Electron-electron interactions and correlations in atomic-scale wires: Luttinger liquids and their spectral signatures

Thesis submitted for the degree of Doctor of Philosophy

Department of Physics and Astronomy,
University College London

Louise Karenza Dash

May 6, 2002

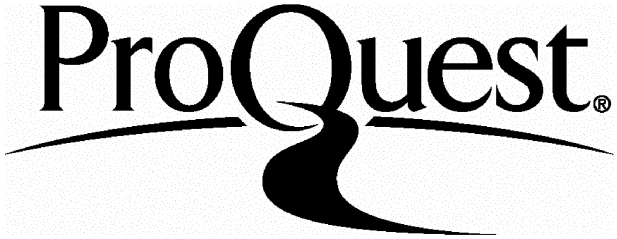

Abstract

It is now possible to create "wires" consisting of a single chain of atoms on an insulating substrate, with possible applications in nanoscale circuitry. However, experimental data on such systems are currently rather limited and as such a thorough theoretical investigation of such systems is required.

In particular, it is useful to know to what extent the behaviour of such wires is one-dimensional—purely one-dimensional systems display Luttinger liquid behaviour, as opposed to the Fermi liquid behaviour characteristic of higher dimensional systems. However, conventional techniques in theoretical surface science are unable to provide a description of electronic correlations at the level required for one dimensional systems.

The existing literature on such atomic wire systems is first reviewed. A discussion of physics in one spatial dimension follows, with a thorough introduction to both the Luttinger liquid and the analytical solutions of the Luttinger model. These concepts are then applied to a simplified model of an atomic wire system—two coupled chains of atoms, on just one of which electron-electron interactions are included. The chain which includes interactions thus represents the wire, while the non-interacting chain represents, albeit incompletely, the influence of the insulating substrate upon which the wire is embedded. Evidence for Luttinger liquid behaviour would be found in the excitation spectra and correlation functions of the system.

A Fortran 90 code was written to implement the above, and both a description of the code and numerical results are presented. The results from excitations and correlation functions of the system indicate that, within the limitations of the model, Luttinger liquid behaviour may well survive. It is possible to calculate for larger and more complicated systems by use of the Density Matrix Renormalization Group (DMRG) algorithm, which relies on keeping only those states of the many particle system needed to describe the ground state and the low-energy excitations. The underlying theory of DMRG is discussed and followed with presentation of preliminary results based on a Hubbard model Hamiltonian.

Acknowledgements

Many people have contributed to and assisted with this thesis. I am very pleased to thank my supervisor, Andrew Fisher, for all the time and effort he has put into guiding me through the maze of my PhD studies. I should also like to thank my other supervisors, Marshall Stoneham and John Gallop at the NPL, for the assistance they have provided, and William Barford at the University of Sheffield for providing the DMRG code used in chapter 6.

Without the help of the staff of the now defunct Birkbeck College Physics Department, I would never have got as far as even starting a PhD. I'd therefore like to thank everyone who taught me, both formally and informally, during my time there as an undergraduate. In particular, special mention should go to Mike de Podesta, Stan Zochowski, Mark Ellerby and Keith McEwen, who have had the somewhat dubious pleasure of having to see me through my postgraduate years as well.

Mike Gillan and Dave Bowler have been exceptionally understanding over the last few months about the amount of time I've been spending writing my thesis rather than doing the research I'm being paid to do—thank you. I should like to thank Hervé Ness for many stimulating conversations and also for helping to keep me sane. Andrew Gormanly has been a fantastic office-mate and has managed to put up with me even when I'm at my most grumpy—I hope to be able to do the same for him when he's in the final stages of writing his thesis! Sarah Harris has also been a great friend over the last year and has helped me keep chilled, while Ché Gannarelli has ensured I have had many more hangovers than was strictly necessary. Callum Wright has been a constant source of encouragement for over eight years and, more recently, has provided invaluable assistance with running the parallel version of my code. I'd also like to thank some recent former members of CMMP: Stephen Shevlin for providing a source of entertainment (come on Steve, we all know it's a wig), Adam Foster for helping me take the piss out of Steve, Hanna Vehkamäki for introducing me to her special brand of Finnish culture and Duncan Harris for introducing me to Fantasy Football.

Finally, I thank all the staff and regulars at the Head of Steam, Euston, for provision of excessive quantities of brain-stimulating refreshment. Without this, I would indubitably have finished my thesis somewhat sooner, more financially solvent and with more brain cells, but it wouldn't have been quite as much fun.

Thank you all.

Contents

I Introduction **9**

1 Introduction **10**

1.1 Background 11
1.2 Aims and motivations 12
1.3 Strong interactions in one dimension 12
1.3.1 The Peierls distortion problem 12
1.3.2 Luttinger liquids 14
1.4 Quantum wires 15
1.4.1 Length scales 15
1.4.2 Quantum waveguides 15
1.4.3 Connection to macroscopic leads 15
1.4.4 Single channel conductance 16
1.5 Atomic scale wires 16
1.5.1 Dangling bond systems 17
1.5.2 Au chains on Si(111) 20
1.5.3 Other candidate Luttinger liquid systems 23
1.6 Summary 23

2 Luttinger liquid theory **24**

2.1 Introduction 25
2.2 One-dimensional systems 25
2.2.1 Fermi liquid breakdown 27
2.3 The Luttinger model 29
2.3.1 Background 29
2.3.2 Haldane's 1981 paper [60] 34
2.4 Spectral functions 39
2.5 Transport 41
2.6 Coupled and crossed chain systems 43
2.6.1 Extensions to the Luttinger model 46

2.7 Non-Luttinger model approaches 48

II Exact calculations **50**

3 Methods **51**

3.1 The model 52

3.1.1 Changes from Haldane's model 53

3.2 Initial calculations 54

3.2.1 Tight-binding chains 54

3.2.2 Results of initial calculations 56

3.3 Green's functions for differential equations 61

3.3.1 Green's functions for the single particle Schrödinger equation 62

3.3.2 The retarded Green's function 63

3.3.3 Finding the Green's function numerically 65

3.4 Exact diagonalization and the Lanczos method 66

3.4.1 Steepest descent — or "How not to do it" 67

3.4.2 The conjugate gradient method 68

3.4.3 The Lanczos algorithm 69

3.4.4 Problems with the Lanczos method 72

3.4.5 Haydock's chain model 73

3.4.6 Finding the eigenvalues and eigenvectors 76

3.4.7 Using the Lanczos method to calculate correlation functions 78

4 Implementation **82**

4.1 Introduction 83

4.1.1 Assumptions and simplifications 83

4.2 Representation of the basis states 85

4.2.1 Single chain basis states 86

4.2.2 Two-chain basis states 86

4.2.3 Numerical representation of the boson system 87

4.2.4 The subroutines `listophys` and `phystolist` 87

4.3 Implementation of the operators 87

4.3.1 The subroutines `field_annihilate` and `field_create`: $\hat{\phi}_p(x)$ and $\hat{\phi}_p^\dagger(x)$ 87

4.3.2 The subroutine `exponentiate`: $e^{i\hat{\phi}_p(x)}$ 88

4.3.3 The `ladder_up` and `ladder_down` subroutines: $\hat{U}_{p,c}$ 92

4.3.4 Electron creation and annihilation: $\hat{\psi}_p^\dagger(x)$ and the `electron` subroutine 93

4.3.5 Normalization 93
4.3.6 Discrete lattice versus the continuum model 97
4.3.7 Implementation of the Hamiltonian for a single chain: The `int_single_hamiltonian` subroutine 98
4.3.8 Book-keeping routines 99
4.3.9 Two coupled Luttinger chains 100
4.4 Implementation of the two-chain Hamiltonian 100
4.4.1 Structure of the coupled Hamiltonian subroutine 101
4.5 Convergence on the eigenstates 104
4.5.1 Calculating moments of the Hamiltonian 105
4.5.2 Lanczos vs conjugate gradient methods 106
4.5.3 To orthogonalize or not to orthogonalize? 107
4.5.4 Precision and errors 108
4.6 Parameters 108
4.7 Parallelization of the code 109

5 Results **112**
5.1 Introduction 113
5.2 Identical chains 113
5.2.1 Ground states 113
5.2.2 Excited states 119
5.2.3 Spectral functions 127
5.2.4 Calculation of the Luttinger parameters 131
5.2.5 Discussion 134
5.3 Non-identical chains 136
5.3.1 Motivation 136
5.3.2 Ground states 136
5.3.3 Excited states 139
5.3.4 Spectral functions 144
5.3.5 Calculation of the Luttinger parameters 144
5.4 Odd numbers of electrons 153
5.5 Summary 157

III DMRG calculations **158**

6 DMRG studies of atomic wires **159**
6.1 Introduction 160
6.2 DMRG theory 160
6.2.1 The algorithm 163

6.3 Applying the theory 164
6.4 Exact calculations 166
6.5 DMRG results 168

7 Conclusions **172**
7.1 Achievements 173
7.2 Proposal for future work 175
7.3 Summary 177

List of Tables

3.1 Conversion between standard mathematical and Haydock's notation 73

4.1 Example notation for basis states of two chains 101
4.2 Convergence properties of the Lanczos and conjugate gradient methods for the eigenvalues of an $L = 4$ non-interacting system. . 106

5.1 Table of ground states for 1 - 5 electrons in two coupled chains each of length 4 sites. This could be extended to chains of any length as long as there are enough available sites on each chain to accommodate all the electrons. While the phases of these states are in principle arbitrary, the phases shown here give $\hat{c}^{\dagger}|\mathrm{gs}_{n=i}\rangle = |\mathrm{gs}_{n=i+1}\rangle$. 115
5.3 Ground states for the $L = 4$, $N = 2$, $t_{\perp} = 0.1$ systems for various interaction strengths I. States with an absolute coefficient of less than 10^{-5} have been omitted 117
5.4 First neutral excited states for the $L = 4$, $N = 2$, $t_{\perp} = 0.1$ systems for various interaction strengths I. Note that the $I = 0.0$ state is a combination of the four degenerate states $\alpha, \beta, \gamma, \delta$ of figure 5.4. States with an absolute coefficient of less than 10^{-5} have been omitted 125
5.5 Ground states for the $L = 4$, $N = 2$, $t_{\perp} = 0.1$ $v_F^A = 1.0, v_F^B = 2.0$ systems for various interaction strengths I. States with an absolute coefficient of less than 10^{-5} have been omitted. 138
5.6 Neutral first excited states for the $L = 4$, $N = 2$, $t_{\perp} = 0.1$ systems for various interaction strengths I. States with an absolute coefficient of less than 10^{-4} have been omitted. 140
5.7 Numerical values of excitation energy corresponding to figure 5.19. 142

List of Algorithms

1 Steepest descent 68
2 Conjugate gradient algorithm 69
3 Basic Lanczos algorithm 72
4 Bisection algorithm for locating the nth eigenvalue λ_n of matrix T_r from the Sturm sequence 77
5 Numerical Renormalization Group outline algorithm 161
6 DMRG infinite system algorithm 164
7 DMRG finite system algorithm 165

Part I

Introduction

Chapter 1

Introduction

> You should never cease to be aware that all aspects of the learning you have acquired, and will acquire, are possible because of their relationship with negation—with that which is not, or which appears not to be.
>
> Glenn Gould, *Advice to a Graduation*, 1964

1.1 Background **11**
1.2 Aims and motivations **12**
1.3 Strong interactions in one dimension **12**
1.4 Quantum wires **15**
1.5 Atomic scale wires **16**
1.6 Summary **23**

1.1 Background

The aim of this work is to investigate the nature of the electron-electron interactions in wires only one atom wide — essentially a chain of atoms. In particular, if such wires are to be used in future atomic-scale circuitry, it is necessary to determine to what extent the wire interacts with its substrate, and if the nature of any such interaction destroys the one-dimensional characteristics of the wire. While the problem of interacting electrons in purely one-dimensional systems, such as an isolated chain of idealized atoms or two coupled chains, has already been the subject of much research [4, 8, 16, 18, 21–24, 28, 34, 35, 40, 42, 43, 46, 47, 56–60, 72, 76, 79, 82–85, 102, 115, 120, 123, 125, 132, 133, 140, 144, 156, 168] the case of a chain of real atoms on a substrate has received less attention.

The work is structured as follows. I begin with a discussion of the aims and motivations underlying the work. The rest of chapter 1 is concerned with the background to the current project—a discussion of what I mean by the term atomic-scale wire, the distinction between this and the term "quantum wire", discussion of the physical systems we are aiming to model, plus a summary of the current state of play of research on these systems.

Chapter 2 is an overview of the theory of physics in one dimension, and in particular a discussion of the Luttinger liquid state and the corresponding Luttinger model, on which most of the current calculations are based. This includes a description of the spectral properties of Luttinger liquids, which is one of our main probes for Luttinger liquid behaviour in the atomic wire system.

Chapter 3 contains a detailed description of our model, with a thorough review of the theoretical and numerical methods we have utilized, particularly exact diagonalization methods for calculating eigenstates and Green's functions of the system.

This is followed in chapter 4 by a full account of the Fortran 95 code written to implement the methods of chapter 3. This includes a discussion of how the Hilbert space is represented numerically and the assumptions and simplifications it was necessary to make.

Chapter 5 consists of the main body of results for the current work. It contains the results for the calculation of eigenstates and correlation functions for two classes of coupled-chain systems, together with a discussion of which aspects of these results lead us to conclude that, within the limitations of the model, such an atomic wire will retain Luttinger liquid properties.

Chapter 6 is concerned with further calculations made using the Density Matrix Renormalization Group (DMRG) method, which allows us to calculate for larger systems than is possible for exact diagonalization techniques.

Finally, chapter 7 summarizes the successes and not-quite-successes of the current work, together with suggestions for future work.

1.2 Aims and motivations

The motivations of this work are twofold. Firstly, from a purely scientific perspective the problem of a one-dimensional system coupled to a higher-dimensional system is inherently interesting and, as yet, has not been fully investigated. Developments in STM techniques have now made it possible to create atomic scale wires, however at present it has not been possible to attach leads to these structures in order to perform transport experiments and thus a theoretical prediction of transport properties would be most useful. Secondly, there are obvious technological applications of such as system, for instance as possible interconnects in a quantum electronic circuit.

1.3 Strong interactions in one dimension

While a full description of physics in one dimension, and the associated concept of a Luttinger liquid is left until chapter 2, it is appropriate at this point to introduce the basic concepts and discuss briefly how and why we expect this to apply to the atomic-scale wire systems in which we are interested.

In a nutshell, physics in one spatial dimension differs greatly from that in higher dimensions, as the phase space available for excitation is so very highly restricted. Consequently, whereas in higher dimensions even strong electron-electron interactions tend to lead to only weak correlation effects, in one dimension even very weak interactions will lead to strong correlations. However, such one-dimensional systems are particularly prone to instabilities, the most important of which is the Peierls distortion.

1.3.1 The Peierls distortion problem

One of the instabilities displayed by one-dimensional conductors is the Peierls distortion, which transforms any one-dimensional conductor to a semiconductor, and can be explained as follows (reference [114], p110ff).

If we take a one-dimensional linear chain with lattice spacing a, and displace every rth atom by a small amount, then the translational symmetry of the system is immediately reduced. The lattice vectors are no longer multiples of a but now of ra, and the basic cell in reciprocal space runs not over $-\frac{\pi}{a} < k < \frac{\pi}{a}$ but over the interval $-\frac{\pi}{ra} < k < \frac{\pi}{ra}$. We can treat the effect of the displacements

perturbatively by considering the resultant change in the periodic potential $\delta V(x)$. The energy curve $E(k)$ is distorted, with discontinuities at $k = \frac{n\pi}{ra}$, and, analogous to the splitting at the Brillouin zone edge for the undistorted chain, the vertical extent of the discontinuities is given by twice the matrix element of the perturbation $\delta V(x)$ between the wavefunction of the undistorted chain $\psi_k(x)$

$$\Delta E = 2 \int \mathrm{d}x \; \psi_k(x)^* \delta V(x) \psi_k(x). \tag{1.1}$$

This is shown in figure 1.1. Now if one of these discontinuities occurs across the Fermi level of the system, then the energies of the highest occupied states will be lowered, whereas the energies of the lowest unoccupied states will be raised. This will lower the overall energy of the system, making the distorted chain energetically preferable to the undistorted chain, and also transforming the system from metallic to semiconducting. Since for any system there will be some value of r for which the discontinuities in $E(k)$ will occur at E_F, a pure one-dimensional conductor is never going to be metallic and will always be subject to this Peierls distortion. As we shall see in later sections, this will occur whenever there is an excitation with momentum transfer exactly equal to $2k_F$. This effect is greatest for small values of r, and so the most common manifestation of the Peierls distortion is where $r = 2$ and the lattice sites of the one-dimensional system pair up to form a dimerized semiconductor. For finite size chains a similar effect occurs, known as the Jahn-Teller distortion.

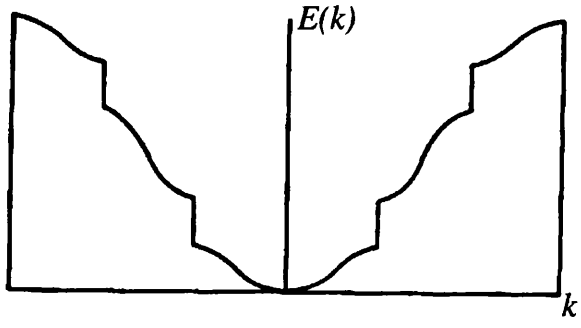

Figure 1.1: Effect on band structure of the Peierls distortion. Reproduced from reference [114].

In practice, however, there exist many one dimensional surface systems that do not experience a Peierls distortion — this occurs when the atoms forming the one-dimensional conductor are rigidly held in place by the substrate atoms, as we shall see in section 1.5, and as a result the effect of Peierls distortion is either decreased, as for the systems discussed in section 1.5.1, or, for all practical purposes, completely suppressed (possibly by the presence of a step

edge on the surface), as in the Au wire system discussed in section 1.5.2.

1.3.2 Luttinger liquids

Although there are many states of matter resulting from the electron-electron interactions in one dimension, depending on the exact nature of the interactions and correlations, the one we are interested here is that of a pure one-dimensional conductor, known as Luttinger liquid, a term first introduced by F.D.M. Haldane [58, 60], which has several distinctive properties. The most notable of these is the existence of power-law dependencies in many of the system's properties, such as the density of states and the conductivity, where the exponent of the power laws is a system-wide constant. In addition, the fundamental excitations of a one dimensional conductor are not fermion-like, but bosonic collective excitations of charge and spin which move at different velocities, leading to uncoupling of the charge and spin degrees of freedom—spin-charge separation.

Luttinger liquids themselves have been well studied, both as isolated entities and as coupled systems [4, 7, 8, 11, 12, 16–18, 21, 23, 24, 26, 28, 29, 34–37, 40–43, 45, 46, 49, 52, 53, 56–60, 62, 66, 68, 69, 72, 73, 78, 79, 82, 87–90, 93–95, 97, 98, 100, 101, 103, 104, 110–112, 115, 119–121, 123–125, 129–133, 135, 137, 140, 143, 144, 148, 150–153, 155, 156, 161, 170]. However, Luttinger liquid systems coupled to higher dimensional systems have, until now, been largely neglected [2, 30].

Much work, however, has been done on "quantum wires", and it is necessary to draw a distinction between these systems, which will be discussed briefly in section 1.4, and the atomic-scale wires of the current work. Typically, quantum wire systems are both much larger than the atomic wires considered here and are semiconductor based. Consequently, although (as their name suggests) they do indeed exhibit quantum effects, such as the quantization of conductance into units of $2e^2/h$, the structure is generally large enough that the electrons still behave fundamentally as a Fermi liquid, rather than the Luttinger liquid predicted for a pure one-dimensional conductors that we believe may be present in quasi-one-dimensional structures such as the true atomic-scale wires such as those under consideration here. However, there has been recent experimental evidence [10] that quantum wires in a GaAs/AlGaAs heterostructure may exhibit properties consistent with Luttinger-liquid like electronic interactions.

1.4 Quantum wires

1.4.1 Length scales

Normally, macroscopic conductors are expected to behave according to Ohm's law, and in particular their conductance G is inversely proportional to their length L and the width W:

$$G = \frac{\sigma W}{L} \tag{1.2}$$

This would seem to imply that the conductance will increase indefinitely as the length of the wire is reduced. However, once certain length scales are reached, this behaviour is destroyed and the conductor behaves in a quite different way. These lengths represent fundamental characteristics of the way individual electrons behave inside a conductor and as such are masked at macroscopic lengths. The first of these is the Fermi wavelength of the conductor, which is proportional to the square root of electron density n_s.

$$\lambda_F = \sqrt{\frac{2\pi}{n_s}} \tag{1.3}$$

We also need to consider the mean free path of the electrons in the conductor, L_m, and the phase-relaxation length, L_ϕ, the distance that an electron travels in the conductor before its initial phase is destroyed [31].

1.4.2 Quantum waveguides

By analogy with electromagnetic waveguides, a narrow conductor will have tranverse modes of electron transmission. These modes, or channels, have well-separated energies if the wire is narrow enough, splitting the dispersion relation into sub-bands. The number of transverse modes is proportional to the width of the conductor, so that in a narrow enough wire, only one channel of conductance will remain. In addition, it is found that the conductance of very small, perfectly transmitting wires no longer decreases linearly with W but is restricted to integer multiples of the quantum of conductance $G_0 = \frac{2e^2}{h}$.

1.4.3 Connection to macroscopic leads

Obviously, in order to be able to measure the conductance of a quantum wire we need to attach leads to it and apply an external bias. If these leads are macroscopic, then we have a problem. We saw in section 1.4.1 that the conductance should be proportional to the length of the wire, and an infinitely narrow wire (i.e. a single channel conductor) should therefore have infinite conductivity, in

other words zero resistance. However it is found that the conductance of such a wire has a maximum limiting value as the length of the wire falls below the mean free path L_m. As $L < L_m$ we expect the electrons' passage through the conductor to be free of collisions, which would also imply zero resistance. In fact the observed resistance is owing to the interface between the macroscopic leads and the wire, where the many transverse modes of the leads have to give way to the single mode of the wire itself, and thus we have a resistance that is independent of the length of the wire.

1.4.4 Single channel conductance

For a single-channel Fermi liquid wire (see section 2.2.1), we can derive the value of the conductance quantum as follows [72]: First we assume that the chemical potentials of the two macroscopic leads (which act as electron reservoirs) are separated by eV. There will then be an excess of $\frac{\kappa eV}{2}$ states carrying current away from the lead at the higher potential, where $\kappa = \frac{\partial n}{\partial \mu}$ is the compressibility. For a non-interacting one-dimensional electron gas the compressiblity is given by

$$\kappa = \frac{1}{v_F \pi \hbar}. \tag{1.4}$$

The current carried by each state will be dependent on the Fermi velocity and the charge, thus giving a total current I of

$$\begin{aligned} I &= \kappa v_F \frac{e^2 V}{2} \\ &= \frac{e^2 V}{2\pi\hbar}. \end{aligned} \tag{1.5}$$

Dividing by V to give the conductance thus gives $G = \frac{e^2}{h}$, and including spin gives an extra factor of 2 to yield the conductance for a single-channel Fermi liquid conductor:

$$G_0 = \frac{2e^2}{h}. \tag{1.6}$$

1.5 Atomic scale wires

While the above discussion serves well for these "conventional" quantum wires, we need to bear in mind that owing to the width of the atomic scale wires we are investigating here, one-dimensional properties will increasingly come into play, and hence we cannot ignore the role of the electron-electron correlations.

Since part of the aim here is to investigate to what extent the Luttinger liquid wire interacts with the surface, and in fact whether the Luttinger liquid

survives the interaction, it is useful to consider the type of physical systems that are relevant to our model (see section 3.1). At present there are several candidate systems that may show Luttinger liquid behaviour, the most promising of which are self-assembled Au lines on silicon, and systems based on dangling-bonds on hydrogen terminated Si surfaces, where the dangling bonds may be left unterminated or saturated with Ga atoms. However, there have been precious few studies of the transport properties of these systems, and effort has been concentrated theoretically on electronic structure calculations, and experimentally on spectroscopic studies.

1.5.1 Dangling bond systems

There has been recent interest in the electronic structure of wires fabricated by taking a hydrogen-passivated Si surface and removing a line of H atoms. The remaining Si atoms thus form a wire of "dangling bonds" which, although obviously too chemically reactive to be of much use in an atomic-scale device, have the advantage of being a relatively simple system on which to perform calculations [33, 158, 159].

For instance, the Si(111)-H system has been examined using density functional theory by Watanabe *et al.*[158]. Here the geometry and electronic structure was calculated using a local-density-functional approach with a pseudopotential used to model the electron-nucleus interaction, with the results showing that the the dangling bond wire is structurally stable. Band structure calculations show that states with a highly one-dimensional character arise in the band gap that are absent from a pure Si(111)-H system, implying that the wire is metallic. It was also shown that no dimerization along the wire of the dangling bonds caused by the Peierls distortion (see section 1.3.1) occurs in this system, but that instead a small (0.023Å) height difference occurs between the Si atoms with dangling bonds and neighbouring Si atoms. This leads to a splitting of the midgap states and the wire becoming semiconducting, although as the magnitude of the splitting is 38meV and the energy gain owing to the distortion only 6.5meV, corresponding to a thermal energy of 75K, the distortion will not occur at room temperature and the wire will be metallic in this regime.

Similar results have been obtained for dangling bond wires on the hydrogen terminated Si(100)2×1 surface [157, 159]. This surface is more anisotropic than the Si(100)1×1 surface and hence more wire geometries are possible. The 2×1 surface reconstruction leads to a dimerization of the H-atoms and dangling bond wires can be formed either along these dimer rows or perpendicular to them, although the geometry of the wires is crucial to the electronic properties—in fact

only the single dangling bond wire parallel to the dimer rows is metallic in this instance, again only above the Peierls threshold, calculated as 75K. Ga atoms can be adsorbed on these dangling bond structures to form rather less reactive wires that promise to be more useful in technological situations [64, 65, 157, 159]. However these structures appear to be largely semiconducting, and none of them purely metallic.

Atoms of As can also be adsorbed onto dangling bonds and it is possible that these may be more promising candidates for metallic wires [165]. In addition, attempts are being made to find a "formula" for both adsorbates and substrates to form "designer" systems with specific required properties [166, 167].

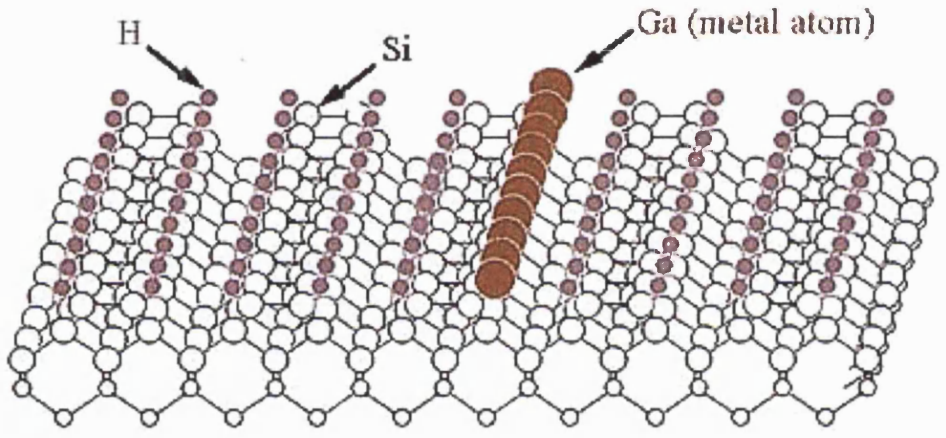

Figure 1.2: Diagram of a Ga atomic wire on the Si(100) surface (Hitachi Advanced Research Laboratory, http://hatoyama.hitachi.co.jp/english/research/hashizu/text.html)

While the distorted and semiconducting forms of these wires will have their transport properties dominated by polaronic transport [19, 105–107], it is possible that metallic atomic wires will exhibit one-dimensional properties despite being coupled to the surface. As yet there have been no published attempts to determine whether or not these infinite wires behave as Luttinger liquids, or indeed any comprehensive work on their electronic transport properties. However, a recent study by P. Doumergue *et al.* [33] used elastic scattering quantum chemistry (ESQC) to calculate the conductance of a finite DB wire on a Si(001)-(2×1)-H surface between two Au contact pads, as in figure 1.4. The conductance was calculated both for a (metallic) undistorted chain and a (semiconducting) Peierls distorted chain. They concluded that the undistorted wire acts as a single ballistic quantum channel, whereas for the Peierls distorted wire

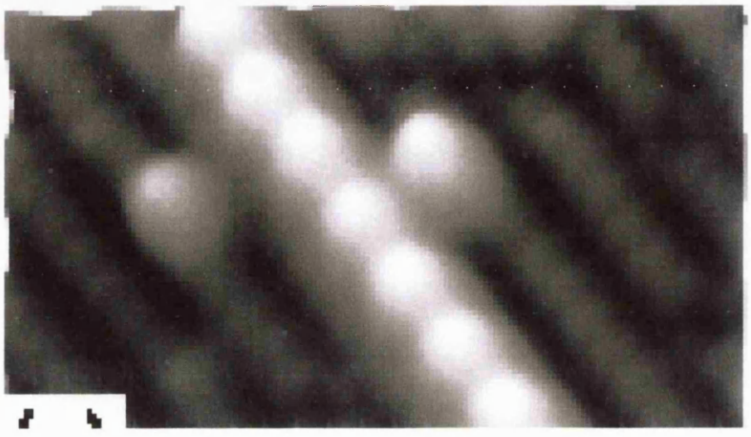

Figure 1.3: STM picture of a dangling bond wire on the Si(100)2×1 surface, from reference [65]

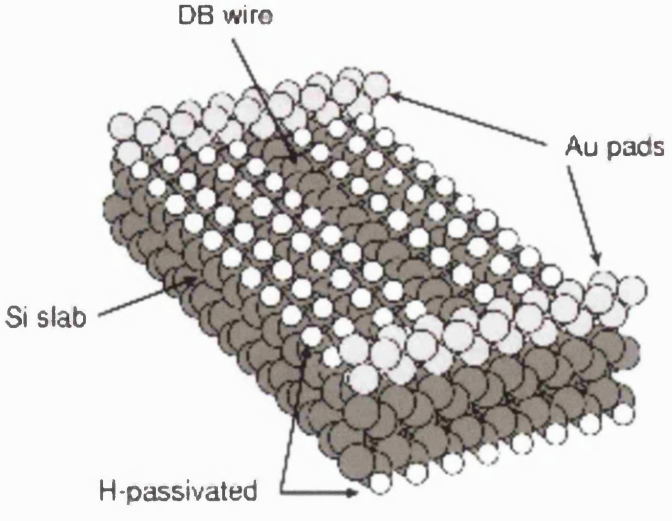

Figure 1.4: Finite DB wire with contact pads (Reproduced from [33])

transport occurs through tunnelling but with a very short inverse decay length. However, neither electron-electron interactions nor electron-phonon interactions were taken into account and since a full description of transport properties of the metallic wire is dependent on the correct treatment of the electron-electron interactions, the results of this paper may not reflect the physical reality of such a system.

1.5.2 Au chains on Si(111)

There has been recent controversy over the potential Luttinger liquid nature of Au chains on a Si(111) substrate [3, 63, 86, 136]. Initially, photoemission data was used to infer spin-charge separation owing to the chains, and hence Luttinger liquid behaviour [136], but more recent work has indicated that this may not be the case [3, 63, 86].

Photoemission is an important spectroscopic probe for many body effects — not least because the data can be directly related to the spectral function, which will be discussed in detail in section 2.4. The process is shown schematically in figure 1.5. An incoming photon ejects an electron from the surface, transferring

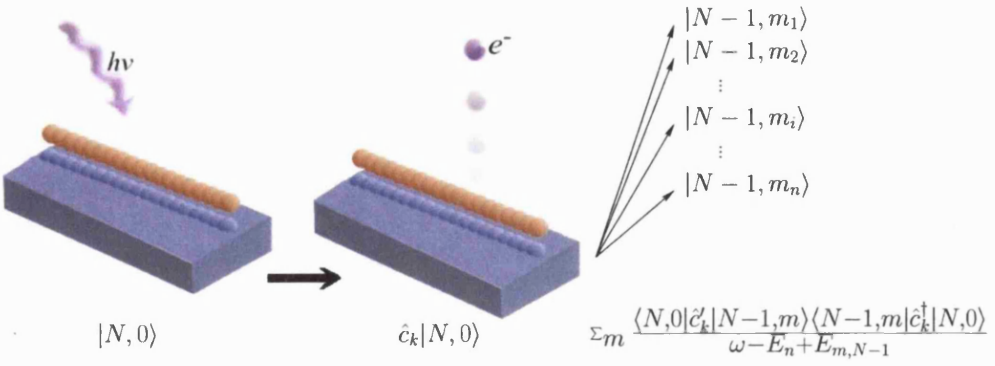

Figure 1.5: Schematic diagram of the photoemission process.

the system from an N-electron state to some combination of $(N-1)$-electron eigenstates. The energy of the emitted electrons can be measured and this data is equivalent to the electron part of the spectral function. The momentum parallel to the surface $k_{||}$ is conserved during this process, and is equal to $\sqrt{2mE_k/\hbar^2}\sin\theta_e$, where E_k is the energy of the emitted electron and θ_e is the angle between the direction of the emitted photon and the normal to the surface [75], and so by varying $k_{||}$ or θ_e it is possible to build up a detailed picture of the spectral function in the vicinity of the Fermi energy.

In the photoemission experiments performed by Segovia *et al.* [136], sam-

ples consisting of vicinal Si(111) cut at an angle of 9.45° were prepared, upon which Au chains were self-assembled by evaporation and annealing, to form the Si(111)5×1-Au structures (equivalently Si(557)-Au) shown in figure 1.6. Angle-resolved photoemission data was collected at 12K using linearly polar-

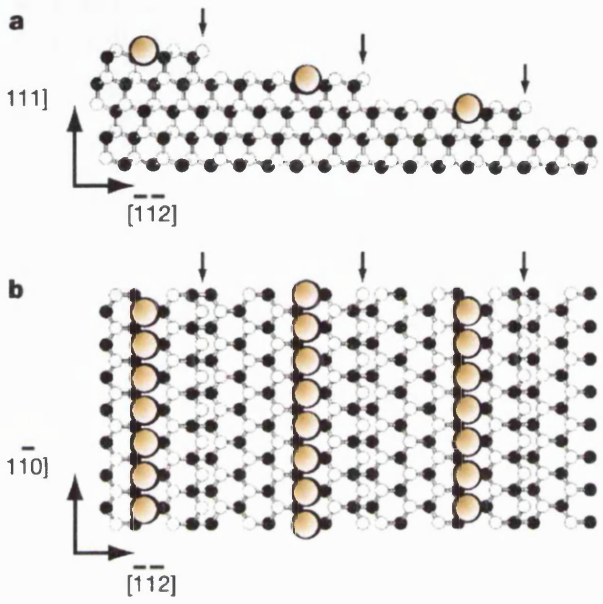

Figure 1.6: Si(111)5×1-Au (Si(557)-Au) side and plan views, from reference [136]

ized monochromatic ultraviolet photons, and no dispersion perpendicular to the chains for the chain state was found, indicating that the chains form a one-dimensional metallic system, and there is no evidence of a Peierls distortion. The results are shown in figure 1.7. The authors claim that the removal of spectral weight at E_F indicates non-Fermi liquid behaviour, and moreover, that the double peak structure visible most clearly at $\theta_e = -13.5°$ is attributable to two separate peaks for the spin and charge excitations. The combination of these two factors is therefore an indicator of potential Luttinger liquid behaviour.

However, the work of Losio and Altmann *et al.* refutes this claim [3, 86]. They too performed angular-resolved photoemission experiments on this system (at the rather higher temperature of 100K), but with higher energy photons ($h\nu$ = 34eV rather than 21.2eV in reference [136]), and find that while the double peak structure is still observed, it does not disappear at $E = E_F$, and therefore is inconsistent with the attribution of the double peak structure to spin charge separation (the spin and charge peaks converge at E_F in a Luttinger liquid). Instead, the authors propose that the double peak structure is owing to

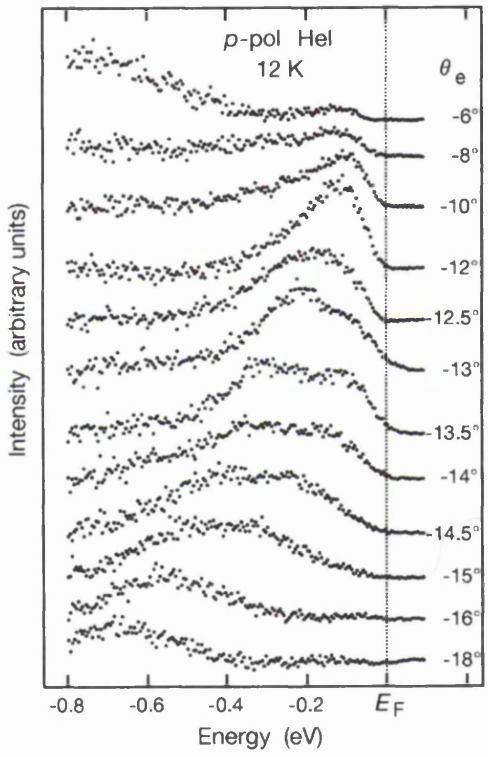

Figure 1.7: Photoemission results from reference [136]

two nearly degenerate bands. This is further borne out by the recent electronic structure work of Sánchez-Portal *et al.* [126] which uses DFT methods to reach the same conclusions—that there are two almost degenerate bands associated with the chains. X-ray diffraction studies [122] also support this. This does not, however, rule out the possibility of a Luttinger liquid in this system.

1.5.3 Other candidate Luttinger liquid systems

While the atomic-scale wires presented in the previous section are the main focus of attention in the present work, there are several other physical systems that have been proposed as possible Luttinger liquid systems. Recently carbon nanotubes have received attention [17, 78, 110, 117, 169]—not least because their physical properties make it possible to attach leads to the nanotubes and measure conductance properties directly. In addition, it has recently been proposed that the coupling of Luttinger liquid carbon nanotubes to a superconductor may provide a useful physical realization of quantum entanglement [13]. It has also been suggested that the edge states in Quantum Hall systems may behave as chiral Luttinger liquids [26, 121, 161]. Finally, the highly anisotropic Bechgaard salts $(TMTSF)_2X$, where TMTSF denotes tetramethyltetraselenofulvalene, have shown optical properties consistent with Luttinger liquid behaviour [14, 52, 135, 142, 151].

1.6 Summary

In summary, we have seen that there are several possible systems that may exhibit properties consistent with Luttinger liquid behaviour in certain regimes. However, owing to the Peierls distortion, a band gap will open in many of these systems at low temperatures to form a semiconducting wire. Nonetheless, at temperatures above the Peierls transition temperature (only 75K in the case of the Si(100)-H based dangling bond wire discussed in section 1.5.1, metallic behaviour, and hence possible Luttinger liquid behaviour, will be restored. While phase diagrams for the temperature dependence of Luttinger liquid behaviour have been generated for some other coupled-chain systems [14, 15], as yet the systems described in section 1.5.1 remain neglected in this regard. Although the present work is not concerned with the exactitudes of electronic structure, we do however attempt to investigate to what extent, given the existence of a metallic wire, the presence of the substrate surface perturbs, or even destroys, the Luttinger liquid behaviour of an isolated wire. With this in mind, chapter 2 describes the theory of interacting electrons in one dimension.

Chapter 2

Luttinger liquid theory

Ma peath hearn pecare oll an beaz
Mouy pobell bohodgack vel pobell broaz.

From *"Reem an parra hearn"*,
attr. John Boson, c1770

2.1 Introduction **25**
2.2 One-dimensional systems **25**
2.3 The Luttinger model **29**
2.4 Spectral functions **39**
2.5 Transport **41**
2.6 Coupled and crossed chain systems **43**
2.7 Non-Luttinger model approaches **48**

2.1 Introduction

This chapter is entirely concerned with the theory underlying the physics of one-dimensional Fermi systems. It begins with a description of their physical properties, and how these properties lead to the breakdown of the Fermi liquid concept in one spatial dimension, to be replaced instead by the concept of a Luttinger liquid.

This is followed by a description of the main model used in the present work—the Luttinger model. A thorough review of Haldane's 1981 solution of the Luttinger model [60] is presented in section 2.3, complete with a description of the operator method of bosonization, as implemented computationally in chapter 4.

A discussion of the relationship between the Luttinger model and the Luttinger liquid properties of one-dimensional systems is contained in section 2.3. This is followed by a description of how the Luttinger model relates to some of the physical properties manifest in real systems, and in particular, how the spectral function and other correlation functions can be calculated.

A description of transport phenomena in the Luttinger liquid follows, in section 2.5. This is followed by a review of recent work in the theory of crossed– and coupled–Luttinger liquid systems in section 2.6.

Finally, in sections 2.6.1 and 2.7, we discuss briefly extensions to the "standard" Luttinger model, and some the most important non-Luttinger model approaches to one-dimensional systems, in particular the Hubbard model, which is utilized in the Density Matrix Renormalization Group work of Chapter 6.

2.2 One-dimensional systems

Consider a system of non-interacting fermions constrained to move on a line. In one dimension the Fermi surface is not continuous, as in higher dimensions, but consists of two points at the Fermi energy, as shown in figure 2.1. The consequences of this are mortiferous for standard Fermi liquid theory—this is discussed in more detail in section 2.2.1, but also results in physical phenomena unique to one-dimensional systems.

It will be noted that there is a region at low energies in the excitation spectrum where there are no allowed excitations, as can be seen from figure 2.2. The reason for the existence of this zero-excitation region becomes clear when the nature of the possible excitations is considered. Minimal energy excitations are only possible with a momentum change either close to zero or about $2k_F$, as can be seen from figure 2.1. This gap also gives rise to a well

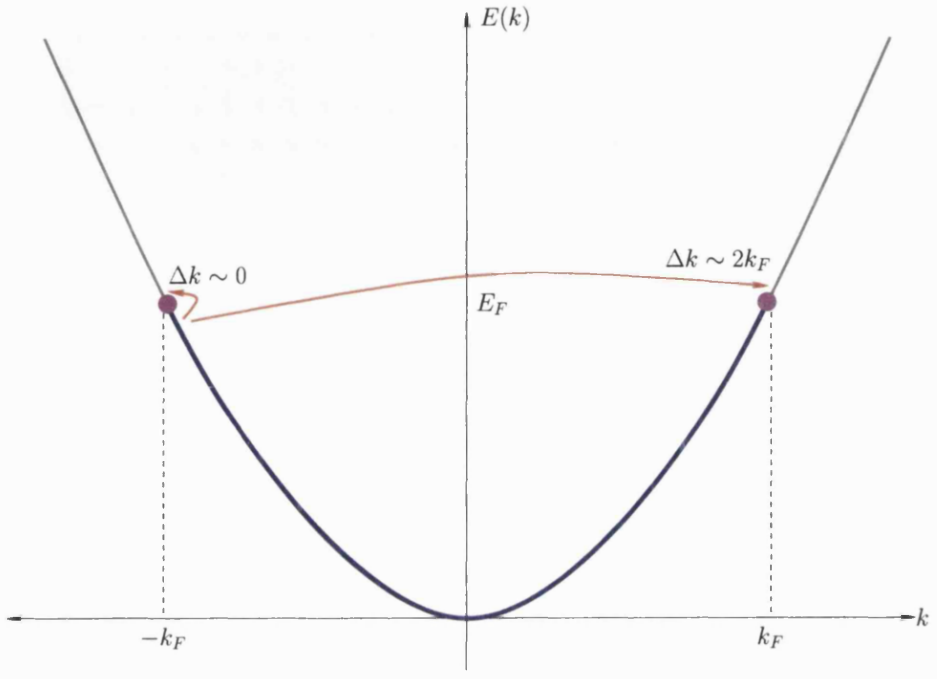

Figure 2.1: Allowed low-energy excitations for a one-dimensional system. The points representing the Fermi surface are shown in purple, occupied states by the blue line.

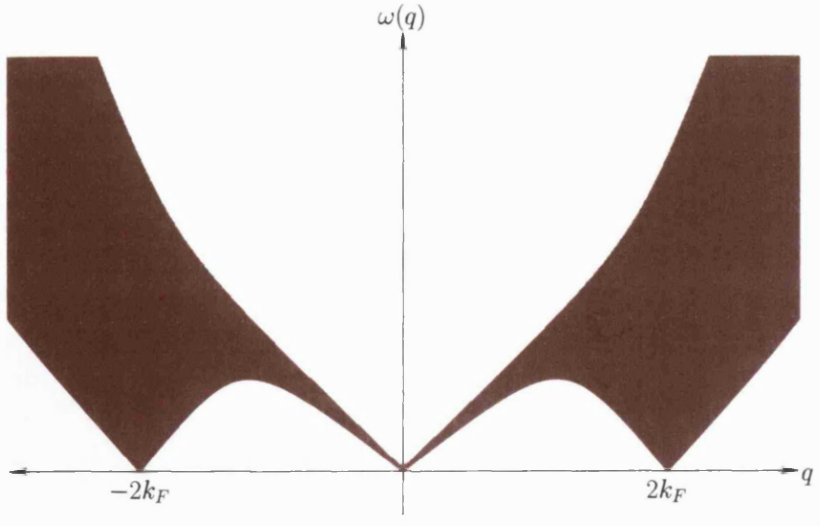

Figure 2.2: Particle-hole excitation spectrum in one dimension.

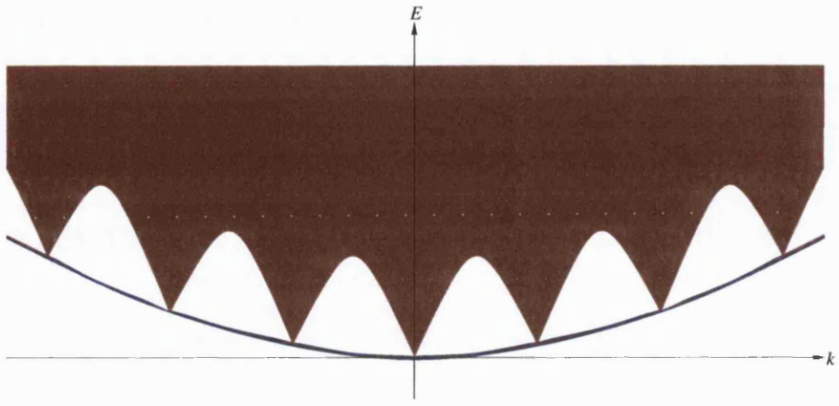

Figure 2.3: Multiple particle-hole excitation spectrum in one dimension.

defined particle-like dispersion of those excitations with $\Delta k \sim 0$, and as a consequence the elementary excitations of an interacting one-dimensional system are not the electron-like excitations familiar to higher dimensional systems, but bosonic collective excitations of charge and spin generally referred to as holons and spinons respectively. Once electron-electron interactions are included, the spinons and holons disperse with different velocities, and this leads to the phenomenon of complete separation of the spin and charge degrees of freedom for one-dimensional systems.

Multiple excitations, of two or more electron-hole pairs, are also possible, giving a full spectrum of the form shown in figure 2.3. This spectrum has the additional feature of a parabolic "envelope", due to the fact that once one minimum-energy excitation has taken place, a subsequent excitation must occur from a lower energy state to a higher one than the original excitation.

For an interacting system, the density of states, $n(\omega)$, becomes continuous and is devoid of the discontinuity at E_F characteristic of higher dimensional systems. In fact, the density of states varies like $|k - k_F|^\alpha$, where α is an interaction dependent exponent which is equal to 1 in the non-interacting limit. Many other physical properties of the system are also characterized by power laws with the same exponent α, in particular the spectral function, which will be discussed in section 2.4, the conductance, which behaves as a power of temperature, $G(T) \sim T^\alpha$, and the I–V characteristics, where $I(V) \sim V^\alpha$. These properties will be discussed further in section 2.5.

2.2.1 Fermi liquid breakdown

In three dimensions the concept of the Fermi liquid is well known—the fundamental excitations of the system can be represented by electron-like quasipar-

ticles that evolve continuously from the real electrons as the electron-electron interactions are switched on. The lifetime of these particles, which tends to infinity as the Fermi surface is approached, is related to the imaginary part of the self-energy Σ, which appears in the electronic Green's function as [144]

$$G(k,\omega) = \frac{1}{\varepsilon_0(k) - \omega - \Sigma(k,\omega)}. \tag{2.1}$$

Here $\varepsilon_0(k)$ is the dispersion of the non-interacting electrons, ω the energy. The self-energy $\Sigma(k,\omega)$ is the energy and wavevector dependent complex energy shift arising from the many body interactions. There will be poles in $G(k,\omega)$ for each value of ω that represents a quasiparticle eigenvalue. Given a single pole in $G(k,\omega)$ for each quasiparticle, without which the quasiparticle description becomes physically meaningless, the residue is given by [144]

$$z_k = \left(1 - \frac{\partial \mathrm{Re}\Sigma(k,\omega)}{\partial\omega}\right)^{-1}_{\omega=\varepsilon_0(k)}, \tag{2.2}$$

which, for a normal Fermi liquid, will satisfy $0 \leq z_k \leq 1$.

In one dimension, however, the situation is somewhat more complicated. The problem of the Peierls transition, caused by interactions between the electrons and phonons, was presented in section 1.3.1. However, the one-dimensional system is highly susceptible to similar instabilities caused by *any* process with a momentum transfer equal to $2k_F$, regardless of its cause, and, due to the perfect nesting of the Fermi "points" in one dimension, interactions between electrons on opposite sides of the Fermi surface result in just such processes.

There is also a problem arising from the assumptions made about the Fermi liquid Green's function. If, for example, we consider a forward scattering process between particles of opposite spin (this will be defined as a $g_{4\perp}$ process in section 2.3.1), then it can be shown [144] that the Green's function gives not one but two solutions for the energy location of the quasiparticle pole

$$\omega = \left(v_F \pm \left|\frac{g_{4\perp}}{\sqrt{8}\pi}\right|\right)(k - k_F). \tag{2.3}$$

This double-valuedness is the origin of the spin–charge separation phenomenon. However, it also violates the fundamental assumptions underlying Fermi liquid theory and as such indicates that no Fermi liquid description is possible for interacting electrons in one dimension.

2.3 The Luttinger model

2.3.1 Background

The Luttinger model has its origins in the work of Tomonaga [141] who, noticing the boson-like properties of the excitations of an interacting one-dimensional electron gas, approximated the Hamiltonian for such a system by describing the excitations as exact bosons, despite the fact that the elementary particles – the electrons – are fermions. By linearizing the dispersion relation around E_F in order to simplify the description of the low-lying excitations (section 3.2.2 demonstrates the validity of this approximation), the Tomonaga Hamiltonian becomes exactly solvable.

Luttinger [89] expanded on this approach by not only separating the electrons into two distinct populations of fermions—left moving (with dispersion slope < 0) and right moving (slope > 0)—but also by extending the dispersions for each population out to $k = \pm\infty$, giving an infinite 'sea' of negative-energy electrons, as shown in in figure 2.4. Although completely unphysical, by doing this the bosonic commutation relationships, only approximate in the Tomonaga model, become exact.

The Luttinger model was solved exactly in 1965 by Mattis and Lieb [93], and although the methods have been widely described in other terms by various authors [90, 130, 140, 144], arguably the definitive picture of the Luttinger model was given in 1981 by F.D.M. Haldane [58–60], whose concise operator methods will be used here.

There are four basic interaction processes available, as shown in figure 2.5. However, only two of these are included in the Luttinger model. The first of these, generally known as a g_1 process, is shown in figure 2.5(a). This represents backward scattering of particles from two different branches, with a corresponding momentum transfer of $2k_F$. The second process, labelled g_2, is shown in figure 2.5(b) and represents forward scattering between momentum branches, with a small transfer of momentum. Umklapp scattering is represented in the g_3 process, figure 2.5(c), although this process is only important if the band is half filled, in which case $4k_F$ is a reciprocal lattice vector and all four of the participating electrons are in the vicinity of the Fermi surface [140]. Finally we have g_4 scattering, as shown in figure 2.5(d), which is forward scattering in which all participating electrons are from the same branch. However, as we shall see, only the g_2 and g_4 processes are included in the Luttinger model.

If we are considering a system which includes spin, then we can also include subscripts $\parallel$ to indicate that the interaction is between particles with the same

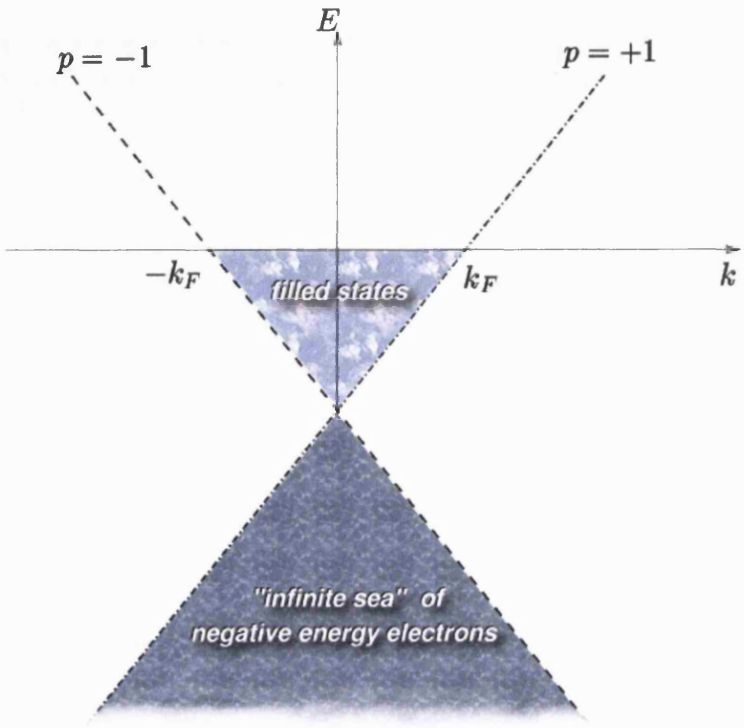

Figure 2.4: Schematic representation of the Luttinger model

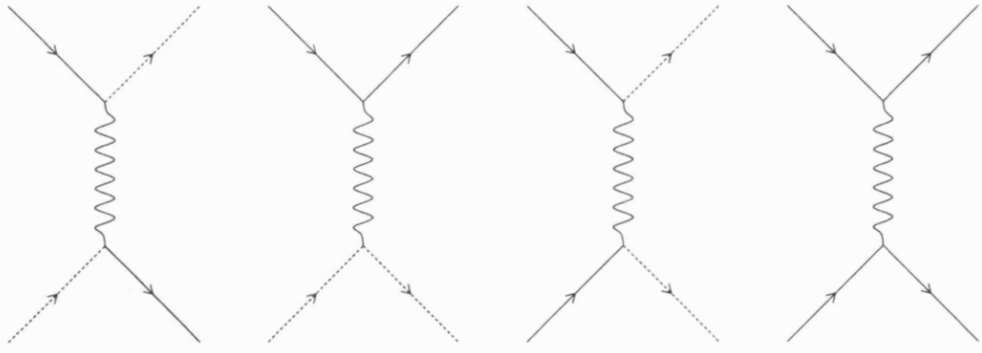

(a) g_1 (b) g_2 (c) g_3 (d) g_4

Figure 2.5: The four possible scattering processes. Solid lines indicate electrons moving with positive momentum, dashed lines electrons moving with negative momentum

spin index, and $\perp$ to indicate that the interaction is between particles with differing spins.

However, not all of these scattering processes are included in the Luttinger model. The $g_{1\perp}$ interaction violates the spin-current conservation between momentum branches inherent in the Luttinger model, and the $g_{3\perp}$ interaction spoils the charge-current conservation between the branches. For spinless fermions, the only interaction processes included in the Luttinger model are those involving g_2 and g_4 scattering.

Before moving onto Haldane's solution [60] of the Luttinger model, it is useful to introduce the Luttinger Hamiltonian in the terminology already used (which follows closely that used in reference [144]) as this formulation appears to be more widely used in the literature. The total Luttinger liquid Hamiltonian can be split into three parts

$$\hat{H} = \hat{H}_0 + \hat{H}_2 + \hat{H}_4, \tag{2.4}$$

where $\hat{H}_0$ is the non-interacting part of the Hamiltonian, and $\hat{H}_2$ and $\hat{H}_4$ contain the g_2 and g_4 interactions respectively.

The non-interacting part of the Hamiltonian is given in second-quantized form as

$$\hat{H}_0 = \sum_{p,q,s} v_F(pq - k_F) : \hat{c}^\dagger_{pqs}\hat{c}_{pqs} :, \tag{2.5}$$

where the operator $\hat{c}^\dagger_{pqs}$ creates a fermion on branch $p = \pm 1$ with momentum q and spin s. The notation $: \ldots :$ denotes normal-ordering[1]. The $\hat{H}_2$ and $\hat{H}_4$ are given by

$$\hat{H}_2 = \frac{1}{L}\sum_{q,s,s'} \left[g_{2\parallel}(q)\delta_{s,s'} + g_{2\perp}(q)\delta_{s,-s'}\right] \hat{\rho}_{+,s}(q)\hat{\rho}_{-,s'}(-q), \tag{2.7}$$

$$\hat{H}_4 = \frac{1}{2L}\sum_{p,q,s,s'} \left[g_{4\parallel}(q)\delta_{s,s'} + g_{4\perp}(q)\delta_{s,-s'}\right] \hat{\rho}_{p,s}(q)\hat{\rho}_{p,s'}(-q), \tag{2.8}$$

Here s indicates the spin index, q momentum and $p = \pm 1$ the branch index. The interaction terms $g_{2\parallel}(q)$, $g_{2\perp}(q)$, $g_{4\parallel}(q)$, $g_{4\perp}(q)$ are the momentum-dependent forms of the interactions as described by figure 2.5. Note that the 1/2 fac-

[1]Usually this would imply that the annihilation operators are all to the right of the creation operators. However, since here we have the infinite sea of negative-energy particles, normal ordering implies that for the negative-energy electrons the reverse is true, e.g.

$$: \hat{c}^\dagger_k\hat{c}_k := \begin{cases} \hat{c}^\dagger_k\hat{c}_k & (\varepsilon_k > 0) \\ \hat{c}_k\hat{c}^\dagger_k & (\varepsilon_k < 0) \end{cases} \tag{2.6}$$

tor in the expression for $\hat{H}_4$ avoids double-counting over the two momentum branches. The density operators $\hat{\rho}$ are defined in terms of the fermion creation and annihilation operators as

$$\hat{\rho}_{p,s}(q) = \sum_k : \hat{c}^\dagger_{p,k+q,s}\hat{c}_{p,k,s} := \sum_k \left(\hat{c}^\dagger_{p,k+q,s}\hat{c}_{p,k,s} - \delta_{q,0}\langle \hat{c}^\dagger_{p,k,s}\hat{c}_{p,k,s}\rangle_0\right). \quad (2.9)$$

We also note that $[\hat{H}_2, \hat{H}_0] \neq 0$, so the $\hat{H}_2$ term is able to modify the ground state by excitation of particle-hole pairs, whereas $[\hat{H}_4, \hat{H}_0] = 0$ and so the $\hat{H}_4$ term cannot modify the ground state, only remove degeneracies in the excitations in much the same way as the introduction of a magnetic field.

The interaction terms may be transformed into charge- and spin-dependent parts as

$$g_{i\rho}(q) = \frac{1}{2}\left(g_{i\parallel}(q) + g_{i\perp}(q)\right), \quad (2.10)$$

$$g_{i\sigma}(q) = \frac{1}{2}\left(g_{i\parallel}(q) - g_{i\perp}(q)\right), \quad (2.11)$$

where here the subscript ρ indicates charge and σ spin. However, as the present work is almost exclusively concerned with spinless models, for the remainder of this section we shall drop the spin indices and assume a spinless Luttinger model.

By removing the spin-dependence of equations (2.7) and (2.8), the interaction parts of the Hamiltonian become

$$\hat{H}_2 = \frac{2}{L}\sum_q g_2(q)\hat{\rho}_+(q)\hat{\rho}_-(-q), \quad (2.12)$$

$$\hat{H}_4 = \frac{1}{L}\sum_{p,q} g_4(q)\hat{\rho}_p(q)\hat{\rho}_p(-q). \quad (2.13)$$

The total spinless Hamiltonian $\hat{H} = \hat{H}_0 + \hat{H}_2 + \hat{H}_4$ can now be diagonalized with a Bogoliubov transformation

$$\tilde{H} = \mathrm{e}^{\mathrm{i}\hat{S}_\rho}\hat{H}\mathrm{e}^{-\mathrm{i}\hat{S}_\rho}, \quad (2.14)$$

where

$$\hat{S}_\rho = \frac{2\pi\mathrm{i}}{L}\sum_{q>0}\frac{\phi_q}{q}\left[\hat{\rho}_+(q)\hat{\rho}_-(-q) - \hat{\rho}_-(q)\hat{\rho}_+(-q)\right]. \quad (2.15)$$

Here we have another interaction-dependent term $\phi(q)$, and the density opera-

tors can also be transformed by

$$\tilde{\rho}_p(q) = \hat{\rho}_p(q)\cosh\phi_q + \hat{\rho}_{-p}(q)\sinh\phi_q. \tag{2.16}$$

The transformed form of the complete Hamiltonian is therefore given by

$$\tilde{H} = \frac{\pi}{L}\sum_{p,\ q\neq 0} v_0(q) : \tilde{\rho}_p(q)\tilde{\rho}_p(-q) : + \frac{\pi}{2L}\left[v_N\left(N_+ + N_-\right)^2 + v_J\left(N_+ - N_-\right)^2\right], \tag{2.17}$$

and is diagonal if we have the following condition on ϕ_q when making the transformation:

$$K_\rho(q) \equiv \mathrm{e}^{2\phi_q} = \sqrt{\frac{\pi v_F + g_4(q) - g_2(q)}{\pi v_F + g_4(q) + g_2(q)}}. \tag{2.18}$$

The spinless Luttinger liquid parameter K_ρ is then obtained by taking the limit of $K_\rho(q)$ as $q \to 0$, i.e.

$$\begin{aligned} K_\rho &\equiv \lim_{q\to 0} K_\rho(q) = \mathrm{e}^{2\phi} \\ &= \sqrt{\frac{\pi v_F + g_4 - g_2}{\pi v_F + g_4 + g_2}}, \end{aligned} \tag{2.19}$$

where the absence of a q subscript in the terms that were previously dependent on q implies that the limit as $q \to 0$ has been taken.

We can now relate the three velocities, v_0 ($\equiv \lim_{q\to 0}$), v_N and v_J as follows

$$v_N v_J = v_0^2, \tag{2.20}$$

$$v_N = \frac{v_0}{K_\rho} = v_0\mathrm{e}^{-2\phi}, \tag{2.21}$$

$$v_J = v_0 K_\rho = v_0\mathrm{e}^{+2\phi}. \tag{2.22}$$

These are also related to the (non-interacting) Fermi velocity as follows

$$v_N = v_F + g_4 + g_2, \tag{2.23}$$

$$v_J = v_F + g_4 - g_2. \tag{2.24}$$

In addition, we can define the Luttinger exponents α and γ, which appear in the power laws governing the single particle properties of the Luttinger liquid. For a spinful Luttinger liquid,

$$\gamma_\nu = \frac{1}{8}\left(K_\nu - \frac{1}{K_\nu} - 2\right); \qquad \nu = \sigma, \rho \tag{2.25}$$

$$\alpha = 2(\gamma_\rho + \gamma_\sigma), \tag{2.26}$$

whereas for a spinless Luttinger liquid, the focus of attention in the current work,

$$\gamma = \frac{1}{4}\left(K_\rho - \frac{1}{K_\rho} - 2\right) \tag{2.27}$$

$$\alpha = 2\gamma \tag{2.28}$$

2.3.2 Haldane's 1981 paper [60]

As the numerical implementation described in chapter 4 is largely based on the form of the solution of the Luttinger model given by Haldane [56–60], we now include a comprehensive review of the relevant parts of Haldane's solution of the Luttinger model.

Firstly, Haldane examines the Hilbert space of the Luttinger model with periodic boundary conditions defined on a ring of length L. Since Haldane is dealing with a continuum rather than a lattice system, the Hilbert space is infinite and care needs to be taken that the operators are well-defined. Haldane therefore chooses to take the (fairly standard) approach of considering only quantities that can be measured using a set of normal ordered creation operators operating on the ground state. The Hamiltonian can therefore be written, in terms of the fermions, as

$$\begin{aligned} \hat{H}^0 &= v_F \sum_{kp} (pk - k_F)(n_{kp} - \langle n_{kp}\rangle_0), \\ &= v_F \int_0^L \sum_p : \hat{\psi}_p^\dagger(x)\,(\mathrm{i}p\nabla - k_F)\,\hat{\psi}_p(x) : dx. \end{aligned} \tag{2.29}$$

Here $p = \pm 1$ is again the branch index, n_{kp} is the number of fermions with momentum k on branch p, and $\langle n_{kp}\rangle_0 \equiv \theta(k_F - pk)$. The fermion operators $\hat{\psi}_p^\dagger(x)$ and $\hat{\psi}_p(x)$ create or annihilate respectively a fermion on branch p at position x.

These creation and annihilation operators can also be expressed in terms of operators that create or annihilate at a specified momentum k, rather than position x, by Fourier transform:

$$\hat{\psi}_p^\dagger(x) = \lim_{\varepsilon \to 0^+} \left(\frac{1}{\sqrt{L}} \sum_k \mathrm{e}^{-\mathrm{i}kx} \mathrm{e}^{-\varepsilon |\frac{kL}{2\pi}|} \hat{c}_{kp}^\dagger \right). \tag{2.30}$$

The limit $\varepsilon \to 0^+$ is usually implicit, but is necessary to ensure an *exact* periodic

delta function in the anticommutation relation for the fermion operators.

$$\begin{aligned}\{\hat{\psi}_p^\dagger(x), \hat{\psi}_p(x)\} &= \delta_{pp'}\left[\lim_{\varepsilon\to 0^+}\left(\frac{1}{L}\sum_k \mathrm{e}^{\mathrm{i}k(x-x')}\mathrm{e}^{-\varepsilon|\frac{kL}{\pi}|}\right)\right] \\ &= \delta_{pp'}\sum_{n=-\infty}^{\infty}\delta(x-x'-nL).\end{aligned} \tag{2.31}$$

In order to solve the model it is necessary to be able to express the fermion operators in terms of boson operators. For this we need the fermion density operator

$$\hat{\rho}_{qp} = \begin{cases}\sum_k \hat{c}_{k+qp}^\dagger \hat{c}_{kp} & (q \neq 0) \\ \equiv N_p = \sum_k n_{kp} - \langle n_{kp}\rangle_0 & (q = 0),\end{cases} \tag{2.32}$$

which has the commutation property[90]

$$[\hat{\rho}_{qp}, \hat{\rho}_{q'p'}] = \delta_{pp'}\delta_{qq'}\left(\frac{Lpq}{2\pi}\right). \tag{2.33}$$

This commutation algebra implies the construction of boson operators of the form

$$\hat{a}_q^\dagger = \sqrt{\frac{2\pi}{L|q|}}\sum_p \theta(pq)\hat{\rho_{qp}} \qquad (q \neq 0, q = \frac{2\pi n}{L}, n = \pm 1, \pm 2, \ldots). \tag{2.34}$$

Note that this is undefined at $q = 0$; there is in fact no $q = 0$ boson mode, but it is represented by the number operator $\hat{N}_p$, which returns the total number of type p fermions and commutes with the boson operators $\hat{a}_q$ $(q \neq 0)$.

The density operator (2.32) can therefore be written in terms of the boson operators as

$$\hat{\rho}_{qp} = \hat{N}_p\delta_{q0} + \sqrt{\frac{L|q|}{2\pi}}\left(\theta(pq)\hat{a}_q^\dagger + \theta(-pq)\hat{a}_{-q}\right). \tag{2.35}$$

A ladder operator $\hat{U}_p$ to raise or lower the fermion charge N_p is also required, but must also commute with $\hat{a}_q$. Due to the way the Hilbert space has been constructed, there is no upper or lower limit to the range of allowed values of $\hat{N}_p$, and so $\hat{N}_p$ cannot be expressed in terms of the raising operator and a lowering operator conjugate to the raising operator. Haldane therefore chooses the ladder operator $\hat{U}_p$ to be unitary, i.e.

$$\hat{U}_p^{-1} = \hat{U}_p^\dagger, \tag{2.36}$$

but it must also, owing to the fermionic nature of the particles, be chosen such that it anticommutes with $\hat{U}_{-p}$ and $\hat{U}_{-p}^{-1}$. The ladder operator should therefore be of the form

$$\hat{U}_p|N_p, N_{-p}\rangle = \eta(p, N_p, N_{-p})|N_p + 1, N_{-p}\rangle, \tag{2.37}$$

where η is a phase factor that must take the values ± 1, but whose exact form is yet to be determined.

In order to reconcile all the required properties of the ladder operator, Haldane writes $\hat{U}_p$ in terms of a further operator $\hat{\phi}_p(x)$:

$$\hat{U}_p(x) = \frac{1}{\sqrt{L}} \int_0^L \mathrm{d}x \; \mathrm{e}^{-\mathrm{i}pk_F x} \mathrm{e}^{-\mathrm{i}\hat{\phi}_p^\dagger(x)} \hat{\psi}_p^\dagger(x) \mathrm{e}^{-\mathrm{i}\hat{\phi}_p(x)}, \tag{2.38}$$

with $\hat{\phi}_p(x)$ defined as

$$\hat{\phi}_p(x) = \lim_{\varepsilon \to 0+} \left[\frac{2\pi \mathrm{i}p}{L} \sum_q \theta(-pq) \frac{\mathrm{e}^{-\mathrm{i}qx}}{q} \mathrm{e}^{-\frac{\varepsilon|q|L}{2\pi}} \hat{\rho}_{qp} \right] \tag{2.39}$$

$$= \left(\frac{p\pi x}{L}\right) N_p + \mathrm{i} \sum_{q \neq 0} \theta(pq) \left(\frac{2\pi}{L|q|}\right)^{1/2} \mathrm{e}^{-\mathrm{i}qx} \hat{a}_q. \tag{2.40}$$

This therefore gives the commutation relation between the ladder operator $\hat{U}_p$ and the fermion density operator $\hat{\rho}_{qp}$ as

$$[\hat{\rho}_{qp}, \hat{U}_p] = \delta_{pp'} \delta_{q0} \hat{U}_p. \tag{2.41}$$

It is at this point that Haldane utilizes the linear fermion dispersion of the Hamiltonian in order to obtain the bosonized form of the Hamiltonian—the entire argument up to this point is independent of the form of the dispersion and depends only on the definition of the vacuum state and the Hilbert space.

The Hamiltonian (2.29) has the following commutation relationships with the density and boson operators:

$$[\hat{H}^0, \hat{\rho}_{qp}] = v_F pq \hat{\rho}_{qp} \tag{2.42}$$

$$[\hat{H}^0, \hat{a}_q^\dagger] = v_F |q| \hat{a}_q^\dagger. \tag{2.43}$$

The energies of those eigenstates $|\{N_p\}\rangle$ of the system that do not contain any boson excitations are given simply by $v_F \pi / L \sum_p \hat{N}_p^2$, whereas a mode q boson contribution to the eigenvalue is given by $v_F |q| n_q$, giving the bosonic form of

the Hamiltonian as

$$\hat{H}^0 = v_F \left[\sum_q |q| \hat{a}_q^\dagger \hat{a}_q + \frac{\pi}{L} \sum_p N_p^2 \right]. \tag{2.44}$$

Haldane then proves that the set of eigenstates produced from the vacuum by successive operation with the ladder operator $\hat{U}_p$ and the boson creation operator $\hat{a}_q^\dagger$ is a complete set, and therefore that equations (2.29) and (2.44) are identities.

Haldane then re-expresses the operators already introduced completely in terms of the boson operators. By inverting equation (2.38) he obtains the bosonized form of the fermion operator

$$\hat{\psi}_p^\dagger(x) = \frac{1}{\sqrt{L}} e^{ipk_F x} \left[e^{i\hat{\phi}_p^\dagger(x)} \hat{U}_p e^{i\hat{\phi}_p(x)} \right]. \tag{2.45}$$

This is, by definition, normal ordered in the $\hat{a}_q$ and is therefore well-defined. The charge and current quantum numbers are also introduced and defined in terms of the charge of the ground state, N_0

$$N_0 = \frac{k_F L}{\pi}, \tag{2.46}$$

$$N = N_0 + \sum_p N_p \quad ; \quad J = \sum_p p N_p. \tag{2.47}$$

Various other quantities can then be defined, however, the ones in which, for the present purposes, we are interested are the Hamiltonian and momentum operators for non-interacting electrons

$$\hat{H}^0 = v_F \left[\sum_q |q| \hat{a}_q^\dagger \hat{a}_q + \frac{\pi}{2L} \left((N - N_0)^2 + J^2 \right) \right]; \tag{2.48}$$

$$\hat{P} = \left[k_F - \frac{\pi}{L}(N - N_0) \right] J + \sum_q q \hat{a}_q^\dagger \hat{a}_q. \tag{2.49}$$

Adding electron-electron interactions

Once the system has been set up for non-interacting electrons, is is then fairly simple, using this representation, to include the electron-electron interactions.

The interactions are represented by two interaction functions $V_1(q)$ and $V_2(q)$, each with dimensions of velocity. They are related to the interaction

functions of section 2.3 and equations (2.12) and (2.13) by

$$\begin{aligned} g_2(q) &= \pi V_2(q) \\ g_4(q) &= \pi V_1(q) \end{aligned} \tag{2.50}$$

Using these the interacting part of the Hamiltonian $\hat{H}^1$ can be written as

$$\hat{H}^1 = \frac{\pi}{L} \sum_{pp'q} \left[V_{1q} \delta_{p,p'} + V_{2q} \delta_{p,-p'} \right] \hat{\rho}_{qp} \hat{\rho}_{-q,p'}, \tag{2.51}$$

where the $\hat{\rho}$ are the fermion density operators of equation (2.32). By defining new velocities for the charge and current density fluctuations v_N and v_J respectively in terms of the Fermi velocity v_F in the same way as equations (2.23) and (2.24), the full Hamiltonian $\hat{H}^0 + \hat{H}^1$ can be written in terms of the boson operators

$$\begin{aligned} \hat{H} = &- \frac{1}{2} \left(\sum_q v_F |q| \right) + \frac{\pi}{2L} \left(v_N N^2 + v_J J^2 \right) \\ &+ \frac{1}{2} \sum_q |q| \left[(v_F + V_{1q}) (\hat{a}_q^\dagger \hat{a}_q + \hat{a}_q \hat{a}_q^\dagger) + V_{2q} (\hat{a}_q^\dagger \hat{a}_q + \hat{a}_q \hat{a}_q^\dagger) \right]. \end{aligned} \tag{2.52}$$

This can be diagonalized using a Bogoliubov transformation, as in section 2.3, to give

$$\hat{H} = E_0 + \sum_q \omega_q \hat{b}_q^\dagger \hat{b}_q + \frac{\pi}{2L} \left(v_N N^2 + v_J J^2 \right), \tag{2.53}$$

where

$$E_0 = \frac{1}{2} \sum_q \left(\omega_q - v_F |q| \right), \tag{2.54}$$

$$\omega_q = | \left(v_F + V_{1q} \right)^2 - \left(V_{2q} \right)^2 |^{\frac{1}{2}} |q|, \tag{2.55}$$

$$\hat{b}_q^\dagger = \cosh(\varphi_q) \hat{a}_q^\dagger - \sinh(\varphi_q) \hat{a}_{-q}, \tag{2.56}$$

$$\tanh(2\varphi_q) = -\frac{V_{2q}}{v_F + V_{1q}}. \tag{2.57}$$

Haldane continues the paper by showing how it is possible to calculate analytically the dynamical correlation functions from these results, and by a discussion of the extension of the pure Luttinger model to more realistic, but no longer completely soluble, models such as those with a non-linear fermion dispersion.

2.4 Spectral functions

We now need to review the spectral properties of a pure Luttinger liquid. This is a well-studied problem [37, 96, 97, 103, 112, 129, 131, 148, 149] but the main results reviewed here are largely taken from the work of Voit [144, 148, 149] and Schönhammer and Meden [97, 129].

For these purposes, the spectral function is defined as

$$\rho_{p,s}(q,\omega) = -\frac{1}{\pi}\Im G^R_{p,s}(k_F + q, \omega + \mu), \tag{2.58}$$

where p is, as usual, the branch index and s the spin index. $G^R(k,\omega)$ is the retarded Green's function as discussed in section 3.3, and is the double Fourier-transformed version of the time-ordered Green's function

$$G^R_{p,s}(x,t) = -\mathrm{i}\theta(t)\langle\{\hat{\psi}_{p,s}(x,t)\hat{\psi}^\dagger_{p,s}(0,0)\}\rangle, \tag{2.59}$$

where $\{\ldots,\ldots\}$ designates the anticommutator.

Voit [148, 149] takes Haldane's result [60] for the bosonized form of the fermion operator $\hat{\psi}$ in terms of bosonic phase fields and obtains an analytical expression for the Luttinger liquid Green's function

$$\begin{aligned} G^R_{p,s}(x,t) = &-\mathrm{i}\frac{\theta(t)}{2\pi}\mathrm{e}^{\mathrm{i}pk_Fx} \\ &\times \lim_{\alpha\to 0}\left[\frac{\Lambda + \mathrm{i}(v_Ft - px)}{\alpha + \mathrm{i}(v_Ft - px)}\prod_{\nu=\rho,\sigma}\frac{1}{[\Lambda + \mathrm{i}(v_\nu t - px)]^{1/2}}\left(\frac{\Lambda^2}{(\Lambda + \mathrm{i}v_\nu t)^2 + x^2}\right)^{\gamma_\nu}\right. \\ &\left. + \begin{pmatrix} x \to -x \\ t \to -t \end{pmatrix}\right], \end{aligned} \tag{2.60}$$

where $\nu = \rho, \sigma$, representing charge or spin respectively. The variable Λ is a momentum cutoff equal to the minimum momentum transfer for an excitation, i.e. $2\pi/L$ for the lattice systems on which the current work is performed. The exponent γ_ν is dependent on the Luttinger parameter K_ν as

$$\gamma_\nu = \frac{1}{8}\left(K_\nu + \frac{1}{K_\nu} - 2\right). \tag{2.61}$$

If the momentum dependence of $v_\nu(q)$ and $K_\nu(q)$ (see section 2.3.1) is neglected completely, then this expression simplifies to

$$G^R_{p,s}(x,t) = -\mathrm{i}\frac{\theta(t)}{2\pi}\mathrm{e}^{\mathrm{i}pk_Fx}\lim_{\alpha\to 0}\left[\prod_{\nu=\rho,\sigma}\frac{1}{[\Lambda + \mathrm{i}(v_\nu t - px)]^{1/2}}\right.$$

$$\times \left(\frac{\Lambda^2}{(\Lambda + \mathrm{i}v_\nu t)^2 + x^2} \right)^{\gamma_\nu} + \begin{pmatrix} x \to -x \\ t \to -t \end{pmatrix} \Bigg]. \quad (2.62)$$

However, in order to calculate the spectral function we require not this form of the Green's function but its double Fourier transform, $G^R_{p,s}(k,\omega)$. Rather than perform a double Fourier transform on equation (2.60), Voit chooses to make use of the property

$$\left[G^R_{p,s}(k,\omega)\right]^* = -G^R_{p,s}(-k,-\omega) \quad (2.63)$$

to calculate the analytical form of the spectral function directly for three example systems—the spinless Luttinger liquid, in which our main interest lies, the single-branch Luttinger liquid, and the spinful Luttinger liquid.

We shall now concentrate on the derivation of the spectral function for the spinless Luttinger liquid, and shall merely discuss the main results for the spinful Luttinger liquid. Voit defines the additional variables

$$s = v_0 t - px \quad ; \quad s' = v_0 t + px, \quad (2.64)$$

and obtains a spectral function of the form

$$\rho_p(q,\omega) = \frac{1}{8\pi^2 v_0 \Lambda} \int_{-\infty}^{\infty} \mathrm{d}s \int_{-\infty}^{\infty} \mathrm{d}s' \, \mathrm{e}^{\mathrm{i}\Omega_1 s} \mathrm{e}^{\mathrm{i}\Omega_2 s'} \times \lim_{\alpha \to 0} \left[\frac{\Lambda + \mathrm{i}(a_F s + b_F s')}{\alpha + \mathrm{i}(a_F s + b_F s')} \left(\frac{\Lambda}{\Lambda + \mathrm{i}s} \right)^{\gamma_0 + 1} \left(\frac{\Lambda}{\Lambda + \mathrm{i}s'} \right)^{\gamma_0} + \begin{pmatrix} s \to -s \\ s' \to -s' \end{pmatrix} \right], \quad (2.65)$$

where the following have been defined

$$q = k - k_F, \quad (2.66)$$

$$\Omega_1 = \frac{\omega}{2v_0} + \frac{pq}{2} \quad ; \quad \Omega_2 = \frac{\omega}{2v_0} - \frac{pq}{2}, \quad (2.67)$$

$$a_F = \frac{1}{2}\left(\frac{v_F}{v_0} + 1 \right) \quad ; \quad b_F = \frac{1}{2}\left(\frac{v_F}{v_0} - 1 \right), \quad (2.68)$$

and γ_0 is given by

$$\frac{1}{4}\left(K_\rho + \frac{1}{K_\rho} - 2 \right) \quad (2.69)$$

with the spinless Luttinger parameter K_ρ defined as in equation (2.19).

Equation (2.65) was solved by Luther and Peschel [88] in the approximation of constant velocity, where $b_F = 0$ and the equation reduces to a single integral over s. Voit, however, solves this exactly to give the result

$$\rho_p(q,s) = \frac{\Lambda}{2v_0\Gamma^2(\gamma_0)}\theta(\omega + pv_0q)\theta(\omega - pv_0q)$$
$$\times\,\gamma\left(\gamma_0, \frac{\Lambda}{2v_0}(\omega + v_0pq)\right)\left(\frac{\Lambda}{2v_0}(\omega - v_0pq)\right)^{\gamma_0-1} e^{-\frac{\Lambda}{2v_0}(\omega - v_0rq)}$$
$$+ \begin{pmatrix}\omega \to -\omega \\ q \to -q\end{pmatrix} \quad (2.70)$$

where $\gamma(\alpha, x)$ is the incomplete gamma function [1].

Whereas for a Fermi liquid we would expect $\rho(0,\omega)$ to be a delta function at the Fermi energy, the situation for a Luttinger liquid is quite different. Spectral weight is repelled from the Fermi surface owing to the virtual particle-hole excitations generated by the inter-branch scattering term g_2, resulting in a broadened peak. As q is increased the Fermi liquid spectral function will merely broaden like q^2, reflecting the finite lifetime of electrons away from E_F, but for a Luttinger liquid there is zero spectral weight within a range $\pm v_0q$ of the Fermi energy. In addition, the negative-frequency contribution is suppressed exponentially with q, and for a continuum Luttinger liquid the positive-frequency contributions have a power law dependence. For $\omega > 0$ this is of the form $\theta(\omega - v_0q)(\omega - v_0q)^{\gamma-1}$ and for $\omega < 0$ it is of the form $\theta(-\omega - v_0q)(-\omega - v_0q)^{\gamma}$, with γ given by equation (2.69)[144]. The relationship between the exponent γ and the spectral function is shown in figure 2.6, whereas figure 2.7 shows the spectral function for a spinful system as a function of both q and ω, clearly showing the spin and charge peaks in the electron part moving at different velocities.

2.5 Transport

Given the breakdown of the Fermi liquid picture of one-dimensional systems we now need to re-evaluate the single-channel conductance properties of the Luttinger liquid conductor. For the interacting electrons of a Luttinger liquid, both the compressibility and the Fermi velocity are renormalized, and we can no longer use the relation of equation 1.4. Instead, a dimensionless parameter is defined [72] (see also [73, 164]):

$$g = \pi\hbar\kappa v. \quad (2.71)$$

The parameter g is equivalent to the Luttinger parameter K_ρ already introduced, however in the context of Luttinger liquid transport the notation g is more in evidence and so we follow convention here. For non-interacting spinless

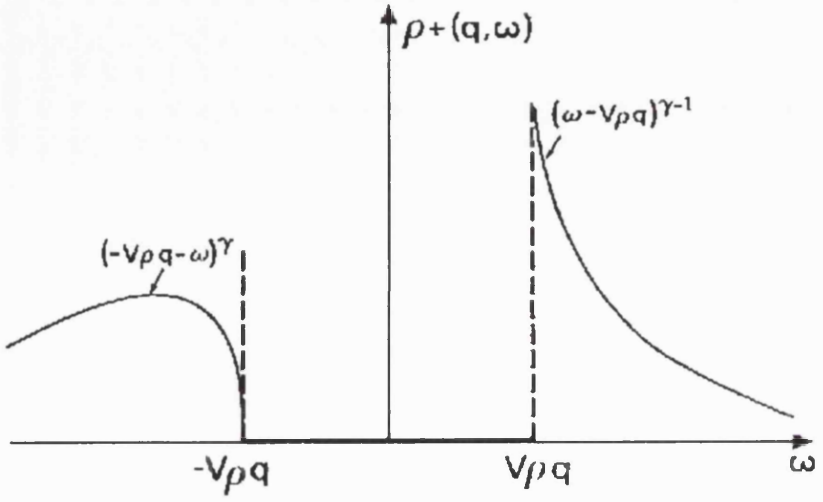

Figure 2.6: Analytical spectral function for a spinless Luttinger liquid. (From reference [149])

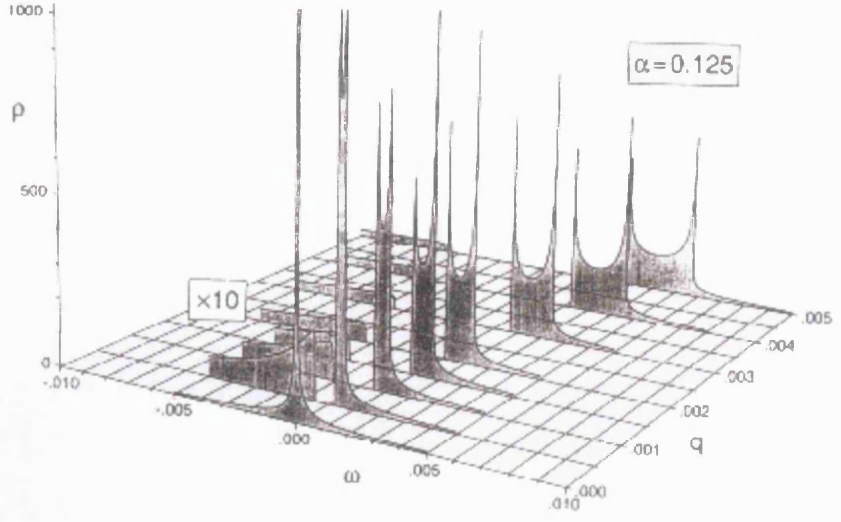

Figure 2.7: Analytical spectral function for a spinful Luttinger liquid, $q > 0$. The double peak structure at positive ω represents the spin and charge excitations separating as q increases. (From reference [144])

electrons, we have $g = 1$ and Fermi liquid behaviour is restored. For repulsive interactions, $g < 1$ and can be approximated by $g^2 \approx \left(1 + \frac{U}{2E_F}\right)^{-1}$, where U is the Hubbard U representing on-site Coulomb interactions (see section 2.7). In addition, it is known that for a repulsively interacting Luttinger liquid with an arbitrarily small barrier, there is no transmission through the barrier at zero temperature. The Luttinger liquid is completely reflected and the conductance becomes zero. At non-zero temperatures, the conductance behaves as a power of temperature T:

$$G(T) \approx T^{\frac{2}{g}-2} \tag{2.72}$$

In addition, the I-V characteristics of the Luttinger liquid are non-Ohmic and of the form

$$I(V) \approx V^{\frac{2}{g}-1} \tag{2.73}$$

For a real wire of length L, the thermal coherence length implies that these relations will only be valid for temperatures greater than

$$T_L = \frac{\hbar v_F}{k_B L} \tag{2.74}$$

Experiments on single wall carbon nanotube (SWNT) systems have confirmed these theoretical predictions [17].

2.6 Coupled and crossed chain systems

Systems of weakly coupled Luttinger liquids have been studied before [7, 8, 18, 22–24, 28, 34, 40, 42, 43, 45, 46, 52, 78, 79, 101, 102, 104, 115, 142, 143], particularly with regard to the c axis conductivity of high temperature superconductors [4, 24, 28, 45, 66]. However the literature is apparently devoid of studies of Luttinger liquids coupled to Fermi liquids—the problem under consideration here. It is, however, instructive to review the main findings of these previous studies.

The main question is regarding the nature of the coupling between the chains—more precisely, whether the interchain transport mechanism survives, and if so, whether the transport is coherent or incoherent. The systems studied are both those consisting of just two coupled chains, and those consisting of a greater number, in some cases an infinite array of chains, although the number of chains involved does not appear to be a major factor in the results.

While the subject of hopping between coupled Luttinger liquids remains controversial, the consensus appears to be that *coherent* interchain transport is suppressed for all but the weakest interacting weakly coupled chains. This can be explained qualitatively in the following way. For coherent hopping of

the form $\sum_c \hat{c}^\dagger_{c+1}\hat{c}_c + \text{H.c.}$ (where c is the chain index) to occur, we need to remove an electron from one chain and place it on the other. However, the fundamental entities within the Luttinger liquid chains are not electrons but collective excitations of charge and spin; moreover these excitations are moving at different velocities. Thus this process is intuitively less likely to occur for weakly coupled interacting chains than for coupled non-interacting chains.

There are several ways of investigating the nature of the interchain hopping for these systems. However, we shall concentrate on two of the most popular methods. The first of these is due to Clarke, Strong and Anderson [28]. Two Hubbard model chains are prepared at time $t = 0$ in their separate ground states with ΔN more right-moving spinful electrons with spin s on one chain than on the other. The interchain hopping $t_\perp$ is then turned on, and the probability $P(t)$ of the system being in its initial state at an intermediate time t is measured. The nature of $P(t)$ will therefore provide an indication of whether the hopping is consistent with coherent interchain transport or not. For two non-interacting chains, $P(t)$ is found to be of the form

$$\begin{aligned} P(t) &= 1 - t_\perp^2 \Delta N t^2 + \dots \\ &= \cos^{2\Delta N}(t_\perp t). \end{aligned} \tag{2.75}$$

The oscillatory nature of $P(t)$ implies that electrons are free to hop back and forth between the chains in a coherent manner. However, once intrachain interactions are switched on, the oscillations in $P(t)$ are destroyed, to be replaced with a rather more complicated expression that depends on many factors. If no hopping whatsoever was taking place, $P(t)$ would be equal to one, and since this is not the case, this is a clear indicator of incoherent hopping.

The second approach, utilized by Capponi, Poilblanc and Mila [24] (see also [22, 23, 25, 115]) examines both the nature of the distortions in the band structure due to the electron-electron interactions and the nature of the transverse (interchain) optical conductivity $\sigma(\omega)$. A system of two or more spinless chains of length L with periodic boundary conditions is constructed with the Hamiltonian

$$\hat{H} = \sum_{j,\beta}(\hat{c}^\dagger_{j+1,\beta}\hat{c}_{j,\beta} + \text{H.c.}) - t_\perp \sum_{j,\beta}(\hat{c}^\dagger_{j,\beta+1}\hat{c}_{j,\beta} + \text{H.c.}) + \sum_{j,\beta,\delta} V(\delta)\hat{n}_{j,\beta}\hat{n}_{j+\delta,\beta}, \tag{2.76}$$

where $1 \leq \beta \leq m$ is the chain index, $1 \leq j \leq L$ is the site index and $V(\delta)$ indicates the intrachain electronic interactions. The system is threaded with an arbitrary magnetic flux, represented by a twist in the boundary conditions

[77], from which the transport properties of the system can be measured.

For a single chain, the Luttinger parameter K_ρ can be calculated from the Drude weight $2\pi D$ and the charge velocity v_ρ, both of which can be obtained from finite size scaling analysis

$$\begin{aligned} 2\pi D &= 2v_\rho K_\rho \\ &= \frac{1}{4\pi}\frac{\partial^2(\frac{E_0}{L})}{\partial\Phi_x^2}, \end{aligned} \tag{2.77}$$

where E_0 is the ground state energy and Φ_x the magnetic flux in the x-direction (along the chains).

For two coupled chains, the charge excitation energy ΔE gives information about the distortion of the band structure. Capponi *et al.* calculate $\Delta E/2t_\perp$ and extrapolate to a $L = \infty$ system for various values of the Luttinger parameter α, whereupon it is found that $\Delta E/2t_\perp \to 0$ at a critical value of α which increases with $t_\perp$, indicating the suppression of coherent hopping and a possible crossover to incoherent hopping. In other words, the bonding and antibonding bands are no longer separated by any finite value (whereas for non-interacting chains they would be separated at the Fermi energy by $2t_\perp$), returning to the same type of band structure that would be expected at $t_\perp = 0$, where the electrons are completely confined to their chains.

For a number of chains $m \geq 3$, it is possible to create a torus geometry of chains such that current can flow in a loop between the chains, and so the conductivity can be measured. The interchain conductivity can be written as the sum of two parts [24, 77, 99, 100, 144]

$$\sigma(\omega) = D\delta(\omega) + \sigma^{\text{reg}}(\omega), \tag{2.78}$$

where D is the Drude weight and $\sigma^{\text{reg}}(\omega)$ is the regular part of the conductivity, given by the current-current correlation function

$$\sigma^{\text{reg}}(\omega) = \frac{\pi}{N}\sum_{n\neq 0}\frac{|\langle\phi_0|\hat{j}|\phi_n\rangle|^2}{E_n - E_0}\delta(\omega - (E_n - E_0)), \tag{2.79}$$

where $|\phi_n\rangle$ is the nth eigenstate with eigenvalue E_n and $\hat{j}$ is the current operator.

The conductivity $\sigma(\omega)$ therefore consists of a peak at $\omega = 0$ the amplitude of the Drude weight plus some frequency dependent component. For non-interacting chains, $[\hat{H}, \hat{j}] = 0$ and therefore the conductivity has no contribution from $\sigma^{\text{reg}}(\omega)$ and contains only a Drude peak. For interacting electrons, however, the Drude peak becomes strongly suppressed as α increases, indicating

corresponding suppression of coherent hopping. There is also a pronounced structure in $\sigma^{\mathrm{reg}}(\omega)$ at finite frequencies, indicating the presence of incoherent interchain transport.

Most of the other papers on this subject are based on one or other of these approaches. However, a thermodynamic approach is also possible [18] to yield essentially the same result of suppression of coherent hopping in the presence of interactions.

It is also possible to consider "crossed" Luttinger liquids, i.e. chains that are coupled not along their entire length but only at one or two points [34, 78, 79, 120]. In these systems the coupling can be considered as an impurity. For example, Durganandini and Rao [34] consider two Luttinger liquids coupled at two points to form an "island" in the middle. An external bias is applied via open boundary conditions, and they find that, while for weak electron-electron interactions the transport is undisturbed, for strong interactions the interwire couplings grow and the charge becomes fixed on the island between the two coupling points.

2.6.1 Extensions to the Luttinger model

While the formalism presented here represents the standard Luttinger model, there are extensions to it which may in the long term prove essential to a full treatment of a real atomic wire: open boundary conditions to model a finite wire, and a treatment of the electron-phonon interactions.

To model a finite wire, we will need to shift from Haldane's periodic boundary conditions to open boundary conditions [37, 41, 94, 131, 151]:

$$\hat{\psi}(x=0) = \hat{\psi}(x=L) = 0. \tag{2.80}$$

This was a problem first considered by Fabrizio and Gogolin [41], who found that the right- and left-moving populations are *no longer independent* but satisfy

$$\hat{\psi}_{p=-1}(x) = -\hat{\psi}_{p=+1}(-x) = 0, \tag{2.81}$$

where the operator $\hat{\psi}$ is formed of a combination of the right- and left-moving fermion operators:

$$\hat{\psi} = \mathrm{e}^{\mathrm{i}k_F x}\hat{\psi}_{p=-1}(x) + \mathrm{e}^{-\mathrm{i}k_F x}\hat{\psi}_{p=+1}(x). \tag{2.82}$$

The right moving field still obeys periodic boundary conditions, but now with

period $2L$:

$$\hat{\psi}_{p=+1}(x+2L) = \hat{\psi}_{p=+1}(x) \tag{2.83}$$

The alteration in boundary conditions has the result that the current quantum number J is no longer a good quantum number, although the charge quantum number N remains good.

The boundary conditions can be expected to have a strong effect on the spectral properties of the Luttinger liquid [37, 94], and in particular it has been predicted [37] that for a finite Luttinger liquid, the spectral density will be dominated by boundary effects at frequencies close to the Fermi energy.

In addition, electron-phonon effects can be included, although this is complicated and introduces many restrictions into the kind of systems that can be studied [27, 39, 55, 91, 92, 119, 145–147]. For the sake of completeness, we review these extended models briefly here. Engelsberg and Varga [39] solved exactly a Luttinger-like Hamiltonian with phonons in 1964, but only small momentum transfer scattering ($q \approx 0$) was included. Marino [91, 92] considered the interaction of many-electrons with acoustic phonons, where a field equation was used to eliminate the phonon field to generate effective Hamiltonian equivalent to the massless Thirring model. However, Voit and Schulz [145] claim that Marino's result is in fact only valid when the phonon sound velocity is roughly equal to v_F. Voit and Schulz also included, starting from the standard Luttinger model, an electron-phonon term to allow electron backscattering through emission or absorption of a phonon with wave vector $|q| \approx 2k_F$ [146, 147]. This results in further renormalization of the coupling constants, and it was found that whereas the charge density fluctuations behave as for the Luttinger model, at low temperatures the spin density fluctuations are frozen out. Chen [27] took a functional integral approach to the problem of electron-phonon forward scattering, and found that the acoustic phonons give rise to a non-local and retarded part in the effective electronic interaction.

However, more recently it has been claimed that a fully interacting electron-phonon system is exactly solvable [119]. Rao takes a total Hamiltonian that is the sum of the free-electron, optical phonon, acoustic phonon, electron-optical phonon, electron-acoustic phonon and electron-electron parts. This can be written entirely in terms of the relevant field operators, and the phonon fields eliminated by introducing Lagrangian density corresponding to $\hat{H}$ and choosing appropriate parameters. The total Hamiltonian can now be written in terms of boson density operators as a sum of free-electron and effective electron-electron terms, which can be diagonalized analytically. It was found that for a certain range of coupling parameters, the spectrum is gapless, implying a polaronic

metal, but that there is nonetheless the possibility of an instability leading to phase transition.

2.7 Non-Luttinger model approaches

In the current work we have used the Luttinger model as it has the significant advantage of being completely solvable and therefore our results can be considered exact. However, any suitable model (i.e. one that includes a proper treatment of the electron-electron interactions) will reveal Luttinger liquid indicators if they are present. The main alternative to the Luttinger model used in the literature to probe for Luttinger liquid behaviour is the Hubbard model [4, 43, 48, 50, 51, 53, 67, 70, 74, 76, 80, 84, 85, 94–96, 100, 102, 115, 116, 128, 131, 134, 140, 142, 151, 168, 170] and as we shall also use the Hubbard model in the Density Matrix Renormalization Group work to be presented in chapter 6, a review is appropriate here.

The basic Hubbard model Hamiltonian is given by

$$\hat{H} = -t\sum_{i,\sigma}(\hat{c}^{\dagger}_{i+1,\sigma}\hat{c}_{i,\sigma} + \text{H.c.}) + U\sum_{i}\hat{n}_{i,\uparrow}\hat{n}_{i,\downarrow} \tag{2.84}$$

where U represents the on-site repulsion and t the hopping matrix element along the chain, and it is assumed that $U \ll t$. In this form the one-dimensional model is fully solvable using the Bethe ansatz [85, 140], however for a half-filled band with $U \neq 0$ Umklapp scattering becomes important and a gap opens in the charge excitation spectrum. The ground state is thus both insulating and antiferromagnetic, although the spin excitation spectrum remains gapless. Phase transitions to insulating states at certain filling factors are a feature of all Hubbard-based models. Note that only on-site electron-electron interactions are included, and that all the electron-electron couplings g_1, g_2, g_3, g_4 of figure 2.5 are included and equal in magnitude. However, for unequal couplings the model has not been solved exactly due to logarithmic divergences, requiring a renormalization group approach in which a large energy cutoff is introduced to alter the effect of the interactions at the Fermi surface [100]. In this form, and away from half-filling, the Hubbard model can be mapped onto the Luttinger model [100, 140].

One of the advantages of the Hubbard model is that it can easily be extended to incorporate other terms and effects. For example, a dimerization of the sites can be included, useful for studying the Bechgaard salts, in which dimerization is an important effect [142]. Nearest-neighbour repulsion can be

included to extend the range of the electron-electron interactions, in other words the Hamiltonian has the form

$$\hat{H} = -t\sum_{i,\sigma}(\hat{c}^{\dagger}_{i+1,\sigma}\hat{c}_{i,\sigma} + \text{H.c.}) + U\sum_{i}\hat{n}_{i,\uparrow}\hat{n}_{i,\downarrow} + V\sum_{i}\hat{n}_{i}\hat{n}_{i+1}, \tag{2.85}$$

which again is not completely solvable but can be mapped onto other models [57]. However, this model becomes insulating at quarter filling for $V = 2t$.

Part II

Exact calculations

Chapter 3

Methods

> We (the undivided divinity operating within us) have dreamt the world. We have dreamt it as firm, mysterious, visible, ubiquitous in space and durable in time; but in its architecture we have allowed tenuous and eternal crevices of unreason which tell us it is false.
>
> Jorge Luis Borges, *Avatars of the Tortoise*

3.1 The model **52**

3.2 Initial calculations **54**

3.3 Green's functions for differential equations **61**

3.4 Exact diagonalization and the Lanczos method . . **66**

3.1 The model

The model we use for the calculation consists of two chains coupled together at each site by a constant interchain hopping matrix element $t_\perp$. We use periodic boundary conditions and the chains are defined on a ring of length L, as shown in figure 3.1. Hopping is therefore only allowed between equal momen-

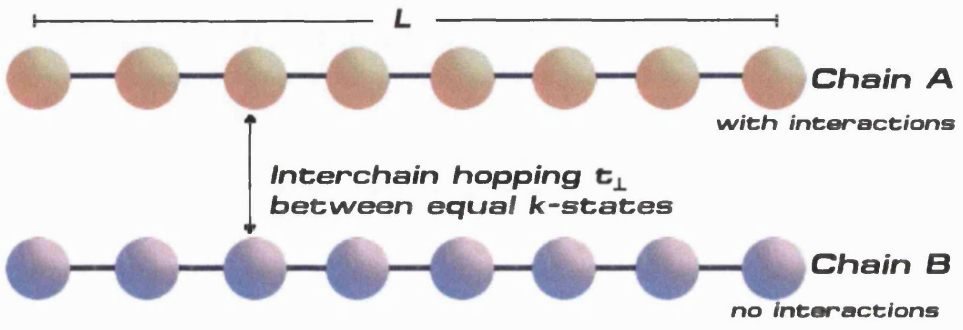

Figure 3.1: Schematic representation of the coupled chains model.

tum states and we neglect any interchain electron-electron interactions, such as Coulomb drag effects. One of the chains, which we label chain A, includes electron-electron interactions, with the intention that this chain represents the wire, while the other, labelled chain B, has no electron-electron interactions and is intended to represent the effect of the substrate. This therefore provides us with an approximation to the situation shown in figure 3.2, where we are representing the physics of the wire (which is, after all, what we are interested in) exactly, while the substrate is represented, admittedly somewhat simplistically and unrealistically, only by the second chain.

The choice of such a model may at first seem strange—what we are ultimately interested in is not the physics of two coupled metallic chains. However, we justify the choice of such a model as follows. We wish to calculate, in as exact a way as possible, both the eigenstates and correlation functions for the system. By choosing the Luttinger model as the basis for our system, rather than, for example, the Hubbard model, we are able to compare our results easily to those of an isolated chain, provided that the wire we represent is metallic.

Moreover, while the subject of two coupled Luttinger liquid chains has been extensively studied (see section 2.6), the problem of a Luttinger liquid coupled to a Fermi liquid, which is essentially what our model represents, has received no attention. We therefore use this Luttinger model based coupled chain system as a starting point for studies in this area, with the obvious caveat that it

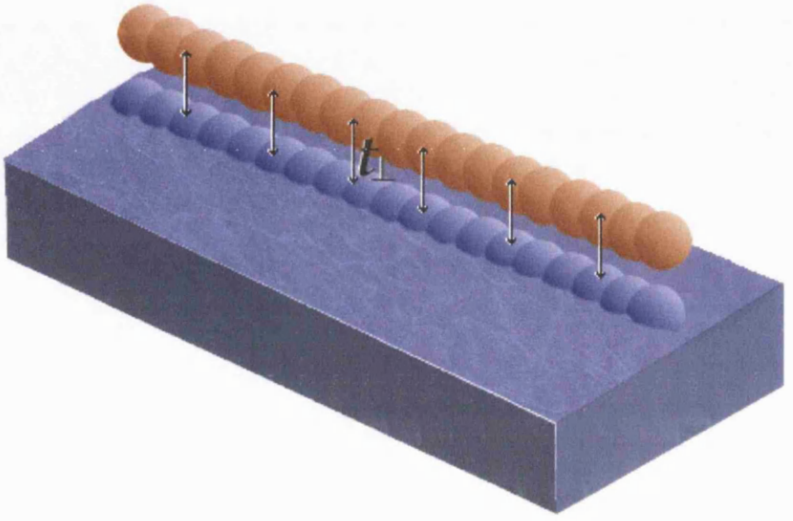

Figure 3.2: Schematic representation of how the model relates to the "atomic wire on a surface" problem.

represents the role of a semiconducting surface inadequately. However, we have to start somewhere, and by choosing this particular model we are able to study the essential aspects of the physics in which we are interested, particularly the nature of the coupling, while still treating the electron-electron interactions of the wire chain exactly, something that is absent from the existing literature.

3.1.1 Changes from Haldane's model

In order to implement this model, it is necessary to make a few alterations to the formalism of Haldane's model [60]. Firstly, we are dealing not with a continuum, but with a discrete lattice, and so rather than integrals over $\mathrm{d}x$ we have sums over x. The implications of this are discussed in section 4.3.6. The presence of the second chain also requires some changes to Haldane's ladder operator of equation (2.38). In order for the ladder operator $\hat{U}$ to produce anticommuting field operators on different chains, it is necessary to introduce a further phase factor into its definition, analogous to Haldane's phase factor $\zeta(p, N_p, N_{-p})$ for ensuring anticommutation between the branches of a single chain. The total ladder operator component of equation (2.45) when two chains are involved

thus takes the form

$$\hat{U}_{p,c} = \zeta(p, N_p, N_{-p})\zeta'(c, N_c, N_{-c})|N_{p,c} + 1, N_{-p,c}\rangle, \tag{3.1}$$

where the subscript $c = \pm 1$ is a chain index. The anticommutation properties originate in the phase factors ζ, which can be written as

$$\zeta_{i=p,c} = (-1)^{(\frac{1}{2}iN_{-i})}. \tag{3.2}$$

3.2 Initial calculations

Although the main advantage of the Luttinger model is that it simplifies the inclusion of electron-electron interactions, for the moment they will be neglected. Once the model is known to be working correctly in the non-interacting limit, the interactions can be added. In addition, as the Luttinger model has complete spin-charge separation, it is also possible to neglect the effects of spin at this stage without losing too many of the physical features of the model, as we have already shown in chapter 2.

3.2.1 Tight-binding chains

In the non-interacting spinless limit it is straightforward to solve the problem of two coupled chains without using the Luttinger model, thus giving simple results that can be used to verify the initial results of the Luttinger model simulation. However, this approach becomes unfeasible once electron-electron interactions are included.

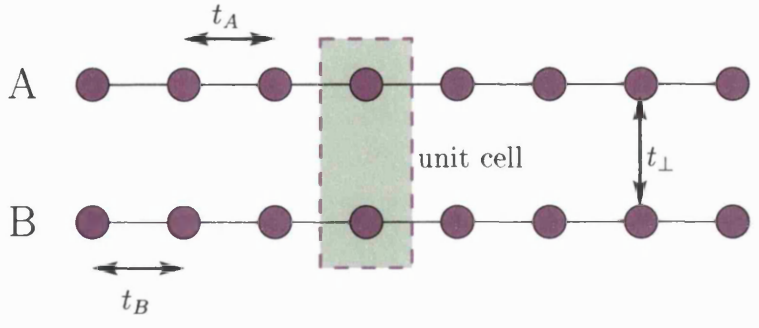

Figure 3.3: Representation of the system used for the tight-binding calculations

Consider two chains, labelled A and B, of atoms, each having a single orbital, arranged on a one dimensional lattice of length N. A schematic representation

of this is shown in figure 3.3. We first consider the wavefunction of chain A. Using a tight-binding approach (see, for example, [9]), we can write

$$|k_A\rangle = \frac{1}{N^{1/2}} \sum_{n=1}^{N} \mathrm{e}^{\mathrm{i}kn} |n_A\rangle \tag{3.3}$$

where $|n_A\rangle$ represents the orbital of a single atom on chain A at lattice site n. We can now include a perturbation to the uncoupled model to allow electrons to "hop" from chain A to chain B and vice versa, with amplitude $t_\perp$:

$$V = \sum_{n=1}^{N} t_\perp \left(|n_A\rangle\langle n_B| + |n_B\rangle\langle n_A| \right) \tag{3.4}$$

We consider the problem in terms of a unit cell consisting of one atom from each chain, as in figure 3.4. The wavefunction for a cell at position n will have

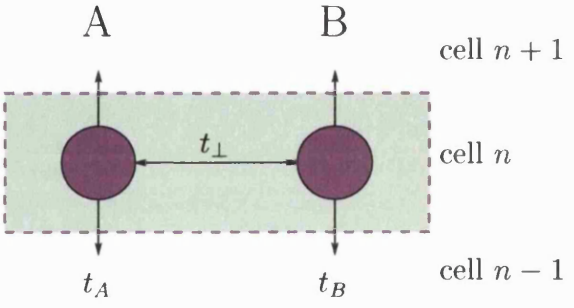

Figure 3.4: Representation of the system used for the tight-binding calculations

components from chain A, labelled α, and from chain B, labelled β, i.e.

$$\psi_n = \begin{pmatrix} \alpha_n \\ \beta_n \end{pmatrix}. \tag{3.5}$$

By introducing the necessary periodic boundary conditions and using Bloch's theorem, we can express the cell's wavefunction as

$$\psi_n = \mathrm{e}^{\mathrm{i}kn} \begin{pmatrix} \alpha \\ \beta \end{pmatrix}. \tag{3.6}$$

Now for a single atom on chain A at site n, contributions to the wavefunction will occur from the atoms on chain A at sites $n+1$ and $n-1$, and from the adjacent atom on chain B at site n. Therefore we can write Schrödinger's

equation as

$$\varepsilon_A \alpha_n - t_\perp \beta_n - t_A(\alpha_{n+1} + \alpha_{n-1}) = E\alpha_n, \tag{3.7}$$

where ε_A is a constant term representing the energy of an electron bound to site n. By substituting from equation 3.6 for α_n and β_n, we obtain

$$\varepsilon_A e^{ikn}\alpha - t_\perp e^{ikn}\beta - t_A(e^{ik(n+1)} + e^{ik(n-1)})\alpha = Ee^{ikn}\alpha, \tag{3.8}$$

and dividing through by e^{ikn} yields

$$(\varepsilon_A - 2t_A \cos k)\alpha - t_\perp \beta = E\alpha. \tag{3.9}$$

By considering the corresponding expression for the atoms on chain B, we can write the Schrödinger equation in matrix form as

$$\begin{pmatrix} \varepsilon_A - 2t_A \cos k & -t_\perp \\ -t_\perp & \varepsilon_B - 2t_B \cos k \end{pmatrix} \begin{pmatrix} \alpha \\ \beta \end{pmatrix} = E \begin{pmatrix} \alpha \\ \beta \end{pmatrix}. \tag{3.10}$$

Since ε_A represents the energy for the uncoupled systems, we can write

$$E_A(k) = \varepsilon_A - 2t_A \cos k, \tag{3.11}$$

and so the eigenvalues of the coupling Hamiltonian are given by

$$E = \frac{1}{2}\left[E_A(k) + E_B(k) \pm \sqrt{[E_A(k) - E_B(k)]^2 + 4t_\perp^2}\right]. \tag{3.12}$$

We can now compare the results so far for the uncoupled and coupled chains. Figure 3.5 shows the dispersion relation for two uncoupled chains with the intrachain interaction included, as given by equation 3.11. The two dispersion relations cross at some value of $\pm k$. Figure 3.6 shows the change when a weak coupling between the chains is included—the dispersion relations split into two separate bands.

3.2.2 Results of initial calculations

Generating the excitation spectra using the tight-binding Hamiltonian

Calculating the single particle-hole excitation spectrum using the tight-binding results of section 3.2.1 is fairly straightforward (giving results as in figure 3.7), merely requiring a double loop structure over all the occupied and unoccupied states in order to account for all the possible excitations. However, most of

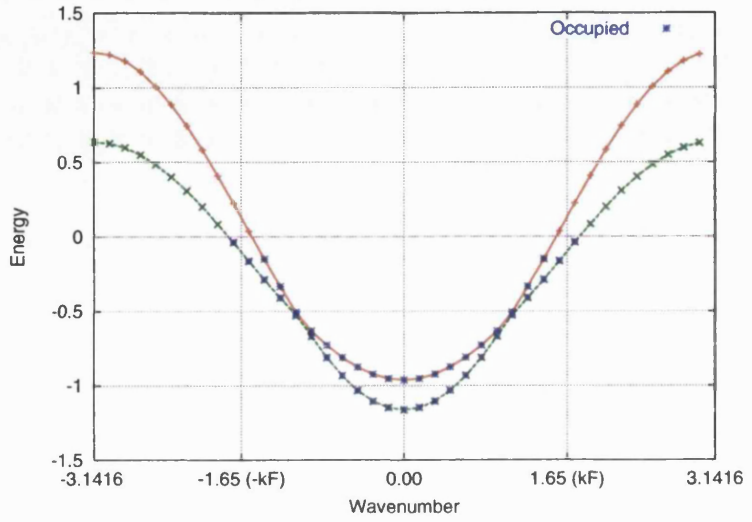

Figure 3.5: Dispersion relation for two uncoupled chains ($L = 40, t_A \neq t_B, \varepsilon_A = \varepsilon_B, t_\perp = 0$, 42 electrons)

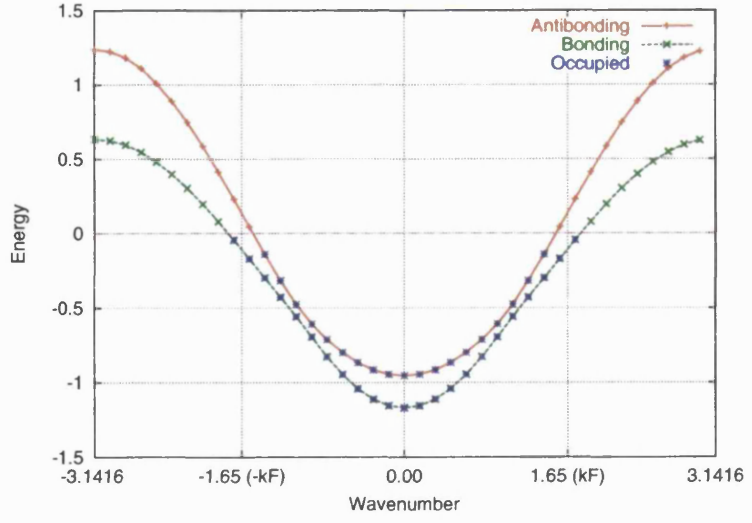

Figure 3.6: Dispersion relation for two weakly coupled chains ($L = 40, t_A \neq t_B, \varepsilon_A = \varepsilon_B, t_\perp = 0.1$, 42 electrons), showing the splitting into separate bands

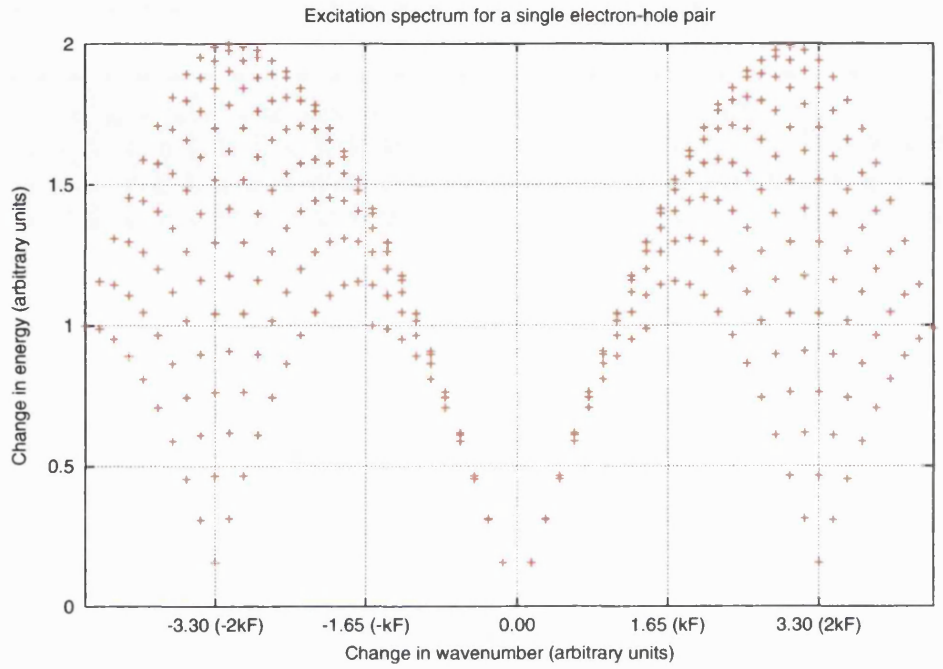

Figure 3.7: Single particle-hole excitation spectrum (single tight-binding chain, $L = 40, t_A = 0.5, \varepsilon_A = 1.0$, 20 electrons).

the multiple particle-hole excitations will be above our low-energy cutoff and so it is computationally more efficient to include the (arbitrary) energy threshold and not calculate any excitations resulting in an energy change greater than the threshold. The result of this is shown in figure 3.8.

Generating the excitation spectra using the Luttinger Hamiltonian

We now need to generate a similar set of multiple excitations for the Luttinger Hamiltonian and confirm that they map exactly onto the results for the linearized tight-binding system. In order to do this we need to represent the various variables of the Luttinger Hamiltonian,

$$\hat{H} = v_F \left[\sum_q |q| \hat{a}^\dagger \hat{a} + \frac{\pi}{2L} \left((N - N_0)^2 + J^2 \right) \right], \tag{3.13}$$

numerically, and in particular we need to establish a computationally efficient way of representing the boson occupations $\{n_q\}$. To do this it is useful to be aware of the physical meaning of the various boson distributions in terms of the excitation spectrum, which should be clear from figure 3.9.

In order to calculate the full excitation spectrum, we need to determine all

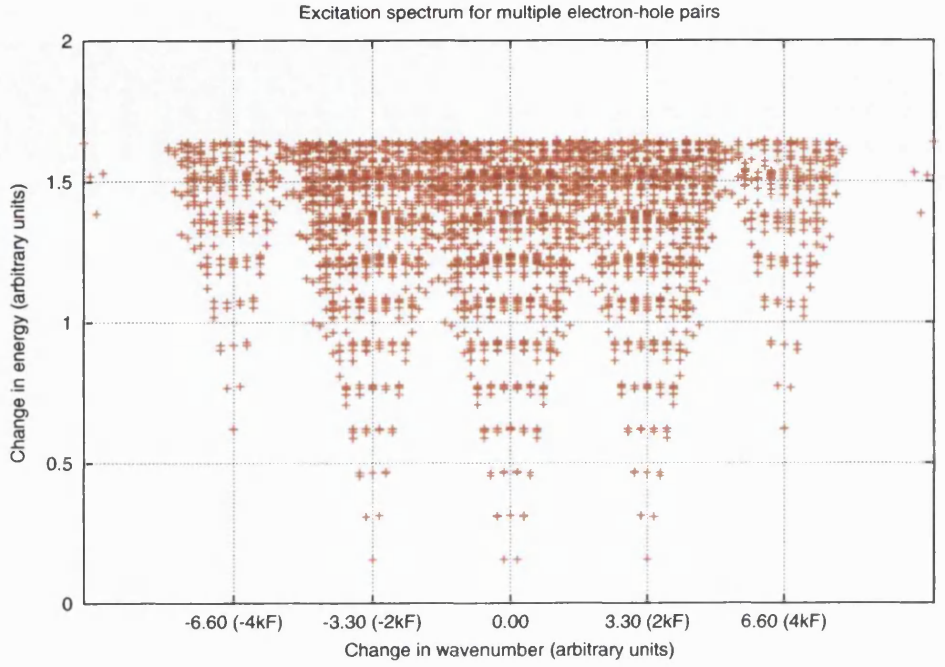

Figure 3.8: Multiple particle-hole excitation spectrum (single tight-binding chain, $L = 40, t_A = 0.5, \varepsilon_A = 1.0$, 20 electrons)

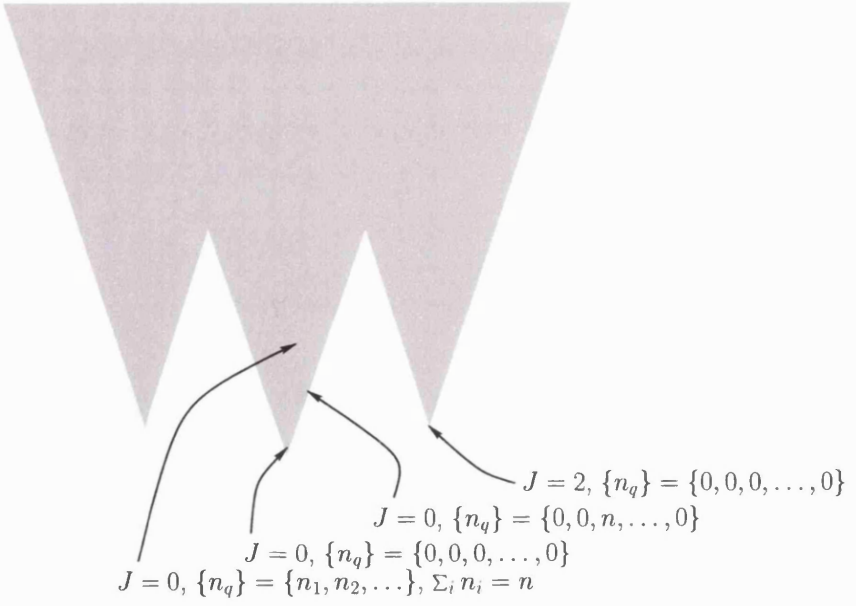

Figure 3.9: Schematic representation of boson occupations in terms of excitation spectrum

possible ways of distributing n bosons among the Q available modes. The most efficient way to do this was concluded to be mapping each combination onto a pair of binomial coefficients and then solving the problem as for the electron excitations in section 3.2.2.

First we represent each combination as a binary sequence with the 1's representing bosons and the 0's representing partitions between the modes, e.g. for two bosons in the first of three available modes, we would represent $\{2\ 0\ 0\} \equiv 2|0|0 \equiv 1100$ where the partitions | of the second term become the 0's of the third, which can then be represented as the pair of binomial coefficients 1 2. Thus the full table of possibilities for two bosons in three modes would be

boson occupations	binary representation	binomial representation
2 0 0	1100	1 2
1 1 0	1010	1 3
1 0 1	1001	1 4
0 2 0	0110	2 3
0 1 1	0101	2 4
0 0 2	0011	3 4

Since we are only interested in the low energy properties of the system we can save a considerable amount of computational time by only calculating those excitations that are low in energy. For these purposes, low in energy means $\Delta\varepsilon \ll v_F k_F$ and so a cutoff was set at this value and excitations exceeding this value were ignored.

For computational reasons it is also necessary to restrict the total number of bosons in the system. It was found that for the low energy excitations of the system, a full representation could be obtained by setting the maximum number of bosons in the system to just two: if it is set to 1 then the characteristic v-shaped outline of the spectrum is obtained, adding the second boson "fills in" the outline to give diamond shapes and it was found that while higher maximum values give similar shapes, they occur at higher energies and can be neglected here.

It is now possible to compare the excitation spectrum resulting from this Hamiltonian with the results from the independent electron Hamiltonian, where the original tight-binding dispersion relation is replaced by a linear one of slope v_F. The results for a chain of length $L = 40$ are shown in figure 3.10, from which it can be seen that the excitations do indeed map onto each other almost exactly.

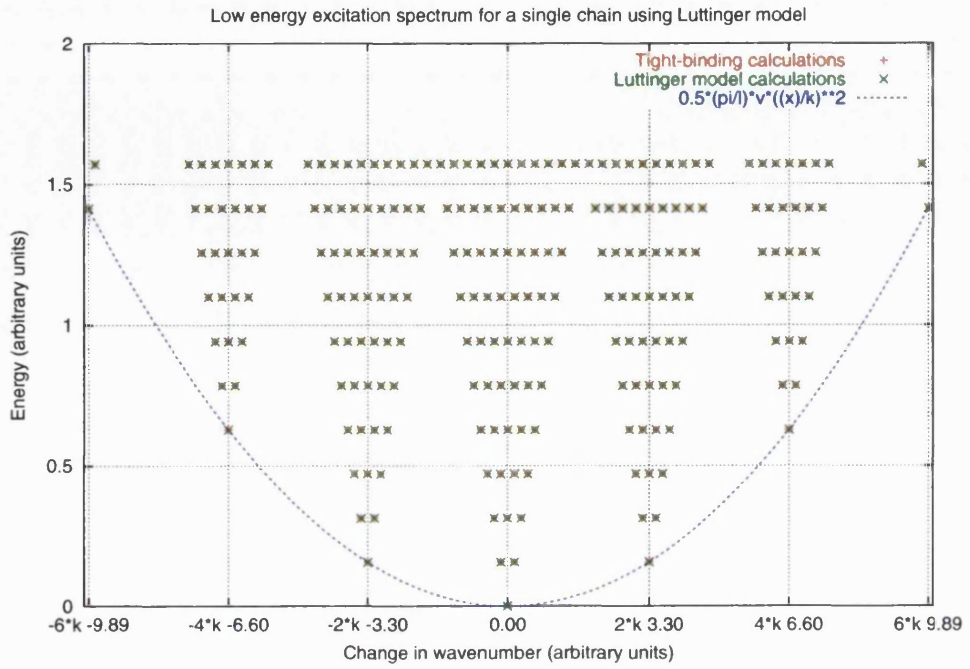

Figure 3.10: Overlaid results for the Luttinger Hamiltonian ($v_F = 1.0$) and the linearized independent-electron single chain Hamiltonian ($L = 40, t_A = 0.5, \varepsilon_A = 1.0$) with a linear dispersion.

These methods for representing the bosons computationally will be greatly expanded on in chapter 4.

3.3 Green's functions for differential equations

We can use Green's functions to solve linear differential equations of the form

$$Lu = f, \tag{3.14}$$

where L is a linear differential operator, u is an unknown function and f is a known function, for example, Poisson's equation

$$\nabla^2 \phi = \frac{\rho}{\varepsilon_0}. \tag{3.15}$$

Imagine that instead we solve the equation

$$\nabla^2 G(r, r') = \delta(r - r'), \tag{3.16}$$

in order that

$$\phi(r) = \int \mathrm{d}r'\, G(r,r')\frac{\rho(r')}{\varepsilon_0}. \tag{3.17}$$

Note that the Green's function G must obey the same boundary conditions as ϕ. Here

$$G(r,r') = \frac{1}{4\pi\varepsilon_0|r-r'|}. \tag{3.18}$$

The Green's function is thus defined as the solution to the equation

$$LG(r,r') = \delta(r-r'). \tag{3.19}$$

3.3.1 Green's functions for the single particle Schrödinger equation

We can use a similar method to solve the single particle Schrödinger equation, which will tell us how a wave function evolves from an initial state $\Psi(r',t')$ to a state $\Psi(r,t)$

$$\begin{aligned} \mathrm{i}\frac{\partial}{\partial t}\Psi &= \left(-\frac{1}{2}\nabla^2 + V\right)\Psi \\ &= \hat{H}\Psi. \end{aligned} \tag{3.20}$$

Suppose we have, by analogy with equation 3.17

$$\Psi(r,t) = \mathrm{i}\int \mathrm{d}r'\, G(r,r',t,t')\Psi(r',t'), \tag{3.21}$$

and we know that the eigenfunctions and eigenvalues of Ψ:

$$\hat{H}\psi_n = E_n\psi_n. \tag{3.22}$$

By utilizing the time evolution operator $e^{-\mathrm{i}\hat{H}t/\hbar}$ we can write that if

$$\begin{aligned} |\Psi(t')\rangle &= \sum_n c_n|\psi_n\rangle, \\ |\Psi(t)\rangle &= \sum_n \mathrm{e}^{-\mathrm{i}E_n(t-t')}c_n|\psi_n\rangle. \end{aligned} \tag{3.23}$$

But since by definition $c_n = \langle\psi_n|\Psi(t')\rangle$ we can write

$$|\Psi(t)\rangle = \sum_n \mathrm{e}^{-\mathrm{i}E_n(t-t')}|\psi_n\rangle\langle\psi_n|\Psi(t')\rangle, \tag{3.24}$$

or in coordinate space notation,

$$\begin{aligned}\Psi(r,t) &= \int \mathrm{d}r' \left[\sum_n e^{-\mathrm{i}E_n(t-t')}\psi_n(r)\psi_n^*(r')\right]\Psi(r',t'),\\ &= \mathrm{i}\int \mathrm{d}r'\, G(r,r',t,t')\Psi(r',t').\end{aligned} \tag{3.25}$$

If we start with a state that is completely localized in space at a point r_0 then the initial state takes the form of a delta function

$$\Psi(r',t') = \delta(r'-r_0), \tag{3.26}$$

and performing the integration in equation (3.25) gives us

$$\Psi(r,t) = \mathrm{i}G(r,r_0,t,t'), \tag{3.27}$$

where the integration of the delta function has picked out the initial point r_0.

3.3.2 The retarded Green's function

The Green's function representing the propagation of a single particle can be represented as

$$G(r,r',t,t') = -\mathrm{i}\langle 0|\hat{\psi}(r,t)\hat{\psi}^\dagger(r',t')|0\rangle\theta(t-t'), \tag{3.28}$$

i.e. we create a particle at position r' at time t', let it propagate in the system for some time, and then attempt to annihilate the particle at position r and time t. Note that here the state $|0\rangle$ is a many-particle groundstate, not the vacuum. The retarded Green's function depends only on the time difference $t-t'$ and so we can Fourier transform it with respect to $t-t'$ to get

$$\begin{aligned}G(r,r',\omega) &= \int_{-\infty}^{\infty} \mathrm{d}t\; G(r,r',t,0)\mathrm{e}^{\mathrm{i}\omega t}\\ &= \sum_n \psi_n(r)\psi_n^*(r')\int_0^{\infty} \mathrm{e}^{\mathrm{i}[\omega-E_n]t}dt.\end{aligned} \tag{3.29}$$

where we can take the lower limit of the integral to be 0 rather than $-\infty$ as we know that the Green's function is 0 for all values of $t < t'$. However, the exponential term involving ω means that this integral will not converge. In order to get around this, we make ω complex by adding an infinitesimally small

imaginary component η to the frequency:

$$\omega \to \omega + \mathrm{i}\eta, \tag{3.30}$$

so that

$$\mathrm{e}^{\mathrm{i}[\omega - E_n]t} \to \mathrm{e}^{\mathrm{i}[\omega - E_n]t}\mathrm{e}^{-\eta t}. \tag{3.31}$$

This introduces an effective damping term $\mathrm{e}^{-\eta t}$ which forces the integral to converge. We therefore have

$$\begin{aligned} \int \mathrm{d}t \ \mathrm{e}^{\mathrm{i}[\omega - E_n]t}\mathrm{e}^{-\eta t} &= \left[\frac{1}{\mathrm{i}(\omega - E_n) - \eta}\mathrm{e}^{[\mathrm{i}(\omega - E_n) - \eta]t}\right]_0^\infty \\ &= \frac{\mathrm{i}}{(\omega - E_n) + \mathrm{i}\eta}, \end{aligned} \tag{3.32}$$

and so

$$G(r, r', \omega) = \sum_n \frac{\psi_n(r)\psi_n^*(r')}{(\omega - E_n) + \mathrm{i}\eta}. \tag{3.33}$$

Since the Green's function is itself a solution to the Schrödinger equation, we have that

$$\hat{H}G = \mathrm{i}\frac{\partial}{\partial t}G, \tag{3.34}$$

except at $t = 0$. As t approaches 0, G will approach the delta function representing the original localized state:

$$G(t \to 0_+) \equiv G(t^+) = \delta(r - r'), \tag{3.35}$$

and so

$$\begin{aligned} G(t^+) - G(t^-) &= \int_{t^-}^{t^+} \frac{\partial G}{\partial t}\mathrm{d}t \\ &= \delta(r - r'). \end{aligned} \tag{3.36}$$

where t^+ indicates $t > t'$ and vice versa, and so

$$\frac{\partial}{\partial t}G = -\mathrm{i}\delta(t - t')\delta(r - r'). \tag{3.37}$$

From this we find that

$$\left[\hat{H} - i\frac{\partial}{\partial t}\right] G = \delta(t - t')\delta(r - r') \tag{3.38}$$

We can then Fourier transform this back to frequency space to obtain

$$\left[\hat{H} - \omega\right] G = -i\delta(r - r') \tag{3.39}$$

$$\hat{G} = (\omega - \hat{H})^{-1}. \tag{3.40}$$

This expression is often known as the resolvent. We can generalize this to an expression for the propagation of a single added particle

$$\hat{G} = \hat{\psi}(r) \left[\omega - \hat{H}\right]^{-1} \hat{\psi}^{\dagger}(r'). \tag{3.41}$$

We can replace the Hamiltonian $\hat{H}$ in this expression with a complete set of eigenstates for the system, thus giving

$$\begin{aligned} G &= -\mathrm{i} \sum_n \langle 0, N | \mathrm{e}^{\mathrm{i}\hat{H}t} \hat{\psi} \mathrm{e}^{-\mathrm{i}\hat{H}t} | n, N+1 \rangle \langle n, N+1 | \mathrm{e}^{\mathrm{i}\hat{H}t'} \hat{\psi}^{\dagger} \mathrm{e}^{-\mathrm{i}\hat{H}t'} | n, 0 \rangle \\ &= -\mathrm{i} \sum_n \mathrm{e}^{-\mathrm{i}(E_{n,N+1} - E_{0,N})(t-t')} \langle 0, N | \hat{\psi} | n, N+1 \rangle \langle n, N+1 | \hat{\psi}^{\dagger} | n, 0 \rangle. \end{aligned} \tag{3.42}$$

Upon Fourier transforming, this becomes

$$G = \sum_n \frac{\langle 0, N | \hat{\psi} | n, N+1 \rangle \langle n, N+1 | \hat{\psi} | 0, N \rangle}{\omega - (E_{n,N+1} - E_{0,N}) + \mathrm{i}\eta}, \tag{3.43}$$

where $|N, 0\rangle$ indicates the ground state of the N particle system, and $|N+1, n\rangle$ indicates the nth state of the $N+1$ particle system.

3.3.3 Finding the Green's function numerically

In order to utilise Green's functions in the present work, we require a method of finding them numerically. We are looking for the retarded Green's function

$$G = \langle 0 | \hat{\psi}(r) \left[\omega - \hat{H} + \mathrm{i}\eta\right]^{-1} \hat{\psi}^{\dagger}(r') | 0 \rangle, \tag{3.44}$$

where $|0\rangle$ presents the N-particle ground state. We can define a state $|1\rangle$ such that

$$|1\rangle = \hat{\psi}^{\dagger}(r') |0\rangle, \tag{3.45}$$

i.e. a state where we have added a particle at r'. We can then define a second state $|\tilde{1}\rangle$ as

$$\left[\omega - \hat{H}\right] |\tilde{1}\rangle = |1\rangle, \tag{3.46}$$

i.e.

$$\begin{aligned} |\tilde{1}\rangle &= \left[\omega - \hat{H}\right]^{-1} |1\rangle \\ &= \left[\omega - \hat{H}\right]^{-1} \hat{\psi}^{\dagger}(r')|0\rangle. \end{aligned} \tag{3.47}$$

If we now define a state $|2\rangle$ such that

$$|2\rangle = \hat{\psi}^{\dagger}(r)|0\rangle, \tag{3.48}$$

then we can write the Green's function as

$$G = \langle 2|\tilde{1}\rangle. \tag{3.49}$$

The hardest part of this to solve numerically is the expression for $|1\rangle$:

$$\left[\omega - \hat{H}\right] |\tilde{1}\rangle = |1\rangle \tag{3.50}$$

but fortunately we can choose an arbitrary ω and solve using the exact diagonalization methods of section 3.4.

3.4 Exact diagonalization and the Lanczos method

In this work exact diagonalization methods [5, 6, 54, 61, 113] are used to find the eigenstates of the system, and in addition to calculate the Green's function of the coupled chain system so that we may obtain the spectral function [54, 61]. In the following sections I present a review of the main methods, their advantages and disadvantages, and the reasons for eventually deciding on the Lanczos method as the method of choice for this problem.

In general the problems we want to solve are of the form $\mathsf{A}|x\rangle = |b\rangle$ where we solve for $|x\rangle$ given an input state $|b\rangle$. In fact, there are two types of problem we want to solve—the first of these is the eigenvalue problem, where we want to solve $\hat{H}|x\rangle = E|x\rangle$, but we also want to solve Green's function problems of the form $(\omega - \hat{H})|\tilde{1}\rangle = |1\rangle$. So, for example, in the eigenvalue problem the matrix A is generally the Hamiltonian $\hat{H}$, and the input state $|b\rangle$ is our best guess at the required eigenstate $|x\rangle$. It is then possible to converge on the eigenstate (usually the ground state), for example, by making an initial guess at $|b\rangle$, solving for $|x\rangle$, and then calculating the energy

$$E = \frac{\langle x|\hat{H}|x\rangle}{\langle x|x\rangle}. \tag{3.51}$$

Then $|x\rangle$ can be normalized

$$|x'\rangle = \frac{|x\rangle}{\langle x|x\rangle}, \tag{3.52}$$

and we can put $|b\rangle = E|x'\rangle$ for the next iteration. There are a number of ways of solving the general $\mathsf{A}|x\rangle = |b\rangle$ problem detailed in the following subsections.

3.4.1 Steepest descent — or "How not to do it"

If the matrix A is positive definite, then instead of solving for $\mathsf{A}|x\rangle = |b\rangle$ directly, we could equivalently find the stationary points of [54]

$$\phi(x) = \frac{1}{2}\langle x|\mathsf{A}|x\rangle - \langle x|b\rangle, \tag{3.53}$$

since taking the negative gradient of equation (3.53) gives

$$-\nabla\phi(x) = |b\rangle - \mathsf{A}|x\rangle, \tag{3.54}$$

and the function ϕ must be decreasing most rapidly in the direction of this negative gradient.

In order to converge on the solution, the residual $|r_c\rangle$ at a point $|x_c\rangle$ is defined as

$$|r_c\rangle = |b\rangle - \mathsf{A}|x_c\rangle. \tag{3.55}$$

Now if $|r_c\rangle \neq 0$, there must exist a positive α such that

$$\phi(x_c + \alpha r_c) < \phi(x_c), \tag{3.56}$$

and in this method of steepest descent, α is set to

$$\alpha = \frac{\langle r_c|r_c\rangle}{\langle r_c|\mathsf{A}|r_c\rangle}. \tag{3.57}$$

The function being minimized is therefore

$$\phi(x_c + \alpha r_c) = \phi(x_c) - \alpha\langle r_c|r_c\rangle = \frac{1}{2}\alpha^2\langle r_c|\mathsf{A}|r_c\rangle. \tag{3.58}$$

The outline algorithm for this method is shown as algorithm 1.

Algorithm 1: Steepest descent

$|x_0\rangle$ = initial guess
$|r_0\rangle = |b\rangle - \mathsf{A}|x_0\rangle$
$k = 0$
while $|r_k\rangle \neq 0$
  $k = k + 1$
  $\alpha_k = \frac{\langle r_{k-1}|r_{k-1}\rangle}{\langle r_{k-1}|\mathsf{A}|r_{k-1}\rangle}$
  $|x_k\rangle = |x_{k-1}\rangle + \alpha_k|r_{k-1}\rangle$
  $|r_k\rangle = |b\rangle - \mathsf{A}|x_k\rangle$
end

However, there are a number of problems with this method that make it unfeasible to use in practice. In particular, because there is no restriction on the relative directions of the gradients used to descend to the minimum, it is possible for the minimization to "get stuck" repeatedly traversing the equivalent of a long, steep sided valley rather than descending down it. It is for this reason that the conjugate gradient method is much more efficient.

3.4.2 The conjugate gradient method

The main difference between the steepest descent method of section 3.4.1 and this method is that in the conjugate gradient algorithm the directions along which to minimize do not correspond directly to the residuals $\{|r_0\rangle, |r_1\rangle, \ldots\}$.

A direction $|p_k\rangle$ is instead chosen that is the closest vector to $|r_{k-1}\rangle$ that is also conjugate[1] to the directions along which we have already minimized $\{|p_0\rangle, |p_1\rangle, |p_{k-1}\rangle \ldots\}$. The most efficient method of calculating the direction $|p_k\rangle$ is the solution to a least squares problem and is discussed in detail in reference [54]. The algorithm for the conjugate gradient method is given in algorithm 2.

[1]In this context we take "conjugate" to mean that $\langle p_l|\mathsf{A}|p_k\rangle = 0, l = 0, \ldots, k-1$.

Algorithm 2: Conjugate gradient algorithm

$k = 0$
$|r_0\rangle = |b\rangle - \mathsf{A}|x_0\rangle$
while $|r_k\rangle \neq 0$
  $k = k + 1$
  if $k = 1$
    $|p_1\rangle = |r_0\rangle$
  else
    $\beta_k = \frac{\langle r_{k-1}|r_{k-1}\rangle}{\langle r_{k-2}|r_{k-2}\rangle}$
    $|p_k\rangle = |r_{k-1}\rangle + \beta_k|p_{k-1}\rangle$
  end if
  $\alpha_k = \frac{\langle r_{k-1}|r_{k-1}\rangle}{\langle p_k|\mathsf{A}|p_k\rangle}$
  $|x_k\rangle = |x_{k-1}\rangle + \alpha_k|p_k\rangle$
  $|r_k\rangle = |r_{k-1}\rangle - \alpha\mathsf{A}|p_k\rangle$
end
$|x\rangle = |x_k\rangle$

3.4.3 The Lanczos algorithm

There is an alternative to the conjugate gradient based algorithms—the Lanczos method, which has the added advantage, as we shall see in section 3.4.7, that it can be used not only to calculate the eigenstates of our system, but also correlation functions.

In the Lanczos method, we aim to compute, with j iterations, a set $\{|q_j\rangle\}$ of j orthonormal vectors of length n (where n is the dimension of the Hilbert space), with $j < n$.

We begin by defining the Rayleigh quotient as

$$r(x) = \frac{\langle x|\mathsf{A}|x\rangle}{\langle x|x\rangle}. \tag{3.59}$$

The Rayleigh quotient thus returns the expectation value of the matrix A operating on the vector $|x\rangle$.

In order to find the extremal eigenvalues of A, we need to find the maximum and minimum values of this expectation value. To do this, we define m_j and M_j as the minimum and maximum values of $r(x)$, i.e. $\lambda_1(\mathsf{A})$ and $\lambda_n(\mathsf{A})$, respectively. The subscript j on m and M indicates that only the subspace spanned by the first j vectors is included.

We can therefore write

$$\begin{aligned} M_j &= \lambda_1(\mathsf{Q}_j^T \mathsf{A} \mathsf{Q}_j) \\ &= \max_{y \neq 0} \frac{\langle y|(\mathsf{Q}_j^T \mathsf{A} \mathsf{Q})|y\rangle}{\langle y|y\rangle} \\ &\leq \lambda_1(\mathsf{A}), \end{aligned} \tag{3.60}$$

and

$$\begin{aligned} m_j &= \lambda_j(\mathsf{Q}_j^T \mathsf{A} \mathsf{Q}_j) \\ &= \min_{y \neq 0} \frac{\langle y|(\mathsf{Q}_j^T \mathsf{A} \mathsf{Q})|y\rangle}{\langle y|y\rangle} \\ &\geq \lambda_j(\mathsf{A}), \end{aligned} \tag{3.61}$$

where $\mathsf{Q_j}$ is a matrix consisting of j column vectors $|q_i\rangle$ such that

$$\mathsf{T} = \mathsf{Q}_j^T \mathsf{A} \mathsf{Q}_j \tag{3.62}$$

is tridiagonal.

What is needed now is to find a way of generating the $|q_i\rangle$ so that the M_j and m_j are increasingly better estimates of the largest and smallest eigenvalues.

Consider a vector $|u_j\rangle$ in the space $\text{span}\{|q_1\rangle, |q_2\rangle, \ldots, |q_j\rangle\}$, chosen such that

$$M_j = r(u_j), \tag{3.63}$$

and similarly a vector $|v_j\rangle \in \text{span}\{|q_1\rangle, |q_2\rangle, \ldots, |q_j\rangle\}$ with

$$m_j = r(v_j). \tag{3.64}$$

Now we want M_j to converge on the highest eigenvalue λ_j as quickly as possible, and since M_j must be increasing most rapidly in the direction of the positive gradient, we require that

$$\nabla r(u_j) \in \text{span}\{|q_1\rangle, |q_2\rangle, \ldots, |q_j\rangle, |q_{j+1}\rangle\}, \tag{3.65}$$

and correspondingly for m_j, which is decreasing most rapidly in the direction of the negative gradient $-\nabla$ and so we require that

$$\nabla r(v_j) \in \text{span}\{|q_1\rangle, |q_2\rangle, \ldots, |q_j\rangle, |q_{j+1}\rangle\}. \tag{3.66}$$

This leaves us with the problem that the required $|q_{j+1}\rangle$ must satisfy both these requirements — how do we find such a $|q_{j+1}\rangle$?

Since we know that

$$r(x) = \frac{\langle x|\mathsf{A}|x\rangle}{\langle x|x\rangle}, \tag{3.59}$$

then

$$\begin{aligned}\nabla r(x) &= \frac{2}{\langle x|x\rangle}\left[\mathsf{A}|x\rangle - r(x)|x\rangle\right] \\ &\in \mathrm{span}\{|x\rangle, \mathsf{A}|x\rangle\}.\end{aligned} \tag{3.67}$$

Therefore, if

$$\mathrm{span}\{|q_1\rangle, |q_2\rangle, \ldots, |q_j\rangle\} = \mathrm{span}\{|q_1\rangle, \mathsf{A}|q_1\rangle, \ldots, \mathsf{A}^{j-1}|q_1\rangle\}, \tag{3.68}$$

then it follows that we can choose $|q_{j+1}\rangle$ so that

$$\mathrm{span}\{|q_1\rangle, |q_2\rangle, \ldots, |q_{j+1}\rangle\} = \mathrm{span}\{|q_1\rangle, \mathsf{A}|q_1\rangle, \ldots, \mathsf{A}^{j-1}|q_1\rangle, \mathsf{A}^j|q_1\rangle\}, \tag{3.69}$$

and thus the problem we actually have to solve is that of computing orthonormal bases for the Krylov subspaces

$$\mathcal{K}(\mathsf{A}, |q_1\rangle, j) \equiv \mathrm{span}\{|q_1\rangle, \mathsf{A}|q_1\rangle, \ldots, \mathsf{A}^j|q_1\rangle\}. \tag{3.70}$$

This is achieved by the requirement on the matrix Q_j that

$$\mathsf{T} = \mathsf{Q}_j^T \mathsf{A} \mathsf{Q}_j \tag{3.62}$$

is tridiagonal.

If $\mathsf{Q} \equiv \mathsf{Q}_n$, i.e. the matrix Q is at its maximum size of an $n \times n$ matrix, then we have

$$\mathsf{AQ} = \mathsf{QT}, \tag{3.71}$$

with

$$\mathsf{T} = \begin{bmatrix} \alpha_1 & \beta_1 & 0 & \ldots & 0 \\ \beta_1 & \alpha_2 & \beta_2 & 0 & \vdots \\ 0 & \beta_2 & \alpha_3 & \beta_3 & \\ \vdots & & & \ddots & \beta_{n-1} \\ 0 & \ldots & & \beta_{n-1} & \alpha_n \end{bmatrix} \tag{3.72}$$

This then gives us the Lanczos recursion relation

$$\mathsf{A}|q_j\rangle = \beta_{j-1}|q_{j-1}\rangle + \alpha_j|q_j\rangle + \beta_j|q_{j+1}\rangle \tag{3.73}$$

with $\beta_0|q_0\rangle = 0$ and $j = 1, \ldots, n-1$.

If the $|q_j\rangle$ are orthonormal, then

$$\alpha_j = \langle q_j|\mathsf{A}|q_j\rangle, \tag{3.74}$$

and $|q_{j+1}\rangle = |r_j\rangle/\beta_j$, where

$$|r_j\rangle = (\mathsf{A} - \alpha_j)|q_j\rangle - \beta_{j-1}|q_{j-1}\rangle \tag{3.75}$$

If a particular $\beta_j = 0$, then the recursion of course breaks down, but in this case we have then already obtained a j-dimensional invariant subspace.

We can therefore write the basic Lanczos algorithm:

Algorithm 3: Basic Lanczos algorithm

$|r_0\rangle = |q_1\rangle$
$\beta_0 = 1$
$|q_0\rangle = 0$
$k = 0$
while $\beta_k \neq 0$
  $|q_{k+1}\rangle = \frac{|r_k\rangle}{\beta_k}$
  $k = k + 1$
  $\alpha_k = \langle q_k|\mathsf{A}|q_k\rangle$
  $|r_k\rangle = (\mathsf{A} - \alpha_k\mathsf{I})|q_k\rangle - \beta_{k-1}|q_{k-1}\rangle$
  $\beta_k = \langle r_k|r_k\rangle$
end

3.4.4 Problems with the Lanczos method

There is one major problem with the Lanczos procedure — loss of orthogonality between the successive Lanczos vectors $|q_i\rangle$. This can be seen from the following argument. First, following Golub and van Loan [54], we define the computational unit roundoff $\mathbf{u}$ as

$$\mathbf{u} = \frac{1}{2}\beta^{1-t} \tag{3.76}$$

where β is the base in which we are computing, and t the precision. It can be shown [54] that the dot product between two adjacent Lanczos vectors is

$$|\langle q_{k+1}|q_k\rangle| \approx \frac{|\langle r_k|q_k\rangle| + \mathbf{u}\mathsf{A}.\mathsf{A}}{|\beta_k|} \tag{3.77}$$

and so, even for small **u**, non-orthogonality will be a problem for small values of β_k. In other words precisely those Lanczos vectors close to convergence are likely to be those seriously affected by loss of orthogonality. However, in practice, the loss of orthogonality does not greatly affect the calculations until linear independence between the Lanczos vectors is also lost [61].

3.4.5 Haydock's chain model

There is also a more physically intuitive method of deriving the Lanczos vectors, due to Haydock [61], which although fully equivalent, complements the mathematical approach above. However, this is based on a slightly different notation than that used in the previous section, and in order to retain consistency with the literature, we use Haydock's notation. The conversion between the two conventions is shown in table 3.1. This is based on a chain model specified by the Lanczos vectors $\{|u_0\rangle, |u_1\rangle, \ldots\}$ and the two sets of real parameters $\{a_0, a_1, \ldots\}$ and $\{b_1, b_2, \ldots\}$. These parameters thus describe the effect of the Hamiltonian on the Lanczos vectors by the 3-term Lanczos recurrence relation first introduced above,

$$\hat{H}|u_n\rangle = a_n|u_n\rangle + b_{n+1}|u_{n+1}\rangle + b_n|u_{n-1}\rangle, \tag{3.78}$$

which is merely a recasting of equation (3.73) in the new notation. The name "chain model" comes from the graphical representation of this system, in which the states $|u_i\rangle$ are represented by vertices, and the Hamiltonian is represented by the edges, the connections between the vertices, as in figure 3.11.

Standard mathematical literature	Haydock [61]
$\|q_0\rangle, \|q_1\rangle, \ldots$	$\|u_0\rangle, \|u_1\rangle, \ldots$
$\alpha_1, \alpha_2, \ldots$	$a_0, a_1, \ldots$ (note subscript index change)
$\beta_1, \beta_2, \ldots$	$b_1, b_2, \ldots$

Table 3.1: Conversion between standard mathematical and Haydock's notation

In a representation where the $|u_n\rangle$ are column vectors consisting of zeros with the exception of the nth element, which is one, the matrix representation

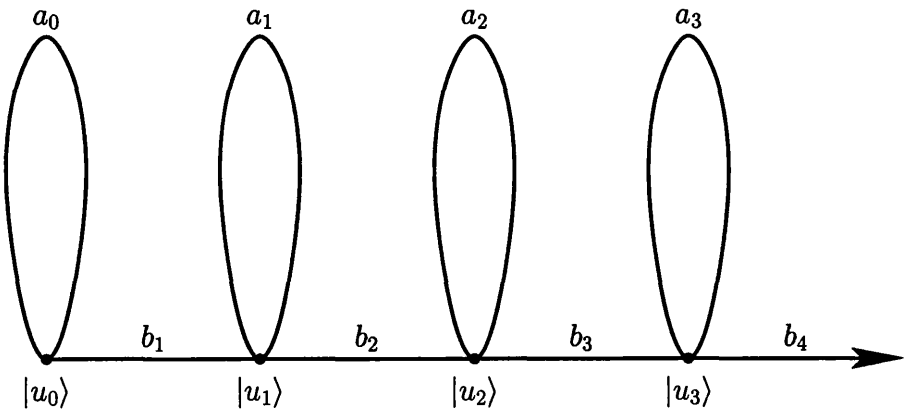

Figure 3.11: Graphical representation of the chain model

of the Hamiltonian is thus

$$\hat{H} = \begin{bmatrix} a_0 & b_1 & 0 & \dots \\ b_1 & a_1 & b_2 & \dots \\ 0 & b_2 & a_3 & \dots \\ \vdots & 0 & b_3 & \dots \\ \vdots & \vdots & \vdots & \ddots \end{bmatrix}. \tag{3.79}$$

Note that this is equivalent in form to equation (3.72). We can therefore see that a chain represents a generalized eigenstate of the system, and therefore that the simplest chain contains just one state $|u_0\rangle$ which is an eigenstate of the Hamiltonian

$$\hat{H}|u_0\rangle = a_0|u_0\rangle. \tag{3.80}$$

A longer chain represents an invariant subspace, such that we have a set of states for which $\hat{H}$ acting on any state returns another state in the subspace. The chain model corresponds to the smallest invariant subspace containing any state on the chain.

Haydock derives the Lanczos procedure for the chain model as follows. First an initial state $|u_0\rangle$ is chosen — this is arbitrary. The only mathematical requirement is that it be normalized, but the exact state to choose will depend on the physics of the system. In the work that follows a state containing random contributions from all the constituent basis states is chosen, this will be discussed further in section 4.5.2. The recurrence relation (equation 3.78) therefore gives

$$\hat{H}|u_0\rangle = a_0|u_0\rangle + b_1|u_1\rangle, \tag{3.81}$$

and all the terms on the LHS are known. We now need to determine a_0, b_1 and $|u_1\rangle$. The orthonormality requirement for $|u_0\rangle$ and $|u_1\rangle$ give us a_0:

$$\begin{aligned}\langle u_0|\hat{H}|u_0\rangle &= \langle u_0|a_0|u_0\rangle + \langle u_0|b_1|u_1\rangle,\\ a_0 &= \langle u_0|\hat{H}|u_0\rangle.\end{aligned} \tag{3.82}$$

We can then subtract $a_0|u_0\rangle$ from both sides of equation (3.81) to give

$$b_1|u_1\rangle = (\hat{H} - a_0)|u_0\rangle, \tag{3.83}$$

and multiplying each side from the left by its hermitian conjugate gives

$$\begin{aligned}(b_1|u_1\rangle)^\dagger b_1|u_1\rangle &= \left[(\hat{H} - a_0)|u_0\rangle\right]^\dagger \left[(\hat{H} - a_0)|u_0\rangle\right]\\ &= |b_1|^2.\end{aligned} \tag{3.84}$$

Since we require all the parameters to be real, $b_1^2 > 0$, and for convenience we take the positive root, to give

$$|u_q\rangle = \frac{(\hat{H} - a_0)|u_0\rangle}{b_1}. \tag{3.85}$$

It is clear that by the nature of this construction, $|u_1\rangle$ is normalized to one and orthogonal to $|u_0\rangle$.

This construction continues in much the same way. We have that

$$\hat{H}|u_n\rangle = a_n|u_n\rangle + b_{n+1}|u_{n+1}\rangle + b_n|u_{n-1}\rangle, \tag{3.73}$$

and so we can first find a_n:

$$\begin{aligned}\langle u_n|\hat{H}|u_n\rangle &= \langle u_n|a_n|u_n\rangle\\ a_n &= \langle u_n|\hat{H}|u_n\rangle,\end{aligned} \tag{3.86}$$

and b_n

$$\begin{aligned}\langle u_{n-1}|\hat{H}|u_n\rangle &= \langle u_{n-1}|b_n|u_n\rangle\\ b_n &= \langle u_{n-1}|\hat{H}|u_n\rangle,\end{aligned} \tag{3.87}$$

and then b_{n+1}:

$$b_{n+1}|u_{n+1}\rangle = (\hat{H} - a_n) - b_n|u_{n+1}\rangle \tag{3.88}$$

$$b_{n+1}^2 = \left[(\hat{H} - a_n)|u_n\rangle - b_n|u_{n-1}\rangle\right]^\dagger \left[(\hat{H} - a_n)|u_n\rangle - b_n|u_{n-1}\rangle\right], \tag{3.89}$$

where again we take the positive root. We can then calculate the next state in the sequence

$$|u_{n+1}\rangle = \frac{\left[(\hat{H} - a_n)|u_n\rangle - b_n|u_{n-1}\rangle\right]}{b_{n+1}}. \tag{3.90}$$

Again, by construction $|u_{n+1}\rangle$ is normalized to one and orthogonal to both $|u_n\rangle$ and $|u_{n-1}\rangle$. However, it also needs to be orthogonal to $|u_{n-2}\rangle, \ldots, |u_0\rangle$, and this can be shown as follows. From equation (3.88) above, we have

$$b_{n+1}|u_{n+1}\rangle = (\hat{H} - a_n) - b_n|u_{n+1}\rangle, \tag{3.88}$$

$$\langle u_m|b_{n+1}|u_n + 1\rangle = \langle u_m|\hat{H}|u_n\rangle \qquad \text{for } m < n - 1,$$

$$b_{n+1}\langle u_m|u_{n+1}\rangle = (\hat{H}|u_m\rangle)^\dagger|u_n\rangle. \tag{3.91}$$

Because of the recursion relation, when $\hat{H}$ operates on $|u_m\rangle$ it produces a linear combination of $|u_{m-1}\rangle, |u_m\rangle$ and $|u_{m+1}\rangle$, all of which have zero overlap with $|u_n\rangle$, and therefore $|u_{n+1}\rangle$ is orthogonal to all the previous states in the chain.

3.4.6 Finding the eigenvalues and eigenvectors

Fortunately, once we have tridiagonalized the Hamiltonian with the Lanczos procedure, finding both the eigenvalues and the corresponding eigenvectors is relatively simple.

We first discuss the method of determining the eigenvalues. It is possible to construct a polynomial $p_r(x)$ equivalent to the secular equation for the tridiagonalized Lanczos matrix after r recursion steps,

$$p_r(x) = (a_r - x)p_{r-1}(x) - b_{r-1}^2 p_{r-2}(x), \tag{3.92}$$

which is a determinantal expansion of the secular equation. For example

$$\mathsf{T}_{r=3} = \begin{bmatrix} a_0 & b_1 & 0 & 0 \\ b_1 & a_1 & b_2 & 0 \\ 0 & b_2 & a_2 & b_3 \\ 0 & 0 & b_3 & a_3 \end{bmatrix}, \tag{3.93}$$

$$p_{r=3}(x) = \begin{bmatrix} a_0 - x & b_1 & 0 & 0 \\ b_1 & a_1 - x & b_2 & 0 \\ 0 & b_2 & a_2 - x & b_3 \\ 0 & 0 & b_3 & a_3 - x \end{bmatrix}, \tag{3.94}$$

and so finding the zeros of $p_r(x)$ is equivalent to finding the eigenvalues of T_r. Thus as r increases, T_r becomes more equivalent to the Hamiltonian and we are finding increasingly better estimates of the eigenvalues of $\hat{H}$.

To do this efficiently numerically, we utilize the Sturm sequence properties of tridiagonal matrices [54, 71]. The Sturm sequence is given by

$$\{p_0(x), p_1(x), \ldots, p_r(x)\}. \tag{3.95}$$

If $m(x)$ equals the number of sign changes between adjacent members of this sequence, then $m(x)$ is also equal to the number of T_r's eigenvalues that are less than x. We can therefore converge on the nth eigenvalue of T_r by a bisection method, adjusting the upper bound z and the lower bound y of the eigenvalue. This is shown as algorithm 4.

Algorithm 4: Bisection algorithm for locating the nth eigenvalue λ_n of matrix T_r from the Sturm sequence

while $|z - y| >$ tolerance
  $x = \frac{y+z}{2}$
  if $m(x) > r - n$
    $z = x$
  else
    $y = x$
  end if
end while
$\lambda_n = x$

For the eigenvectors, we start with the estimate of the eigenvalue (here labelled τ) as found above and an initial random guess at the corresponding eigenvector, $|b\rangle$. We then solve the system by inverse iteration [118] as follows. We have

$$(\mathsf{A} - \tau\mathsf{I})|y\rangle = |b\rangle, \tag{3.96}$$

where I is the identity matrix. We shall now show that if this procedure is iterated by putting $|b_{\text{new}}\rangle = |y\rangle$ then the solution $|y_{\text{final}}\rangle$ will be the eigenvector corresponding to the true eigenvalue λ.

The vectors $|y\rangle$ and $|b\rangle$ can both be expanded in terms of the eigenvectors $|x_j\rangle$ of A:

$$|y\rangle = \sum_j \alpha_j |x_j\rangle \quad ; \quad |b\rangle = \sum_j \beta_j |x_j\rangle. \tag{3.97}$$

Equation (3.96) can therefore be expanded as

$$\sum_j (\lambda_j - \tau)\alpha_j |x_j\rangle = \sum_j \beta_j |x_j\rangle, \tag{3.98}$$

and so

$$\alpha_j = \frac{\beta_j}{\lambda_j - \tau} \tag{3.99}$$

and

$$|y\rangle = \sum_j \frac{\beta_j |x_j\rangle}{\lambda_j - \tau}. \tag{3.100}$$

Now if we are searching for the nth eigenvector and $\lambda_n \approx \tau$, as it will be if we have a good enough original estimation of the eigenvalue, then for $\lambda_n = \lambda_j$ the denominator of equation (3.100) will be close to zero and thus the contribution to $|y\rangle$ from this $|x_n\rangle$ will be larger than for any of the other $|x_j\rangle$. Therefore as the procedure is iterated, the solution $|y\rangle$ will converge on the required eigenvector $|x_n\rangle$.

3.4.7 Using the Lanczos method to calculate correlation functions

Haydock [61] has also used the Lanczos method to calculate correlation functions of a system by using it to calculate the Green's function 3.3. Haydock defines the local Green's function as

$$G_0(E) = \langle v|\mathsf{S}(E - \hat{H})^{-1}|u\rangle \tag{3.101}$$

where E is a complex energy that is not an eigenvalue of $\hat{H}$, and S is the matrix measuring the overlap of the basis states of the system. For an orthogonal basis set, such as we are using here, S becomes the identity matrix and so we shall omit it from the following explanation. $G_0(E)$ therefore describes the propagation of the system from state $|u\rangle$ to state $|v\rangle$ at energy E.

The spectral decomposition of the Green's function is given by

$$G_0(E) = \langle v| \left[\sum_\alpha |w_\alpha\rangle (E - E_\alpha)^{-1} \langle w_\alpha| \right] |u\rangle, \tag{3.102}$$

where the $\{|w_\alpha\rangle\}$ are an orthonormal set of eigenstates of $\hat{H}$ with corresponding eigenvalues $\{E_\alpha\}$. This has a pole at each eigenvalue E_α, and so a contour integral of $G_0(E)$ picks out the eigenstates $\{|w_\alpha\rangle\}$ that couple to $|u\rangle$ and $|v\rangle$.

This form of the Green's function can be related exactly to the chain model

of section 3.4.5. First consider some of the properties of $G_0(E)$ — as $E \to \infty$, $G_0(E) \to 0$ like $1/E$. Also,

$$\begin{aligned} G_0(E)^\dagger &= \langle u_0|(E-\hat{H})^\dagger|u_0\rangle \\ &= \langle u_0|(E^\dagger-\hat{H}^\dagger)|u_0\rangle \\ &= G_0(E^\dagger), \end{aligned} \tag{3.103}$$

as $\hat{H}^\dagger = \hat{H}$ by definition. From equation (3.102) it can also be seen that the residue of each eigenvalue in $G_0(E)$ is positive, and so the imaginary part of $G_0(E)$ is negative in the upper half of the complex energy plane, and positive in the lower half plane. In addition, the poles of $G_0(E)$ are real, and occur at eigenvalues of $\hat{H}$, and the zeroes of $G_0(E)$ are also real and separate the poles along the real E-axis.

Such a function can be written as a continued fraction:

$$\cfrac{1}{E-a_0-\cfrac{b_1^2}{E-a_1-\cfrac{b_2^2}{E-a_2-\ldots-\cfrac{b_{N-1}^2}{E-a_n\ldots}}}} \tag{3.104}$$

where we shall now show that the $\{a_n\}$ and $\{b_n\}$ here are the same as for the corresponding chain model. Firstly, note that the continued fraction of equation (3.104) can be written as a recursion:

$$G_n(E) = \frac{1}{[E-a_n-b_{n+1}^2 G_{n+1}(E)]} \tag{3.105}$$

and has the following properties: If a_n is real, b_{n+1}^2 positive and E is in the upper half of the complex E-plane, not only is $G_{n+1}(E)$ in the lower half-plane but so is G_n. Also, if $G_{n+1}(E) \to 1/E$ as $E \to \infty$, so does $G_n(E)$, and $G_{n+1}(E^\dagger) = G_{n+1}(E)^\dagger$ implies that $G_n(E^\dagger) = G_n(E)^\dagger$.

Now since we have already shown that the Hamiltonian can be tridiagonalized

$$\hat{H} = \begin{bmatrix} a_0 & b_1 & 0 & \ldots \\ b_1 & a_1 & b_2 & \ldots \\ 0 & b_2 & a_3 & \ldots \\ \vdots & 0 & b_3 & \ldots \\ \vdots & \vdots & \vdots & \ddots \end{bmatrix}, \tag{3.79}$$

then the Green's function can be written as

$$\begin{aligned} G_0(E) &= \langle u_0|(E-\hat{H})^{-1}|u_0\rangle \\ &= \begin{bmatrix} E-a_0 & -b_1 & 0 & \dots \\ -b_1 & E-a_1 & -b_2 & \dots \\ 0 & -b_2 & E-a_3 & \dots \\ \vdots & 0 & -b_3 & \dots \\ \vdots & \vdots & \vdots & \ddots \end{bmatrix}^{-1}_{00}, \end{aligned} \tag{3.106}$$

where the 00 subscript implies the 00 element of the matrix, which is given by the ratio of the cofactor of $E-a_0$ to the determinant of the whole matrix. If we write the determinant of the matrix with the first n rows and columns removed as $D_n(E)$, then

$$\begin{aligned} G_0(E) &= \frac{D_1(E)}{D_0(E)} \\ &= \frac{D_1(E)}{[(E-a_0)D_1(E) - b_1^2 D_2(E)]} \\ &= \dots \quad \text{etc.}, \end{aligned} \tag{3.107}$$

which produces another continued fraction. Note however that this depends on the orthogonality of the $\{|u_n\rangle\}$.

From this we can calculate the local density of states, which is related to the residues of $G_0(E)$ at its singularities. If we write the residue of each pole as ρ_α, corresponding to the pole at each eigenvalue with energy E_α, then the density of states is equivalent to the density of $G_0(E)$

$$n_0(E) = \sum_\alpha \rho_\alpha \delta(E - E_\alpha), \tag{3.108}$$

and since

$$G_0(E) = \langle u_0|w_\alpha\rangle(E-E_\alpha)\langle w_\alpha|u_0\rangle \tag{3.109}$$

we see that ρ_α is just $|\langle w_\alpha|u_0\rangle|^2$.

Now if we consider the imaginary part of $G_0(E)$ parallel to the real axis but just above it, we see that

$$n_0(E) = \lim_{\varepsilon\to 0} -\frac{1}{\pi}\Im\left[G_0(E+\mathrm{i}\varepsilon)\right], \tag{3.110}$$

and that each pole on the real E-axis produces a delta function in the limit.

Note that the real part of $G_0(E)$ along the real axis is the Hilbert transform

of the density of states

$$\Re[G_0(E)] = \int_{-\infty}^{+\infty} \frac{n_0(E')}{(E - E')} \mathrm{dE}' \tag{3.111}$$

and is related physically to the resistance of the system to excitation at energies other than the eigenenergies.

Chapter 4

Implementation

> "1 + 1" it could manage ("2"), and "1 + 2" ("3") and "2 + 2" ("4") or tan 74 ("3.4874145"), but anything above "4" it represented merely as "A Suffusion of Yellow"
>
> Douglas Adams, *"The Long Dark Teatime of the Soul"*

4.1 Introduction **83**
4.2 Representation of the basis states **85**
4.3 Implementation of the operators **87**
4.4 Implementation of the two-chain Hamiltonian . . . **100**
4.5 Convergence on the eigenstates **104**
4.6 Parameters **108**
4.7 Parallelization of the code **109**

4.1 Introduction

This chapter consists of a description of the Fortran 90/95 code written to perform the calculations, and a discussion of problems that arose in the process and how they were resolved. It was necessary to make a number of assumptions about the model in order to proceed with the implementation; these are discussed in section 4.1.1. The way the basis states are represented for computational purposes is discussed in section 4.2, which is followed by a detailed description of how Haldane's operators were implemented in section 4.3. Section 4.4 describes how these various elements are combined into the most important subroutine of the code—the implementation of the coupled chain Hamiltonian. The chapter concludes with a discussion of the various parameters required and how they were chosen, together with a consideration of the precision of the calculations and the extent of numerical errors in the results.

Figure 4.1 shows the main subroutines of the code and how they relate to each other—each item in this diagram corresponds to a subsection of section 4.3.

4.1.1 Assumptions and simplifications

In order to translate Haldane's vision of the Luttinger model into a working computer code, it was necessary to make a few assumptions and simplifications. Firstly, it was assumed that all of the negative energy electron states are filled and are not available for excitation—after all, they exist only as a mathematical convenience in order to ensure the correct behaviour of the Hilbert space. Consequently these states can neither be annihilated nor created—for these purposes a "zero-electron state" refers to a state in which there are no positive energy electrons. Secondly, it was necessary to make a decision about the electron states on each chain at $k = 0$. These states have an indeterminate p-value and as such cannot be said to belong to either of the two Luttinger model branches. It was decided to assume that, as with the negative energy states, these states are permanently occupied and not available for excitation.

The problems introduced by considering a discrete lattice of atomic sites to represent the chains rather than the continuum of states used by Haldane are discussed in section 4.3.6.

It is also necessary to truncate the Hilbert space in order to produce a problem of computationally manageable size. As already mentioned in section 3.2.2, the simplest way of doing this is to restrict the maximum number of bosons in each mode. Computationally this is achieved by setting of the global variable

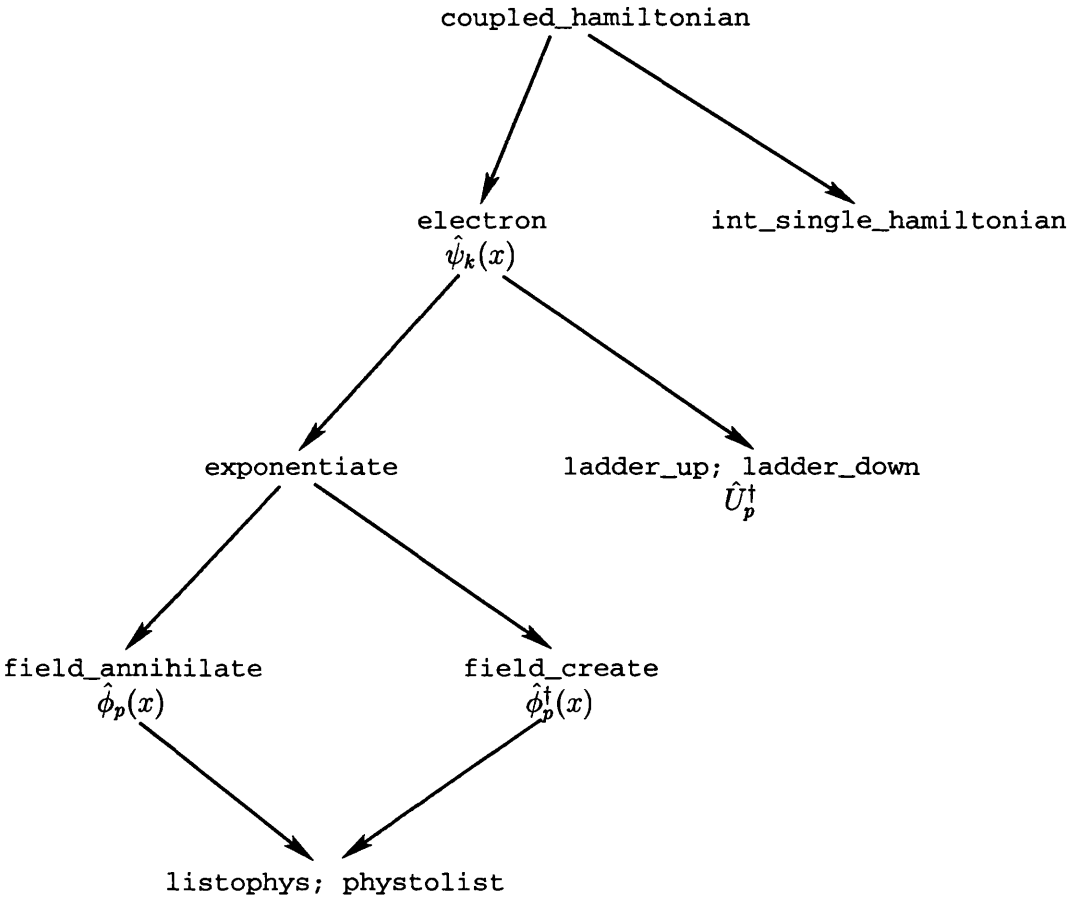

Figure 4.1: Schematic diagram showing the structure and interdependence of the various subroutines

`limit`, and it was found that setting `limit = 1` was sufficient to reproduce the low energy characteristics of the model with a reasonable Hilbert space. This was verified by sample calculations for both eigenstates and correlation functions, whereupon it was found that both the `limit = 1` and `limit = 2` calculations gave the same results to a precision comparable to the noise in the calculations (see section 4.5.4).

The size of the Hilbert space, together with the number of elements in the matrix required for the implementation of the coupled Hamiltonian, is shown in figure 4.2.

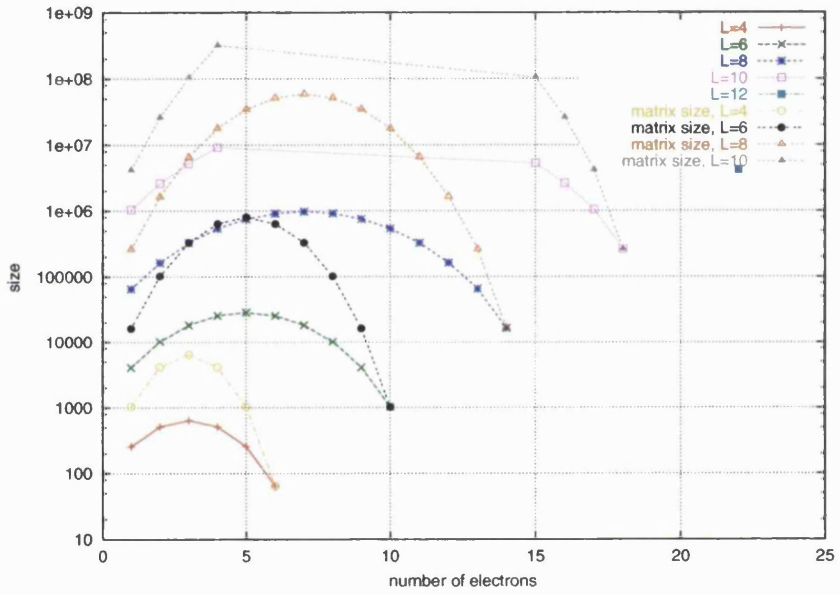

Figure 4.2: Size of the computational Hilbert space for various chain lengths and occupations with `limit` = 1. The corresponding size of the matrix required for the coupled Hamiltonian is also shown, this is discussed in section 4.4. Certain of the extremal values for very large systems have been omitted for computational ease.

4.2 Representation of the basis states

It is necessary to decide on a way to represent the basis states computationally. Fortunately, Fortran 90/95's ability to handle derived types simplifies this matter considerably [38]. Since, as we shall see in subsequent sections, in the course of the code implementation we shall have cause to deal with states involving both just one chain and the two chains, we define two separate Fortran derived types for each circumstance.

4.2.1 Single chain basis states

In order to describe a state for a single chain, it is necessary to know various quantum numbers and also the coefficient of the state. The derived type for these states is therefore of the form

$$\texttt{coefficient} \mid \texttt{index J N\_ N}_{+} \texttt{ N}_{\texttt{L}} \texttt{ N}_{\texttt{0}}\rangle$$

The coefficient part of the state consists of a `complex` variable defined to have a minimum of 15 decimal digits. The quantum numbers of the state are all represented by integers—the integers `J`, $\texttt{N\_}$ and $\texttt{N}_{+}$ have their usual quantum number meaning here, and in addition we include $\texttt{N}_{\texttt{L}}$—the number of (positive energy) electrons in the Luttinger chain system (i.e. on both chains) and $\texttt{N}_{\texttt{0}}$—the number of electrons on the other chain. The inclusion of these additional numbers is required in order to calculate the phase factors for the ladder operators $\hat{U}_{p,c}$ correctly, as will be discussed in section 4.3.3. It will be noticed that there is some redundancy of information in this representation, as $\texttt{N\_} + \texttt{N}_{+} = \texttt{N}_{\texttt{L}} - \texttt{N}_{\texttt{0}}$, but this is retained as it provides a useful check against numerical errors. The `integer` variable `index` represents the boson occupations, as described in section 4.2.3.

4.2.2 Two-chain basis states

For most of the code we want to describe states of the two-chain system, which we do as follows. We again represent the coefficient as a `complex` variable with a minimum of 15 decimal digits, and the quantum numbers as `integers`. In this case the state is of the form

$$\texttt{coefficient} \mid \texttt{index}_{\texttt{A}} \texttt{ J}_{\texttt{A}} \texttt{ N\_}_{\texttt{A}} \texttt{ N}_{+\texttt{A}} \texttt{ ; index}_{\texttt{B}} \texttt{ J}_{\texttt{B}} \texttt{ N\_}_{\texttt{B}} \texttt{ N}_{+\texttt{B}}\rangle$$

$\texttt{index}_{\texttt{A}}$ and $\texttt{index}_{\texttt{B}}$ represent the boson indices of chain A and chain B respectively (see section 4.2.3). The integers $\texttt{J}_c, \texttt{N\_}_c$ and $\texttt{N}_{+c}$, with $c = \text{A, B}$ represent the current and branch-charge quantum numbers on the relevant chain respectively, as before.

By representing the basis states in such a manner, it becomes simple to extract the relevant one-chain information from one of the two-chain states whenever required. Moreover, as we shall show in the next section, representation of the boson occupation by an `integer` index variable significantly reduces the amount of space such a state requires. It should be noted that it would also be possible to represent the entire state by such an index—however this alternative was rejected in favour of the transparency and speed of processing the above approach gives.

4.2.3 Numerical representation of the boson system

The most efficient way of representing the boson occupations is as a single integer, which can be implemented by treating each set of boson occupations $\{n_q\}$ as a base (`limit` + 1) number, where `limit` is the global maximum limit on the number of bosons in the system (see section 3.2.2). For the sake of computational convenience, the numbers were converted in the following way, best illustrated by the a simple example. For the $p = +1$ branch of a chain of length $L = 6$ (i.e. 6 boson modes with labels running from -3 to $+2$), and `limit` = 1 the following boson distributions are possible:

Mode:	-3	-2	-1	0	1	2	Index
(value	*1*	*2*	*4*	*8*	*16*	*32)*	
	0	0	0	0	0	0	1
	0	0	0	0	1	0	17
	0	0	0	0	0	1	33
	0	0	0	0	1	1	49

In order to avoid an index of 0 for a state with zero boson occupation, 1 is added to all indices. Note that the conversion is made with values increasing from left to right rather than the more familiar right to left.

4.2.4 The subroutines `listophys` and `phystolist`

In order to use these boson representations effectively, we need an efficient way to convert from the index representation to the actual boson occupations. This will allow us to operate on the bosons with the annihilation and creation operators $\hat{a}_q$ and $\hat{a}_q^\dagger$. Since this merely involves a form of base conversion, this is fairly trivial. Two subroutines were created—listophys to convert from the index representation (a base 10 integer) to the real boson occupations (a base `limit` + 1 number), and phystolist to convert from the real boson occupations in base `limit` + 1 to the index in base 10.

4.3 Implementation of the operators

4.3.1 The subroutines `field_annihilate` and `field_create`: $\hat{\phi}_p(x)$ and $\hat{\phi}_p^\dagger(x)$

The purpose of these subroutines is to implement the lowest level of Haldane's bosonization operators, the boson field operator $\hat{\phi}_p^{(\dagger)}(x)$ (reference [60] equation

3.22)

$$\hat{\phi}_p(x) = \left(\frac{p\pi x}{L}\right) N_p + \mathrm{i} \sum_{q \neq 0} \theta(pq) \left(\frac{2\pi}{L|q|}\right)^{1/2} \mathrm{e}^{-\mathrm{i}qx} \hat{a}_q, \tag{2.40}$$

$$\hat{\phi}_p^\dagger(x) = \left(\frac{p\pi x}{L}\right) N_p - \mathrm{i} \sum_{q \neq 0} \theta(pq) \left(\frac{2\pi}{L|q|}\right)^{1/2} \mathrm{e}^{\mathrm{i}qx} \hat{a}_q^\dagger. \tag{4.1}$$

The input to these subroutines, which are called by the routine that calculates $\mathrm{e}^{\mathrm{i}\hat{\phi}_p(x)}$, **exponentiate** (section 4.3.2), is an array of single-chain basis states. The main body consists of a loop over all the input states. Then, for each input state, the "number operator" term $\left(\frac{p\pi x}{L}\right) N_p$ is calculated. In order to calculate the terms which alter the (boson) quantum numbers of the input state, the basis state is first converted to its actual form using `listophys`, and then the sum over boson modes is performed and the bosons annihilated or created as required. Once the annihilations or creations have taken place, `phystolist` converts the new boson occupations back to the index representation, with the resulting single-chain basis states held in a temporary array. Once all the states in the input array have been processed, the temporary result state is sent to the book-keeping routines (section 4.3.8) for arithmetic simplification and removal of duplicate states. The result array is then sent as output to the calling routine, **exponentiate**, discussed in the following section.

4.3.2 The subroutine exponentiate: $\mathrm{e}^{\mathrm{i}\hat{\phi}_p(x)}$

This subroutine is designed to calculate the exponential of the field operator, equation (2.40), and is a necessary component of the fermion operator (equation 2.45). However, $\hat{\phi}_p(x)$ is non-hermitian, and to take the exponential of a non-hermitian operator causes some complications.

Therefore implementing $\mathrm{e}^{\mathrm{i}\hat{\phi}_p(x)}$ numerically is non-trivial, as a result to machine accuracy is required in order to construct the other operators accurately. In addition, this routine will be called many thousands of times in a typical run to calculate an eigenstate or correlation function, and thus it is essential to perform this calculation in as computationally efficient a way as possible. Before discussing the eventual structure of the subroutine therefore, it is appropriate to discuss how the most efficient way to proceed with this calculation was determined.

Calculating $e^{i\hat{\phi}_p(x)}$

It is fairly well known that theoretically the most efficient way to calculate the exponential of an hermitian operator is to use the approach of Kosloff [81] which uses an algorithm based on the Chebyshev expansion and Newtonian interpolation. The efficiency of this method is dependent on knowing the range of the eigenvalues of the operator, which for a hermitian operator will lie on the real axis, However, since here the range of eigenvalues of $\hat{\phi}_p(x)$ will lie in the complex plane, it was important to confirm that this approach would indeed be superior to a simple power series expansion of the exponential.

In order to use the Chebyshev expansion effectively, we need to determine the region in the complex plane where the eigenvalues of $\hat{\phi}_p(x)$ lie. Since $\hat{\phi}_p(x)$ non-hermitian, exact determination of the eigenvalues is not practicable. However, it is possible to bound the region in which they lie in the following manner.

Using Dirac's phase operator [32] we can write the general annihilation operator as

$$\hat{a} = e^{i\hat{\theta}}\hat{n}^{1/2}, \tag{4.2}$$

where $\hat{n}$ represents the number operator, with eigenvalues $0, 1, 2, \ldots, n_{\max}$ (here $n_{\max}$ represents the total number of bosons in the distribution $\{n_q\}$, which has a maximum value of `limit`). We also know that

$$\hat{a}|n\rangle = \sqrt{n}|n-1\rangle, \tag{4.3}$$

and from this we deduce that the eigenvalues of $\hat{a}$ must lie within a circle of radius equal to the maximum eigenvalue of $\hat{a}$, i.e. $\sqrt{n_{\max}}$, and centred at the origin of the complex plane, as in figure 4.3.

Now since the operator we are trying to bound the eigenvalues for is

$$\hat{\phi}_p(x) = p\left(\frac{\pi x}{L}\right)\hat{N}_p + i\sum_{q\neq 0}\theta(pq)\left(\frac{2\pi}{L|q|}\right)^{1/2} e^{iqx}\hat{a}_q, \tag{4.4}$$

where N_p is simply the number of fermions on branch p, each of the annihilation operators in the summation over all modes q will contribute a "radius" analogous to the above, of length $\sqrt{n_{q\ \max}}$, scaled by a factor

$$i\theta(pq)\left(\frac{2\pi}{L|q|}\right)^{1/2} e^{iqx} = \alpha_q. \tag{4.5}$$

Adding these together and recentring the circle at $p\left(\frac{\pi x}{L}\right)N_p = \beta N_p$ we deduce

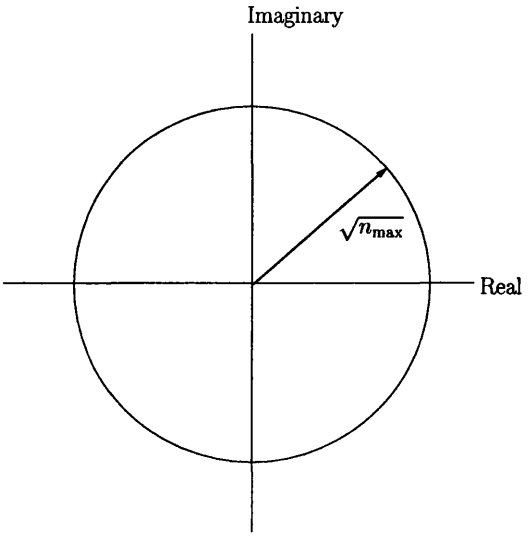

Figure 4.3: Domain of eigenvalues for the annihilation operator $\hat{a}$.

that the eigenvalues of the operator $\theta_p(x)$ will lie within a circle of radius

$$R = \sum_{q \neq 0} \alpha_q \sqrt{n_{q\ \max}} \tag{4.6}$$

and centred on the point on the real axis given by βN_p, as in figure 4.4.

In order to implement the above, a subroutine was created to use the Newtonian interpolation method together with the Chebyshev polynomials [81] to calculate the operator $e^{i\phi_p(x)}$. Another subroutine was also created using a simple power series expansion

$$e^{i\phi_p(x)} = 1 + i\phi_p(x) - \frac{1}{2!}\phi_p(x)^2 - \frac{i}{3!}\phi_p(x)^3 + \ldots \tag{4.7}$$

in order to check the results. However, it was found that the Chebyshev approach was, in this case, inferior to the simple power series expansion. While the convergence of the Chebyshev approach was slightly superior for values near the boundary of the "eigenvalue circle", for points nearer the centre of the circle the power expansion converged significantly faster, as perhaps may have been expected. Although the Chebyshev/Newton approach is theoretically the most efficient, it was hampered in this instance by difficulty in bounding the eigenvalues sufficiently well to give optimum results. For this reason the Chebyshev approach was abandoned and the power series subroutine implemented with a cutoff such that further terms in the series were not calculated once adjacent terms for the coefficients of all the boson occupation states differed by less than

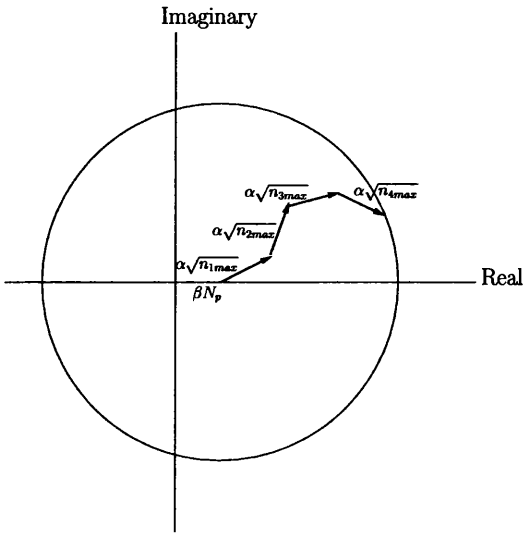

Figure 4.4: Domain of eigenvalues for $\phi_p(x)$.

10^{-13}. It should be noted that the power series remains numerically stable in this instance as the coefficients of the results do not represent any conserved quantity or physical observable. If the operator were the Hamiltonian, for instance, then a second order differencing version of the power series would be more appropriate and would allow for the energy to be conserved.

Implementation

The structure of the subroutine is therefore as follows. The input to the routine (called from `electron`, section 4.3.4) is a single-chain basis state array. The first term in the power series is simply $1\times$ the input array, and so the main body of the code consists of a loop over the successive terms in the power series, up to a maximum number of terms after which an error is declared if the series has not converged by the time this maximum is reached. Empirical observations revealed that 100 is an appropriate number for this limit, and in most cases the series converged well before this limit is approached.

The loop operates with $\hat{\phi}_p^{(\dagger)}(x)$, using `field_annihilate` or `field_create` as appropriate, on the output of the previous iteration of the loop. The output of this is then added to the existing result from the previous iteration. Because of the number of terms typically returned from this operation, the book-keeping routines are called after each iteration of the main loop. The convergence criteria are met when a comparison of the coefficients of all the states in the result array differ from their counterparts in the result array from the previous

iteration by less than a specified cutoff, in this case 10^{-13}.

4.3.3 The `ladder_up` and `ladder_down` subroutines: $\hat{U}_{p,c}$

The purpose of these routines is to implement Haldane's ladder operator $\hat{U}_p$, equation (2.38), which adds or removes a unit of charge from the system. As discussed in section 3.1.1, an additional phase factor is necessary to ensure the correct anticommutation properties of the resultant fermion operator $\hat{\psi}_p^c(x)$ when we include more than one chain in the system. There is one further complication we need to take into account when implementing this operator computationally. Because of the discrete size of the system , there is a maximum number of electrons that each branch can accommodate—for instance, on the $p = +1$ branch of an $L = 6$ chain, there are only two states available, as shown in figure 4.5, and this imposes a maximum limit of 2 on the value of $\mathtt{N}_+$ for this chain. Also, since for computational purposes we are disregarding the negative energy electron states (as discussed in section 4.1.1), there is a lower limit on $\mathtt{N}_{-,+}^{\mathtt{A,B}}$ of 0.

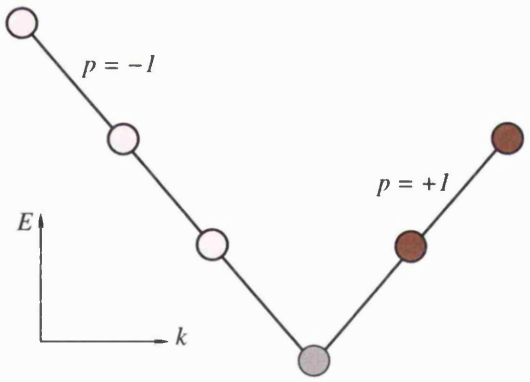

Figure 4.5: Schematic band structure for a chain with $L = 6$. There are only two available states for electrons on the $p = +1$ branch of the $L = 6$ chain. The state at $k = 0$ is not available, as discussed in section 4.1.1.

The subroutines therefore take as their input an array of single chain basis states, and for each state in the array check to see if a unit of charge can be annihilated or created, as appropriate, i.e. to see if the new values of $\mathtt{N}_{-,+}^{\mathtt{A,B}}$ would be within the limits discussed above. If not, then a null result is returned—no result is produced for this element of the input array. If however, the new value of $\mathtt{N}_{-,+}^{\mathtt{A,B}}$ is valid, then the phase factor is calculated, based on both the number of electrons on the other branch of the same chain, and on the total number of electrons on both branches of the other chains—this is where the inclusion of $\mathtt{N}_0$

in the definition of the single-chain basis state derived type becomes essential (section 4.2.1). The states are returned as an array with the new values of $\mathtt{N}^{\mathtt{A,B}}_{-,+}$ and the coefficients multiplied by the appropriate phase factors.

4.3.4 Electron creation and annihilation: $\hat{\psi}^\dagger_p(x)$ and the `electron` subroutine

Once we have the `ladder_up`, `ladder_down` and `exponentiate` subroutines, it is relatively simple to string them together to form the fermion operator $\hat{\psi}_{p,c}(x)$, which creates a momentum-type p fermion at position x on chain c. For two chains, this takes the form (compare with Haldane's single chain form of equation (2.45))

$$\hat{\psi}^\dagger_{p,c}(x) = \frac{1}{\sqrt{L}} \mathrm{e}^{\mathrm{i}pk_F x} \left[\mathrm{e}^{\mathrm{i}\hat{\phi}^\dagger_p(x)} \hat{U}_{p,c} \mathrm{e}^{\mathrm{i}\hat{\phi}_p(x)} \right] \tag{4.8}$$

The subroutine `electron` achieves this for both the creation and annihilation forms of the fermion operator. It takes as its input an array of single-chain basis states, and first calls `exponentiate` with the input array and appropriate arguments to calculate $\mathrm{e}^{\mathrm{i}\hat{\phi}}$, $\mathrm{e}^{-\mathrm{i}\hat{\phi}}$, $\mathrm{e}^{\mathrm{i}\hat{\phi}^\dagger}$ or $\mathrm{e}^{-\mathrm{i}\hat{\phi}^\dagger}$ as required. The result of this is then sent to the appropriate ladder routine, and then the intermediate result is sent to `exponentiate` once more with the new appropriate arguments. This result is then simplified using the book-keeping routines and returned to the calling routine, `coupled_hamiltonian`, discussed in section 4.4.

The routine `electron` and its dependent subroutines thus represent the heart of the code—it can create or remove fermions, with the appropriate anticommutation properties, despite being composed of bosonic operator subroutines which are perfectly commuting in nature.

4.3.5 Normalization

In order to check that the correct results were being generated, the normalizations of the operators were examined. It is possible, to consider this problem analytically in order to check the veracity of the numerical results.

As an example, consider the simple case of a chain of length $L = 6$, with one electron at the $k = 0$ position and therefore no electrons on either branch of the Luttinger dispersion relation. Note also that due to the boundary conditions on the Brillouin zone there are three empty states on the right hand branch (corresponding to $p = -1$) and two on the left hand branch ($p = +1$). This difference in the number of available fermion states will lead to a corresponding difference in the number of boson states, resulting in different normalizations

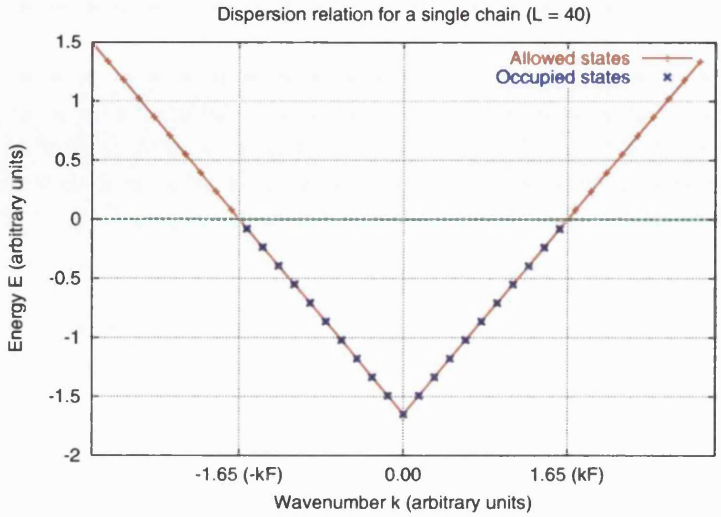

Figure 4.6: Dispersion relation for a chain of length 40 atoms, shown with 20 electrons and $v_F = 1$.

for each branch.

If we first consider the $p = +1$ right hand branch (which has $L/2 - 1 = 2$ available boson modes) then the initial zero-electron ground state can be given by

$$|0\rangle = |N_+, J, \{n_{q>0}\}\rangle = |0, 0, 0, 0\rangle, \tag{4.9}$$

i.e. $N_+ = 0$, $J = 0$ and $n_1 = n_2 = 0$. Operating on this vacuum with the first part of the fermion creation operator $\hat{\phi}_p(x)$ only requires the use of the field annihilation operator $\hat{\phi}_p(x)$ and, since there is nothing here to annihilate, results once more in the vacuum state. Now application of the next part of $\hat{\psi}_p(x)$, the ladder operator $\hat{U}_p$, increases both N_+ and J by one to give the state

$$|\Psi\rangle = |N_+, J, \{n_{q>0}\}\rangle = |1, 1, 0, 0\rangle. \tag{4.10}$$

We now need to operate on this state with the final part of the fermion creation operator, $\hat{\psi}_p^\dagger(x)$, and calculate $\exp \hat{\phi}_p^\dagger(x)$. Then

$$\phi^\dagger_{p=+1}(x)|\Psi\rangle = \left[\left(\frac{p\pi x}{L}\right) N_p + \mathrm{i}\sum_{q\neq 0} \theta(pq) \left(\frac{2\pi}{L|q|}\right)^{1/2} \mathrm{e}^{\mathrm{i}qx} \hat{a}_q\right] |\Psi\rangle \tag{2.40}$$

$$= \frac{\pi x}{L}|\Psi\rangle + \mathrm{i}\left[\sqrt{\frac{2\pi}{L|q_1|}}\mathrm{e}^{-\mathrm{i}q_1 x}|1110\rangle + \sqrt{\frac{2\pi}{L|q_2|}}\mathrm{e}^{-\mathrm{i}q_2 x}|1101\rangle\right] \tag{4.11}$$

$$= \frac{\pi x}{L}|\Psi\rangle + \mathrm{i}\left[\mathrm{e}^{-\mathrm{i}q_1 x}|1110\rangle + \frac{1}{\sqrt{2}}\mathrm{e}^{-\mathrm{i}q_2 x}|1101\rangle\right],$$

where the q are required to be $2\pi/L$ times an integer. Given the form of this expression, we can now use a binomial expansion to obtain

$$\begin{aligned}
e^{i\phi_+(x)} &= \frac{1}{n!}[i\phi_+(x)]^n \\
&= \frac{1}{n!}\sum_{r=0}^{n}\binom{n}{r}\left(\frac{i\pi x}{L}\right)^{n-r}\left[-e^{-iq_1x}\hat{a}_1 - \frac{1}{\sqrt{2}}e^{-iq_2x}\hat{a}_2\right]^r|\Psi\rangle \\
&= \frac{1}{n!}\left(\frac{i\pi x}{L}\right)^n|1100\rangle - \frac{1}{(n-1)!}\left(\frac{i\pi x}{L}\right)^{n-1}\left[e^{-iq_1x}|1110\rangle + \frac{1}{\sqrt{2}}e^{-iq_2x}|1101\rangle\right] \\
&\quad + \frac{1}{(n-2)!}\frac{1}{\sqrt{2}}\left(\frac{i\pi x}{L}\right)^{n-2}e^{-iq_1x}e^{-iq_2x}|1111\rangle,
\end{aligned} \tag{4.12}$$

where all subsequent terms in the expansion become zero due to our condition on the boson Hilbert space that no more than one particle is allowed in each mode (see section 3.2.2). Since we are trying to calculate $\langle\Psi|\Psi\rangle = \sum_n |a_n|^2$ we now need to include the summation over all values of n:

$$\begin{aligned}
\sum_{n=0}^{\infty}[\phi_+(x)]^n|\Psi\rangle &= \sum_{n=0}^{\infty}\left[\frac{1}{n!}\left(\frac{i\pi x}{L}\right)^n\right]|1100\rangle \\
&\quad - i\left[\sum_{n=1}^{\infty}\frac{1}{(n-1)!}\left(\frac{i\pi x}{L}\right)^{n-1}\right]\left(e^{-iq_1x}|1110\rangle + \frac{e^{-iq_2x}}{\sqrt{2}}|1101\rangle\right) \\
&\quad + \frac{1}{\sqrt{2}}\left[\sum_{n=2}^{\infty}\frac{1}{(n-2)!}\left(\frac{i\pi x}{L}\right)^{n-2}\right]\left(e^{-iq_1x}e^{-iq_2x}|1111\rangle\right) \\
&= e^{\frac{i\pi x}{L}}|1100\rangle + ie^{\frac{i\pi x}{L}}\left[e^{-iq_1x}|1110\rangle + \frac{1}{\sqrt{2}}e^{-iq_2x}|1101\rangle\right] \\
&\quad - \frac{e^{\frac{i\pi x}{L}}}{\sqrt{2}}\left[e^{-i(q_1+q_2)x}|1111\rangle\right].
\end{aligned} \tag{4.13}$$

Now we find that when we also include the $L^{-1/2}\exp(ipk_Fx)$ factor from the expression for $\psi_p(x)$ we can evaluate exactly the coefficients for each term:

$$\begin{aligned}
\psi_+(x)|0\rangle &= \frac{1}{\sqrt{L}}e^{ipk_Fx}\sum_n[\phi_+(x)]^n|\Psi\rangle \\
&= \frac{1}{\sqrt{L}}e^{ipk_Fx}\left[e^{\frac{i\pi x}{L}}|1100\rangle + ie^{\frac{i\pi x}{L}}\left[e^{-iq_1x}|1110\rangle + \frac{1}{\sqrt{2}}e^{-iq_2x}|1101\rangle\right]\right. \\
&\quad \left. - \frac{e^{\frac{i\pi x}{L}}}{\sqrt{2}}\left[e^{-i(q_1+q_2)x}|1111\rangle\right]\right]
\end{aligned} \tag{4.14}$$

Furthermore, we can calculate the square of this sum to determine the overall normalization, whence we find that

$$\begin{aligned}\left|\frac{1}{\sqrt{L}}\mathrm{e}^{\mathrm{i}pk_Fx}\sum_{n=0}^{\infty}[\phi_+(x)]^n\,|\Psi\rangle\right|^2 &= \frac{1}{L}\left[1+1+\frac{1}{2}+\frac{1}{2}\right]\\ &= \frac{1}{L}.\frac{L}{2}\\ &= \frac{1}{2}.\end{aligned} \tag{4.15}$$

which is independent of L. The veracity of this is confirmed by comparison of these results with those obtained numerically.

Now we can consider the $p=-1$ (left hand) branch in the same manner. The only difference between the two cases is that here three boson modes (i.e. $L/2$ modes) are available. This then gives

$$\begin{aligned}\frac{1}{\sqrt{L}}\mathrm{e}^{\mathrm{i}pk_Fx}\mathrm{e}^{\mathrm{i}\phi_-^\dagger(x)}|\Psi\rangle &= \frac{1}{n!}\left[\mathrm{i}\phi_-^\dagger(x)\right]^n\\ &= \frac{1}{\sqrt{L}}\mathrm{e}^{\mathrm{i}pk_Fx}\mathrm{e}^{\frac{\mathrm{i}\pi x}{L}}\left[|1,-1,0,0,0\rangle-\frac{\mathrm{e}^{-\mathrm{i}q_{-3}x}}{\sqrt{3}}|1,-1,1,0,0\rangle\right.\\ &\quad-\frac{\mathrm{e}^{-\mathrm{i}q_{-2}x}}{\sqrt{2}}|1,-1,0,1,0\rangle-\mathrm{e}^{-\mathrm{i}q_{-1}x}|1,-1,0,0,1\rangle\\ &\quad+\frac{\mathrm{e}^{-\mathrm{i}(q_{-3}+q_{-2})x}}{\sqrt{2}\sqrt{3}}|1,-1,1,1,0\rangle\\ &\quad+\frac{\mathrm{e}^{-\mathrm{i}(q_{-3}+q_{-1})x}}{\sqrt{3}}|1,-1,1,0,1\rangle+\frac{\mathrm{e}^{-\mathrm{i}(q_{-2}+q_{-1})x}}{\sqrt{2}}|1,-1,0,1,1\rangle\\ &\quad\left.+\frac{\mathrm{e}^{-\mathrm{i}(q_{-3}+q_{-2}+q_{-1})x}}{\sqrt{3}\sqrt{2}}|1,-1,1,1,1\rangle\right],\end{aligned} \tag{4.16}$$

and using the same principle as before

$$\begin{aligned}\left|\frac{1}{\sqrt{L}}\sum_{n=0}^{\infty}[\phi_-(x)]^n\,|\Psi\rangle\right|^2 &= \frac{1}{L}\left[1+\frac{1}{3}+\frac{1}{2}+1+\frac{1}{6}+\frac{1}{3}+\frac{1}{2}+\frac{1}{6}\right]\\ &= \frac{1}{L}.\frac{2L}{3}\\ &= \frac{2}{3}.\end{aligned} \tag{4.17}$$

Again, this is confirmed by the numerical results.

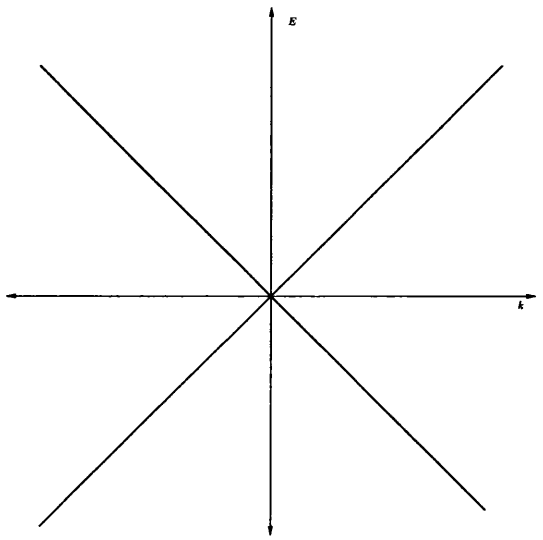

Figure 4.7: Band structure for the continuum model

4.3.6 Discrete lattice versus the continuum model

It will be noticed that while Haldane [60] assumes a continuum of x-values, here we are dealing with a discrete lattice and have been taking only integer values of x as allowed. This leads to an interesting effect in the operator $c^{\dagger}_{kp}$ when the terms involving the exponentials of the boson modes q add up to an integer multiple of 2π, e.g. in the above example the coefficient for the state $|1,-1,1,1,1\rangle$ includes the term $\exp -\mathrm{i}(q_{-3}+q_{-2}+q_{-1})x = \exp \frac{2\pi \mathrm{i}}{L}(-3-2-1) = \exp 2\pi\mathrm{i}$. This leads to a non-vanishing contribution to the energy from this boson state, whereas the creation of an extra fermion in the system should lead only to a change in the values of N_p and J – there should still be a ground state of the boson excitations. This actually represents a mixture of fermion states which can be explained as follows. Our discrete lattice of x-values gives us the Brillouin zone that we have assumed throughout, but so far we have neglected consideration of the band structure outside the first Brillouin zone. Whereas Haldane's continuum model has k-values extending to plus and minus infinity (as in figure 4.7) by representing the lattice model in the reduced zone scheme (as in figure 4.8) it becomes apparent that this factor of 2π leads to the creation of an excitation with momentum $k' = k + 2\pi$. For longer chains, higher multiples of 2π may be created, representing excitations on higher energy bands. This is also indicated on figure 4.8. Note also that the higher energy excitations can only occur on the same branch as the low energy excitation — in this case a right-moving branch ($p = +1$).

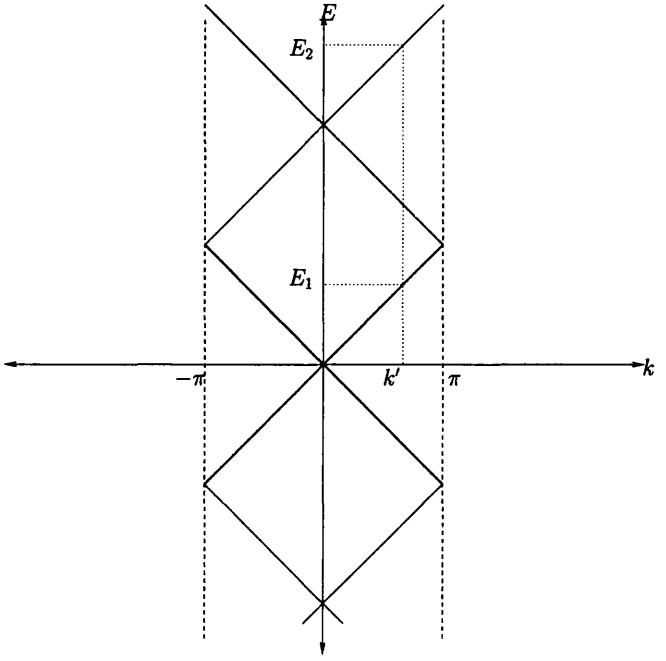

Figure 4.8: Band structure (reduced zone scheme) for the lattice model. Note that there is more than one possible energy (E_1, E_2) for a given value of k'

For the purposes of these calculations, however, the creation of these states is unwanted, and fortunately they may be suppressed easily by substituting the sum over integer values of x in $\hat{c}^{\dagger}_{kp}$ by a numerical "integration" over smaller intervals of x — in this case an interval as large as $\Delta x = 0.1$ was adequate to suppress the higher excitations and give accurate results without an excessive increase in processing time.

4.3.7 Implementation of the Hamiltonian for a single chain: The `int_single_hamiltonian` subroutine

The purpose of this subroutine is to calculate the Hamiltonian for the interacting chain, in other words, an implementation of Haldane's equation 4.13 (reference [60])

$$H = E_0 + \sum_q \omega_q \hat{b}^{\dagger}_q \hat{b}_q + \frac{\pi}{2L}\left(v_N N^2 + v_J J^2\right), \tag{2.53}$$

$$E_0 = \frac{1}{2}\sum_q \left(\omega_q - v_F|q|\right).$$

This can be split into three parts—a part independent of the boson modes q and only dependent on N and J $(\frac{\pi}{2L}\left(v_N N^2 + v_J J^2\right))$, and the ground state

energy shift E_0, which is dependent on q but does not contain any operators. These are both trivial to calculate; the third part, however, is a term involving the number operator for the Bogoliubov–transformed bosons $\sum_q \omega_q \hat{b}_q^\dagger \hat{b}_q$. Since we have formulated our representation in terms of the original boson operators $\hat{a}_q^\dagger$, $\hat{a}_q$, we cannot treat $\hat{b}_q^\dagger \hat{b}_q$ as a simple number operator. Instead, we need to transform it back to the $\hat{a}_q^\dagger$, $\hat{a}_q$ representation, i.e.

$$\begin{aligned}\hat{b}_q^\dagger \hat{b}_q &= \left[\cosh\phi_q \hat{a}_q^\dagger - \sinh\phi_q \hat{a}_{-q}\right]\left[\cosh\phi_q \hat{a}_q - \sinh\phi_q \hat{a}_{-q}^\dagger\right] \\ &= \cosh^2\phi_q \hat{a}_q^\dagger \hat{a}_q + \sinh^2\phi_q \hat{a}_{-q}\hat{a}_{-q}^\dagger - \sinh\phi_q \cosh\phi_q \left(\hat{a}_{-q}\hat{a}_q + \hat{a}_q^\dagger \hat{a}_{-q}^\dagger\right) \\ &= \cosh^2\phi_q \hat{n}_q + \sinh^2\phi_q (\hat{n}_{-q} - 1) - \sinh\phi_q \cosh\phi_q \left(\hat{a}_{-q}\hat{a}_q + \hat{a}_q^\dagger \hat{a}_{-q}^\dagger\right)\end{aligned} \tag{4.18}$$

where $\hat{n}_q$ is the number operator corresponding to the pre-Bogoliubov transformed boson operators $\hat{a}_q^\dagger$, $\hat{a}_q$. In this representation, therefore, it is simple to transform the boson index into its boson mode occupations using `listophys`, and then annihilate or create in the modes q as required. The result of this can then be sent to the book-keeping routines for simplification and return as output.

4.3.8 Book-keeping routines

The book-keeping subroutines exist to simplify an input state generated by one of the Haldane operator subroutines of section 4.3. The input is typically an unordered array of basis states with many duplicates, and in order for the code to work both correctly and efficiently, these duplicates need to be removed at each step of the calculation.

The first step in the procedure is to sort the input array into some kind of ordered array. This is achieved using a modified heapsort algorithm [118] whereby the sorting criteria are defined by the quantum number parts of each basis state, with the least significant bit being the rightmost integer, e.g. $\mathtt{N}_+^{\mathtt{B}}$ for a two-chain input array.

Once the original input array has been sorted in this fashion, it becomes easy to remove the duplicate states in a single scan of the sorted input array. The final result state is generated cumulatively—if one of the input states matches the quantum numbers of a state already in the output array, then its coefficient is added to the relevant output coefficient, otherwise the new state and its coefficient are appended to the output array. This method thus provides an exceptionally efficient way of simplifying basis state arrays and keeping track of the states at every stage of the calculation.

In addition, in order to prevent cumulation of errors resulting from the inevitable noise in the calculations, it was found necessary to include a subroutine that deletes all basis states with a coefficient of less than 10^{-20} from an input array. This is called only twice—at the end of the `electron` subroutine and at the end of the `coupled_hamiltonian` subroutine.

4.3.9 Two coupled Luttinger chains

We now have all the elements we need to construct a Hamiltonian describing the hopping of an electron from one chain to the other in terms of the Luttinger model.

The coupling Hamiltonian includes the Hamiltonians of the uncoupled chains $\hat{H}^0 = \hat{H}^A + \hat{H}^B$ as well as contributions (most of which will be zero) from hopping from chain A to chain B and chain B to chain A at each value of k on the chains:

$$\hat{H}^{\text{coupled}} = \hat{H}' = \hat{H}^0 + t_\perp \sum_k \left(\hat{c}^{A\dagger}_{kp} \hat{c}^B_{kp} + \hat{c}^{B\dagger}_{kp} \hat{c}^A_{kp} \right). \tag{4.19}$$

For the moment we only allow hopping between states that both have equal momenta and have the same branch (of the same type p).

We can rewrite this in terms of the field operators. As

$$\hat{c}^\dagger_{kp} = \sum_x \mathrm{e}^{-\mathrm{i}kx} \hat{\psi}^\dagger_p, \tag{4.20}$$

the coupling Hamiltonian becomes

$$\begin{aligned} \hat{H}' &= \hat{H}^0 + t_\perp \sum_k \sum_x \sum_{x'} \mathrm{e}^{-\mathrm{i}kx} \mathrm{e}^{-\mathrm{i}kx'} \left[\hat{\psi}^{A\dagger}_p \hat{\psi}^B_p + \hat{\psi}^{B\dagger}_p \hat{\psi}^A_p \right] \\ &= \hat{H}^0 + t_\perp \sum_x \left[\hat{\psi}^{A\dagger}_p \hat{\psi}^B_p + \hat{\psi}^{B\dagger}_p \hat{\psi}^A_p \right], \end{aligned} \tag{4.21}$$

because

$$\sum_k \mathrm{e}^{-\mathrm{i}kx} \mathrm{e}^{-\mathrm{i}kx'} = \delta_{x,x'}. \tag{4.22}$$

4.4 Implementation of the two-chain Hamiltonian

The Hamiltonian for two chains coupled together with amplitude $t'_\perp$ is given by

$$\begin{aligned} \hat{H}^{\text{coupled}} &= \hat{H}^A + \hat{H}^B + t_\perp \sum_k \left[\hat{c}^{A\dagger}_{kp} \hat{c}^B_{kp} + \hat{c}^{B\dagger}_{kp} \hat{c}^A_{kp} \right] \\ &= \hat{H}^A + \hat{H}^B + t_\perp \sum_x \left[\hat{\psi}^{A\dagger}_p \hat{\psi}^B_p + \hat{\psi}^{B\dagger}_p \hat{\psi}^A_p \right]. \end{aligned} \tag{4.23}$$

Although these two expressions are analytically equivalent, in terms of computational cost the Hamiltonian written in terms of $\hat{c}_k^\dagger$ is much more expensive, as it consists of $L\delta x$ iterations of $\hat{\psi}_p^\dagger(x)$:

$$c_{kp}^\dagger = \frac{1}{\sqrt{L}} \sum_{x=1}^{L} \mathrm{e}^{-\mathrm{i}kx} \psi_p^\dagger(x) \tag{4.24}$$

Also, the states of the two chains are most efficiently stored as a Fortran 90 derived type array consisting of the (complex) coefficient and the (integer) quantum numbers for each chain This means that applying the operator subroutines

$(\frac{1}{\sqrt{2}}, 0)$	$\|0001$	0	0	0	;	0001	-1	1	$0\rangle$
(coeff)	| boson idx.A	J^A	N_-^A	N_+^A	;	boson idx.B	J^B	N_-^B	$N_+^B\rangle$

Table 4.1: Example notation for basis states of two chains

in the subroutine for the coupled Hamiltonian in the manner naïvely suggested by equation (4.23) would require at least (4× the number of input states) calls to the relevant fermion creation or annihilation subroutine. For a large number of input states, such as the random start state used by the Lanczos method for finding the ground state (section 3.4.3) this can therefore prove very expensive!

However there are several ways to improve the efficiency, and in this case we chose to group the input states into a sets of chain A states and sets of chain B states.

By forming a matrix where the columns consist of states with identical chain A quantum numbers and the rows consist of states with identical chain B quantum numbers we can significantly reduce the number of calls to each operator subroutine:

$$\begin{array}{ccccc} |1;1\rangle & |1;2\rangle & \cdots & \cdots & |1;n\rangle \\ |2;1\rangle & |2;2\rangle & \vdots & & \vdots \\ |3;1\rangle & \cdots & |i;i\rangle & & \vdots \\ \vdots & & & \ddots & \vdots \\ |n;1\rangle & \cdots & \cdots & \cdots & |n;n\rangle \end{array}, \tag{4.25}$$

where the notation $|m,n\rangle$ indicates a chain A state m and a chain B state n.

4.4.1 Structure of the coupled Hamiltonian subroutine

The coupled Hamiltonian can be written in pseudocode as

```
input:  MATRIX(ROWS,COLS)
do TYPE = -1,1
  do X = 0, L
    set COUNT, COUNT1, COUNT2, TEMP_COUNT = 0
    do ROWS
      find the first non-zero element
      annihilate on the chain B part
      multiply result by each non-zero chain A element in this row
      now have COUNT1 terms in RESULT1
    end do ROWS
    tidy RESULT1 into TEMP_RESULT with TEMP_COUNT terms
    form a new matrix from TEMP_RESULT with N-1 electrons
    do ROWS
      find the first non-zero element
      create on the chain A part
      multiply result by each non-zero chain A element in this row
      now have COUNT2 terms in RESULT2
    end do ROWS
    tidy RESULT2 into RESULT with COUNT terms
    reset COUNT1, COUNT2, TEMP_COUNT = 0
    do ROWS
      find the first non-zero element
      annihilate on the chain A part
      multiply result by each non-zero chain A element in this row
      now have COUNT1 terms in RESULT1
    end do ROWS
    tidy RESULT1 into TEMP_RESULT with TEMP_COUNT terms
    form a new matrix from TEMP_RESULT with N-1 electrons
    do ROWS
      find the first non-zero element
      create on the chain B part
      multiply result by each non-zero chain A element in this row
      now have COUNT2 terms in RESULT2
    end do ROWS
    tidy RESULT2 into TEMP_RESULT with TEMP_COUNT terms
    add the contents of TEMP_RESULT to RESULT
  end do X
  add contents of RESULT to CUMULATIVE_RESULT with CUMULATIVE_COUNT terms
```

```
end do TYPE
tidy CUMULATIVE_RESULT into RESULT.
```

So what results do we expect to get from this Hamiltonian? It is again useful to compare the computational results with an analysis to check that the correct results are being given.

First consider the case where we have two chains with an equal number of electrons on each. It is intuitive that due to the exclusion principle there can be no hopping between two occupied states, and that as the number of electrons is equal for both chains and hopping is only allowed between equal k states, no hopping will occur and the coupling part of the Hamiltonian (equation 4.19) will be zero. This can be shown explicitly as follows. First we need to calculate the *total* energy of a single isolated chain. With linear dispersion, each state has an individual energy of $v_F k$, and since the states are separated by $\frac{2\pi}{L}$ the total energy of the chain is given by the sum over occupied states

$$\begin{aligned} E_{\text{total}} &= \int_{-k_F}^{k_F} \frac{L}{2\pi} v_F |k_F - k| \mathrm{d}k \\ &= \frac{v_F L}{\pi} \int_0^{k_F} (k_F - k) \mathrm{d}k \\ &= \frac{v_F L}{2\pi} k_F^2. \end{aligned} \tag{4.26}$$

We can define "effective" Fermi wavevectors for the anti-bonding and bonding bands k_F^- and k_F^+ such that the horizontal splitting of the bands is given by

$$\frac{2t_\perp}{v_F} = k_F^+ - k_F^- \tag{4.27}$$

Then from conservation of particles we must have that $k_F^+ + k_F^- = 2k_F$, giving

$$k_F^+ = k_F + \frac{t_\perp}{v_F} \tag{4.28}$$

If we now consider two coupled chains, then the total energy, by analogy with before, is

$$\begin{aligned} E_{\text{total}} &= \frac{v_F L}{2\pi} \left({k_F^+}^2 + {k_F^-}^2 \right) \\ &= \frac{v_F L}{2\pi} \left(\left[k_F + \frac{t_\perp}{v_F} \right]^2 + \left[k_F - \frac{t_\perp}{v_F} \right]^2 \right) \\ &= \frac{v_F L}{\pi} \left({k_F}^2 + \frac{{t_\perp}^2}{{v_F}^2} \right). \end{aligned} \tag{4.29}$$

There is no term linear in $t_\perp$ here, demonstrating that the inter-chain hopping is a second-order rather than a first-order effect. In other words, we have

$$E = \langle\psi_0|\hat{H}_0|\psi_0\rangle + \langle\psi_0|\hat{H}_1|\psi_0\rangle + \mathrm{O}(\mathrm{t}_\perp^2), \tag{4.30}$$

where the term proportional to the hopping part of the Hamiltonian $\hat{H}_1$, which would be of order $t_\perp$, is zero.

This Hamiltonian was implemented and gave results as expected: For the case where hopping is attempted between two identical chains with equal numbers of electrons the hopping term returned zero, as there are no vacant states to hop between, as predicted by equations (4.30) and (4.29).

For chains where there is one more electron on one than there is on the other, a state is available for hopping and the hopping part of the Hamiltonian then returns the resultant state with a coefficient of 1, which is then scaled by the hopping coefficient $t_\perp$. Note also that in this case, in order for the creation and annihilation operators to work correctly, we need to be careful about how E_F is defined, and in fact in this case it corresponds to

$$E_F = \frac{1}{2}\left(\mathtt{HOMO} + \mathtt{LUMO}\right). \tag{4.31}$$

4.5 Convergence on the eigenstates

Now that the coupling Hamiltonian (equation (4.19)) has been implemented, it is possible to combine it with the Lanczos and/or conjugate gradient methods described in sections 3.4.3 and 3.4.2 to produce a driver subroutine that will converge either on the ground state or another low-lying eigenstate specified by the user.

To do this, we first require an efficient method of determining how close a state generated at each iteration of the driver procedure is to an eigenstate of the system—the procedure will only have converged when the correct eigenstate is obtained. The most convenient method of doing this is to make a measure of the moments of the Hamiltonian, which can tell us how broad a spread there is in the basis states resulting from the operation of the Hamiltonian on an arbitrary input state.

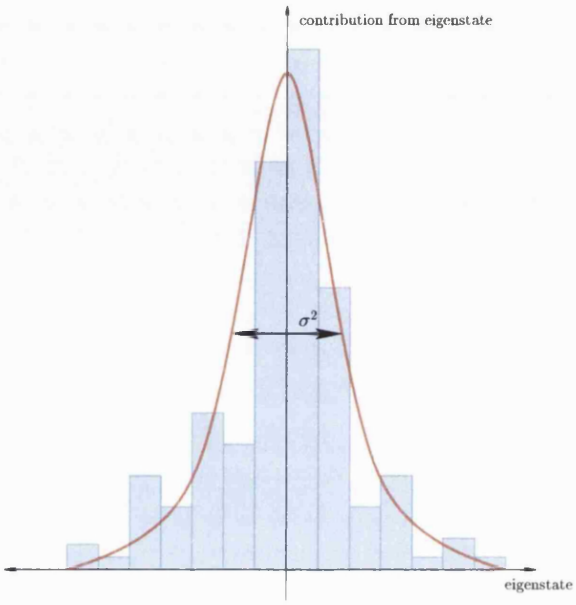

Figure 4.9: The variance σ^2 of a general state depends on its constituent spread of eigenstates. An true eigenstate of the system will have a single eigenstate contribution, and will thus have zero variance.

4.5.1 Calculating moments of the Hamiltonian

We define the variance σ^2 of a general state of the system $|\Psi\rangle = \sum_n c_n|\psi_n\rangle$, where the $|\psi_n\rangle$ are eigenstates, as

$$\begin{aligned}\sigma^2 &= \langle (E - \langle E\rangle)^2\rangle \\ &= \langle E^2\rangle - \langle E\rangle^2.\end{aligned} \tag{4.32}$$

This is depicted schematically in figure 4.9. The expectation value of the energy, $\langle E\rangle$, is defined in the standard way as

$$\langle E\rangle = \langle\Psi|\hat{H}|\Psi\rangle, \tag{4.33}$$

$$\langle E^2\rangle = \langle\Psi|\hat{H}\hat{H}|\Psi\rangle, \tag{4.34}$$

where equation (4.33) is equal to the energy E for an eigenstate. The variance gives us a measure of how close the arbitrary state $|\Psi\rangle$ is to an eigenstate of the system—a variance of zero implies that $|\Psi\rangle$ is a perfect eigenstate of the system.

We can therefore calculate σ^2 with two calls to `coupled_hamiltonian`—the first to calculate the value of $\langle\Psi|\hat{H}|\Psi\rangle$, and the second to calculate $\langle\Psi|\hat{H}\hat{H}|\Psi\rangle$,

from which the variance is given as

$$\sigma^2 = \langle \hat{H}\hat{H} \rangle - (\langle \hat{H} \rangle)^2 \tag{4.35}$$

In practice, of course, a variance of precisely zero is never encountered and therefore it is necessary to imply a realistic cutoff for the variance below which the eigenstate can be said to be effectively converged. Empirical observations showed that 10^{-16} was a suitable value for this cutoff, which typically returns the eigenvalue correct to approximately six decimal places, as compared to an analytically obtained value.

4.5.2 Lanczos vs conjugate gradient methods

While in theory the Lanczos and conjugate gradient methods are equivalent [54], in practice they have different properties that can lead to radical differences in the rate of convergence. It therefore becomes necessary to evaluate the methods' relative efficiency of converging on both the eigenvalues and eigenstates. Once both methods had been implemented, a comparison was made between the relative performance, as summarized in table 4.2. The following points, however, should be noted. Firstly, that starting from a fully randomized state, for a non-interacting system the conjugate gradient implementation showed a marked proclivity to converge not on the ground state eigenvalue but the first excited state eigenvalue (i.e. the antibonding state rather than the bonding state). Secondly, following evaluation of this comparison many further optimizations were made both to the `coupled_hamiltonian` and driver subroutines, although the extent to which the Lanczos implementation outperforms the conjugate gradient implementation is unlikely to be affected greatly by this. The Lanczos implementation was thus decided to be the superior method for eigenvalue convergence for the two coupled chains system.

	Conjugate gradient	Lanczos
Approximate number of iterations of driver routine required to obtain converged eigenvalue:	35	15
Number of calls to `coupled_hamiltonian`:	$\sim 30 \times 35 = 1050$	$\sim 1 \times 15 = 15$

Table 4.2: Convergence properties of the Lanczos and conjugate gradient methods for the eigenvalues of an $L = 4$ non-interacting system.

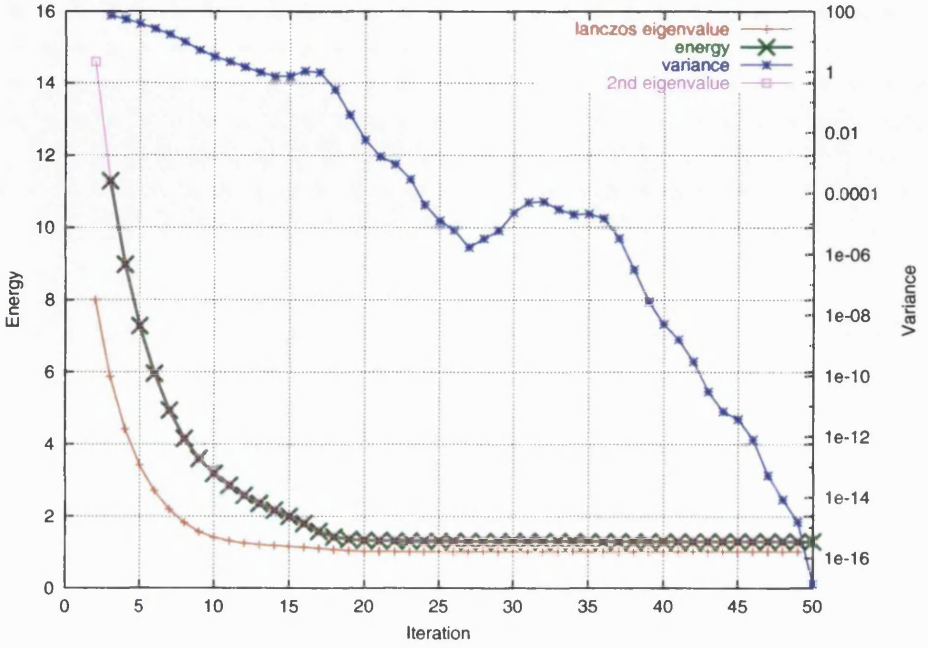

Figure 4.10: A sample run showing typical convergence properties. This is for an $L = 6, N = 2$ system with $I = 0.4$, converging on the first excited eigenstate. The Lanczos ground state eigenvalue is shown in red, the first excited state in pink. The green data indicates the eigenvalue produced by the Lanczos-calculated target eigenstate. Note that while the eigenvalue converges very quickly, within about 20 iterations, the eigenvector converges much more slowly, as indicated by the variance (right hand axis).

4.5.3 To orthogonalize or not to orthogonalize?

In view of the known problems with loss of orthogonality with the Lanczos method (see section 3.4.4 and references [54] and [61]), it was decided to include an orthogonalization step at each iteration of the driver routine, in order to ensure that orthogonality between the Lanczos vectors was being retained. A version of the Gram-Schmidt orthogonalization procedure [54] was therefore implemented in a subroutine and called at each stage of the driver routine.

However, it was found that in fact the inclusion of this orthogonalization actually *decreased* the stability of the Lanczos procedure, presumably an indicator of Haydock's prediction [61] that the real problem with the Lanczos procedure is not loss of orthogonality but loss of linear independence between the Lanczos vectors. For this reason, therefore, the call to the Gram-Schmidt orthogonalization routine was removed from the driver routine.

The results for a sample eigenstate run are shown in figure 4.10.

4.5.4 Precision and errors

Obviously, with a code such as this numerical errors will tend to accumulate. However, by maintaining a high level of accuracy throughout the calculation we believe that we have kept the accumulation of errors at a minimum. Real and complex variables have a minimum of 15 decimal digits (corresponding to a 16-byte number on most machines), and the book-keeping routines (section 4.3.8) delete only those states whose coefficient has a magnitude of less than 10^{-20}. By setting the cutoff for the variance in the eigenstate calculations (section 4.5) to 10^{-16}, we find that the eigenstates are accurate to around six decimal places, more than adequate for analysis of the results presented in chapter 5, although it will be noticed that nonetheless some numerical noise is evident in some of the results.

4.6 Parameters

Parameters involving cutoffs have already been discussed in the preceding section. Of the remaining parameters used in the code, the most important involve the form and range of the electron-electron interactions.

The choice of a specific form for the interactions $g_2(q)$ and $g_4(q)$ is arbitrary, as the Luttinger liquid remains completely solvable for any interaction that fulfils certain conditions [60]. We choose a Gaussian form for the interaction and set $g_2(q) = g_4(q) = 2\pi V(q)$ with

$$V(q) = I \exp\left(-2q^2/r\right) \tag{4.36}$$

as this has the advantage that it maintains the same form in both real and momentum space. Other forms, such as a screened Coulomb interaction, would also be possible. The parameter I can be varied to control the "strength" of the interaction, and r controls the range of the interactions. The range of the interaction was fixed at $r = 1$ for all the results presented in chapter 5, although other possible values for both the range and form of the interaction will be discussed in section 7.2. The Luttinger variables for the interacting chain A, ϕ, v_0, v_N and v_J, are dependent only on the form and strength of the interaction and the Fermi velocity v_F, and so for the interaction of equation (4.36) with $r = 1$ they are given by

$$\phi^A = \frac{1}{4} \ln\left(\frac{v_F^A}{v_F^A + 2I}\right), \tag{4.37}$$

$$v_0^A = \sqrt{v_F^{A2} + 2I v_F^A}, \tag{4.38}$$

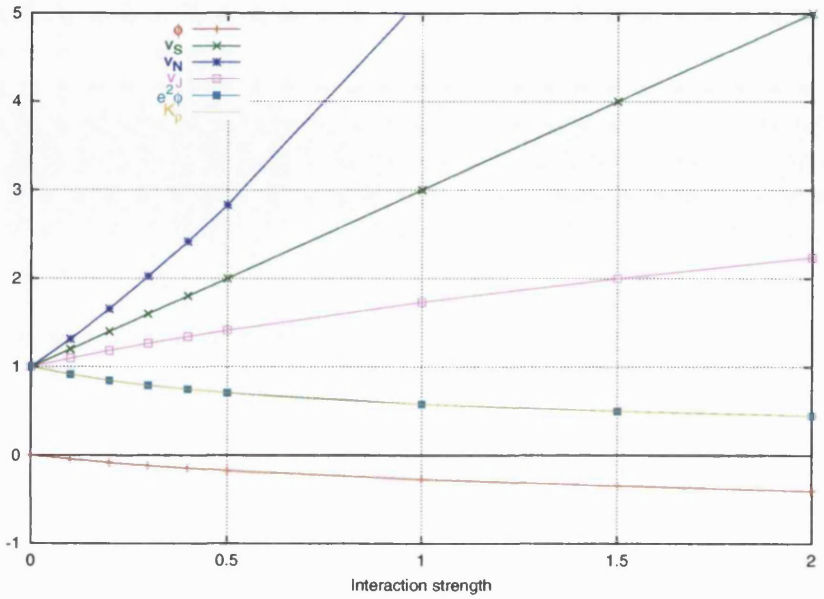

Figure 4.11: Comparison of computed Luttinger velocities for chain A with analytical results.

$$v_N^A = v_0^A e^{-2\phi^A}, \tag{4.39}$$

$$v_J^A = v_0^A e^{+2\phi^A}. \tag{4.40}$$

The Luttinger velocity K_ρ^A for chain A is then given by

$$K_\rho^A = e^{2\phi^A}. \tag{4.41}$$

These values are plotted for various interaction strengths in figure 4.11. The effect of the range parameter r on the chain-A Luttinger parameter K_ρ^A is shown in figure 4.12. The two main parameters that can be varied by the user on each run of the code are therefore the Fermi velocities v_F^A and v_F^B, which can be set individually for each chain, and the interaction strength I. The only other information required is the length of the chains, L, and the number of electrons, N.

4.7 Parallelization of the code

In order to make full use of the available computational resources, a parallel version of the code was created and run on UCL's HiPerSpace Centre SGI Origin 2000 computer.

Nearly all of the computational cost in running the code is calculating the

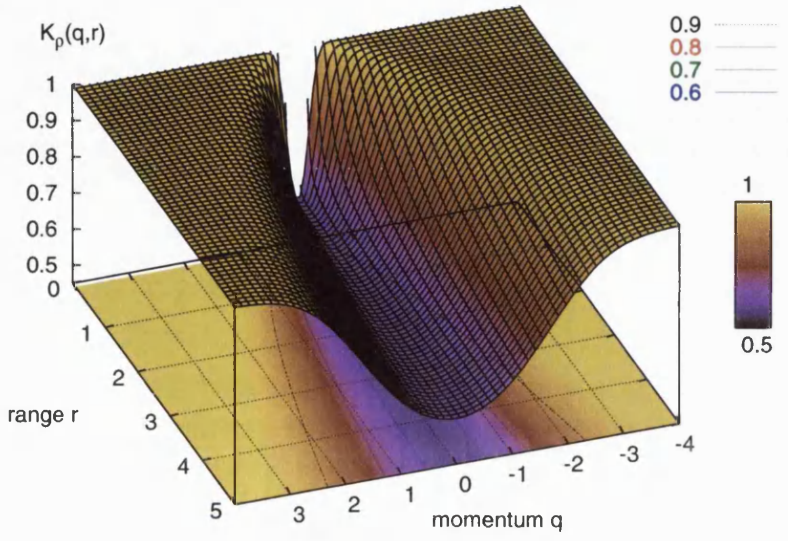

Figure 4.12: Effect on $K_\rho^A(q,r)$ of altering the range parameter r for an electron-electron interaction of the form $V(q) = I\exp\left(-2q^2/r\right)$. Note that $K_\rho^A(0,r) = K_\rho^A$, i.e. independent of range.

hopping part of the Hamiltonian,

$$\hat{H}^{\text{hopping}} = t_\perp \sum_x \left[\hat{\psi}_p^{A\dagger}\hat{\psi}_p^B + \hat{\psi}_p^{B\dagger}\hat{\psi}_p^A\right]. \tag{4.42}$$

Fortunately, since this consists of the sum of a series of calculations on the same input state, with only the value of x changing at each step, this part of the code is trivially parallelizable. To do this, the MPI (Message Passing Interface) parallelization standard was used. This is based on a master-slave paradigm—one of the computational processes acts as a master and passes out the required work to the remaining processes, the slaves.

The parallel version of the `coupled_hamiltonian` subroutine is thus essentially the same as that described in section 4.4.1, except that the main loop over x is controlled by the master process, which broadcasts the input state to the slave processes and sends each required value of x to one of the slave processes, sending a new value as soon as one of the slaves completes the current calculation. The slaves return the results of the individual x-calculation back to the master process for processing by the tidying and book-keeping routines.

In this manner it was possible to create an efficient coarse-grid parallelization of the code. However, due to the cost of communication between the processes,

the optimum number of processors to use for these calculations was found to be four—with eight processors only a marginal improvement in total computing time over the four-processor calculations was achieved.

Chapter 5

Results

Make it so.

Jean-Luc Picard, *USS Enterprise*

5.1 Introduction 113
5.2 Identical chains 113
5.3 Non-identical chains 136
5.4 Odd numbers of electrons 153
5.5 Summary 157

5.1 Introduction

In this chapter I present the main body of results for the two-chain Luttinger model. The first section (section 5.2) consists of the results of the calculations for chains with equal Fermi velocities, the salient points of which have already been published as reference [30].

This is followed by results for chains with different Fermi velocities. The rationale for this is presented fully in section 5.3, but in summary, this is intended to reflect a situation where the substrate has different properties from the wire, and in particular, has a gap in the vicinity of the Fermi energy, as would be expected for an insulating or semiconducting surface. All these sections refer to states where there are two electrons available for excitation - this is the minimum number needed to give meaningful results but enables us to analyse the underlying physics of the system fully.

The chapter concludes with some results for systems with an odd number of electrons.

5.2 Identical chains

In the first instance I have calculated for two chains that are *identical* with respect to their non-interacting properties and have equal H_0 (see section 2.3.2), in other words, the only difference between them is that the surface chain has its interaction strength set to zero throughout, but that the wire chain may have its interaction strength varied. The band structure for a typical non-interacting system of this type is shown in figure 5.1.

The results are presented in the following order: First the ground states of the system for both chain lengths $L = 4, 6$ are discussed in section 5.2.1, followed by the corresponding excited states in section 5.2.2. The spectral functions for the system are then calculated (section 5.2.3) and used to derive effective values of the Luttinger parameters K_ρ and α. Finally the conclusions we may derive from these calculations are discussed.

5.2.1 Ground states

For two coupled but non-interacting chains, it is reasonably straightforward to construct the ground state from first principles. By considering the bonding and anti-bonding bands (as in figure 5.1) we can see that it is possible to construct analytically the ground state of N electrons distributed among the two chains as follows:

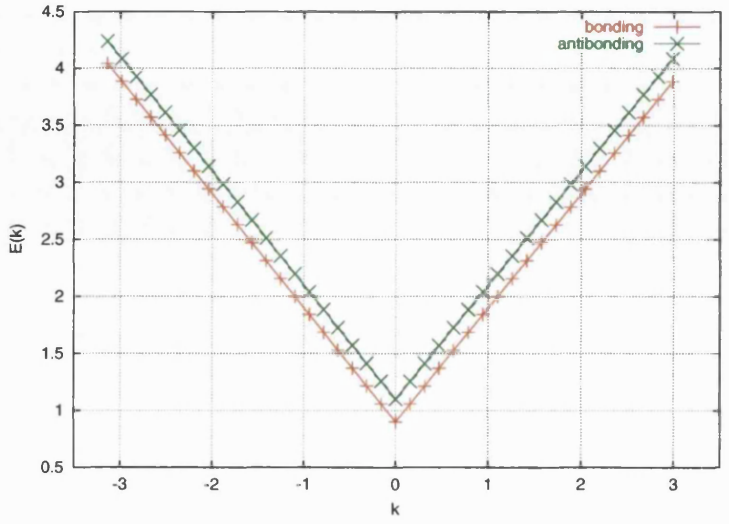

Figure 5.1: Band diagram for a system of chain length $L = 40$, both with Fermi velocity $v_F = 1$ and with coupling matrix element $t_\perp = 0.1$, thus separating the bonding and anti-bonding bands by $2t_\perp = 0.2$.

In order to avoid confusion, we designate states corresponding to chains A or B with upper case subscripts, and bonding b states or antibonding a states with lower case subscripts. Then acting on a vacuum state with no positive energy electrons with, for example, 6 creation operators results in

$$|\mathrm{gs}_{n=6}\rangle = \hat{c}^\dagger_{b(k=-2)}\hat{c}^\dagger_{a(k=+1)}\hat{c}^\dagger_{a(k=-1)}\hat{c}^\dagger_{b(k=+1)}\hat{c}^\dagger_{b(k=-1)}\hat{c}^\dagger_{b(k=0)}|0\rangle \tag{5.1}$$

where the subscripts k refer to the momentum index and the exact order of the creation operators depends on the relative energy at which they create. Note that this of course assumes that $t_\perp$ is small enough with respect to $2\pi v_F/L$ that an antibonding state with momentum $k_{|i|}$ has lower energy than an bonding state with momentum $k_{|i+1|}$. We can easily calculate the list of allowed states and their energies for the coupled chain using the earlier tight-binding results, and so by sorting these in order of ascending energy, we know which creation operators to apply in order to get the ground state.

The creation operators for the bonding and anti-bonding bands are constructed from the operators for chains A and B, viz.

$$\begin{aligned}\hat{c}^\dagger_b &= \frac{1}{\sqrt{2}}\left(\hat{c}^\dagger_A - \hat{c}^\dagger_B\right)\\ \hat{c}^\dagger_a &= \frac{1}{\sqrt{2}}\left(\hat{c}^\dagger_A + \hat{c}^\dagger_B\right)\end{aligned} \tag{5.2}$$

(assuming a positive value for $t_\perp$[1].) There are however a number of points we need to bear in mind when constructing these operators. Because the branch p is undefined at $k = 0$, we cannot create (or annihilate) there and so we neglect all states at $k = 0$ (in fact we assume that for each chain the state at $k = 0$ is always occupied).

The non-interacting ground states of the two coupled chains can therefore be constructed as detailed in table 5.1

No. of electrons	ground state
1	$\frac{1}{\sqrt{2}}|$00001 0 0 0 ; 00001 -1 1 0$\rangle$ - $\frac{1}{\sqrt{2}}|$00001 -1 1 0 ; 00001 0 0 0$\rangle$
2	$-\frac{i}{2}|$00001 0 1 1 ; 00001 0 0 0$\rangle$ $-\frac{i}{2}|$00001 -1 1 0 ; 00001 1 0 1$\rangle$ $+\frac{i}{2}|$00001 1 0 1 ; 00001 -1 1 0$\rangle$ $-\frac{i}{2}|$00001 0 0 0 ; 00001 0 1 1$\rangle$
3	$+\frac{i}{\sqrt{2}}|$00001 0 1 1 ; 00001 -1 1 0$\rangle$ $+\frac{i}{\sqrt{2}}|$00001 -1 1 0 ; 00001 0 1 1$\rangle$
4	$+1|$00001 0 1 1 ; 00001 0 1 1$\rangle$
5	$+\frac{i}{\sqrt{2}}|$00001 -1 2 1 ; 00001 0 1 1$\rangle$ $-\frac{i}{\sqrt{2}}|$00001 0 1 1 ; 00001 -1 2 1$\rangle$

Table 5.1: Table of ground states for 1 - 5 electrons in two coupled chains each of length 4 sites. This could be extended to chains of any length as long as there are enough available sites on each chain to accommodate all the electrons. While the phases of these states are in principle arbitrary, the phases shown here give $\hat{c}^\dagger|\mathrm{gs}_{n=i}\rangle = |\mathrm{gs}_{n=i+1}\rangle$.

While the ground state of such non-interacting systems may be calculated from first principles in this way, for the purposes of checking the code, it is more useful to verify that the Lanczos based subroutines described in chapter 3 are operating correctly by setting the interaction strength on both chains to zero and confirming that we do indeed obtain results equivalent to these manual calculations.

[1]The assumption of a positive value for $t_\perp$ leads to a rather unfamiliar form in which the signs for the bonding and antibonding combinations are reversed from the standard convention. Note however that this could be transformed to the conventional $t_\perp < 0$ form without affecting any of the results presented here.

The results of a sample calculation of the ground state for a system with $L = 4$, $N = 2$ and $t_\perp = 0.1$ are

```
(  0.113000E+00  0.487100E+00) *| 00001  0  1  1 ; 00001  0  0  0 >
( -0.113000E+00 -0.487100E+00) *| 00001 -1  1  0 ; 00001  1  0  1 >
(  0.113000E+00  0.487100E+00) *| 00001  1  0  1 ; 00001 -1  1  0 >
(  0.113000E+00  0.487100E+00) *| 00001  0  0  0 ; 00001  0  1  1 >
```

A second calculation gave the result:

```
( -0.49931730E+00  0.26120872E-01) *| 00001  0  1  1 ; 00001  0  0  0 >
( -0.49931730E+00  0.26120902E-01) *| 00001 -1  1  0 ; 00001  1  0  1 >
(  0.49931724E+00 -0.26120916E-01) *| 00001  1  0  1 ; 00001 -1  1  0 >
( -0.49931709E+00  0.26120883E-01) *| 00001  0  0  0 ; 00001  0  1  1 >
```

It can be seen that the exact phase of the result is arbitrary, as expected, and actually depends only on the (random) phase of the start state for the Lanczos procedure. However, it is obvious that the calculated ground state for this system, as expected, has equal magnitude of electrons on either branch of either chain as the manual results.

The ground and neutral first excited states were then calculated (with the interaction form as described in section 4.6) for different interaction strengths I on the "wire" chain A. Sample results for these calculations are shown in table 5.3, and it will be immediately noticed that the interacting ground states include basis states with bosons on the interacting chain A, and also that there is (at somewhat lower magnitude) a non-zero contribution from basis states containing bosons on the *non-interacting* chain B. This occurs because, as detailed in chapter 3, we have chosen to work with a Hilbert space with a set of basis states consisting of the untransformed boson operators, i.e. the $\hat{a}^\dagger, \hat{a}$ operators rather than the transformed $\hat{b}^\dagger, \hat{b}$ boson operators of equation (2.56). The amplitude for states with bosons on chain B only is negligble, as implied by equation (5.3).

Each eigenstate of the system can be decomposed into basis states with no bosons on either chain, bosons on chain A only, or bosons on both chains. As the states are normalized, we therefore have

$$\sum |\text{neither}|^2 + \sum |\text{A-only}|^2 + \sum |\text{both}|^2 = 1 \qquad (5.3)$$

where $\sum |\text{neither}|^2$ refers to the sum of the squares of the coefficients of all the basis states with no bosons on either chain, etc. We can plot the relationship between the interaction strength and the boson contributions from each chain for all the calculated states, as in figures 5.2 and 5.3. Also included in these plots

I	Ground state
0.5	(0.1783E-01 0.2090E-01) *| 00001 0 1 1 ; 00001 0 0 0 > (0.1442E+00 0.1690E+00) *| 00001 -1 1 0 ; 00001 1 0 1 > (-0.1442E+00 -0.1690E+00) *| 00001 1 0 1 ; 00001 -1 1 0 > (0.6158E+00 0.7220E+00) *| 00001 0 0 0 ; 00001 0 1 1 > (-0.3054E-04 -0.3621E-04) *| 00009 -1 1 0 ; 00003 1 0 1 > (-0.7912E-05 -0.9618E-05) *| 00009 0 0 0 ; 00003 0 1 1 > (0.3037E-04 0.3630E-04) *| 00003 1 0 1 ; 00009 -1 1 0 > (-0.6737E-05 -0.9673E-05) *| 00003 0 0 0 ; 00009 0 1 1 > (-0.2098E-04 -0.2484E-04) *| 00011 0 1 1 ; 00001 0 0 0 > (-0.2273E-03 -0.2663E-03) *| 00011 -1 1 0 ; 00001 1 0 1 > (0.2270E-03 0.2667E-03) *| 00011 1 0 1 ; 00001 -1 1 0 > (-0.1089E-02 -0.1278E-02) *| 00011 0 0 0 ; 00001 0 1 1 >
1.0	(0.6396E-02 -0.4354E-02) *| 00001 0 1 1 ; 00001 0 0 0 > (0.1013E+00 -0.6893E-01) *| 00001 -1 1 0 ; 00001 1 0 1 > (-0.1013E+00 0.6894E-01) *| 00001 1 0 1 ; 00001 -1 1 0 > (0.8141E+00 -0.5542E+00) *| 00001 0 0 0 ; 00001 0 1 1 > (-0.7285E-04 0.4970E-04) *| 00009 -1 1 0 ; 00003 1 0 1 > (-0.9116E-05 0.6210E-05) *| 00009 0 0 0 ; 00003 0 1 1 > (0.7288E-04 -0.4973E-04) *| 00003 1 0 1 ; 00009 -1 1 0 > (-0.9085E-05 0.6168E-05) *| 00003 0 0 0 ; 00009 0 1 1 > (-0.1147E-04 0.7863E-05) *| 00011 0 1 1 ; 00001 0 0 0 > (-0.2881E-03 0.1961E-03) *| 00011 -1 1 0 ; 00001 1 0 1 > (0.2881E-03 -0.1961E-03) *| 00011 1 0 1 ; 00001 -1 1 0 > (-0.2888E-02 0.1966E-02) *| 00011 0 0 0 ; 00001 0 1 1 >
2.0	(-0.1131E-02 0.1652E-02) *| 00001 0 1 1 ; 00001 0 0 0 > (-0.3561E-01 0.5200E-01) *| 00001 -1 1 0 ; 00001 1 0 1 > (0.3561E-01 -0.5200E-01) *| 00001 1 0 1 ; 00001 -1 1 0 > (-0.5628E+00 0.8217E+00) *| 00001 0 0 0 ; 00001 0 1 1 > (0.8406E-04 -0.1223E-03) *| 00009 -1 1 0 ; 00003 1 0 1 > (-0.8387E-04 0.1223E-03) *| 00003 1 0 1 ; 00009 -1 1 0 > (0.1690E-03 -0.2463E-03) *| 00011 -1 1 0 ; 00001 1 0 1 > (-0.1694E-03 0.2466E-03) *| 00011 1 0 1 ; 00001 -1 1 0 > (0.3980E-02 -0.5810E-02) *| 00011 0 0 0 ; 00001 0 1 1 >

Table 5.3: Ground states for the $L = 4$, $N = 2$, $t_\perp = 0.1$ systems for various interaction strengths I. States with an absolute coefficient of less than 10^{-5} have been omitted

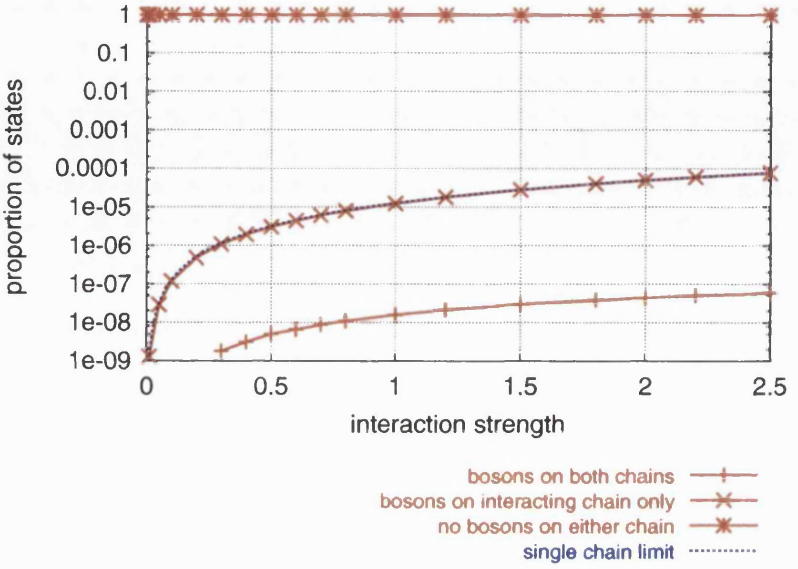

Figure 5.2: Contribution of bosonic basis states to the ground states of the $L = 4$, $N = 2$, $t_\perp = 0.1$ system as a function of interaction strength I.

is the boson contribution expected on a single, isolated continuum Luttinger liquid chain for the same interaction form and strength. This is calculated as follows.

Since the Bogoliubov transformation of the boson operators is defined as

$$\begin{aligned} \hat{b_q}^\dagger &= \cosh\phi_q \hat{a}_q^\dagger - \sinh\phi_q \hat{a}_{-q} \\ \hat{b_q} &= \cosh\phi_q \hat{a}_{-q} - \sinh\phi_q \hat{a}_q^\dagger \end{aligned} \tag{5.4}$$

we can invert this to give the untransformed boson operators in terms of the transformed ones:

$$\begin{aligned} \hat{a_q}^\dagger &= \cosh\phi_q \hat{b}_q^\dagger - \sinh\phi_q \hat{b}_{-q} \\ \hat{a_q} &= \cosh\phi_q \hat{a}_q - \sinh\phi_q \hat{a}_{-q}^\dagger \end{aligned} \tag{5.5}$$

Now if we consider just a single boson mode q, we can count the number of untransformed bosons in this mode in the ground state of the Bogoliubov-transformed Hilbert space, $|\tilde{0}\rangle$:

$$\begin{aligned} \langle\tilde{0}|\hat{a}_q^\dagger\hat{a}_q|\tilde{0}\rangle &= \langle\tilde{0}|\left(\cosh\phi_q\hat{b}_q^\dagger + \sinh\phi_q\hat{b}_{-q}\right)\left(\cosh\phi_q\hat{b}_q + \sinh\phi_q\hat{b}_{-q}^\dagger\right)|\tilde{0}\rangle \\ &= \langle\tilde{0}|\sinh^2\phi_q\hat{b}_q\hat{b}_{-q}^\dagger|\tilde{0}\rangle \\ &= \sinh^2\phi_q. \end{aligned} \tag{5.6}$$

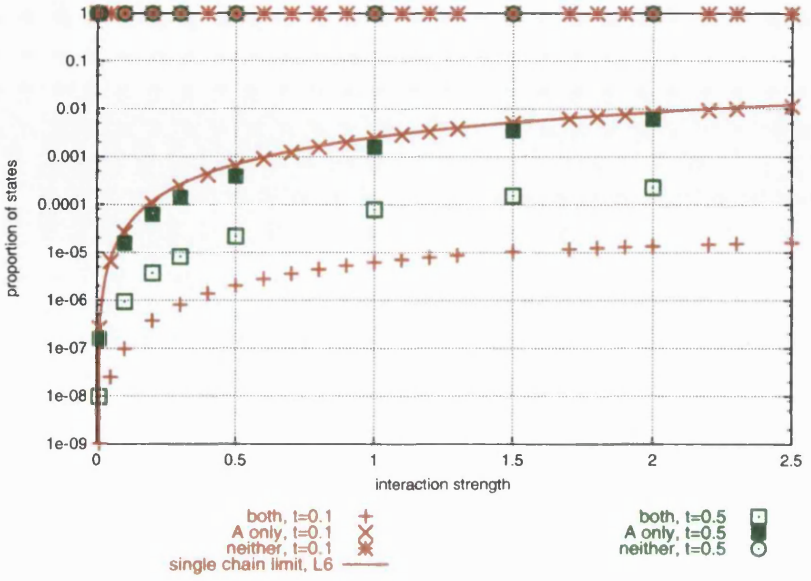

Figure 5.3: Contribution of bosonic basis states to the ground states of the $L = 6$, $N = 2$, $t_\perp = 0.1$ and $L = 6$, $N = 2$, $t_\perp = 0.5$ systems as a function of interaction strength I. See text for a full explanation.

Therefore we can sum over all the modes q to give the total number of untransformed bosons in this ground state.

$$\text{no. of bosons} = \sum_q \sinh^2 \phi_q, \tag{5.7}$$

where ϕ_q is determined by the form and strength of the interaction on chain A (see section 4.6).

The single-LL data match almost exactly those for the the interacting chain for both $L = 4$ and $L = 6$, with $t_\perp = 0.1$ and $t_\perp = 0.5$. This suggests that, for both values of $t_\perp$, we are in a regime where the two chains can said to be weakly coupled.

5.2.2 Excited states

When considering the neutral excited states of this system it is extremely informative to consider the $L = 4, N = 2$ states as a specific simple example. In order to do this I now now introduce a graphical representation of glyphs based on both the bonding and antibonding band structures of the non-interacting system (such as figure 5.1), and the individual chains' band structures. This will allow us to understand fully the effects of adding interactions to the non-interacting system.

In this glyph scheme the bonding and antibonding bands are labelled by lowercase b and a respectively, while the individual bands for chain A and chain B (that relate directly to individual zero-boson basis states) are labelled by an uppercase A or B as appropriate. Empty states are represented by empty circles, filled states in the bonding-antibonding glyphs are represented by filled green circles, in the separate chain glyphs by filled red circles. Therefore the glyph

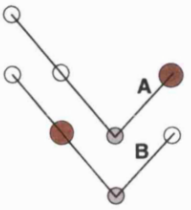

represents a state where there is one electron in the $k = \pi/2$ state on chain A, and one electron in the $k = -\pi/2$ state on chain B:

```
| 00001  1  0  1 ; 00001 -1  1  0 >
```

whereas the glyph

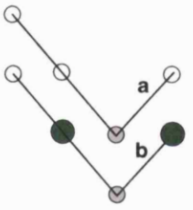

indicates that there are two electrons filling states in the bonding band at $k = -\pi/2$ and $k = \pi/2$. In fact this is the non-interacting ground state described fully in section 5.2.1 and is the 2-electron state of table 5.1.

While this is the sole ground state for this system, there are a number of ways of forming a combination of bonding and antibonding states with these 2 electrons, leading to a 4-fold degeneracy of the first excited state, as shown in figure 5.4. Once we include interactions, however weak, this degeneracy is lifted. This is perhaps clearer when we deconstruct these states into their constituent chain A and chain B bases.

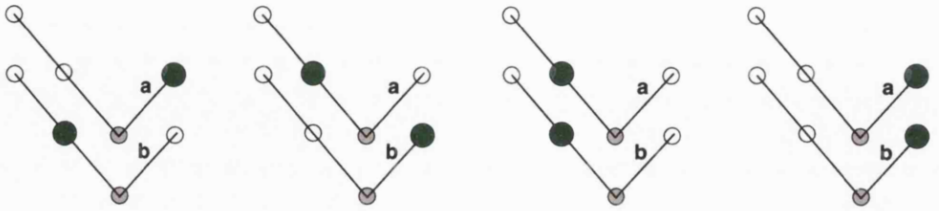

(a) State α (b) State β (c) State γ (d) State δ

Figure 5.4: Degenerate first excited states for 2 electrons

Firstly state α:

$$
\begin{aligned}
&= \hat{c}^\dagger_{b-}\hat{c}^\dagger_{a+}|0\rangle \\
&= \left(\hat{c}^\dagger_{A-} - \hat{c}^\dagger_{B-}\right)\left(\hat{c}^\dagger_{A+} + \hat{c}^\dagger_{B+}\right)|0\rangle \\
&= \left(\hat{c}^\dagger_{A-}\hat{c}^\dagger_{A+} + \hat{c}^\dagger_{A-}\hat{c}^\dagger_{B+} - \hat{c}^\dagger_{B-}\hat{c}^\dagger_{A+} - \hat{c}^\dagger_{B-}\hat{c}^\dagger_{B+}\right)|0\rangle \\
&=
\end{aligned}
\tag{5.8}
$$

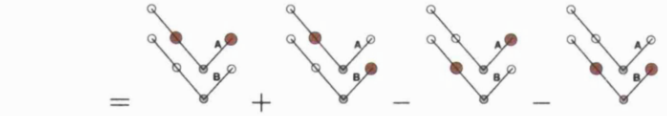

Now β:

$$
\begin{aligned}
&= \hat{c}^\dagger_{a-}\hat{c}^\dagger_{b+}|0\rangle \\
&= \left(\hat{c}^\dagger_{A-} + \hat{c}^\dagger_{B-}\right)\left(\hat{c}^\dagger_{A+} - \hat{c}^\dagger_{B+}\right)|0\rangle \\
&= \left(\hat{c}^\dagger_{A-}\hat{c}^\dagger_{A+} - \hat{c}^\dagger_{A-}\hat{c}^\dagger_{B+} + \hat{c}^\dagger_{B-}\hat{c}^\dagger_{A+} - \hat{c}^\dagger_{B-}\hat{c}^\dagger_{B+}\right)|0\rangle \\
&=
\end{aligned}
\tag{5.9}
$$

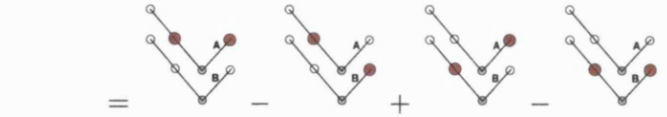

State γ:

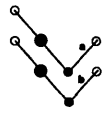

$$\begin{aligned} &= \hat{c}^\dagger_{a-}\hat{c}^\dagger_{b-}|0\rangle \\ &= \left(\hat{c}^\dagger_{A-} + \hat{c}^\dagger_{B-}\right)\left(\hat{c}^\dagger_{A-} - \hat{c}^\dagger_{B-}\right)|0\rangle \\ &= \left(\hat{c}^\dagger_{A-}\hat{c}^\dagger_{A-} - \hat{c}^\dagger_{A-}\hat{c}^\dagger_{B-} + \hat{c}^\dagger_{B-}\hat{c}^\dagger_{A-} - \hat{c}^\dagger_{B-}\hat{c}^\dagger_{B-}\right)|0\rangle \end{aligned} \tag{5.10}$$

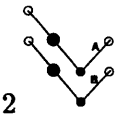

$= 2$

And finally δ:

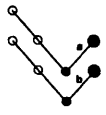

$$\begin{aligned} &= \hat{c}^\dagger_{a+}\hat{c}^\dagger_{b+}|0\rangle \\ &= \left(\hat{c}^\dagger_{A+} + \hat{c}^\dagger_{B+}\right)\left(\hat{c}^\dagger_{A+} - \hat{c}^\dagger_{B+}\right)|0\rangle \\ &= \left(\hat{c}^\dagger_{A+}\hat{c}^\dagger_{A+} - \hat{c}^\dagger_{A+}\hat{c}^\dagger_{B+} + \hat{c}^\dagger_{B+}\hat{c}^\dagger_{A+} - \hat{c}^\dagger_{B+}\hat{c}^\dagger_{B+}\right)|0\rangle \end{aligned} \tag{5.11}$$

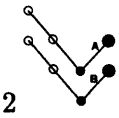

$= 2$

Notice that states α and β each contain states that are strongly "ionic" in nature – i.e. the electrons are both confined to one chain. The rest of the states are more "covalent" in nature – one electron on each chain. We shall see that in fact these purely ionic states are strongly suppressed as soon as interactions are added, but are present in the ground state. States γ and δ however, have non-zero net momentum. Note also that there is no adequate way of representing the influence of the bosons by this method.

With this analysis in place we are now in a position to examine fully the excited states of the interacting system. By taking the calculated eigenstates for $L = 4, 6$ and $N = 2$, we can deconstruct the states in to the contributions from states with both electrons on chain A ("ionic-A"), both electrons on chain B ("ionic-B"), and one electron on each chain ("covalent"). This is plotted for both the ground states and the excited states as a function of interaction strength in figures 5.5 and 5.6. It can be seen that while the interacting ground states evolve smoothly from the non-interacting ground state, there is a discontinuity in the charge distribution of the excited states as soon as even very

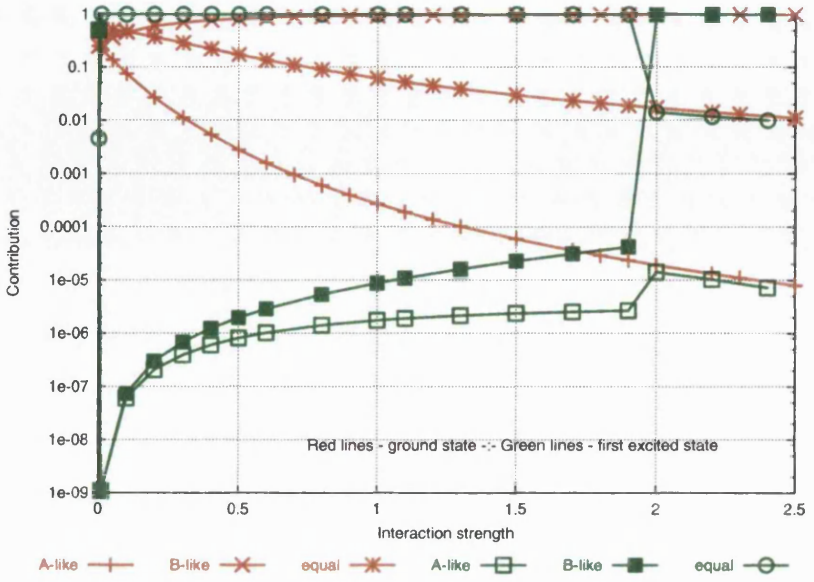

Figure 5.5: Contributions to the ground and first excited states for the $L = 6$, $N = 2$, $t_\perp = 0.1$ system from electrons on each chain as a function of interaction strength I. See text for a full explanation.

weak interactions are included. Table 5.4 shows the calculated eigenstates for the first excited states at interaction strengths $I = 0.0, 0.01$ and 0.1. It will be observed that the ionic contributions (the first and last basis states of the $I = 0.0$ state), strongly present in the non-interacting state, are absent in even the very weakly interacting states.

Now that we have both the ground and excited states, the nature of the neutral excitations can be probed. The excitation energies for the $L = 4$ and $L = 6$ systems are plotted as a function of I in figures 5.7 and 5.8. For the $L = 6$ case, we can see that the ground state energy has a region of roughly linear dependence on I in the region $0 \lesssim I \lesssim 0.5$ and thereafter is rather less dependent on I.

The first excited state, however, is linear in I for $I \lesssim 2.0$, at which point it becomes completely independent of I. The $L = 4$ states follow a similar pattern, except that the dependence on I of the ground state energy for $I \lesssim 2.0$ is rather stronger than that for $L = 6$. For both cases, however, we see that the non-interacting excitation energy is equal to $2t_\perp$, indicating that for this size of system the first excitation is one between the bonding and antibonding bands with zero net momentum change. As the interactions increase in strength, the bonding and antibonding bands begin to distort, and since, as we have already seen, the excited states are rather more sensitive to the presence of interactions

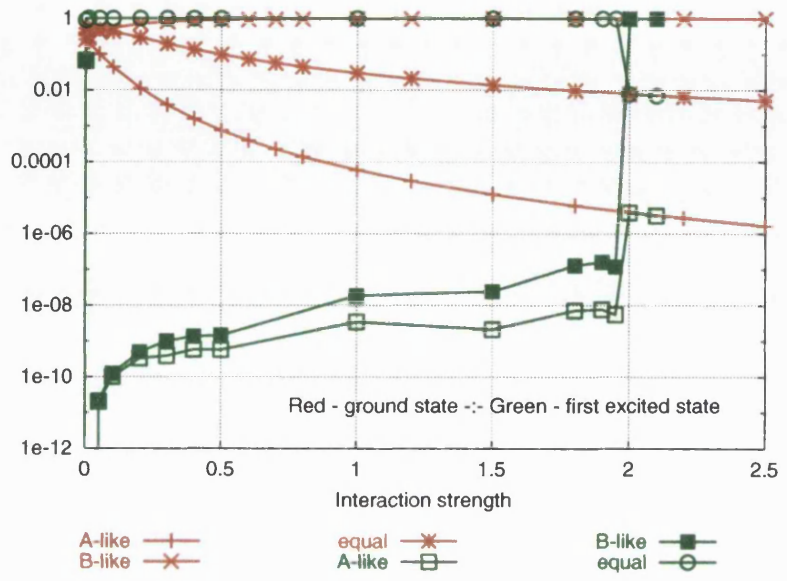

Figure 5.6: Contributions to the ground and first excited states for the $L = 4$, $N = 2$, $t_\perp = 0.1$ system from electrons on each chain as a function of interaction strength I. See text for a full explanation.

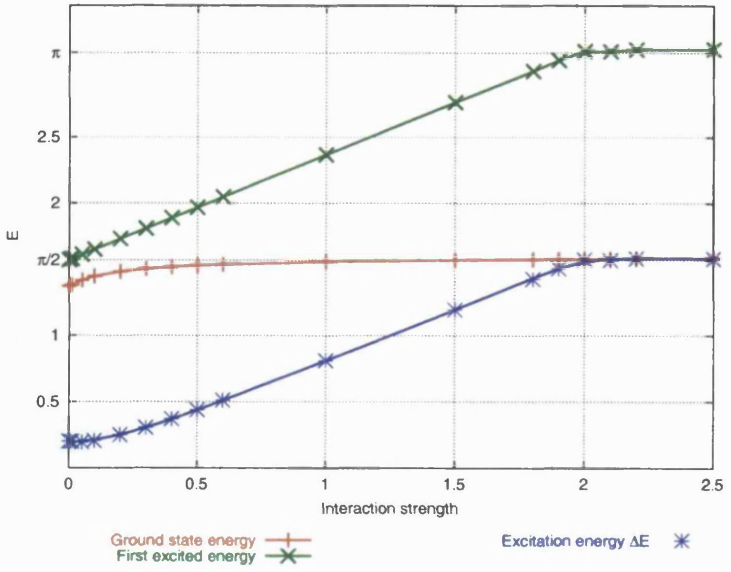

Figure 5.7: Energies for the ground state and neutral first excited state for the $L = 4$, $N = 2$, $t_\perp = 0.1$ system as a function of interaction strength I.

I	First neutral excited state
0.0	(0.1443E+00 0.2132E+00) *| 00001 0 1 1 ; 00001 0 0 0 > (-0.3393E+00 0.4936E+00) *| 00001 -1 1 0 ; 00001 -1 1 0 > (-0.5586E-01 0.8073E-01) *| 00001 -1 1 0 ; 00001 1 0 1 > (-0.5586E-01 0.8073E-01) *| 00001 1 0 1 ; 00001 -1 1 0 > (-0.3746E+00 0.5908E+00) *| 00001 1 0 1 ; 00001 1 0 1 > (-0.1443E+00 -0.2132E+00) *| 00001 0 0 0 ; 00001 0 1 1 >
0.01	(0.4108E+00 0.4612E+00) *| 00001 -1 1 0 ; 00001 -1 1 0 > (-0.1597E+00 -0.2148E+00) *| 00001 -1 1 0 ; 00001 1 0 1 > (-0.1597E+00 -0.2148E+00) *| 00001 1 0 1 ; 00001 -1 1 0 > (-0.3882E+00 0.5697E+00) *| 00001 1 0 1 ; 00001 1 0 1 > (-0.1480E-04 -0.1661E-04) *| 00011 -1 1 0 ; 00001 -1 1 0 > (0.1395E-04 -0.2048E-04) *| 00011 1 0 1 ; 00001 1 0 1 >
0.1	(0.5760E+00 -0.3206E+00) *| 00001 -1 1 0 ; 00001 -1 1 0 > (0.4682E+00 -0.6886E-01) *| 00001 -1 1 0 ; 00001 1 0 1 > (0.4682E+00 -0.6886E-01) *| 00001 1 0 1 ; 00001 -1 1 0 > (-0.3323E+00 -0.8434E-01) *| 00001 1 0 1 ; 00001 1 0 1 > (-0.2074E-03 0.1154E-03) *| 00011 -1 1 0 ; 00001 -1 1 0 > (-0.1686E-03 0.2479E-04) *| 00011 -1 1 0 ; 00001 1 0 1 > (-0.1686E-03 0.2479E-04) *| 00011 1 0 1 ; 00001 -1 1 0 > (0.1194E-03 0.3031E-04) *| 00011 1 0 1 ; 00001 1 0 1 >

Table 5.4: First neutral excited states for the $L = 4$, $N = 2$, $t_\perp = 0.1$ systems for various interaction strengths I. Note that the $I = 0.0$ state is a combination of the four degenerate states $\alpha, \beta, \gamma, \delta$ of figure 5.4. States with an absolute coefficient of less than 10^{-5} have been omitted

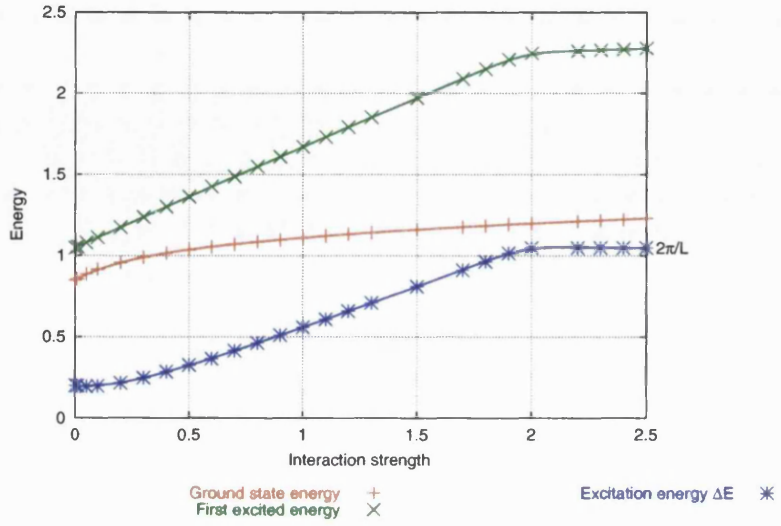

Figure 5.8: Energies for the ground state and neutral first excited state for the $L = 6$, $N = 2$, $t_\perp = 0.1$ system as a function of interaction strength I.

than the ground states, the gap between the ground and excited states begins to widen. Eventually, however, the bands are distorted to such an extent that, at $I \approx 2.0$, in both cases the lowest excitation becomes not one *between* bands with zero net momentum change, but an intraband one with net momentum change $2\pi v_F/l$.

It is at this point, however, that we notice that something rather interesting has occurred — for a Luttinger liquid, we would expect the velocity v in this expression to be the Luttinger velocity v_0 (as in equation (2.17)) rather than the Fermi velocity v_F, leading to a continued I-dependence for ΔE. However, it is clear from figures 5.8 and 5.7 that this is not the case for either of these systems: the excitation energy for $I \gtrsim 2.0$ remains constant and equal to $2\pi v_\mathrm{F}/L = \pi/3$ for $L = 6$ and $\pi/2$ for $L = 4$. (Remember that for these examples $v_\mathrm{F} = 1$.) This can be explained as follows — as I is increased the single-chain energy levels on chain A increase (since the interaction is repulsive), while those on the non-interacting chain B remain constant. It therefore becomes energetically preferable for the electrons to move to the non-interacting chain B rather than remain on the (interacting) chain A, until the point is reached at which the system is predominantly populated by electrons on chain B. This chain is still Fermi liquid-like, thus shifting the properties of the system as a whole back from partially Luttinger liquid-like to Fermi liquid-like.

This is confirmed by a reexamination of the location of the electrons for both the ground and first excited states (as in figures 5.5 and 5.6). First consider the

ground states. We have already seen that for the non-interacting ground state the electrons are distributed equally between the chains, and once interactions are switched on we evolve continuously towards a regime where basis states with electrons on chain A are strongly suppressed in favour of states with both electrons on chain B. We have also already explained the discontinuity in the excited states at $I = 0.0$.

However, there is a second discontinuity in the excited states just below $I = 2.0$, the point at which the nature of the excitations changes from zero net momentum change to $\Delta k = 2\pi v_{\mathrm{F}}/L$. The electron contributions from this point for the excited states match those for the ground state. This would indicate that there is no interchain electron hopping involved in these excitations, and as both the ground and excited states are dominated by chain B basis states, this would support the conclusion that these states are likely to be more Fermi liquid-like than Luttinger liquid-like.

5.2.3 Spectral functions

The spectral function is defined as

$$\rho(q,\omega)_{p,c} = -\frac{1}{\pi}\Im\left[G^R_{p,c}(k_{\mathrm{F}}+q,\omega+\mu)\right], \tag{5.12}$$

with $q = k_{\mathrm{F}} - k$, and the retarded Green's function $G^R_{p,c}$ defined as the double Fourier transform of

$$G^R_{p,c}(x,t) = -\mathrm{i}\theta(t)\langle\{\hat{\psi}_{p,c}(x,t),\hat{\psi}^\dagger_{p,c}(0,0)\}\rangle, \tag{5.13}$$

and thus describes the ability of the system to absorb or emit an electron of energy ω. This is identical to equation (3.28) of chapter 3, with the addition of the branch index p and the chain index c.

The relationship between the Green's function $G^R_{p,c}$ and the spectral function has already been discussed in section 2.4, as has a review of spectral function calculations for Luttinger liquid systems (section 1.5.2).

As it is not possible to obtain an analytical form for the spectral function of this system [97, 129, 148], we utilize the numerical methods discussed in section 3.4.7 to calculate the Green's function

$$G^R(k,k',\omega) = \langle N|\hat{c}_k\left[\omega-\hat{H}+\varepsilon_N\right]^{-1}\hat{c}^\dagger_{k'}|N\rangle + \langle N|\hat{c}^\dagger_{k'}\left[\omega+\hat{H}-\varepsilon_N\right]^{-1}\hat{c}_k|N\rangle. \tag{5.14}$$

In order to ensure convergence, we put $\omega \to \omega + \mathrm{i}\eta$, where η is an imaginary component of the energy roughly equal to the level spacing of the system [61].

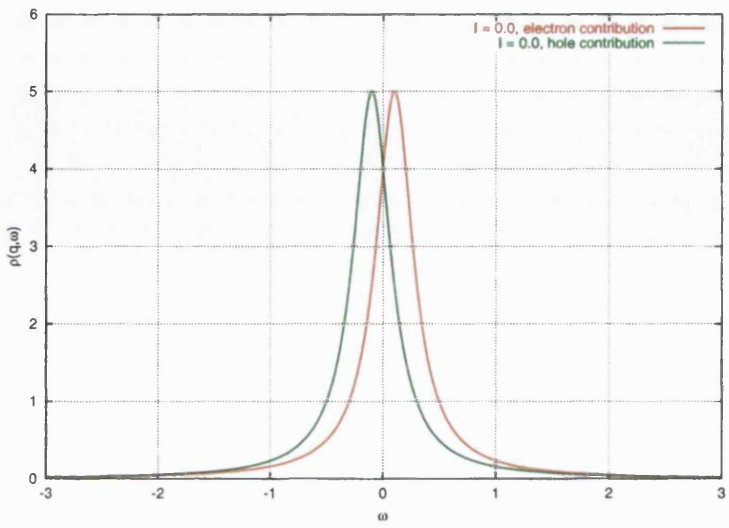

Figure 5.9: Hole (left peak) and electron (right peak) contributions to the spectral function $\rho(q = 0, \omega)$. $t_\perp = 0.1$, $\eta = 2t_\perp$ for two non-interacting chains ($I = 0.0$). In order to show the splitting clearly, the electron and hole contributions are shown as equal in magnitude.

$|N\rangle$ is the N-electron ground state, with energy ε_N.

As previously discussed, for a Fermi liquid we would expect the spectral function for $q = 0$ (i.e. absorption or emission of an electron at the Fermi energy) to be a delta function (corresponding to the step function discontinuity in the density of states). The calculated spectral function $\rho(q = 0, \omega)$ for our non-interacting system is plotted in figure 5.9[2].

It will be noticed immediately that this is not a delta function. In fact, there are two sources of deviation from the expected result. Firstly, the two peaks, separated by $2t_\perp$ ($= 0.2$ in this example) arises from the splitting of the energy levels into bonding and antibonding bands. Secondly, the two peaks are broadened from delta functions into Lorentzians by the presence of the imaginary energy η in the calculations. Figure 5.10 shows the numerical results overlaid with Lorentzians

$$P(x) = \frac{1}{\pi} \frac{1/2\eta}{(x - \varepsilon)^2 + (1/2\eta)^2} \tag{5.15}$$

of width η and centred on the eigenvalues ε, showing a clear agreement. Figure 5.11 shows the results for interacting systems with various interaction

[2]Except where explicitly stated otherwise, all the spectral functions presented here are normalized such that the hole and electron parts have equal magnitude. This enables us to calculate accurately the *position* of the peaks.

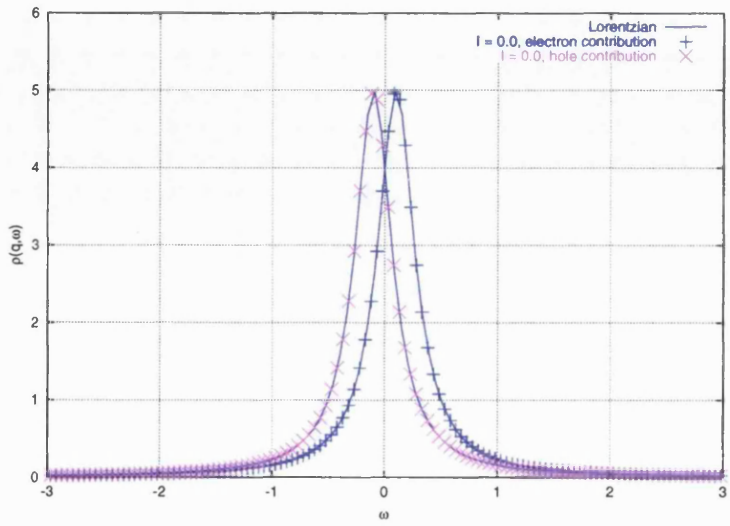

Figure 5.10: Calculated data (points) and Lorentzians $\frac{1}{\pi}\frac{1/2\eta}{(x-\varepsilon)^2+(1/2\eta)^2}$ (lines) centred on the eigenvalues. The plots have been shifted to be symmetric about $\omega = 0$

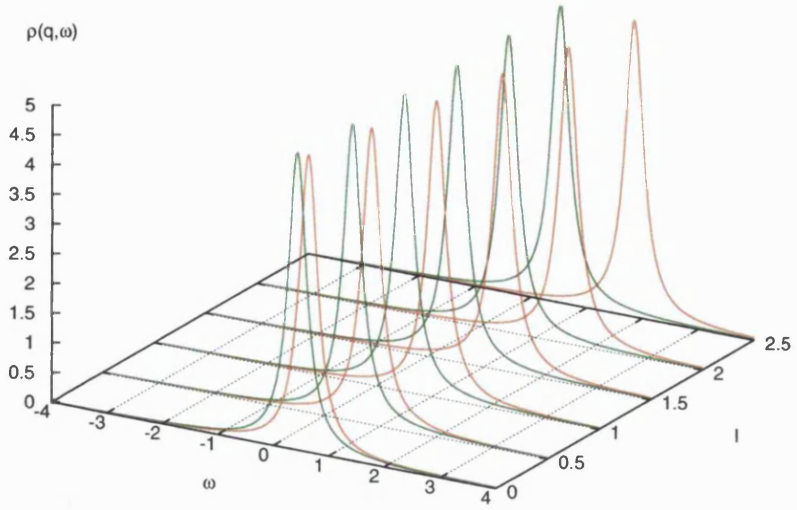

Figure 5.11: Spectral functions $\rho(0,\omega)$ for various interaction strengths. The hole contributions are shown in green, the electron contributions in red.

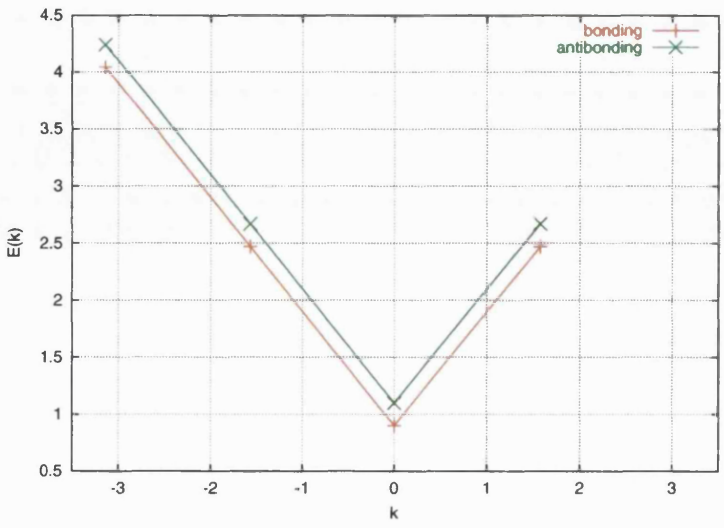

Figure 5.12: Band structure for a $L = 4$ system. There is only one k-state on the right hand ($p = +1$) branch, and hence the $q \neq 0$ spectral function can only be calculated for the left hand ($p = -1$) branch.

strengths I. It will be noticed that a further broadening of the peaks is evident, and furthermore, that this separation is dependent of the interaction strength. This is a clear indicator of Luttinger liquid-like behaviour.

We can also calculate the spectral functions for $q \neq 0$. However, due to the size and discrete nature of our system, there are severe limitations on the number of values of q that can be used. For example, for $L = 4$ and $N = 2$ (where we have $k_F = \pi/2$) the only value of q that is possible is

$$q = |k - k_F| = | - \pi - (-\pi/2)| = \pi/2 \tag{5.16}$$

as the negative-momentum branch is the only one with more than one k-value (as can be seen from figure 5.12).

For the $L = 6$ system, we have a choice of two values of q — either $|k - k_F| = -\pi/3$ or $-2\pi/3$. We can now also calculate for either momentum branch of the system, as can be seen from figure 5.13.

We find that, as before, the hole part of the spectral function is strongly suppressed, but increases as the interaction strength is increased. In general however, for the interaction strengths considered here, the hole contribution to the spectral function is of the order of 10^7 times smaller than the electron contribution. Since we are more interested in the position of the electron and hole peaks rather than their magnitude, we normalize the hole part of the calculations to be of roughly the same magnitude as the electron part, thus

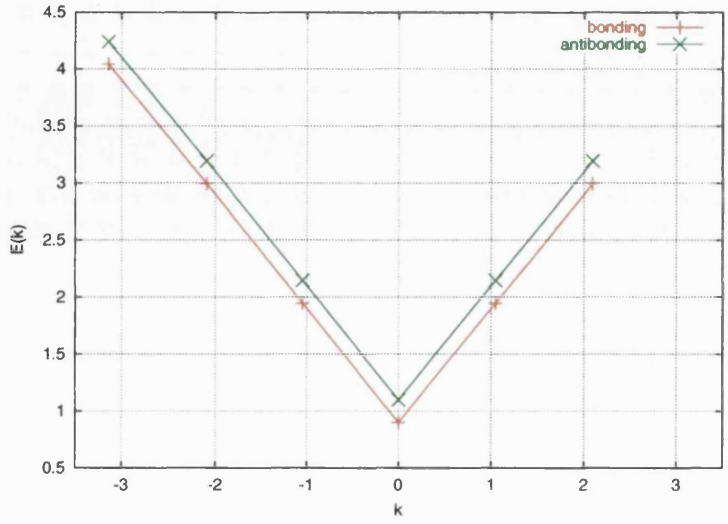

Figure 5.13: Band structure for a $L = 6$ system. With $N = 2$, there are now two "empty" k-states on the right hand ($p = +1$) branch, and one on the left hand ($p = -1$) branch.

allowing us to determine the location of the peaks accurately.

Obviously, as well as the choice of the value of q that we use to calculate the spectral function, we can also choose on which chain to create or annihilate. In fact, this makes remarkably little difference to the results, as can be seen in figure 5.14.

Wherever it is not explicitly stated otherwise, all calculated spectral functions in this chapter are for both creation and annihilation on the interacting chain (chain A).

5.2.4 Calculation of the Luttinger parameters

For continuum systems it is possible to calculate the Luttinger parameter K_ρ directly from the slope of the electron and hole contributions to the spectral function, as in references [97, 129, 144] and as is clear from figure 2.6. However, for the discrete systems under consideration here this is not possible — no accurate measure of the slope can be made.

However, it is still possible to derive an effective value of K_ρ for our coupled chain system. This relies not on the measurement of the slope of the spectral function but on an accurate measurement of the electron-hole peak separation for $\rho(q \neq 0, \omega)$, in other words, a measurement of the Luttinger velocity v_0. For a single Luttinger liquid the (continuum) contributions to $\rho(q \neq 0, \omega)$ are separated by $2v_0 q$ [97, 129, 144], whereas for our non-interacting coupled chain

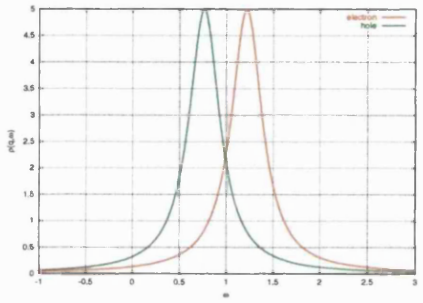

(a) Creation on chain A, annihilation on chain A

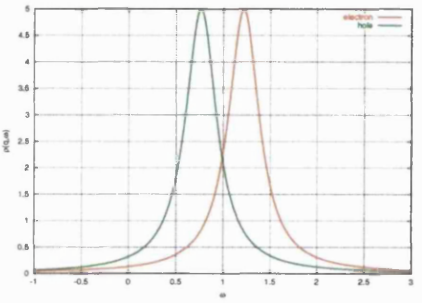

(b) Creation on chain B, annihilation on chain B

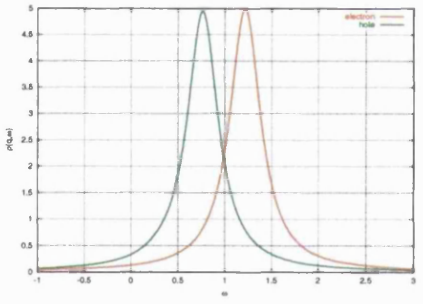

(c) Creation on chain A, annihilation on chain B

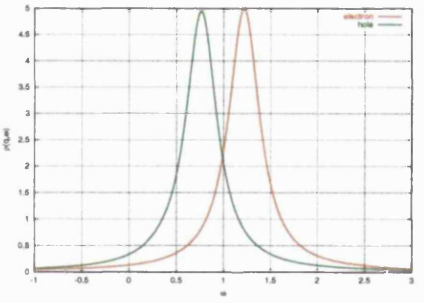

(d) Creation on chain B, annihilation on chain A

Figure 5.14: Spectral function results for creation and annihilation on different chains. $L = 4, N = 2$, interaction strength 0.5 and interchain hopping $t_\perp = 0.1$.

system the electron and hole components are separated by $2t_\perp$ (see section 5.2.3).

We therefore define an effective Luttinger velocity v_0^{eff} in terms of the peak splitting $\Delta\omega$ by the relation

$$\Delta\omega = 2(v_0^{\text{eff}} q + t_\perp). \tag{5.17}$$

This can be used to calculate the Luttinger parameter K_ρ for our system as follows. Starting from from Voit's equation 3.55 (reference [144] page 1003[3]) and the expression for the Luttinger velocity v_0 (v_S in Haldane's [60] notation):

$$v_0(q) = \sqrt{(v_F + V_{1q})^2 - V_{2q}^2} \tag{5.19}$$

Since in our calculations we have the two interaction terms V_{1q} and V_{2q} equal, we put $V_{1q} = V_{2q} \equiv V_q$ and take the limit as $q \to 0$ to give

$$v_0 = \sqrt{(v_F + V_q)^2 - V_q^2} = \sqrt{v_F^2 + 2v_F V_q} \tag{5.20}$$

This can be rearranged to give the interaction in terms of the Luttinger and Fermi velocities

$$V_q = \frac{v_0^2 - v_F^2}{2v_F} = \frac{1}{2}\left[\frac{v_0^2}{v_F} - v_F\right]. \tag{5.21}$$

Now since, from Voit's eqn 3.55 (Haldane's equation 4.3), we can express the velocity associated with the charge quantum number, v_N, as

$$v_N = v_F + V_{1q} + V_{2q} \tag{5.22}$$

However, from Voit's equation 3.32 (page 999) (Haldane's eqn 4.7) this can also be written as

$$v_N = v_0 \mathrm{e}^{-2\phi}. \tag{5.23}$$

We can therefore express these two expressions to give

$$v_F + 2V_q = v_0 \mathrm{e}^{-2\phi}, \tag{5.24}$$

[3]Throughout I take the following relationship between Voit's [144] and Haldane's [60] interaction functions for *spinless* fermions, as implied by comparison of Voit's equation 3.55 (p.1003) and Haldane's equation 4.3:

$$V_{1q} = \frac{g_4(q)}{2\pi} \quad ; \quad V_{2q} = \frac{g_2(q)}{2\pi} \tag{5.18}$$

I use Haldane's notation throughout as it avoids the factors of π.

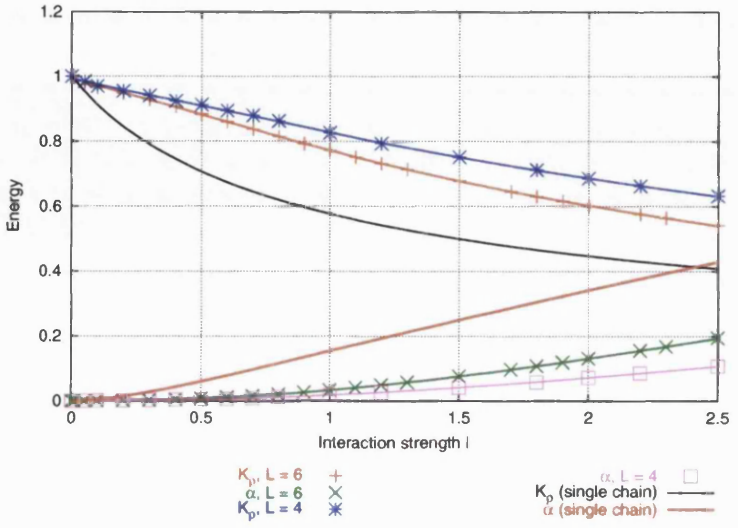

Figure 5.15: Luttinger parameters K_ρ and α for the coupled-chain system, both $L = 6$ and $L = 4$, and for an isolated chain in the continuum ($L \to \infty$) limit.

thus giving us our expression for the Luttinger parameter K_ρ

$$\begin{aligned} e^{-2\phi} &\equiv K_\rho^{-1} && (5.25)\\ &= \frac{v_F + 2V_q}{v_0} && (5.26)\\ &= \frac{1}{v_0}\left[v_F + \frac{(v_0^2 - v_F^2)}{v_F}\right] && (5.27)\\ &= \frac{v_0}{v_F}. && (5.28) \end{aligned}$$

Since for all our calculations in this section we have $v_F = 1$,

$$K_\rho = \frac{v_F}{v_0} = \frac{1}{v_0} \tag{5.29}$$

5.2.5 Discussion

Our calculations approach the question of whether our model exhibits Luttinger liquid behaviour from several complementary directions. We have presented results for the nature of the ground state, for the nature of excited states (charged and neutral) and the related response functions governing the response of the system to excitation. We have also estimated the exponents in certain power-laws characterizing the Luttinger liquid state.

Our results display a certain ambiguity with regard to whether or not this

system is a Luttinger liquid. Roughly speaking, the evidence from the bosonic nature of the ground state, the charged excited states, and the values of the scaling parameters is all broadly consistent with Luttinger liquid behaviour, modified by the presence of the second chain.

Specifically, the one-particle spectral function is consistent with Luttinger liquid behaviour. At $q = 0$, the total spectral function is broadened by separation of the electron and hole parts—this separation is much greater than the $2t_\perp$ expected in a non-interacting two-chain system. For $q \neq 0$, there is additional separation of the electron and hole parts, consistent with the further suppression of spectral weight near the Fermi energy. (For $q > 0$, corresponding to probing the occupancy of states with $k > k_F$ — see equation (5.12)) — the hole part of the spectral function is strongly suppressed, even for relatively strong interactions.) Further support for the Luttinger liquid hypothesis comes from the composition of that portion of the ground state in which bosons are excited on chain A: this fraction closely tracks the fraction that would be expected in an isolated single-chain Luttinger liquid (Figures 5.2 and 5.3).

Moreover, we are able to derive indirectly from $\rho(q > 0, \omega)$ values for two Luttinger liquid parameters: K_ρ (which determines the ratio of the different velocities) and α (which determines the asymptotic behaviour of the correlation functions). Although our analysis presupposes the validity of relations characterizing the Luttinger liquid state (equation (5.29))), the results are self-consistent in the sense that they show $K_\rho < 1$ and $\alpha > 0$, i.e., departures from the Fermi-liquid values. The degree of departure from Fermi-liquid values is, however, somewhat less than would be expected for a single-chain system with the same interaction strength (see figure 5.15).

However, we also have evidence that there is some residual Fermi liquid behaviour. This comes principally from the distribution of charge across the two chains, as a function of interaction strength, in the ground and neutral excited states. Transfer of charge to the non-interacting chain at higher values of I results in the resurrection of a Fermi-liquid like neutral excitation spectrum (although we are still able to extract non-Fermi liquid values for the Luttinger parameters for these interaction strengths, as explained above).

This implies that while the neutral excitation spectrum undergoes a transformation to Fermi liquid behaviour at large I, the charged excitation spectrum does not. It remains to be seen how the apparent conflict between these different views on the same underlying quantum state is resolved.

5.3 Non-identical chains

5.3.1 Motivation

Ideally, we would like to be able to calculate for a metallic chain coupled to an insulating or semiconducting chain. Unfortunately, the metallic nature of our chains is inherent in the Luttinger model and so this is not possible with the present model.

However, we can reproduce some of the most important characteristics of such a system within the constraints of the current model. The calculations presented in section 5.2 are for chains with equal Fermi velocities, i.e. $v_F^{\mathrm{SYSTEM}} = v_F^A = v_F^B = 1$. However, we are not restricted to this and it is possible to repeat most of these calculations with $v_F^A \neq v_F^B$.

In particular, we are interested in systems where $v_F^A < v_F^B$, i.e. the Fermi velocity for the interacting chain is less than that of the non-interacting chain. The result of this is that the electrons find it energetically preferable to reside on the interacting chain, which is one of the characteristics we would expect for a metal-semiconductor chain system. This has several consequences for the band structure of the coupled system, as can be seen more clearly in figure 5.16. The bands are no longer parallel and are not separated by $2t_\perp$. The bands anticross at $E = 0$, which is E_F for our reference state of no participating electrons. Also, for "equal" chains, $v_F^A = v_F^B = v_F^{\mathrm{bonding}} = v_F^{\mathrm{antibonding}}$, whereas here we have $v_F^A(= 1.0) \approx v_F^{\mathrm{bonding}}(= 1.002)$ and $v_F^B(= 2.0) \approx v_F^{\mathrm{antibonding}}(= 1.998)$.

5.3.2 Ground states

As before, the ground and neutral first excited states were calculated for different interaction strengths on chain A. Sample states are shown in table 5.5. We again find that the interacting ground states include basis states with bosons on the interacting chain A, and a finite contribution from basis states that also contain bosons on chain B, as shown in figure 5.17. The data for boson contributions on chain A again match the single Luttinger liquid data almost exactly, although possibly slightly less well than for the identical chains, and the magnitude of the contributions from states with bosons on both chains is comparable to that found for the results from identical chains. In this respect, therefore, we find remarkably few differences from the results obtained for the identical chains, and therefore conclude that once more we are in a weakly coupled regime.

If we look closely at table 5.5 however, and compare it to the states in table 5.3, we see that the electrons are much more likely to reside on the interacting

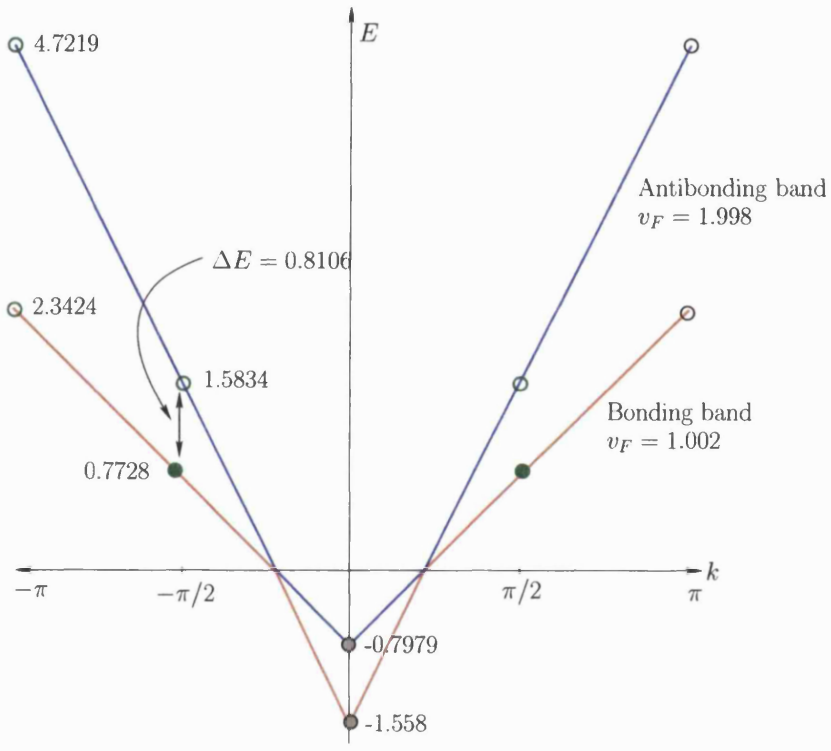

Figure 5.16: Band structure and ground state for the non-interacting system with $L = 4$, $N = 2$, $t_\perp = 0.1$ $v_F^A = 1.0, v_F^B = 2.0$. Filled green circles represent occupied states, unfilled green circles empty states.

I	Ground state
0.0	(0.4967E+00 0.8500E+00) *| 00001 0 1 1 ; 00001 0 0 0 > (0.6225E-01 0.1065E+00) *| 00001 -1 1 0 ; 00001 1 0 1 > (-0.6225E-01 -0.1065E+00) *| 00001 1 0 1 ; 00001 -1 1 0 > (0.7802E-02 0.1335E-01) *| 00001 0 0 0 ; 00001 0 1 1 >
1.0	(-0.4045E-01 0.4333E-01) *| 00001 0 1 1 ; 00001 0 0 0 > (-0.3475E+00 0.3723E+00) *| 00001 -1 1 0 ; 00001 1 0 1 > (0.3475E+00 -0.3723E+00) *| 00001 1 0 1 ; 00001 -1 1 0 > (-0.4717E+00 0.5053E+00) *| 00001 0 0 0 ; 00001 0 1 1 > (0.1843E-04 -0.1975E-04) *| 00009 0 1 1 ; 00003 0 0 0 > (0.3309E-04 -0.3545E-04) *| 00009 -1 1 0 ; 00003 1 0 1 > (0.2438E-04 -0.2611E-04) *| 00009 0 0 0 ; 00003 0 1 1 > (0.1843E-04 -0.1975E-04) *| 00003 0 1 1 ; 00009 0 0 0 > (-0.3309E-04 0.3545E-04) *| 00003 1 0 1 ; 00009 -1 1 0 > (0.2438E-04 -0.2611E-04) *| 00003 0 0 0 ; 00009 0 1 1 > (0.9369E-04 -0.1004E-03) *| 00011 0 1 1 ; 00001 0 0 0 > (0.1187E-02 -0.1271E-02) *| 00011 -1 1 0 ; 00001 1 0 1 > (-0.1187E-02 0.1271E-02) *| 00011 1 0 1 ; 00001 -1 1 0 > (0.1611E-02 -0.1726E-02) *| 00011 0 0 0 ; 00001 0 1 1 >
2.0	(-0.2410E-02 0.4561E-02) *| 00001 0 1 1 ; 00001 0 0 0 > (-0.5710E-01 0.1080E+00) *| 00001 -1 1 0 ; 00001 1 0 1 > (0.5710E-01 -0.1080E+00) *| 00001 1 0 1 ; 00001 -1 1 0 > (-0.4602E+00 0.8708E+00) *| 00001 0 0 0 ; 00001 0 1 1 > (0.5847E-04 -0.1106E-03) *| 00009 -1 1 0 ; 00003 1 0 1 > (0.6789E-05 -0.1285E-04) *| 00009 0 0 0 ; 00003 0 1 1 > (-0.5847E-04 0.1106E-03) *| 00003 1 0 1 ; 00009 -1 1 0 > (0.6789E-05 -0.1285E-04) *| 00003 0 0 0 ; 00009 0 1 1 > (0.6876E-05 -0.1301E-04) *| 00011 0 1 1 ; 00001 0 0 0 > (0.3230E-03 -0.6112E-03) *| 00011 -1 1 0 ; 00001 1 0 1 > (-0.3230E-03 0.6112E-03) *| 00011 1 0 1 ; 00001 -1 1 0 > (0.3241E-02 -0.6133E-02) *| 00011 0 0 0 ; 00001 0 1 1 >

Table 5.5: Ground states for the $L = 4$, $N = 2$, $t_\perp = 0.1$ $v_F^A = 1.0, v_F^B = 2.0$ systems for various interaction strengths I. States with an absolute coefficient of less than 10^{-5} have been omitted.

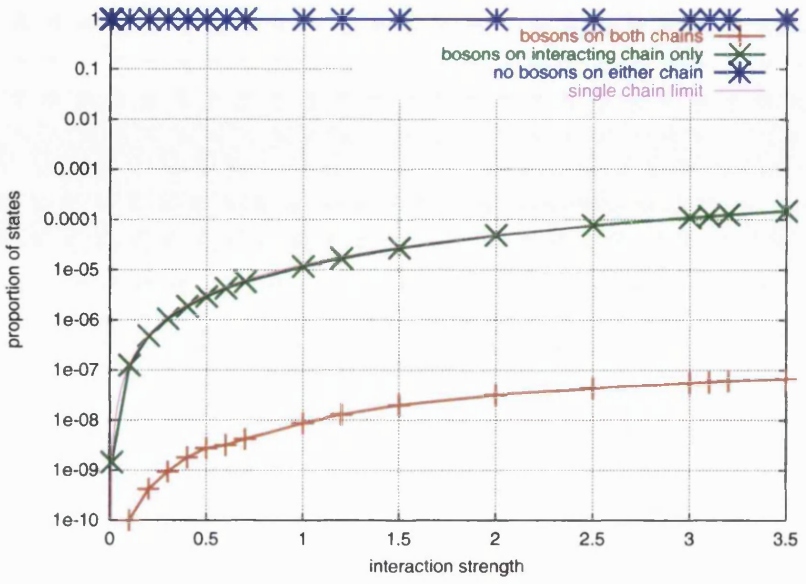

Figure 5.17: Contribution of bosonic basis states to the ground states of the $L = 4$, $N = 2$, $t_\perp = 0.1$ $v_F^A = 1.0, v_F^B = 2.0$ system as a function of interaction strength I.

chain A, as desired. This can be seen clearly from the $I = 0.0$ data in figure 5.18. However, as the interactions are turned on, the states with both electrons on chain A decrease in importance in favour of those with one electron on each chain. In the region $0.4 \lesssim I \lesssim 1.0$ the eigenstates are dominated by the equal distribution basis states, and then, as for the system with $v_F^{\text{SYSTEM}} = v_F^A = v_F^B = 1$, the distortion of the electronic structure due to the interactions leads to states with both electrons on the non-interacting chain B becoming dominant.

5.3.3 Excited states

We now look at the nature of the neutral excitations. Samples of the eigenstates are given in table 5.6, while the charge distribution between the chains is plotted for both the ground and excited states as a function of I in figure 5.18. The excitation energies are plotted as a function of I in figure 5.19.

We notice immediately that the excitation energy for the non-interacting limit $I = 0$ is no longer equal to $2t_\perp$. This is consistent with the altered band structure diagram of figure 5.16.

With regard to the eigenstates, we again note that the non-interacting eigenstate is a combination of the four degenerate states $\alpha, \beta, \gamma, \delta$ of figure 5.4, although this time the coefficients are not equal in magnitude with respect to distribution between the two chains, as they are (almost) in the equal v_F case.

From figure 5.18, we again notice a discontinuity in the charge distribution as soon as the interactions are switched on, and notice from table 5.5 that the $I = 0.01$ eigenstate contains no contribution from the "ionic"-like basis states with both electrons on the same chain.

I	First neutral excited state
0.0	(0.6838E-01 0.4442E-01) *| 00001 0 1 1 ; 00001 0 0 0 > (-0.4331E+00 0.3654E+00) *| 00001 -1 1 0 ; 00001 -1 1 0 > (-0.2433E-01 -0.3552E-01) *| 00001 -1 1 0 ; 00001 1 0 1 > (0.5127E+00 0.3133E+00) *| 00001 1 0 1 ; 00001 -1 1 0 > (-0.4587E+00 0.3038E+00) *| 00001 1 0 1 ; 00001 1 0 1 > (-0.6837E-01 -0.4441E-01) *| 00001 0 0 0 ; 00001 0 1 1 >
0.01	(0.2376E+00 -0.3492E-01) *| 00001 -1 1 0 ; 00001 -1 1 0 > (-0.5536E+00 0.3946E-01) *| 00001 -1 1 0 ; 00001 1 0 1 > (-0.5536E+00 0.3944E-01) *| 00001 1 0 1 ; 00001 -1 1 0 > (0.5033E+00 -0.2702E+00) *| 00001 1 0 1 ; 00001 1 0 1 >
0.1	(-0.3397E+00 -0.4117E+00) *| 00001 -1 1 0 ; 00001 -1 1 0 > (-0.5376E-01 0.1173E+00) *| 00001 -1 1 0 ; 00001 1 0 1 > (-0.5377E-01 0.1173E+00) *| 00001 1 0 1 ; 00001 -1 1 0 > (0.3114E+00 -0.7648E+00) *| 00001 1 0 1 ; 00001 1 0 1 > (0.1215E-03 0.1470E-03) *| 00011 -1 1 0 ; 00001 -1 1 0 > (-0.1126E-03 0.2754E-03) *| 00011 1 0 1 ; 00001 1 0 1 >

Table 5.6: Neutral first excited states for the $L = 4$, $N = 2$, $t_\perp = 0.1$ systems for various interaction strengths I. States with an absolute coefficient of less than 10^{-4} have been omitted.

For the sake of clarity, the exact values of the excitation energy for different values of interaction strength $I < 3.5$ are shown in table 5.7. As we noted at the beginning of this section, the excitation energy for the non-interacting limit is now not equal to $2t_\perp$, but is equal (apart from a numerical error) to the excitation energy expected from inspection of figure 5.16. However, as the interactions increase, the excitation energy *decreases* and is close to zero within the region $0.4 \lesssim I \lesssim 1.0$, the same region for which we noted the charge distribution dominated by "covalent" states. This is owing to the ground state energy increasing much more rapidly than the first excited state energy, which is roughly linear for $I \lesssim 3.0$. The ground state energy saturates at a value of 3.17 at $I \approx 1.5$ although it does continue increasing very slowly. This corresponds to the point in figure 5.18 where the charge distribution becomes almost completely dominated by chain B states. The saturation of the excited state energy to

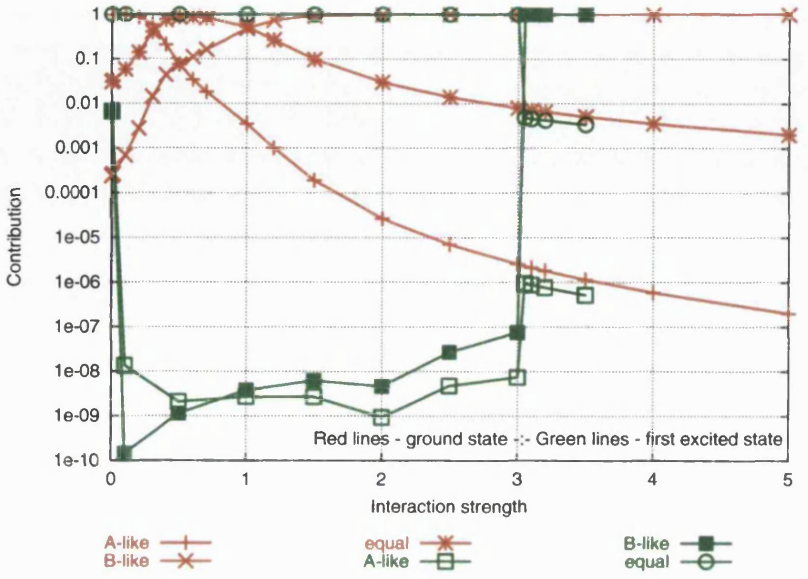

Figure 5.18: Contributions to the ground and first excited states for the $L = 4$, $N = 2$, $t_\perp = 0.1$, $v_F^A = 1.0, v_F^B = 2.0$ system from electrons on each chain as a function of interaction strength I.

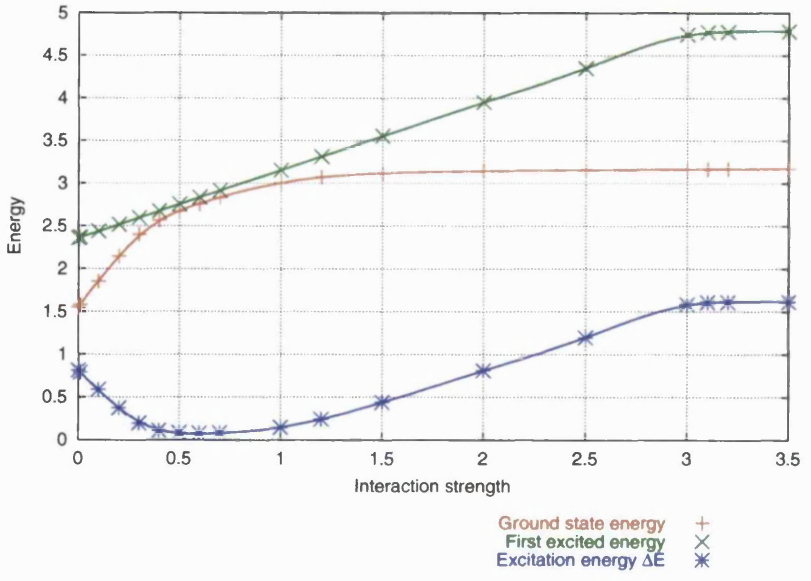

Figure 5.19: Energies for the ground state and neutral first excited state for the $L = 4$, $N = 2$, $t_\perp = 0.1$, $v_F^A = 1.0, v_F^B = 2.0$ system as a function of interaction strength I.

4.77 at $I = 3.0$ corresponds to the discontinuity in charge distribution as the lowest energy excitation shifts from a zero momentum excitation to one with $\Delta k = 2\pi/L$.

I	ΔE	I	ΔE
0	0.81046	1.0	0.14736
0.01	0.78766	1.2	0.24260
0.1	0.58714	1.5	0.43893
0.2	0.37121	2.0	0.81021
0.3	0.19644	2.5	1.19487
0.4	0.10947	3.0	1.58345
0.5	0.08392	3.1	1.60909
0.6	0.07913	3.2	1.61004
0.7	0.08373	3.5	1.61303

Table 5.7: Numerical values of excitation energy corresponding to figure 5.19.

However, as can be seen from table 5.7, the excitation energy does not completely flatten of in the region $I > 3.0$, but continues to grow, albeit slowly. In fact, neither the ground state energy nor the excited state energy have completely saturated. Furthermore, whereas in section 5.2.2 the excitation energy saturated at a value of $2\pi v_F/L$, here the final value of the excitation energy is around 1.6, rather more than the value $2\pi v_F^A/L = \pi/2$. In any case, we would expect this to converge on a value dependent on $v_F^B = 2.0$, the Fermi velocity for the *non*-interacting chain, on which almost all the electrons are residing, rather than v_F^A!

This gradual increase in ΔE for high values of I is clearer in a system in which the two Fermi velocities differ by a greater amount. Figure 5.20 shows the excitation energy for a system with $v_F^A = 0.5$ and $v_F^B = 2.0$. The data points for the excitation energy are shown in magenta, the blue line is a linear least squares fit to this data for $2.5 \leq I \leq 5.0$ which yields a slope of 0.1.

How may this be explained? For the $v_F^A = 1.0, v_F^B = 2.0$ system, at $I = 0.0$ the bonding branch is almost completely chain A-like and the antibonding branch chain B-like, i.e. $v_F^A(= 1.0) \approx v_F^{\text{bonding}}(= 1.002)$ and $v_F^B(= 2.0) \approx v_F^{\text{antibonding}}(= 1.998)$, as confirmed by the $I = 0.0$ data from figure 5.18. Once the chain A interactions are switched on, however, the band structure of figure 5.16 begins to distort. Because it is the chain A states that are affected by the interactions (for weak interactions at least, we have already demonstrated in section 5.2.1 that for strong chain A interactions weak interaction effects manifest themselves on chain B), it is the bonding band that is raised in energy while the antibonding band remains static, thus reducing the excitation energy for both charged and neutral excitations.

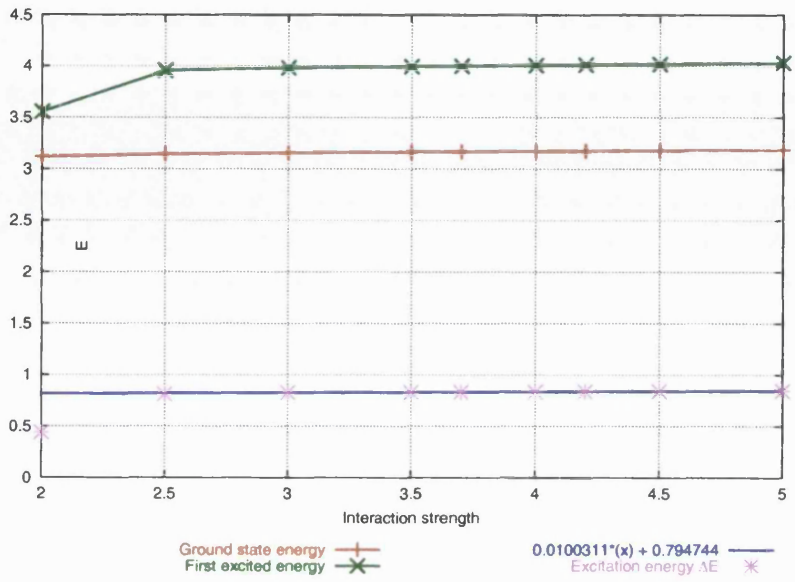

Figure 5.20: Energies for the ground state and neutral first excited state for the $L = 4$, $N = 2$, $t_\perp = 0.1$, $v_F^A = 0.5, v_F^B = 2.0$ system as a function of interaction strength I.

However, this effect weakens the link between the bonding band and its chain A-like nature. Charge is removed from chain A in favour of the covalent states and chain B-like states, as can be seen from figure 5.18. The bonding and antibonding bands therefore do not discriminate with respect to the chains in the region of $I \sim 0.5$, where the neutral excitation energy ΔE approaches zero.

From this point on the situation becomes much as for the case with $v_F^A = v_F^B$—charge is removed from chain A as the interactions increase in strength and the chain A states increase in energy, until we come to the point (at $I \sim 3.0$ in this case) where the lowest energy neutral excitation is no longer one with $\Delta k = 0$ but one with $\Delta k = 2\pi/L$. The charge at this point is all on chain B, so we might expect the excitation energy for these states to be $\Delta E = 2\pi v_F^B/L$, but it seems to remain at $\Delta E = 2\pi v_F^{\text{bonding}}/L \approx 2\pi v_F^A/L$, subject to the small additional increase in energy noted above and discussed in the next paragraph.

The reason for the slowly increasing energies can also be explained. We can decompose the ground state energies into contributions from chain A only (i.e. $\langle \text{g.s.}|\hat{H}^A|\text{g.s}\rangle$), chain B only (i.e. $\langle \text{g.s.}|\hat{H}^B|\text{g.s}\rangle$) and the hopping terms, $\langle \text{g.s.}|t_\perp \sum_x \left[\hat{\psi}_p^{A\dagger}\hat{\psi}_p^B + \hat{\psi}_p^{B\dagger}\hat{\psi}_p^A\right]|\text{g.s}\rangle = \langle \text{g.s.}|\hat{H}^{AB}|\text{g.s}\rangle$. This is plotted in figure 5.21. The energy contribution from the chain A part of the Hamiltonian is decreasing in the region $I \lesssim 3.5$, due to the decrease in contributions to the

ground state from chain A states (as shown in figure 5.22). However, there is a minimum at $I \approx 3.5$ beyond which the $\hat{H}^A$ contributions begin to increase. Hence we conclude that at $I \approx 3.5$ the effect of the chain A interactions (in the form of additional boson contributions) overtakes that of the effect of charge being removed from chain A. Similarly, the contribution from $\hat{H}^B$ is increasing throughout the region shown in figure 5.21—this is due to the induced boson excitations on chain B, as can be seen from figure 5.23. The hopping part of the total energy is also increasing with I, owing to the frustration of favourable interchain coherence caused by the interactions.

5.3.4 Spectral functions

We now examine the spectral functions for this system, which are calculated in an identical manner to those discussed in section 5.2.3. Figure 5.24 shows the spectral function $\rho(q = 0, \omega)$ for the $I = 0.0$ system, where the peak separation, and hence the charged excitation energy, corresponds exactly to that in figure 5.16. The corresponding spectral functions for $I > 0.0$ are shown in figures 5.25, 5.26 and 5.27. We note that, as for the neutral excitations, the peaks first become closer as I increases, indicating a decrease in the charged excitation energy, but this reaches a minimum at $I \approx 0.5$ whereupon the peaks continue to separate with increasing I, again leading us to believe that spectral weight is being removed from the Fermi surface and that Luttinger liquid properties are extant in this system. We also note the two-branch structure around $I \approx 0.5$ evident in both the hole (figure 5.26) and particularly the electron (figure 5.27) parts. This is because of an interchange of predominance between the "covalent" and "ionic" parts of the ground states, and will be discussed in more detail in section 5.3.5.

5.3.5 Calculation of the Luttinger parameters

Can we use the information from section 5.3.4 to calculate the Luttinger liquid parameters for the system as we did for the identical chains? We believe so, subject to some modifications to the method of section 5.2.4. Whereas for the identical chains we had $v_F^{\text{SYSTEM}} = v_F^A = v_F^B$, here we have $v_F^A \neq v_F^B$ and it is not immediately clear what value v_F^{SYSTEM} takes. However, the results of section 5.3.3 would lead us to believe that the properties of the system are dominated by the Fermi velocity of the bonding band, and hence we put

$$v_F^{\text{SYSTEM}} = v_F^{\text{bonding}} = 1.002. \tag{5.30}$$

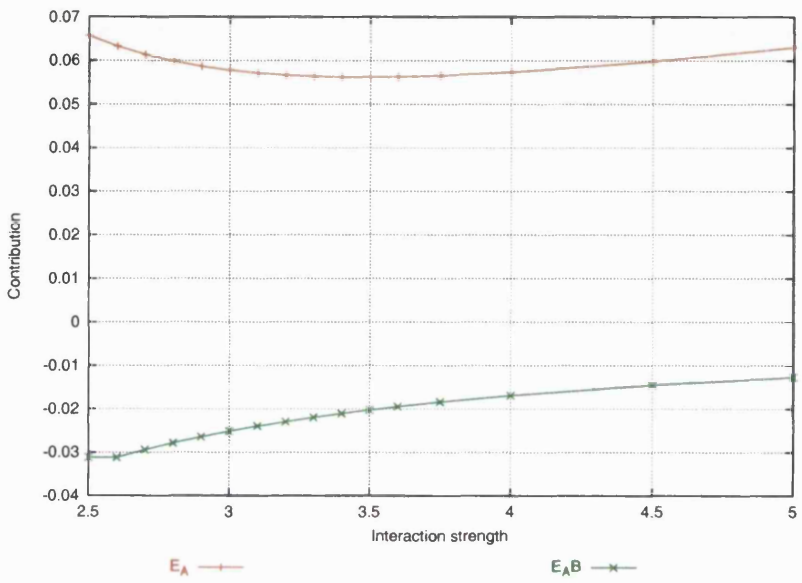

(a) $\langle \text{g.s}|\hat{H}^{AB}|\text{g.s}\rangle$ (green) and $\langle \text{g.s}|\hat{H}^{A}|\text{g.s}\rangle$ (red)

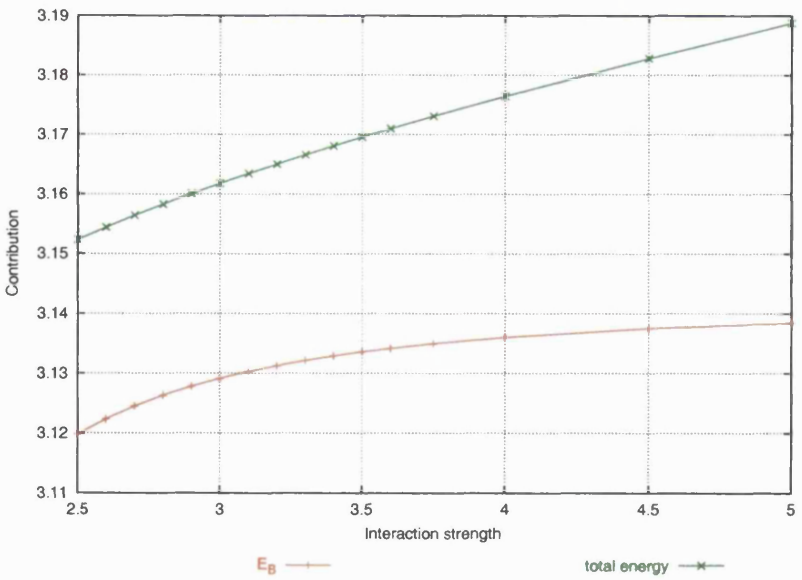

(b) $\langle \text{g.s}|\hat{H}^{\text{TOTAL}}|\text{ g.s}\rangle$ (green) and $\langle \text{g.s}|\hat{H}^{B}|\text{g.s}\rangle$ (red)

Figure 5.21: Decomposition of ground-state energy contributions for $L = 4$, $N = 2$, $t_\perp = 0.1$, $v_F^A = 1.0, v_F^B = 2.0$ system.

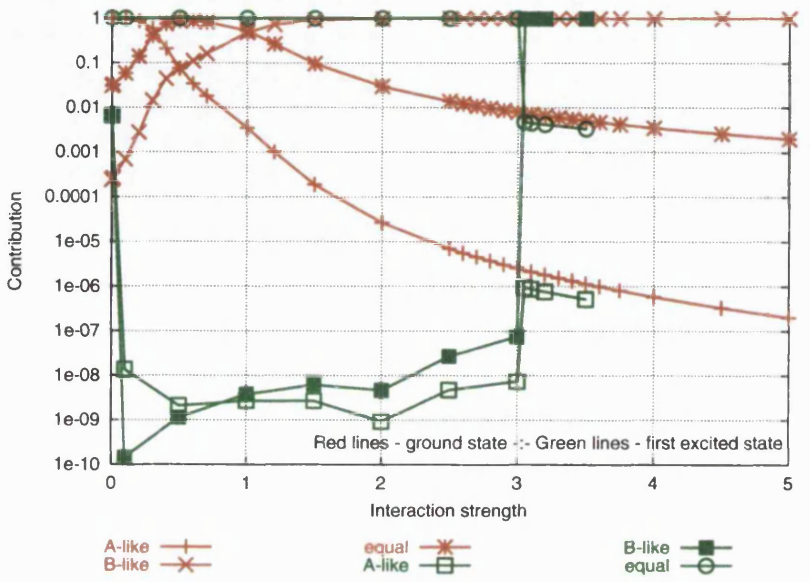

Figure 5.22: Charge distribution for the $L = 4$, $N = 2$, $t_\perp = 0.1$, $v_F^A = 1.0, v_F^B = 2.0$ system including the high I region.

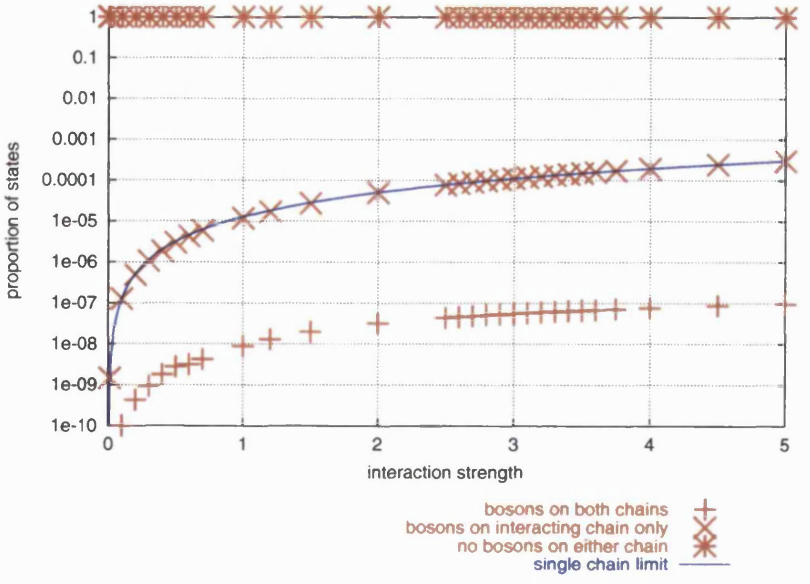

Figure 5.23: Boson contributions for the $L = 4$, $N = 2$, $t_\perp = 0.1$, $v_F^A = 1.0, v_F^B = 2.0$ system including the high I region.

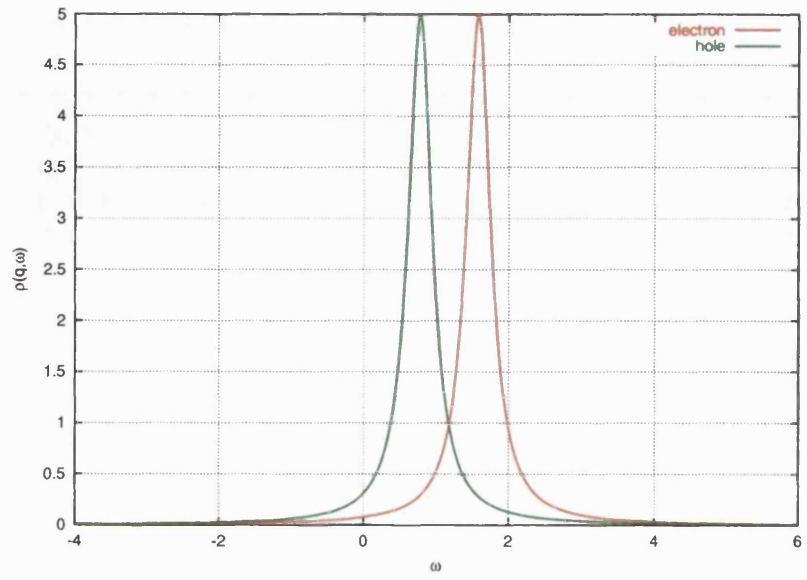

Figure 5.24: Spectral function $\rho(0,\omega)$ for the $L = 4$, $N = 2$, $t_\perp = 0.1$, $v_F^A = 1.0, v_F^B = 2.0$ system with $I = 0$. The hole peak is at $\omega = 0.7729$, the electron peak at $\omega = 1.584$, i.e. separation $\Delta\omega = 0.8105$.

The nature of the band structure also complicates matters somewhat. With parallel bands, as we had for the equal-v_F system, it is clear that for $q > 0$ the added contribution to the electron-hole peak separation of $\rho(|q| > 0, \omega)$ will still be equal to $2t_\perp$. For the case of two unequal chains however, this is no longer true. In particular, for our case of $L = 4$ and $q = 2\pi/L = \pi/2$ the bonding/antibonding splitting will be of order $q|v_F^A - v_F^B|$, and since this is much greater than $2t_\perp$, we can safely ignore any bonding/antibonding splitting for the $q = 2\pi/L$ calculations.

We therefore reassess equation (5.17) and write

$$v_0^{\text{eff}} = \begin{cases} \frac{\Delta\omega - 2t_\perp}{2q} & (v_F^A = v_F^B), \\ \frac{\Delta\omega}{2q} & |v_F^A - v_F^B| q \gg 2t_\perp. \end{cases} \tag{5.31}$$

We may then proceed as before to calculate v_0^{eff} and hence $K_\rho = v_F^{\text{SYSTEM}}/v_0^{\text{eff}}$ for this system.

There is one further complication awaiting us, however. It can be seen from figures 5.27 and 5.29 that there are two "branches" to the electron part of $\rho(q,\omega)$. This is also evident, to a lesser extent, in the hole contributions, as can be seen from figures 5.30 and 5.28. For $\rho(q = \pi/2, \omega)$, there is a single peak in the electron contributions at $I \lesssim 0.3$, but for $0.3 \lesssim I \lesssim 0.8$ there is a

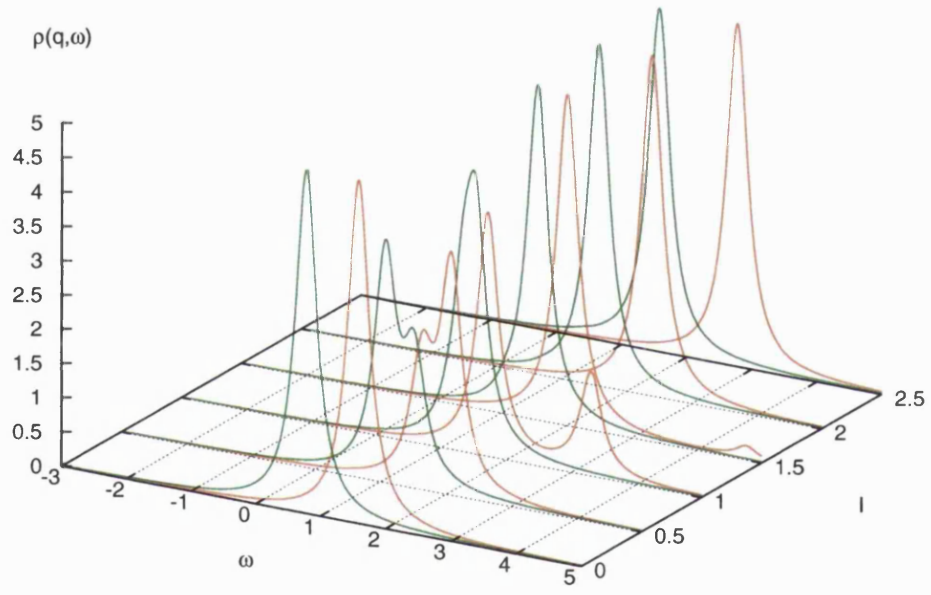

Figure 5.25: Spectral functions $\rho(0,\omega)$ for the $L = 4$, $N = 2$, $t_\perp = 0.1$, $v_F^A = 1.0, v_F^B = 2.0$ system. Electron contributions are shown in red, hole contributions in green. As normal, the hole parts have been renormalized such that they are equal in magnitude to the electron parts. This data is replotted as density maps in figures 5.26 and 5.27.

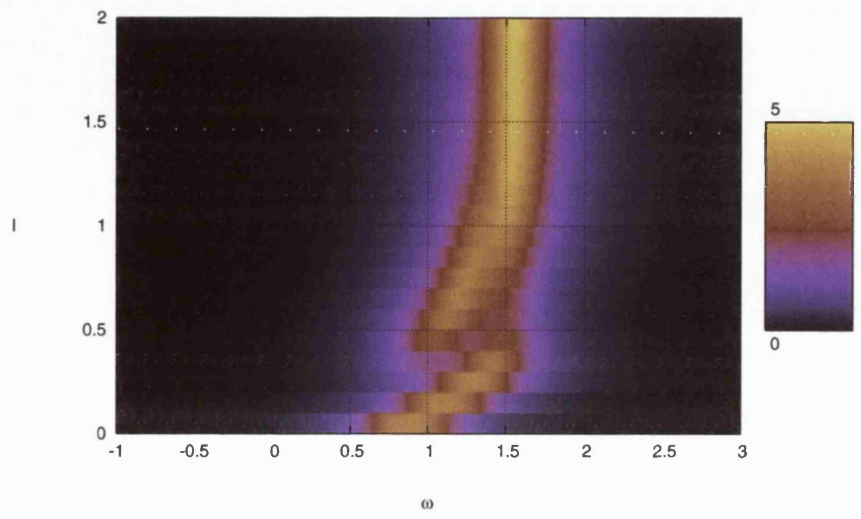

Figure 5.26: Density map of the hole part of the spectral functions $\rho(q = 0, \omega)$ for the $L = 4$, $N = 2$, $t_\perp = 0.1$, $v_F^A = 1.0, v_F^B = 2.0$ system as a function of interaction strength.

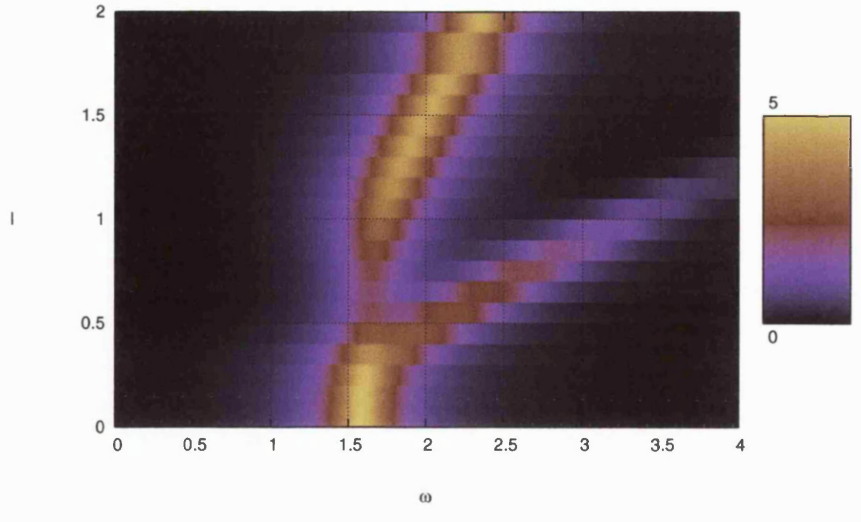

Figure 5.27: Density map of the electron part of the spectral functions $\rho(0, \omega)$ for the $L = 4$, $N = 2$, $t_\perp = 0.1$, $v_F^A = 1.0, v_F^B = 2.0$ system as a function of interaction strength.

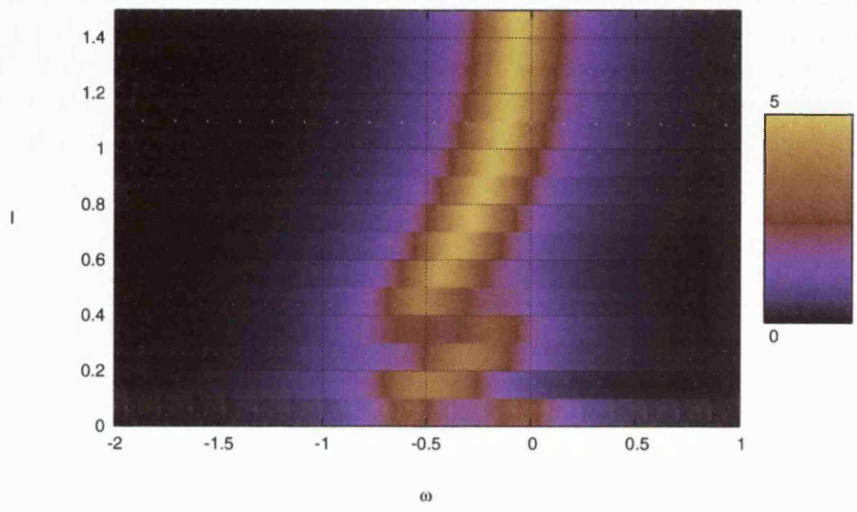

Figure 5.28: Density map of the hole part of the spectral functions $\rho(q = 2\pi/L, \omega)$ for the $L = 4$, $N = 2$, $t_\perp = 0.1$, $v_F^A = 1.0, v_F^B = 2.0$ system as a function of interaction strength.

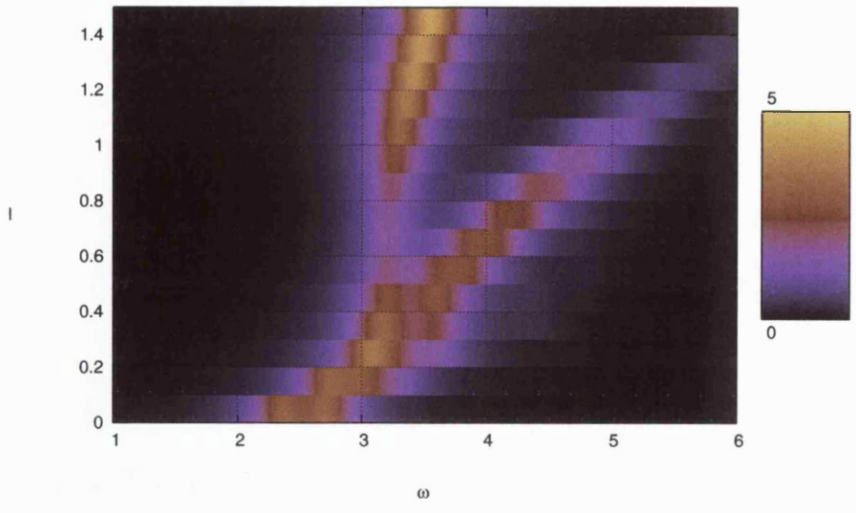

Figure 5.29: Density map of the electron part of the spectral functions $\rho(q = 2\pi/L, \omega)$ for the $L = 4$, $N = 2$, $t_\perp = 0.1$, $v_F^A = 1.0, v_F^B = 2.0$ system as a function of interaction strength.

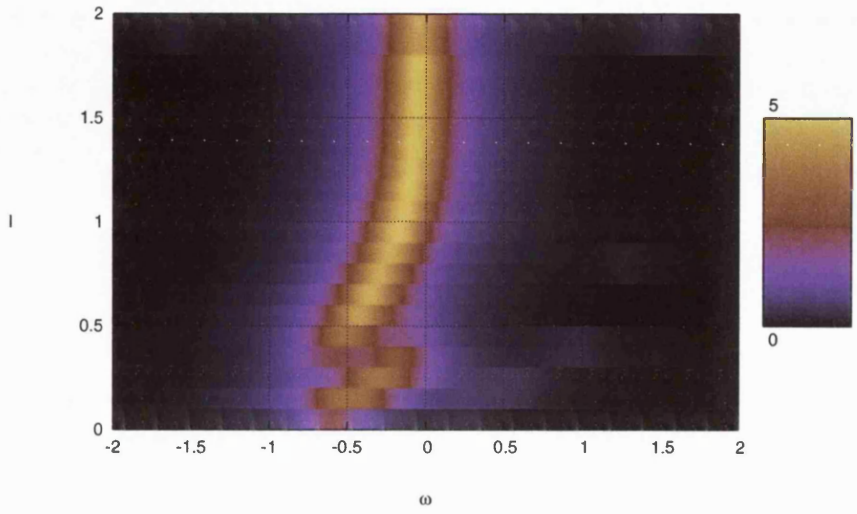

Figure 5.30: Density map of the hole part of the spectral functions $\rho(q = 2\pi/L, \omega)$ where the hole has been created on chain B rather than chain A, for the $L = 4$, $N = 2$, $t_\perp = 0.1$, $v_F^A = 1.0, v_F^B = 2.0$ system as a function of interaction strength.

double peak structure, dominated by the peak at higher energy. For $I \gtrsim 0.8$, this high energy peak fades as it moves off to higher energies and the electron contribution becomes dominated by the lower energy peak, which is also moving off to higher energies as I increases. Which of these peaks do we use to calculate K_ρ?

The answer to this comes to us through an analysis of the nature of the peak structure for the electron part of $\rho(q, \omega)$. We can project out the "chain A only", "chain B only" and "equal" parts (as defined in section 5.2.2) of the ground state and use these to recalculate the spectral function. The result of this for an interaction strength $I = 0.7$ is plotted in figure 5.32. The peaks for the chain A only, chain B only and equal parts are the same height as they are normalized, but it is clear that the peak in the electron part of $\rho(q = 0, \omega)$ at higher energy is due to states with one electron on each chain ("covalent"), while the lower energy peak is due to states with charge only on chain B ("ionic"). Results for other values of the interaction strength in the region $0.5 < I < 1.0$ confirm this, as does a similar analysis for $\rho(q = \pi/2, \omega)$. We can therefore say that the two branches of the electron contribution to figures 5.27 and 5.29 are due to this ionic/covalent splitting, and while initially the covalent branch of

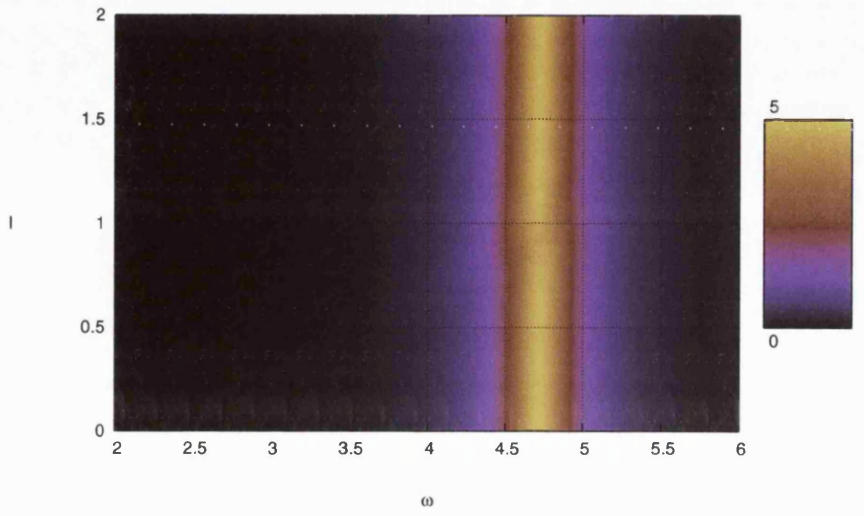

Figure 5.31: Density map of the electron part of the spectral functions $\rho(q = 2\pi/L, \omega)$ where the electron has been created on chain B rather than chain A for the $L = 4$, $N = 2$, $t_\perp = 0.1$, $v_F^A = 1.0, v_F^B = 2.0$ system as a function of interaction strength.

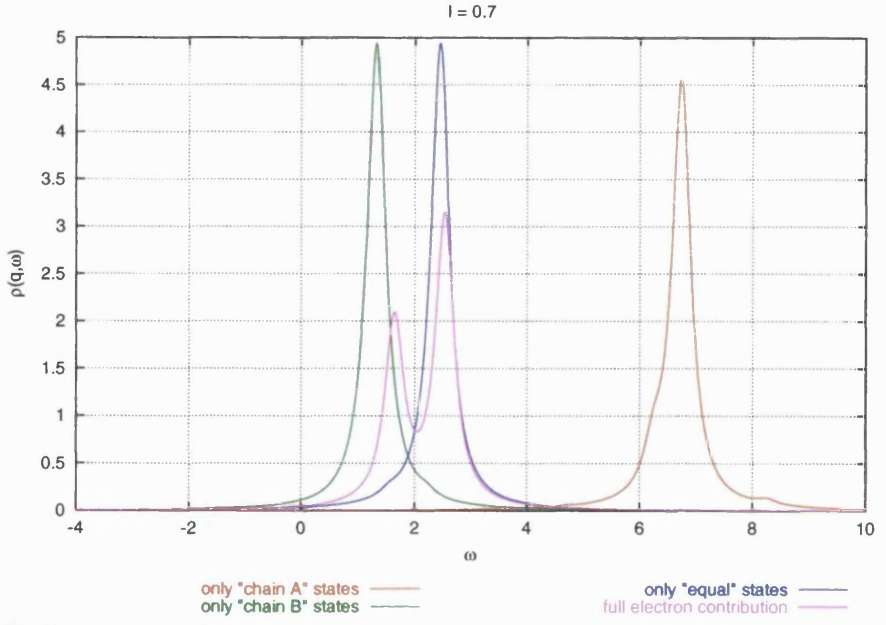

Figure 5.32: Decomposition of $\rho(q = 0, \omega)$ for the electron contribution at $I = 0.7$.

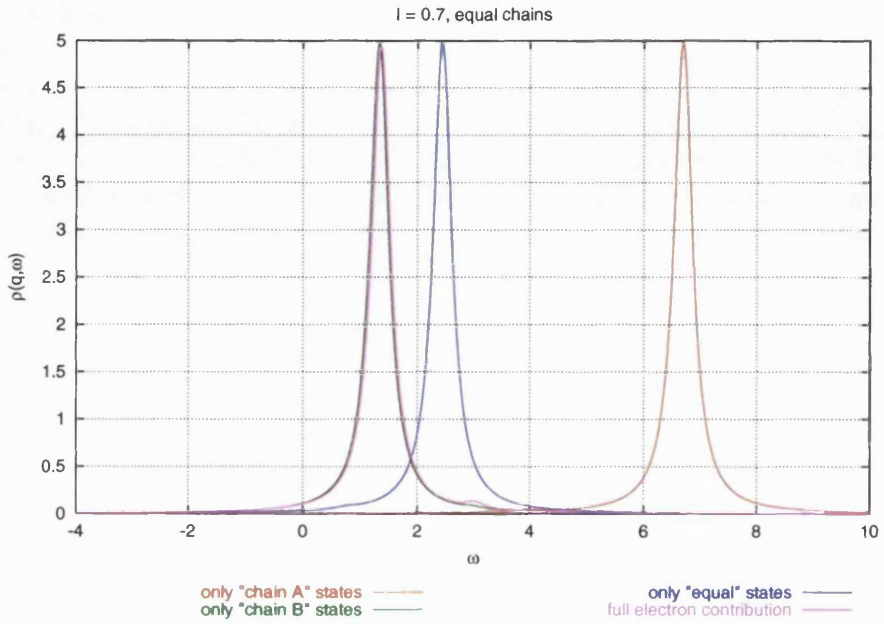

Figure 5.33: Decomposition of $\rho(q = 0, \omega)$ for the electron contribution at $I = 0.7$ for the equal chain system.

the spectral function dominates, at higher interaction strengths the ionic chain B part gives a greater contribution. The same explanation holds true for the hole contributions. Note, however, that a similar analysis for the equal chain spectral function is completely chain B dominated (no "covalent" contribution at all), as shown in figure 5.33. The Luttinger parameter was calculated using both branches of the spectral function and the result is plotted in figure 5.34, with the $L = 4$ equal chain results and the single chain data for comparison. We can see that for $I \lesssim 1.0$, this system is *more* Luttinger-liquid like than the equal chain system, but for $I \gtrsim 1.0$ the covalent branch peters out and the system is *less* Luttinger liquid-like than the equal chains system. However, there does not seem to be a sharp cutoff between the two types of behaviour and this could lead to interesting effects in the system at $I \approx 1.0$.

5.4 Odd numbers of electrons

Finally, we present some results for the equal-chain system with three, rather than two, electrons available for excitation. Figure 5.35 shows the ground and first excited state energies for this system. We see that in the non-interacting limit, the neutral excitation energy is $0.2 = 2t_\perp$, and that in the region $0 \lesssim I \lesssim 0.5$ the excitation energy increases, to a maximum at $I \approx 0.5$. At this point there

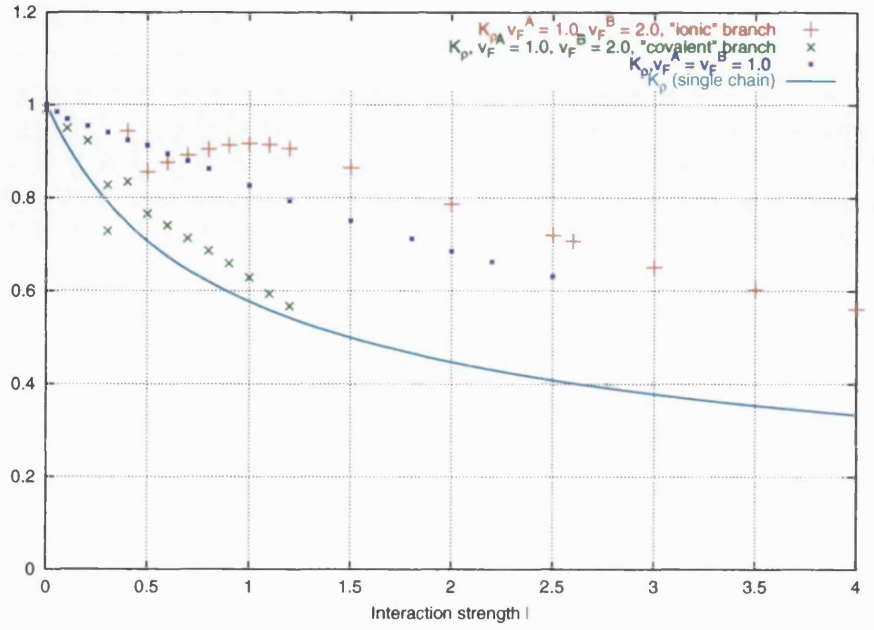

Figure 5.34: Luttinger parameters for the $L = 4, N = 2, v_F^A = 1.0, v_F^B = 2.0$ system.

is a change in the slope of the first excited state energy, which is now less than the slope of the ground state energy. Consequently the excitation energy falls in the region $0.5 \lesssim I \lesssim 2.0$, until it is almost zero at $I \approx 2.0$. Here the ground state and first excited state energies "anticross", and the excitation energy grows once more. We cannot be certain if there is a crossing or anticrossing at this point, as we have not searched parameter space for a zero in the excitation energy. Examination of figure 5.36, which shows the boson contributions to the ground state, shows a discontinuity at $I \approx 2.0$ that is not in evidence in the other systems studied in this chapter, all of which evolve smoothly. What is the cause of this discontinuity? This is revealed in figure 5.37, which shows the charge distribution for these ground states. Since we have three electrons here, there are four possible distributions of them between the two chains: all on chain A, all on chain B, two on chain A and one on chain B, or one on chain A and two on chain B. In the non-interacting limit ($I = 0$), we see that the mixed (covalent) states are predominant. As the interactions are introduced, however, the charge gradually moves away from the states with two electrons on chain A and one on chain B, in favour of the states with one electron on chain A and two on chain B. This is as we would expect from the raising in energy of the chain A biased states as I is increased. At the same time, states with all three electrons on chain B become more important, while those with all three

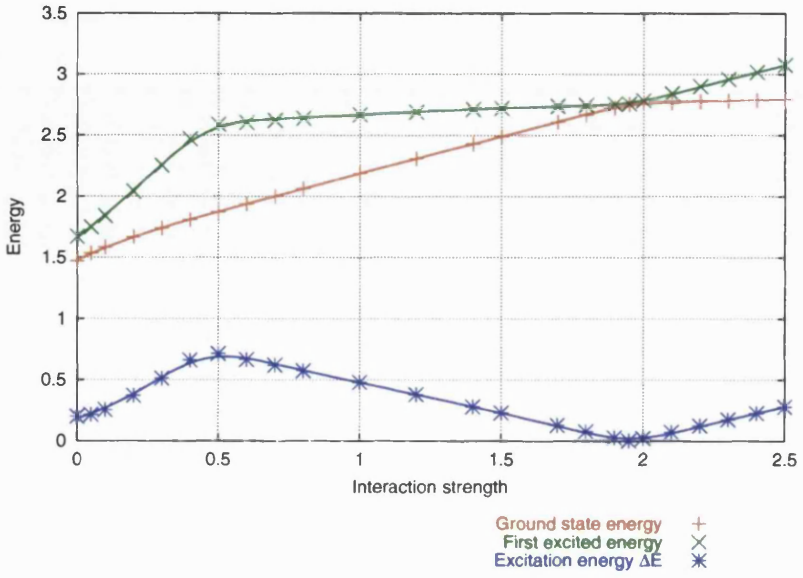

Figure 5.35: Energies for the ground state and neutral first excited state for the $L = 6$, $N = 3$, $t_\perp = 0.1$, $v_F^A = v_F^B = 1.0$ system as a function of interaction strength I.

electrons on chain A, which give only a small contribution at very low values of I, become negligble. However, at $I \approx 2$ we again encounter a discontinuity. This discontinuity in the *ground state* charge distribution does not occur for any of the two-electron systems studied here. At $I = 1.95$ the dominant charge contributions are from the states with one electron on chain A and two on chain B, with significant but lesser contributions from states with two electrons on chain A and one on chain B, and from states with all three electrons on chain B. At $I = 2.0$, however, the charge distribution is dominated by states with all three electrons on chain B, while the contributions from the two types of covalent states decrease by more than an order of magnitude, and there is a significant increase in the small contribution from states with all three electrons on chain A.

The discontinuities at $I \approx 2$ in the energy properties of this three-electron system thus represent a shift in emphasis away from the dominance of covalent-type states at low values of I to the dominance of ionic-type states, with all three electrons on the non-interacting chain B, at high values of I. It was not possible, within the timescale of this thesis, to examine the spectral properties and hence Luttinger parameters, of this system, but it is to be hoped that this may be done in the near future.

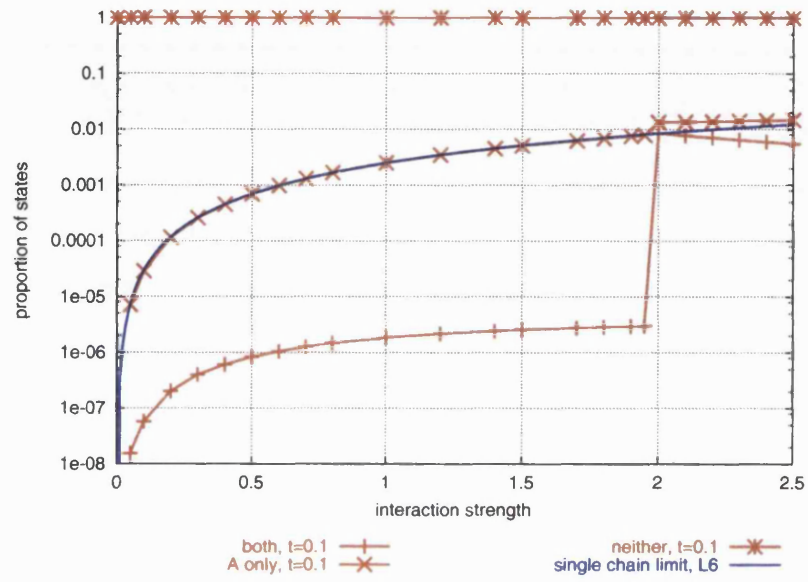

Figure 5.36: Contribution of bosonic basis states to the ground states of the $L = 6$, $N = 3$, $t_\perp = 0.1$ $v_F^A = v_F^B = 1.0$ system as a function of interaction strength I.

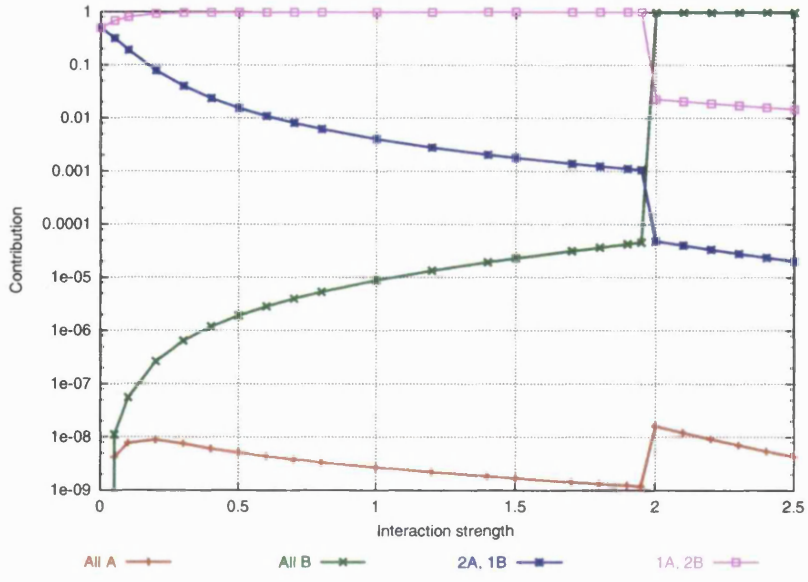

Figure 5.37: Charge distribution for the $L = 6$, $N = 3$, $t_\perp = 0.1$, $v_F^A = v_F^B = 1.0$ system as a function of interaction strength I.

5.5 Summary

In this chapter we have presented results for the Luttinger model coupled-chain systems with equal Fermi velocities, different Fermi velocities and different numbers of electrons. We have calculated the eigenstates and eigenvalues, examined the spectral properties, and calculated Luttinger liquid parameters that suggest that electron-electron interaction effects are likely to be important for atomic scale wires on a surface. Suggestions for further work on these systems is given in chapter 7. However, we have only been able to perform these exact calculations on relatively small systems. In the next chapter we examine the possibility of using the Density Matrix Renormalization Group method to calculate the properties of larger, more realistic systems.

Part III

DMRG calculations

Chapter 6

DMRG studies of atomic wires

> The illusion of 'finding' is perhaps the most pleasant kind of vertigo and one to which one would like to surrender if one did not know that, like the euphoria produced by cold or depth, it can be fatal.
>
> Pierre Boulez, *"The Elliptical Geometry of Utopia"*,1979

6.1 Introduction **160**
6.2 DMRG theory **160**
6.3 Applying the theory **164**
6.4 Exact calculations **166**
6.5 DMRG results **168**

6.1 Introduction

There are several potential advantages in using a numerical method such as the Density Matrix Renormalization Group (DMRG) method for studying problems of this kind, and indeed, such attempts have met with not inconsiderable success [20, 44, 51, 108, 127, 128, 131, 134, 138, 139, 154, 162]. Firstly, the most obvious benefit is that it is possible to calculate for much larger systems than with the exact diagonalization methods detailed in chapter 3, making it much easier to perform a finite-size-scaling analysis to obtain information about the properties of a system. In particular, there is an advantage for the two-coupled chain problem presented in the current work. For the work involving the Luttinger model presented in the earlier chapters, it was impossible to calculate for an insulating substrate chain. By using a density matrix renormalization group approach combined with a Hubbard-like Hamiltonian, it was hoped to rectify this by reducing the intrachain hopping matrix element for the substrate chain.

However, significant problems were encountered adapting the code[1] and it proved impossible within the constraints of time to generate results that could be used to calculate the Luttinger parameters and complement the exact diagonalization results of the earlier chapters. Nonetheless, some results were possible and they are presented in this chapter together with a brief account of the DMRG method.

6.2 DMRG theory

In essence, the DMRG method iteratively increases the size of the system under investigation while only keeping the "most important" eigenstates at each iteration, thus keeping the Hilbert space to a manageable size. We shall now review the details of the DMRG method [109, 139, 162].

As we have already noted in section 2.7, one-dimensional lattice models such as the Hubbard model

$$\hat{H} = -t\sum_{i,\sigma}(\hat{c}^{\dagger}_{i+1,\sigma}\hat{c}_{i,\sigma} + \text{H.c.}) + U\sum_{i}\hat{n}_{i,\uparrow}\hat{n}_{i,\downarrow}, \tag{2.84}$$

are exactly solvable (via the Bethe ansatz), but more information, such as correlation functions, can be extracted from exact diagonalization methods. However, there is a limit to the size of the systems that can be treated in this way.

[1] Kindly provided by William Barford at Sheffield University

A solution to this was provided by Kenneth Wilson [163] by integrating out "unimportant" degrees of freedom by using an algorithm of the following form

Algorithm 5: Numerical Renormalization Group outline algorithm

(1) Create a system with L sites, small enough to diagonalize $\hat{H}_L$ exactly
(2) **while** $L <$ required system length
(3) Obtain the m lowest eigenstates and eigenvalues of $\hat{H}_L$
(4) Transform $\hat{H}_L$ to a new basis of the m lowest eigenstates of $\hat{H}_L$: $\hat{H}_L \rightarrow \tilde{H}_L$
(5) Add a site to form $\hat{H}_{L+1}$
(6) **end**

This became known as the numerical renormalization group method (NRG) and works well for the problem Wilson used it to treat - the s-wave Kondo Hamiltonian for a single magnetic impurity in a non-magnetic metal, but works much less well for Hubbard-type Hamiltonians due to problems with the boundary conditions [109], resulting in accuracy being lost after only a few iterations.

There are two ways of solving this problem. The first of these involves using a combination of open and closed boundary conditions, while the second chooses new bases for the expanded systems made up of more than two copies of the original block. The extra blocks then provide the boundaries that the transformed blocks would see as part of the larger system, and so as the number of included blocks is increased, this method tends towards being equivalent to exact diagonalization of the whole system. DMRG is an extension of this idea.

The DMRG technique defines a system as comprising a *system block*—the part of the system we're interested in constructing a basis for, and a *environment block*—the rest of the system, which together form the *superblock*, as shown schematically in figure 6.1. If we label the states of the system block as $|i\rangle$ and those of the environment block as $|j\rangle$, then any state $|\psi\rangle$ of the superblock can be written as a linear combination of system block and environment block states

$$|\psi\rangle = \sum_{ij} \psi_{ij} |i\rangle |j\rangle. \tag{6.1}$$

The reduced density matrix for the system block is then defined as

$$\rho_{ii'} = \sum_{j} \psi^*_{ij} \psi_{i'j}. \tag{6.2}$$

For normalized states, we have $\mathrm{Tr}\rho = 1$. If we label the eigenstates of the diagonalized density matrix as $|u^\alpha\rangle$ and the eigenvalues w_α, then $\sum_\alpha w_\alpha = 1$ because $\mathrm{Tr}\rho = 1$. Because of the nature of the density matrix, for any operator $\hat{A}$ that acts on the system block only, then the expectation value of the operator is given by

$$\langle\hat{A}\rangle = \sum_{ii'} \hat{A}_{ii'}\rho_{i'i} = \mathrm{Tr}\rho\hat{A}, \tag{6.3}$$

and therefore

$$\langle\hat{A}\rangle = \sum_\alpha w_\alpha \langle u^\alpha|\hat{A}|u^\alpha\rangle. \tag{6.4}$$

This property can be used to decide which eigenstates of ρ to be kept at each iteration—if, for a particular α with $w_\alpha \approx 0$, there is no significant error introduced into the action of $\hat{A}$ by discarding the eigenstate $|u^\alpha\rangle$, then we can choose this state as one to discard.

This problem therefore reduces to one of finding a set of m system block states

$$|u^\alpha\rangle = \sum_{\alpha=1}^{m} u_i^\alpha |i\rangle \tag{6.5}$$

that are optimal for representing some eigenstate $|\psi\rangle$ of the superblock. Since we can write a superblock state as a combination of system block and environment block states, we can expand our eigenstate as

$$|\psi\rangle \approx |\tilde{\psi}\rangle = \sum_{\alpha=1}^{m}\sum_j a_{\alpha,j}|u^\alpha\rangle|j\rangle. \tag{6.6}$$

In order for this to be an accurate expansion, we need to minimize the difference between the two representations $||\psi\rangle - |\tilde{\psi}\rangle|$, which will depend on finding both optimal values of the coefficients $a_{\alpha,j}$ and the states $|u_\alpha\rangle$. We can put this in the form

$$|\tilde{\psi}\rangle = \sum_{\alpha=1}^{m} a_\alpha |u^\alpha\rangle|v_\alpha\rangle \tag{6.7}$$

where $\langle j|v^\alpha\rangle = N_\alpha a_{\alpha,j}$, where the N_α normalize the $|v^\alpha\rangle$. This is equivalent to solving a singular value decomposition of the eigenstate $|\psi\rangle$[118]

$$|\psi\rangle = \mathsf{UDV}^T, \tag{6.8}$$

where U is an $l \times l$ orthogonal matrix consisting of columns of the $|u^\alpha\rangle$ we seek, V is an $J \times l$ orthogonal matrix whose columns are the $|v^\alpha\rangle$ we seek, and D is an $l \times l$ diagonal matrix containing the singular values of $|\psi\rangle$—the m largest elements of this are the required values of a_α. The matrix dimension J is given

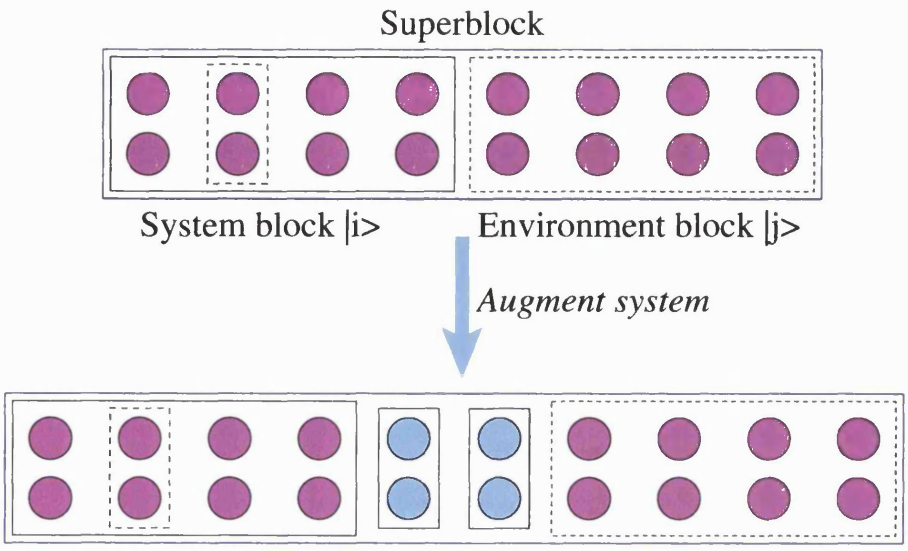

Figure 6.1: Schematic diagram of the DMRG procedure for a two chain system.

by the number of environment basis states being used, and $l \geq J$.

Now since we have originally defined the $|u^{\alpha}\rangle$ to be the eigenvectors of ρ, which itself is given by

$$\rho_{ii'} = \sum_{j} \psi^{*}_{ij}\psi_{i'j}, \tag{6.2}$$

then if the $\psi_{i'j}$ are assumed to be real, we can write

$$\begin{aligned} \rho &= \mathsf{U}\mathsf{D}\mathsf{V}^{T}\mathsf{V}\mathsf{D}\mathsf{U}^{T} \\ &= \mathsf{U}\mathsf{D}^{2}\mathsf{U}^{T}, \end{aligned} \tag{6.9}$$

in other words, the matrix U diagonalizes the density matrix ρ.

6.2.1 The algorithm

Having shown that the optimal states to keep are the m largest eigenstates of the system block density matrix, obtained from an eigenstate of the superblock by the above method, we now come to a description of the DMRG algorithms. There are two basic algorithms, the first, known as the infinite system algorithm, builds up the system to the required size. The second, the finite system algorithm, then successively improves the system generated by the infinite system.

In the infinite system algorithm, the system block is built up one site at a time, and the environment block is chosen for convenience to be a reflection of the system block. This is shown in the top part of figure 6.1. The algorithm is

then given by algorithm 6.

Algorithm 6: DMRG infinite system algorithm

(1) Create a system with L sites, small enough to diagonalize exactly, consisting of a system block, an environment block (each with $l = L/2 - 1$ sites), and two extra sites
(2) **while** $L <$ required system length
(3) Diagonalize the superblock $\hat{H}_L^{\text{superblock}}$ and obtain the ground state $|\psi\rangle$ and its eigenvalue
(4) Add one of the extra sites to the system block, which now has $l + 1$ sites.
(5) Form $\rho_{ii'}$
(6) Diagonalize $\rho_{ii'}$ and obtain the m eigenstates with largest eigenvalues
(7) Construct $\hat{H}_{l+1}$ and the other required operators for the new system block and transform them to the basis set of ρ
(8) Form a superblock of size $L+2$ using the transformed Hamiltonian $\tilde{H}_{l+1}$ plus a single site for the system block, and a reflection $\tilde{H}^R_{l'+1}$ plus a single site for the environment block
(9) $L + 2 \rightarrow L$; $\hat{H}^{\text{superblock}}_{L+2} \rightarrow \hat{H}^{\text{superblock}}_L$
(10) **end**

Once this procedure has been carried out we will need to refine the superblock. The finite system algorithm achieves this by choosing the environment block such that the size of the superblock is kept constant at each step. The finite system method is given by algorithm 7.

6.3 Applying the theory

We can now begin to apply the DMRG theory to the problem in hand. For the moment, let this remain as the problem of two identical chains coupled together by matrix element $t_\perp$. We use a Hubbard model to give the system Hamiltonian

$$\hat{H} = U^A \sum_i \left(n^A_{i,\uparrow} - \frac{1}{2}\right)\left(n^A_{i,\downarrow} - \frac{1}{2}\right) + t_\perp \sum_{\sigma,i} \left[\hat{c}^{\dagger A}_i \hat{c}^B_i + \text{h.c.}\right] + \sum_{\sigma,\alpha,i} t^\alpha_\parallel \left[\hat{c}^{\dagger\alpha}_{\sigma,i}\hat{c}^\alpha_{\sigma,i+1} + \text{h.c.}\right] + \varepsilon \sum_{\sigma,\alpha,i} n^\alpha_{\sigma,i}. \quad (6.10)$$

The first term gives us the on-site electron-electron interaction for the first chain only, which represents the wire. By using this form rather than merely $Un_\uparrow n_\downarrow$ we ensure proper particle-hole symmetry, i.e. the same energy penalty

Algorithm 7: DMRG finite system algorithm

(1) Perform algorithm 6 until the required system size L is reached, storing the operators at each step
(2) **until** convergence achieved
(3) **while** $l' > 1$ ("left to right" phase)
(4) Obtain $\tilde{H}_{l+1}$ as in algorithm 6
(5) Form a size L superblock using $\tilde{H}_{l+1}$, two single sites and $\tilde{H}^R_{l'-1}$, i.e. $l' = L - l - 2$
(6) $l + 1 \rightarrow l; l' - 1 \rightarrow l'$
(7) **end**
(8) **while** $l > 1$ ("right to left"phase)
(9) Using the method of algorithm 6 obtain $\tilde{H}^R_{l'+1}$ by reversing the roles of $\tilde{H}_l$ and $\tilde{H}^R_{l'}$
(10) $l - 1 \rightarrow l; l' + 1 \rightarrow l'$
(11) **end**
(12) **end**

will apply to a site occupied by two holes as to a site occupied by two electrons. The second term of the Hamiltonian is the interchain hopping for electrons with spin $\sigma = \uparrow, \downarrow$. The third term is the intrachain hopping for the two chains $\alpha = A, B$ of electrons with spin σ from site i to site $i+1$. The "semiconducting" properties of the substrate chain B relative to the "metallic" properties of the wire chain A can be achieved by using different values of the intrachain hopping parameter $t_{||}$ for each of the chains. Finally we have the on-site energy with parameter α, which we have set to zero.

There are several ways of using DMRG results to determine the Luttinger parameters of the system. It is possible to determine K_ρ directly from the correlation functions, but this involves numerical calculation of the exponent of a power law and is therefore difficult. In some systems the asymptotic form of the Friedel oscillations can be used to generate K_ρ, as in reference [139]. However, as one of the advantages inherent in the DMRG method is that it expands the size of the system at each step, a finite size scaling method appears an obvious choice.

By considering the scaling of the charge excitation energy Δ_{ch} as well as that of the first two neutral excitations, it is possible to determine both the Luttinger velocity v_0 and K_ρ directly. In a simple approach, such as that used by Weiße *et al.* [160] and Bursill *et al.* [20], the scaling properties of the ground state energy E_g

$$\frac{E_g}{N} \approx \varepsilon_\infty - \frac{\pi v_0}{6N^2}, \tag{6.11}$$

(where ε_∞ is the bulk ground-state energy density) can be used to obtain v_0. The scaling form of the charge excitation Δ_{ch}

$$\Delta_{\mathrm{ch}} = \frac{\pi v_0}{2K_\rho N}, \tag{6.12}$$

can then be used to obtain K_ρ. However, there are non-linear correction terms to equation (6.12) and so this simple approach may lead to unreliable results. Bursill *et al.* [20] include these correction terms to obtain an expression using both the charge and second neutral excitation energy scaling Δ_2

$$\Delta_{\mathrm{ch}} + \Delta_2 \approx \frac{2\pi v_0}{N}\left[\frac{3}{4K_\rho} + K_\rho\right] + \mathrm{O}\left(\frac{1}{(\ln N)^2}\right). \tag{6.13}$$

In this way it was hoped to obtain the Luttinger parameters for our system.

6.4 Exact calculations

For the limiting case of two non-interacting chains, we can again obtain exact results with which we can compare the DMRG-generated results. We first set up a 2-chain Hubbard model with hopping both between chains and with intra-chain nearest neighbour hopping as given by equation (6.10) with $t_{||}^A = t_{||}^B$.

The Hamiltonian matrix can be constructed as follows. We first have, for each chain, a block allowing nearest neighbour hopping with matrix element $t_{||}$:

$$\text{Intrachain block} = \begin{bmatrix} 0 & t_{||} & 0 & \dots & \dots \\ t_{||} & 0 & t_{||} & 0 & \dots \\ 0 & t_{||} & 0 & t_{||} & \dots \\ \vdots & & \ddots & & \ddots \\ \dots & & & 0 & t_{||} \\ \dots & & 0 & t_{||} & 0 \end{bmatrix} \tag{6.14}$$

We also need to allow hopping between the two chains with matrix element $t_\perp$, which gives a complete Hamiltonian of the form

$$\hat{H} = \begin{bmatrix} \begin{pmatrix} \text{chain 1} \\ \text{intrachain part} \end{pmatrix} & \begin{pmatrix} \text{chain 2-1} \\ \text{interchain part} \end{pmatrix} \\ \begin{pmatrix} \text{chain 1-2} \\ \text{interchain part} \end{pmatrix} & \begin{pmatrix} \text{chain 2} \\ \text{intrachain part} \end{pmatrix} \end{bmatrix} \tag{6.15}$$

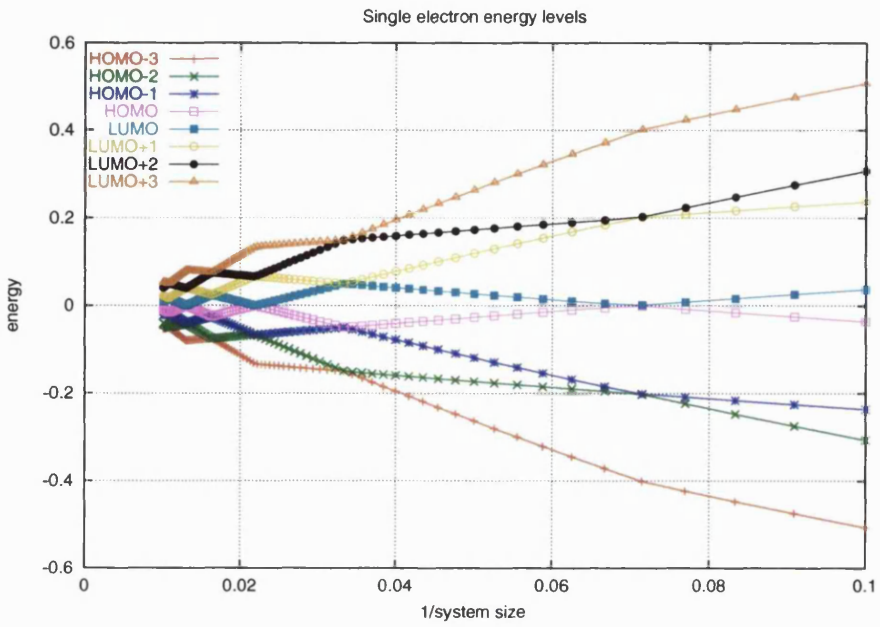

Figure 6.2: One-electron energies as a function of inverse system length for a non-interacting two-chain Hubbard system at half-filling

For example, for two chains each of length 4, we have

$$\hat{H}_{L=4} = \begin{bmatrix} 0 & t_{||} & 0 & 0 & t_{\perp} & 0 & 0 & 0 \\ t_{||} & 0 & t_{||} & 0 & 0 & t_{\perp} & 0 & 0 \\ 0 & t_{||} & 0 & t_{||} & 0 & 0 & t_{\perp} & 0 \\ 0 & 0 & t_{||} & 0 & 0 & 0 & 0 & t_{\perp} \\ t_{\perp} & 0 & 0 & 0 & 0 & t_{||} & 0 & 0 \\ 0 & t_{\perp} & 0 & 0 & t_{||} & 0 & t_{||} & 0 \\ 0 & 0 & t_{\perp} & 0 & 0 & t_{||} & 0 & t_{||} \\ 0 & 0 & 0 & t_{\perp} & 0 & 0 & t_{||} & 0 \end{bmatrix} \tag{6.16}$$

This can be easily diagonalized by using a LAPACK subroutine such as `dsyev`, and we can thus obtain the one-electron eigenvalues and eigenvectors. As we are interested in fillings close to or equal to half filling, we can also calculate the total energy for these states.

For half-filling, we can examine the structure of the one-electron states in the vicinity of the LUMO and HOMO states as a structure of the system length. This is plotted in figure 6.2.

We can see that as the system size increases the single electron levels, as would be expected, grow closer to each other. There are in fact a series of bands

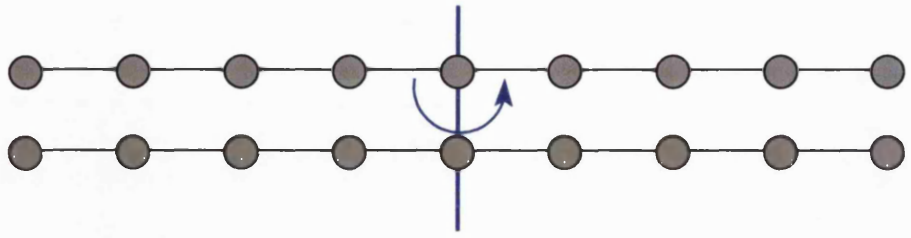

Figure 6.3: A reflection about the short axis of the system corresponds to parity between the ends of the chains

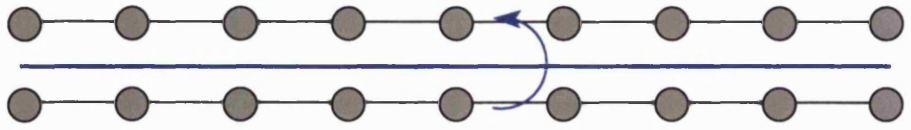

Figure 6.4: A reflection about the long axis of the system corresponds to parity between the chains

initially separated by values of $2t_\perp$ — for example, the HOMO-1 level and HOMO levels are separated by $2t_\perp$ in the region $L < 14$ $(1/L \gtrsim 0.7)$. The HOMO and LUMO levels converge, and subsequently cross, at $L = 14$, and at this point the parities of the HOMO and LUMO levels swap.

In a system such as this, there are two types of parity, corresponding to reflections about the short and long axes of symmetry for the system. Firstly, we have "long" parity between the ends of the chains, which corresponds to a reflection about the short axis of the system, as shown in figure 6.3. Secondly, we can reflect the system about its long axis, to measure the "short" parity between the chains, as shown in figure 6.4. The parities of all the single-electron states can be measured by examination of the eigenvalues returned by the exact-calculation code. For now, we merely note that the HOMO/LUMO crossing at $L = 14$ gives a change in parity for both the long and short axis reflections, while the crossing at $L = 29, 30$ corresponds to a change in the short parity (long axis reflection) but no change in the long parity (short axis reflection).

6.5 DMRG results

We can use these exact results to compare with the $U = 0.0$ DMRG results at half filling. The ground state and first excited state energies are plotted in figures 6.5 and 6.6 respectively. The values given by the DMRG code and the exact results are plotted as a function of system size on the left hand axis, while

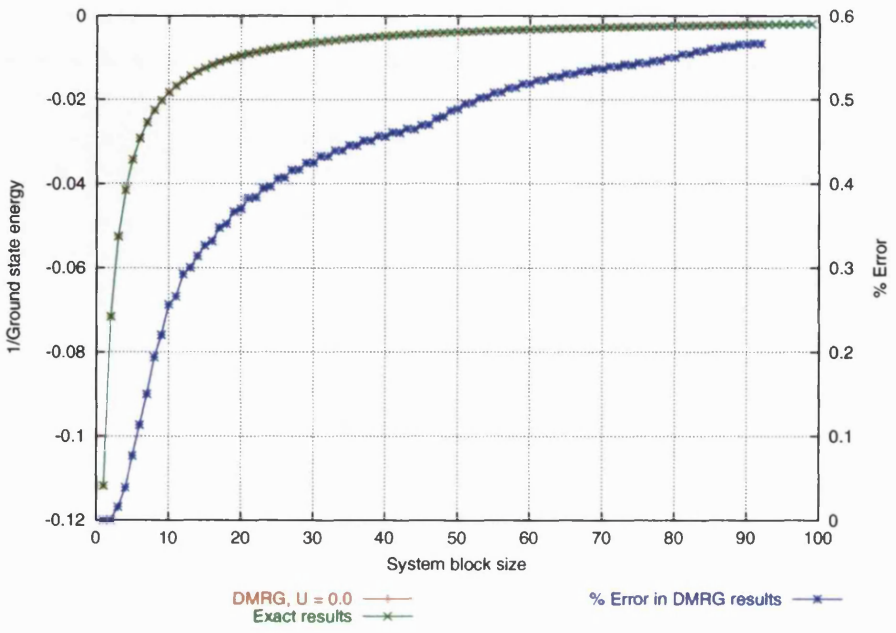

Figure 6.5: Exact and DMRG results for the ground state energies of the $U = 0.0$ half filling system. The percentage error is plotted on the right hand axis.

the percentage error between the two values is shown on the right hand axis. We note that the errors are small—of the order of 0.5%—and increase with the system size, as would be expected. However, a problem arises when we attempt to evaluate the excitation energy, the difference between the ground state and first excited state energies. This is plotted in figure 6.7. If we examine the exact results (plotted in green), we see that the excitation energy successively goes to zero, grows again to a maximum, and then reduces once more. This corresponds directly to the vertical distance between the HOMO and LUMO levels of figure 6.2. However, the DMRG results match the exact results only for system sizes of $L < 30$, and for larger systems the DMRG results bear no relation to the exact results. The DMRG code appears to successfully pick up the parity change at $L = 14$, but *not* the short parity only change at $L = 30$. This result was found both for runs of the DMRG code with short parity turned off and runs with short parity included. As we had hoped to use the excitation energy to directly evaluate the Luttinger parameters for the system, this would seem to present us with a major problem.

Moreover, we appear to have a problem even for the shorter ($L < 30$) systems, where at first glance the DMRG results appear to be in good agreement with the exact results. Figure 6.8 shows various results for the deviation of the DMRG results from the exact results for the half filled system as a function

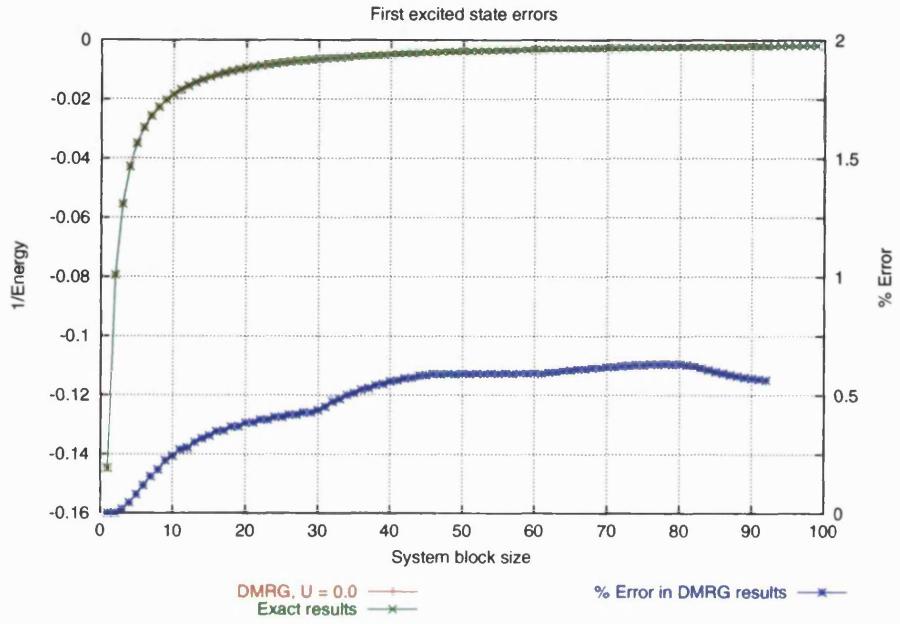

Figure 6.6: Exact and DMRG results for the first excited state energies of the $U = 0.0$ half filling system. The percentage error is plotted on the right hand axis.

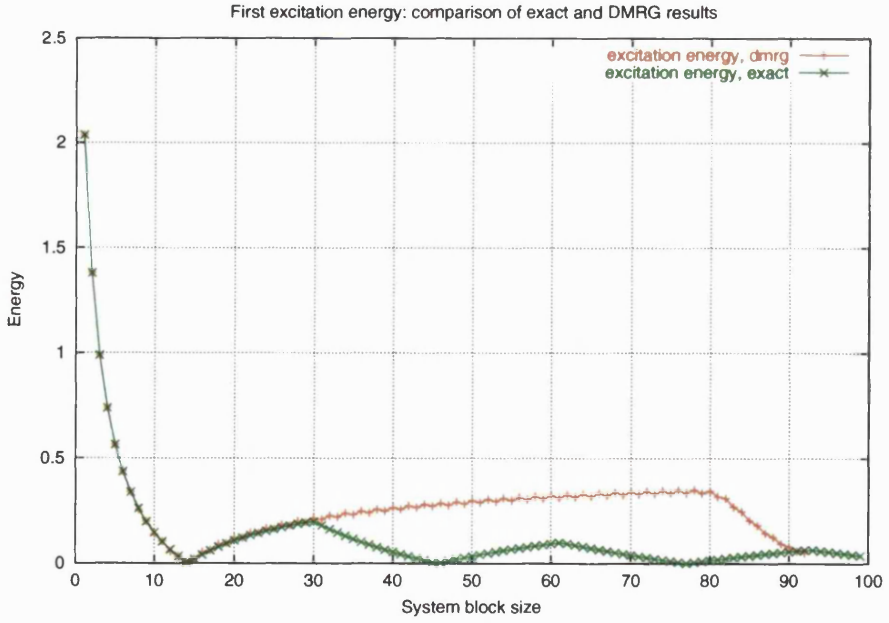

Figure 6.7: First excitation energies as calculated exactly and using the DMRG code

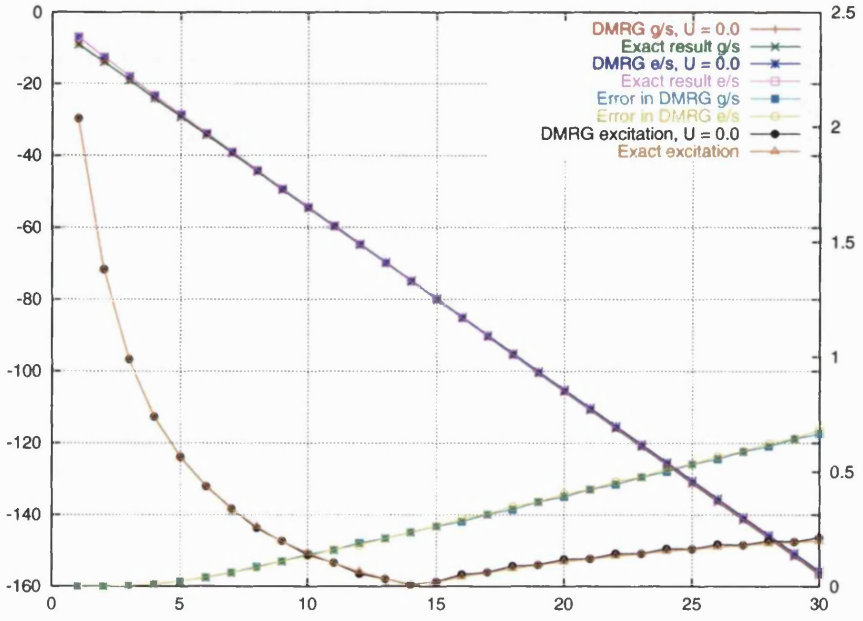

Figure 6.8: Error comparison for the DMRG results

of system length for $L < 30$. The DMRG ground state energy, exact ground state energy, DMRG excited state energy and exact excited state energy are plotted against the left hand axis and overlap almost entirely at this scale. The exactly-calculated excitation energy (shown in orange) and the DMRG excitation energy (black) are plotted against the right hand axis, and, as we have already noted, appear to be in good agreement. The difference between the exact and DMRG ground state energies are also plotted (in turquoise) against the right hand axis, together with the difference between the exact and DMRG excited state energies (yellow). It is clear from figure 6.8 that while the errors in the ground state and first excited state energies are indeed small, systematic and roughly equal to each other within this range of system sizes, they are nonetheless *greater* than the quantity we are trying to measure, the excitation energy, for all system sizes with $L > 10$!

It is unclear how these errors would propagate into $U > 0.0$ systems, but as these systems cannot easily be solved exactly, we have no way of quantifying this. Therefore, unfortunately, the DMRG results as calculated here cannot reliably be used to calculate the Luttinger liquid properties of the system.

Chapter 7

Conclusions

> You usually find something, if you look, but it is not always quite the something you were after.
>
> J.R.R. Tolkien, *"The Hobbit"*

7.1 Achievements **173**

7.2 Proposal for future work **175**

7.3 Summary **177**

7.1 Achievements

We conclude this study with a discussion of the results presented in the earlier chapters. Atomic-scale wires represent a class of systems of utmost relevance to today's world. As candidates for components in future atomic-scale devices, it is essential to know more about their electronic properties. We have shown in chapter 1 that while the electronic structure of such systems has been well studied recently, transport and other properties have been considered only by incomplete methods that do not treat electron-electron interactions adequately. We have reviewed, in chapter 2, the known properties of pure one-dimensional conducting systems and how these theories have been applied to related problems such as systems of coupled Luttinger chains. The spectral properties of such systems have been reviewed and we have discussed how these properties can be used as a probe for Luttinger liquid behaviour in atomic-wire systems, both experimentally by utilizing photoemission techniques and by the theoretical methods discussed in chapter 3. We have thoroughly reviewed these exact diagonalization techniques, used to calculate the eigenstates and correlation functions, and introduced the model for the atomic-wire system.

While this model represents the substrate surface in an inadequate and simplistic manner, we have justified the choice of this simplification as necessary to treat the problem, which has not been studied before, in an accessible way. The basic question we are attempting to answer is whether the coupling of an Luttinger liquid wire to a surface destroys any or all of its one-dimensional properties. We have attempted to answer this question purely by examination of the eigenstates and correlation functions of the model system. A more direct way of answering this question would indeed be to measure the transport properties directly. However this would require substantial changes to the model which we believe would run the risk of obscuring the basic question: whether one-dimensional metallic systems coupled to surfaces *in general* retain their one-dimensional properties, regardless of the influence of such external sources as leads. The potential for extending the current work in this area will, however, be discussed in section 7.2.

We believe that we have gone a long way on the path to answering these questions in chapter 5. First, we have presented results for a system of two chains, identical except for the presence of electron-electron interactions on one chain, representing the wire. We have shown that the coupling to the surface is weak in nature even for coupling parameters as high as $t_\perp = 0.5$, as the contribution to the ground state from basis states involving bosons remains comparable to that for an isolated Luttinger-liquid chain. We have seen that

there is a fundamental change in the nature of the low-lying neutral excitations at a certain value of the interaction strength, owing mainly to the finite length of the chains. However, this shift, from interband excitations with $\Delta k = 0$ to intraband excitations with $\Delta k = 2\pi v_F/L$ also leads to a transfer of charge away from the interacting "wire" chain to the non-interacting "substrate" chain, resulting in the restoration of some Fermi liquid properties. In particular the excitation energy in this region depends *not* on the Luttinger velocity v_0 but on the Fermi velocity v_F. However, the spectral properties, which depend on the nature of the charged rather than the neutral excitations, indicate that Luttinger liquid behaviour survives at values of the interaction strength not only below this threshold, but also above it. This behaviour manifests itself in the removal of spectral weight from the Fermi surface, and we have used this feature to calculate effective values of the Luttinger parameters K_ρ and α for our system. These calculated values of K_ρ and α indicate definitive Luttinger liquid behaviour for the system as a whole, and moreover, tend toward the values for an isolated continuum chain as the system length L increases.

We have also calculated for a system where the two chains have different non-interacting properties, by assigning differing values of v_F to the two chains. While this in no way fully reflects the reality of an insulating or semiconducting substrate, such a system nonetheless includes some or the required properties, and furthermore, is interesting in its own right. We have found that many of the results from the equal-v_F system also hold for this system. These include the weak coupling nature indicated by the presence of bosonic basis states in the ground state, the nature of the neutral excitations (although the transition to the $\Delta k = 2\pi v_F/L$ excitations occurs at a higher value of I, as would intuitively be expected), and the removal of spectral weight from the Fermi surface as interactions are introduced. The corresponding Luttinger parameters have also been calculated. However, here we find that there are two branches of the spectral function $\rho(|q| > 0, \omega)$, which yield differing values of K_ρ, implying that the system is strongly Luttinger liquid-like at low interaction strengths, but that at values of interaction strength $I \gtrsim 1.0$, the system is *less* Luttinger liquid-like than the equal v_F system. This threshold at $I \approx 1.0$ is much lower than the threshold for the change in nature of the neutral excitations, which occurs in the vicinity of $I \approx 3.0$ for this system. Nonetheless, the obtained values of K_ρ for the $I > 1.0$ region still indicate the system has a non-Fermi liquid nature, merely to a lesser extent.

We have also reported results for a system with an odd number of electrons available for excitation. These results, although preliminary, indicate properties

that may lead to behaviour different from that for the even-occupancy systems. In particular, there are discontinuities in the ground-state properties that are absent from the ground states of the two-electron system, although similar to those found in the excited states. Calculation of the spectral functions of this system was not possible within the current time frame, although it is hoped that these calculations may be performed in the near future.

We have also presented, in chapter 6, initial yet inconclusive DMRG results for a similar system. However, this Hubbard model-based system is much more extensible to represent an insulating substrate. It is to be regretted that it did not prove possible to extract the required information needed to determine the presence or otherwise of Luttinger liquid behaviour in this system, and it is hoped that this too may be rectified in the future.

7.2 Proposal for future work

The achievements of the present work notwithstanding, there are many questions still to be answered—in effect we have only begun to scratch the surface of this important problem. Obviously, the most immediate improvement that could be made to the present model would be to include a true insulating substrate; longer term, it would be useful to be able to combine electronic structure techniques with the methods presented here and study a complete wire/surface system. However, this is a long way off.

There are several calculations that can be performed in the short term with little or no change to the current setup. Calculations with different numbers of electrons can be performed, in particular it is planned to generate a complete set of 3-electron calculations to complete the work presented in section 5.4. Calculations on longer systems may become possible as computing power increases; however it is unlikely that it will ever be possible to calculate for systems very much larger than those discussed here as the size of the Hilbert space scales so badly with system length. Nonetheless it may prove possible to extract some finite-size scaling information to complement the present results. In addition, it is simple to calculate for other electron-electron interaction forms and ranges, and in particular it would be interesting to examine the effects of a more realistic potential, such as a screened Coulomb interaction.

In the longer term, there are several extensions that can be made that would require rather more work. Ultimately, it would be ideal to study transport properties, and in particular the effect of leads on the system—obviously for these wires to be useful in future devices the effect of the connections to the

rest of the circuit must be fully accounted for. This would initially involve a change of boundary conditions from the periodic boundary conditions used here to open boundary conditions. The implications of such a change has been discussed in section 2.6.1. Since the main alteration appears to be that the right- and left-moving fermion populations are no longer independent but have a simple interdependence, this would be relatively simple to implement within the current model. It would then be necessary to evaluate the resulting boundary effects before proceeding. The effect of macroscopic leads could also then be included—this is a problem that has already been considered for a Luttinger liquid with no longitudinal surface coupling [68, 73, 78, 104, 125].

In this way it would be possible to build up a much more detailed picture of the nature of atomic scale wires on surface. However, without the inclusion of an insulating substrate the usefulness of this would be limited. Owing to the construction of our basic Hamiltonian in the form $\hat{H}^A+\hat{H}^B+\hat{H}^{\text{hopping}}$, however, if it was possible to find a suitable (i.e. non-Luttinger model) insulating form for $\hat{H}^B$ that could be represented in a way compatible with the Luttinger model representation then it might prove possible to rectify this.

There are a few other directions the work could take. It could prove possible to include more than one chain to represent the surface, although this would further limit the size of the system on which we could perform exact diagonalization procedures. In addition, it would be necessary to convince ourselves that the secondary surface chains would have a significant effect on the properties of the wire. As experimental results show that these wires appear to have a truly one-dimensional nature, this may well not prove to be the case.

No phonons have been included in the current work, and indeed, no lattice distortions are allowed for in the pure Luttinger model. However, controversy remains as to what extent electron-phonon interactions may be of importance in one-dimensional conductors and so it would also be interesting to include this in future work. In particular, the work of Rao *et al.* [119] may provide a path to implement this.

We have also assumed that there is no interaction between the wire electrons and the surface electrons. In the form of Coulomb drag [78, 104], it is possible that this may have an effect on our wire/surface system and it would be interesting to investigate the likelihood of this possibility.

7.3 Summary

In summary, therefore, we have investigated the problem of electron-electron interactions in an atomic scale wire on a surface. We have presented results that indicate that the resulting system does not behave as a pure Luttinger liquid but nonetheless retains many characteristics consistent with Luttinger liquid behaviour. It is clear from our results, however, that there is an important caveat to be borne in mind for hybrid systems such as this—that the results obtained depend very much on the properties of the system one chooses to measure.

Bibliography

[1] Milton Abramowitz and Irene A. Stegun, editors. *Handbook of Mathematical Functions.* Dover, 1965.

[2] Alexander Altland, C.H.W. Barnes, F.W.J. Hekking, and A.J. Schofield. Magnetotunneling as a probe of Luttinger-liquid behaviour. *Physical Review Letters*, 83:1203–1206, 1999. Preprint at cond-mat/9907459.

[3] K. N. Altmann, J. N. Crain, A. Kirakosian, J.-L. Lin, D.Y. Petrovykh, F.J. Himpsel, and R. Losio. Electronic structure of atomic chains on vicinal Si(111)-Au. *Physical Review B*, 64:035406, 2001.

[4] P.W. Anderson and Yong Ren. *The theory of superconductivity in the high T_c cuprates*, chapter 5 :The one-dimensional Hubbard model. Princeton University Press, 1997.

[5] M. Aoki, P. Gumbsch, and D.G. Pettifor. *Interatomic potentials and structural stability*, volume 114 of *Springer Series in Solid-State Sciences*, chapter Angularly-dependent many-atom bond order potentials. Springer, 1993.

[6] Masato Aoki. A rapidly convergent bond order expansion for atomistic simulations. *Physical Review Letters*, 71(23):3842–3845, 1993.

[7] E. Arrigoni. Crossover to Fermi-liquid behaviour for weakly coupled Luttinger liquids in the anisotropic large-dimension limit. *Physical Review B*, 61(12):7909–7929, 2000.

[8] Enrico Arrigoni. Crossover from Luttinger- to Fermi-liquid behaviour in strongly anisotropic systems in large dimensions. *Physical Review Letters*, 83(1):128–131, 1999.

[9] N.W. Ashcroft and N.D. Mermin. *Solid State Physics.* Saunders College, Philadelphia, International edition, 1976.

[10] O.M. Auslaender, A. Yacoby, R. de Picciotto, K.W. Baldwin, L.N. Pfeiffer, and K.W. West. Tunneling spectroscopy of the elementary excitations in a one-dimensional wire. *Science*, 295:825–828, 2002.

[11] O.M. Auslaender, A. Yacoby, R. de Picciotto, K.W. Baldwin, L.N. Pfeiffer, and K.W. West. Experimental evidence for resonant tunneling in a Luttinger liquid. *Physical Review Letters*, 84(8):1764–1767, 2000.

[12] V.S. Babichenko. Metal-insulator transition of the quasi-one-dimensional Luttinger liquid due to the long-range character of the Coulomb interaction. *Physics Letters A*, 261:102–107, 1999.

[13] Cristina Bena, Smitha Vishveshwara, Leon Balents, and Matthew P.A. Fisher. Quantum entanglement in carbon nanotubes. cond-mat/0202102, February 2002.

[14] S. Biermann, A. Georges, T. Giamarchi, and A. Lichtenstein. Quasi-one-dimensional organic conductors: dimensional crossover and some puzzles. cond-mat/0201542, January 2002.

[15] S. Biermann, A. Georges, A. Lichtenstein, and T. Giamarchi. Deconfinement transition and Luttinger to Fermi liquid crossover in quasi-one-dimensional systems. *Physical Review Letters*, 87(27):276405, 2001.

[16] Ya.M. Blanter, F.W.J. Hekking, and M. Büttiker. Interaction constants and dynamic conductance of a gated wire. *Physical Review Letters*, 81:1925–1928, 1998.

[17] Marc Bockrath, David H. Cobden, Jia Lu, Andrew G. Rinzler, Richard E. Smalley, Leon Balents, and Paul L. McEuen. Luttinger-liquid behaviour in carbon nanotubes. *Nature*, 397:598–601, February 18 1999.

[18] Daniel Boies, C. Bourbonnais, and A.-M.S. Tremblay. One-particle and two-particle instability of coupled Luttinger liquids. *Physical Review Letters*, 74(6):968–971, 1995.

[19] D. R. Bowler and A. J. Fisher. Small polaron formation in dangling-bond wires on the Si(001) surface. *Physical Review B*, 63:035310, 2000.

[20] Robert J. Bursill, Ross H. McKenzie, and Chris J. Hamer. Phase diagram of the one-dimensional Holstein model of spinless fermions. *Physical Review Letters*, 80(25):5607–5610, 1998.

[21] Krzysztof Byczuk and Tomaszz Dietl. Realistic electron-electron interaction in a quantum wire. *Physical Review B*, 60(3):1507–1510, 1999.

[22] S. Capponi and D. Poilblanc. Transverse transport in coupled strongly correlated electronic chains. *Zeitschrift für Physik B*, 103:173–176, 1997.

[23] S. Capponi, D. Poilblanc, and E. Arrigoni. Universal scaling behaviour of coupled chains of interacting fermions. *Physical Review B*, 57:6360–6369, 1998.

[24] S. Capponi, D. Poilblanc, and F. Mila. Confinement and transverse conductivity in coupled Luttinger liquids. *Physical Review B*, 54:17,547–17,556, 1996.

[25] Sylvain Capponi, Didier Poilblanc, and Thierry Giamarchi. Effects of long-range electronic interactions on a one-dimensional electron system. *Physical Review B*, 61(20):13,410–13,417, 2000.

[26] A.M. Chang, L.N. Pfeiffer, and K.W. West. Observation of chiral Luttinger behaviour in electron tunnelling into fractional quantum Hall edges. *Physical Review Letters*, 77(12):2538–2541, 1996.

[27] Y. Chen, D.K.K. Lee, and M.U. Luchini. Functional-integral approach to an exactly solvable one-dimensional electron-phonon system. *Physical Review B*, 38(12):8497–8500, 1988.

[28] David G. Clarke, S.P. Strong, and P.W. Anderson. Incoherence of single particle hopping between Luttinger liquids. *Physical Review Letters*, 72(20):3218–3221, 1994.

[29] C.E. Creffield, Wolfgang Häusler, and A.H. Macdonald. Spin and charge Luttinger-liquid parameters of the one-dimensional electron gas. cond-mat/0005354, May 2000.

[30] L.K. Dash and A.J. Fisher. Does Luttinger liquid behaviour survive in an atomic wire on a surface? *Journal of Physics: Condensed Matter*, 13:5035–5046, 2001.

[31] Supriyo Datta. *Electronic transport in mesoscopic systems.* Cambridge studies in semiconductor physics and microelectronic engineering. Cambridge University Press, 1995.

[32] P.A.M. Dirac. *The principles of quantum mechanics.* Clarendon Press, Oxford, fourth edition, 1958.

[33] P. Doumergue, L. Pizzagalli, C. Joachim, A. Altibelli, and A. Baratoff. Conductance of a finite missing hydrogen atomic line on Si(001)-(2×1)-H. *Physical Review B*, 59(24):15,910–15,916, 1999.

[34] P. Durganandini and Sumathi Rao. Transport in double-crossed Luttinger liquids. *Physical Review B*, 59(20):13 122–13 125, 1999.

[35] Reinhold Egger and Hermann Grabert. Applying voltage sources to a Luttinger liquid with arbitrary transmission. *Physical Review B*, 58(16):10,761–10,767, 1998.

[36] Sebastian Eggert. Scanning tunneling microscopy of a Luttinger liquid. *Physical Review Letters*, 84(19):4413–4416, 2000.

[37] Sebastian Eggert, Henrik Johannesson, and Ann Mattsson. Boundary effects on spectral properties of interacting electrons in one dimension. *Physical Review Letters*, 76(9):1505–1508, 1996.

[38] T.M.R. Ellis, Ivor R. Philips, and Thomas M. Lahey. *Fortran 90 programming*. Addison-Wesley, 1994.

[39] Stanley Engelsberg and B.B. Varga. One-dimensional electron-phonon model. *Physical Review*, 136(6A):A1582–A1598, 1964.

[40] M. Fabrizio. Role of transverse hopping in a two-coupled chains model. *Physical Review B*, 48(21):15 838–15 860, 1993.

[41] M. Fabrizio and Alexander O. Gogolin. Interacting one-dimensional electron gas with open boundaries. *Physical Review B*, 51(24):17,827–17,841, 1995.

[42] M. Fabrizio and A. Parola. Spin-charge separation in a model of two coupled chains. *Physical Review Letters*, 71(2):226–229, 1993.

[43] M. Fabrizio, A. Parola, and E. Tosatti. Strong-coupling phases of two Hubbard chains with interchain hopping. *Physical Review B*, 46(5):3159–3162, 1992.

[44] G. Fano, F. Ortolani, A. Parola, and L. Ziosi. Unscreened Coulomb repulsion in the one-dimensional electron gas. *Physical Review B*, 60(23):15,654–15,659, 1999.

[45] Paul Fendley and Chetan Nayak. Tunneling between Luttinger liquids. *Physical Review B*, 63:115102, 2001.

[46] A.M. Finkelstein and A.I. Larkin. Two coupled chains with Tomonaga-Luttinger interactions. *Physical Review B*, 47(16):10 461–10 473, 1993.

[47] M Fowler. Quantum integrable systems in one dimension. *Physica D*, 86:189–197, 1995.

[48] Holger Frahm and V.E. Korepin. Critical exponents for the one-dimensional Hubbard model. *Physical Review B*, 42(16):10,553–10,565, 1990.

[49] Akira Furusaki and Naoto Nagaosa. Single-barrier problem and Anderson localization in a one-dimensional interacting electron system. *Physical Review B*, 47(8):4631–4643, 1993.

[50] Florian Gebhard and Andrei E. Ruckenstein. Exact results for a Hubbard chain with long-range hopping. *Physical Review Letters*, 68(2):244–247, 1992.

[51] G.A. Gehring, R.J. Bursill, and T. Xiang. Applications of the density matrix renormalization group to problems in magnetism. cond-mat/9608127, August 1996.

[52] Antoine Georges, Thierry Giamarchi, and Nancy Sandler. Interchain conductivity of coupled Luttinger liquids and organic conductors. *Physical Review B*, 61(24):16,393–16,396, 2000.

[53] T. Giamarchi. Umklapp process and resistivity in one-dimensional fermion systems. *Physical Review B*, 44(7):2905–2913, 1991.

[54] Gene H. Golub and Charles F. van Loan. *Matrix Computations.* Johns Hopkins University Press, Baltimore, 3rd edition, 1996.

[55] G.Q. Hai, F.M. Peeters, and J.T. Devreese. Screening of the electron-phonon interaction in quasi-one-dimensional semiconductor structures. *Physical Review B*, 48(16):12,016–12,022, 1993.

[56] F.D.M. Haldane. Coupling between charge and spin degrees of freedom in the one-dimensional Fermi gas with backscattering. *Journal of Physics C*, 12:4791–4799, 1979.

[57] F.D.M. Haldane. General relation of correlation exponents and spectral properties of one-dimensional Fermi systems: Application to the anisotropic $s = \frac{1}{2}$ Heisenberg chain. *Physical Review Letters*, 45:1358–1362, 1980.

[58] F.D.M. Haldane. Demonstration of the "Luttinger liquid" character of Bethe-ansatz-soluble modelsof 1-D quantum fluids. *Physics Letters*, 81A:153–155, 1981.

[59] F.D.M. Haldane. Effective harmonic-fluid approach to low-energy properties of one-dimensional quantum fluids. *Physical Review Letters*, 47(25):1840–1843, 1981.

[60] F.D.M. Haldane. "Luttinger liquid theory" of one-dimensional quantum fluids: I Properties of the Luttinger model and their extension to the general 1D interacting spinless Fermi gas. *Journal of Physics C*, 14:2585–2609, 1981.

[61] Roger Haydock. The recursive solution of the Schrödinger equation. *Solid State Physics*, 35:215–294, 1980.

[62] R. Heidenreich, R. Seiler, and D.A. Uhlenbrock. The Luttinger model. *Journal of Statistical Physics*, 22(1):27–57, 1980.

[63] F.J. Himpsel, K.N. Altmann, R. Bennewitz, J.N. Crain, A. Kirakosian, J.-L. Lin, and J.L. McChesney. One-dimensional electronic states at surfaces. *Journal of Physics: Condensed Matter*, 13:11.097–11,113, 2001.

[64] Taro Hitosugi, T. Hashizume, S. Heike, H. Kajiyama, Y. Wada, S. Watanabe, T. Hasegawa, and K. Kitazawa. Scanning tunneling microscopy / spectroscopy of dangling-bond wires fabricated on the Si(100)-2×1-H surface. *Applied Surface Science*, 130-132:340–345, 1998.

[65] Taro Hitosugi, S. Heike, T. Onogi, T. Hashizume, S. Watanabe, Z.-Q. Li, K. Ohno, Y. Kawazoe, T. Hasegawa, and K. Kitazawa. Jahn-Teller distortion in dangling-bond linear chains fabricated on a hydrogen-terminated Si(100)-2 × 1 surface. *Physical Review Letters*, 82:4034–4037, 1999.

[66] A. Houghton, H.-J. Kwon, and J.B. Marston. Multidimensional bosonization. *Advances in Physics*, 49(2):141–228, 2000.

[67] J. Hubbard. Electron correlations in narrow energy bands. *Proceedings of the Royal Society of London Series A*, 276:238–257, 1963.

[68] S. Hügle, R. Egger, and H. Grabert. Static and dynamic image potential for tunneling into a Luttinger liquid. cond-mat/0004305, April 2000.

[69] Aníbal Iucci and Carlos Naón. Exact electronic Green functions in a Luttinger liquid with long-range interactions. *Physical Review B*, 61(23):15,530–15,533, 2000.

[70] E.A. Jagla, K. Hallberg, and C.A. Balseiro. Numerical study of charge and spin separation in low-dimensional systems. *Physical Review B*, 47(10):5849–5853, 1993.

[71] Alan Jennings and J.J. McKeown. *Matrix Computation.* Wiley, 2nd edition, 1992.

[72] C.L. Kane and Matthew P.A. Fisher. Transmission through barriers and resonant tunneling in an interacting one-dimensional electron gas. *Physical Review B*, 46(23):15,233–15,262, 1992.

[73] C.L. Kane and Matthew P.A. Fisher. Transport in a one-channel Luttinger liquid. *Physical Review Letters*, 68(8):1220–1223, 1992.

[74] Y. Kawahito, H. Kasai, H. Nakanishi, and A. Okiji. Effects of intra-site Coulomb interaction on quantized conductance in a quantum wire between an STM tip and a metal surface. *Surface Science Letters*, 409:L709–714, 1998.

[75] S.D. Kevan and Eli Rothenberg. Many body effects at surfaces and interfaces. *Journal of Electron Spectroscopy and Related Phenomena*, 117-118:57–70, 2001.

[76] S. Kirchner, H.G. Evertz, and W. Hanke. Transport properties of one-dimensional hubbard models. *Physical Review B*, 59(3):1825–1833, 1999.

[77] Walter Kohn. Theory of the insulating state. *Physical Review*, 133(1A):A171–A181, 1964.

[78] A. Komnik and R. Egger. Transport and Coulomb drag for two interacting carbon nanotubes. *European Physical Journal B*, 19:271–280, 2001.

[79] Andrei Komnik and Reinhold Egger. Nonequilibrium transport for crossed Luttinger liquids. *Physical Review Letters*, 80(13):2881–2884, 1998.

[80] V.E. Korepin, N.M. Bogoliubov, and A.G. Izergin. *Quantum inverse scattering method and correlation functions.* Cambridge University Press, 1993.

[81] R. Kosloff. Propagation methods for quantum molecular dynamics. *Annual Review of Physical Chemistry*, 45:145–178, 1994.

[82] I.V. Krive. Resonant heat transport through a Luttinger liquid. *Physical Review B*, 59(19):12,338–12,343, 1999.

[83] I.V. Krive and E.R. Mucciolo. Transport properties of quasiparticles with fractional exclusion characteristics. *Physical Review B*, 60(3):1429–1432, 1999.

[84] E.H. Lieb and W. Liniger. Exact analysis of an interacting Bose gas. I The general solution and the ground state. *Physical Review*, 130:1605–1616, 1963.

[85] E.H. Lieb and F.Y. Wu. Absence of Mott transition in an exact solution for the short-range, one-band model in one dimension. *Physical Review Letters*, 20:1444–1448, 19683.

[86] R. Losio, K.N. Altmann, A. Kirakosian, J.-L. Lin, D.Y. Petrovykh, and F.J. Himpsel. Band splitting for Si(557)-Au: Is it spin-charge separation? *Physical Review Letters*, 86(30):4632–4635, 2001.

[87] A. Luther and V.J. Emery. Backward scattering in the one-dimensional electron gas. *Physical Review Letters*, 33(10):589–592, 1974.

[88] A. Luther and I. Peschel. Single-particle states, Kohn anomaly and pairing fluctuations in one dimension. *Physical Review B*, 9(7):2911–2919, 1974.

[89] J.M. Luttinger. *Journal of Mathematical Physics*, 15:609, 1960.

[90] Gerald D Mahan. *Many particle physics.* Plenum Press, second edition, 1990.

[91] E.C. Marino. Field-theoretical approach to the dynamical many-polaron system in one spatial dimension. *Physical Review Letters*, 55(27):2991–2994, 1985.

[92] E.C. Marino. Field-theoretical approach to the dynamical many-polaron system in one spatial dimension: Reply. *Physical Review Letters*, 59(3):371, 1987.

[93] D.C. Mattis and E.H. Lieb. Exact solution of a many-fermion system and its associated boson field. *Journal of Mathematical Physics*, 6:304–312, 1965.

[94] Ann E. Mattsson, Sebastian Eggert, and Henrik Johannesson. Properties of a Luttinger liquid with boundaries at finite temperature and size. *Physical Review B*, 56(24):15,615–15,628, 1997.

[95] V. Meden, W. Metzner, U. Schollwöck, O. Schneider, T. Stauber, and K. Schönhammer. Luttinger liquids with boundaries : Power-laws and energy scales. cond-mat/0002215, February 2000.

[96] V. Meden, W. Metzner, U. Schollwöck, O. Schneider, T. Stauber, and K. Schönhammer. Luttinger liquids with boundaries : Power-laws and energy scales, 2000.

[97] V. Meden and K. Schönhammer. Spectral functions for the Tomonaga-Luttinger model. *Physical Review B*, 46(24):15,753–15,760, 1992.

[98] Augusto A. Melgarejo and Fernando Vericat. Modified Luttinger model and quantum wires. *Physica E*, 8:57–65, 2000.

[99] Kristel Michielsen and Hans De Raedt. Quantum molecular dynamics study of the Su-Schrieffer-Heeger model. *Zeitschrift für Physik B*, 103:391–400, 1997.

[100] F. Mila and K. Penc. Model calculations for 1D correlated systems. *Journal of Electron Spectroscopy and Related Phenomena*, 117-118:451–467, 2001.

[101] P.K. Mohanty and Sumathi Rao. Transport in multi-chain models of interacting fermions. *Journal of Physics A*, 33:7363–7378, 2000.

[102] H. Mori. Localizations in coupled electronic chains. *Physical Review B*, 58:12,699–12,703, 1998.

[103] A.V. Moroz and C.H.W. Barnes K.V. Samokhin and. Spin-orbit coupling in interacting quasi-one-dimensional electron systems. *Physical Review Letters*, 84(18):4164–4167, 2000.

[104] Yuli V. Nazarov and D.V. Averin. Current drag in capacitively coupled Luttinger constrictions. *Physical Review Letters*, 81(3):653–656, 1998.

[105] H. Ness and A.J. Fisher. Quantum inelastic conductance through molecular wires. *Physical Review Letters*, 83(2):452–455, 1999.

[106] H. Ness and A.J. Fisher. Transmission through Peierls distorted one-dimensional atomic wires: quantum coherent electron-phonon coupling. *Applied Surface Science*, 162-163:613–619, 2000.

[107] H. Ness, S.A. Shevlin, and A.J. Fisher. Coherent electron-phonon coupling and polaronlike transport in molecular wires. *Physical Review B*, 63:125422, 2001.

[108] T. Nishino, T. Hikihara, K. Okunishi, and Y. Hieida. Density matrix renormalization group: Introduction from a variational point of view. *International Journal of Modern Physics B*, 13(1):1–24, 1999.

[109] Reinhard M. Noack and Steven R. White. *Density matrix renormalization: A new numerical method in physics*, chapter The density matrix renormalization group. Lecture notes in physics. Springer, Berlin, 1999.

[110] Arkadi A. Odintsov and Hideo Yoshioka. Correlated electrons in carbon nanotubes. cond-mat/9911427, November 1999.

[111] Masao Ogata and P.W. Anderson. Transport properties in the Tomonaga-Luttinger liquid. *Physical Review Letters*, 70(20):3087–3090, 1993.

[112] Dror Orgad. Spectral functions for the Tomonaga-Luttinger and Luther-Emery liquids. cond-mat/0005181, May 2000.

[113] C.C. Paige and M.A. Saunders. Solution of sparse indefinite systems of linear equations. *SIAM Journal of Numerical Analysis*, 12(4):617–629, 1975.

[114] R.E. Peierls. *Quantum theory of solids.* Oxford University Press, 1955.

[115] D. Poilblanc, H. Endres, F. Mila, M.G. Zacher, S. Capponi, and W. Hanke. One-particle interchain hopping in coupled Hubbard chains. *Physical Review B*, 54:10,261–10,264, 1996.

[116] Thomas J. Pollehn, Arno Schindlmayr, and R.W. Godby. Assessment of the *GW* approximation using Hubbard chains. *Journal of Physics C*, 10:1273–1283, 1998.

[117] Henk W. Ch. Postma, Mark de Jonge, Zhen Yao, and Cees Dekker. Electrical transport through carbon nanotube junctions created by mechanical manipulation. *Physical Review B*, 62(16):R10653–R10656, 2000.

[118] William H. Press, Saul H. Teukolsky, William T. Vetterling, and Brian P. Flannery. *Numerical recipes in FORTRAN - The art of scientific computing.* Cambridge University Press, second edition, 1992.

[119] Ch Sambasiva Rao, Phani Murali Krishna, Soma Mukhopadhyay, and Ashok Chatterjee. A fully interacting many-electron-phonon system in one dimension: an exactly solvable model. *Journal of Physics: Condensed Matter*, 13:L919–L924, October 2001.

[120] Sumathi Rao. Transport in Luttinger liquids, 1999. cond-mat/9905049. Talk presented at the 'Symposium on Quantum Many-Body Physics', Delhi, March 1999.

[121] Scot R. Renn and Daniel P. Arovas. Nonlinear $I(V)$ characteristics of Luttinger liquids and gated Hall bars. *Physical Review B*, 51(23):16,832–16,839, 1995.

[122] I.K. Robinson, P.A. Bennett, and F.J. Himpsel. Structure of quantum wires in Au/Si(557). *Physical Review Letters*, 88(9):096104, 2002.

[123] V.A. Sablikov and B.S. Shchamkahlova. Coulomb interaction during coherent transport of electrons in quantum wires. *JETP Letters*, 67(3):196–202, 1998.

[124] I. Safi. A dynamic scattering approach for a gated interacting wire. *European Physical Journal B*, 12:451–455, 1999.

[125] Inès Safi and H.J. Schulz. Interacting electrons with spin in a one-dimensional dirty wire connected to leads. *Physical Review B*, 59(4):3040–3059, 1999.

[126] Daniel Sánchez-Portal, Julian D. Gale, Alberto García, and Richard M. Martin. Two distinct metallic bands associated with monatomic Au wires on the Si(557)-Au surface. *Physical Review B*, 65:081401, 2002.

[127] Peter Schmitteckert and Ulrich Eckern. Phase coherence in a random one-dimensional system of interacting fermions: A density-matrix renormalization group study. *Physical Review B*, 53(23):15,397–15,400, 1996.

[128] K. Schönhammer, O. Gunnarson, and R.M. Noack. Density-functional theory on a lattice: Comparison with exact numerical results for a model with strongly correlated electrons. *Physical Review B*, 52(4):2504–2510, 1995.

[129] K. Schönhammer and V. Meden. Nonuniversal spectral properties of the Luttinger model. *Physical Review B*, 47(24):16,205–16,215, 1993.

[130] K. Schönhammer and V. Meden. Fermion-boson transmutation and comparison of statistical ensembles in one dimension. *American Journal of Physics*, 64(9):1168–1176, 1996.

[131] K. Schönhammer, V. Meden, W. Metzner, U. Schollwöck, and O. Gunnarson. Boundary effects on one-particle spectra of luttinger liquids. *Physical Review B*, 61(7):4393–4396, 2000.

[132] H.J. Schulz, G. Cuniberti, and P. Pieri. Fermi liquids and Luttinger liquids. cond-mat/9807366, 1998. Lecture notes from a summer school at Chia Laguna, Italy, September 1997.

[133] H.J. Schulz and B.S. Shastry. A new class of exactly solvable interacting fermion models in one dimension. *Physical Review Letters*, 80:1924–1927, 1998.

[134] C. Schuster and U. Eckern. Interaction versus dimerization in one-dimensional Fermi systems. *European Physical Journal B*, 5:395–402, 1998.

[135] A. Schwartz, M. Dressel, G. Grüner, V. Vescoli, L. Degiorgi, and T. Giamarchi. On-chain electrodynamics of metallic $(TMTSF)_2X$ salts: Observation of Tomonaga-Luttinger liquid response. *Physical Review B*, 58(3):1261–1271, 1998.

[136] P. Segovia, D. Purdie, M. Hengsberger, and Y. Baer. Observation of spin and charge collective modes in one-dimensional metallic chains. *Nature*, 402:504–507, December 1999.

[137] David Sénéchal. An introduction to bosonization. *cond-mat/9908262*, August 18 1999.

[138] Naokazu Shibata. Thermodynamics of the anisotropic Heisenberg chain calculated by the density matrix renormalization group method. *Journal of the Physical Society of Japan*, 66(8):2221–2223, 1997.

[139] Naokazu Shibata and Kazuo Ueda. The one-dimensional Kondo lattice model studied by the density matrix renormalization group method. *Journal of Physics C*, 11(2):R1–R30, 1999.

[140] J. Sólyom. The Fermi gas model of one-dimensional conductors. *Advances in Physics*, 28(2):201–303, 1979.

[141] S. Tomonaga. *Progress of Theoretical Physics*, 5:544, 1950.

[142] M. Tsuchiizu, P. Donohue, Y. Suzumura, and T. Giamarchi. Commensurate-incommensurate transition in two-coupled chains of nearly half-filled electrons. *European Physical Journal B*, 19:185–193, 2001.

[143] Ashvin Vishwanath and David Carpentier. Two dimensional anisotropic non Fermi-liquid phase of coupled Luttinger liquids. *Physical Review Letters*, 86(4):676–679, 2001.

[144] J. Voit. One-dimensional Fermi liquids. *Reports on Progress in Physics*, 58:977–1116, 1995.

[145] J. Voit and H. Schulz. Field theoretical approach to the dynamical many-polaron in one spatial dimension: Comment. *Physical Review Letters*, 59(3):370, 1987.

[146] J. Voit and H.J. Schulz. Electron-phonon interaction and phonon dynamics in one-dimensional conductors: spinless fermions. *Physical Review B*, 36(2):968–979, 1987.

[147] J. Voit and H.J. Schulz. Electron-phonon interaction and phonon dynamics in one-dimensional conductors. *Physical Review B*, 37(17):10,068–10,085, 1988.

[148] Johannes Voit. Charge-spin separation and the spectral properties of Luttinger liquids. *Journal of Physics C*, 5:8305–8336, 1993.

[149] Johannes Voit. Charge-spin separation and the spectral properties of Luttinger liquids. *Physical Review B*, 47(11):6740–6743, 1993.

[150] Johannes Voit. A brief introduction to Luttinger liquids. cond-mat/0005114, May 2000.

[151] Johannes Voit, Yupeng Wang, and Marco Grioni. Bounded Luttinger liquids as a universality class of quantum critical behaviour. *Physical Review B*, 61(12):7930–7940, 2000.

[152] D.W. Wang, A.J. Millis, and S. Das Sarma. The Coulomb Luttinger liquid. cond-mat/0010241, October 2000.

[153] D.W. Wang, A.J. Millis, and S. Das Sarma. Where is the Luttinger liquid in one dimensional semiconductor quantum wire structures? *Physical Review Letters*, 85(21):4570–4573, 2000.

[154] Xiaoqun Wang and Tao Xiang. Transfer-matrix density-matrix renormalization-group theory for thermodynamics of one-dimensional quantum systems. *Physical Review B*, 56(9):5061–5064, 1997.

[155] Y. Wang, J. Voit, and Fu-Cho Pu. Exact boundary critical exponents and tunneling effects in integrable models for quantum wires. *Physical Review B*, 54(12):8491–8500, 1996.

[156] Yupeng Wang. Fermi-liquid features of the one-dimensional Luttinger liquid. *International Journal of Modern Physics B*, 12(32):3465–3473, 1998.

[157] S. Watanabe, Y.A. Ono, T. Hashizume, and Y. Wada. First principles study of atomic wires on a H-terminated Si(100) – (2 × 1) surface. *Surface Science*, 386:340–342, 1997.

[158] Satoshi Watanabe, Yohimasa A. Ono, Tomihiro Hashizume, Yasuo Wada, Jun Yamamuchi, and Masaru Tsukada. Electronic structure of an atomic wire on a hydrogen terminated Si(111) surface: First-principles study. *Physical Review B*, 52:10,768–10,771, 1995.

[159] Satoshi Watanabe, Yoshimasa A. Ono, Tomihiro Hashizume, and Yasuo Wada. Theoretical study of atomic and electronic structures of atomic wires on an H-terminated Si(100)2x1 surface. *Physical Review B*, 54(24):308–311, 1996.

[160] A. Weiße, H. Fehkse, G. Wellein, and A.R. Bishop. Optimized phonon approach for the diagonalization of electron-phonon problems. *Physical Review B*, 62(2):R747–R750, 2000.

[161] X.G. Wen. Chiral Luttinger liquid and the edge excitations in the fractional quantum Hall states. *Physical Review B*, 41(18):12,838–12,844, 1990.

[162] Steven R. White. Density-matrix algorithms for quantum renormalization groups. *Physical Review B*, 48(14):10,345–10,356, 1993.

[163] Kenneth G. Wilson. The renormalization group: Critical phenomena and the Kondo problem. *Reviews of Modern Physics*, 47(4):773–840, 1975.

[164] A. Yacoby, H.L. Stormer, Ned S. Wingreen, L.N. Pfeiffer, K.W. Baldwin, and K.W. West. Nonuniversal conductance quantization in quantum wires. *Physical Review Letters*, 77(22):4612–4615, 1996.

[165] Akio Yajima, Masaru Tsukada, Satoshi Watanabe, Masahiko Ichimura, Yuji Suwa, Toshiyuki Onigi, and Tomihiro Hashizume. First-principles calculations of As atomic wires on a H-terminated Si(100) surface. *Physical Review B*, 60(3):1456, 1999.

[166] Toshishige Yamada. Atomic wires and their electronic properties. *Journal of Vacuum Science and Technology B*, 15(4):1019–1026, 1997.

[167] Toshishige Yamada, Charles W. Bauschlicher, and Harry Partridge. Substrate for atomic chain electronics. *Physical Review B*, 59(23):15,430–15,436, 1999.

[168] C.N. Yang. Some exact results for the many-body problem in one dimension with repulsive delta-function interaction. *Physical Review Letters*, 19:1312–1315, 1967.

[169] Zhen Yao, Henk W. Ch. Postma, Leon Balents, and Cees Dekker. Carbon nanotube intramolecular junctions. *Nature*, 402:273–276, 1999.

[170] M.G. Zacher, E. Arrigoni, W. Hanke, and J.R. Schrieffer. Systematic numerical study of spin-charge separation in one dimension. *Physical Review B*, 57(11):6370–6375, 1998.